Vibration and Buckling Analysis of Unitized Structure Using Meshfree Method and Kriging Model

Ali Yeilaghi Tamijani

Dissertation submitted to the faculty of the Virginia Polytechnic Institute and State University in partial fulfillment of the requirements for the degree of

Doctor of Philosophy
In
Engineering Mechanics

Rakesh K. Kapania
Muhammad R. Hajj
Mayuresh J. Patil
Saad A. Ragab
Robert L. West Jr

May 6, 2011
Blacksburg, Virginia

Keywords: Vibration, Buckling, Random vibration, Curvilinear stiffener, Stiffened plate, Functionally Graded Material, Optimization, Meshfree, Element Free Galerkin, Surrogate model, Kriging

Vibration and Buckling Analysis of Unitized Structure Using Meshfree Method and Kriging Model

Ali Yeilaghi Tamijani

Abstract

The Element Free Galerkin (EFG) method, which is based on the Moving Least Squares (MLS) approximation, is developed here for vibration, buckling and static analysis of homogenous and FGM plate with curvilinear stiffeners. Numerical results for different stiffeners configurations and boundary conditions are presented. All results are verified using the commercial finite element software ANSYS® and other available results in literature.

In addition, the vibration analysis of plates with curvilinear stiffeners is carried out using Ritz method. A 24 by 28 in. curvilinear stiffened panel was machined from 2219-T851 aluminum for experimental validation of the Ritz and meshfree methods of vibration mode shape predictions. Results were obtained for this panel mounted vertically to a steel clamping bracket using acoustic excitation and a laser vibrometer. Experimental results appear to correlate well with the meshfree and Ritz method results.

In reality, many engineering structures are subjected to random pressure loads in nature and cannot be assumed to be deterministic. Typical engineering structures include buildings and towers, offshore structures, vehicles and ships, are subjected to random pressure. The vibrations induced from gust loads, engine noise, and other auxiliary electrical system can also produce noise inside aircraft. Consequently, all flight vehicles operate in random vibration environment. These random loads can be modeled by using their statistical properties. The dynamical responses of the structures which are subjected to random excitations are very complicated. To investigate their dynamic responses under random loads, the meshfree method is developed for random vibration analysis of curvilinearly-stiffened plates .

Since extensive efforts have been devoted to study the buckling and vibration analysis of stiffened panel to maximize their natural frequencies and critical buckling loads, these structures are subjected to in-plane loading while the vibration analysis is considered. In these cases the natural frequencies calculated by neglecting the in-plane compression are usually over predicted. In order to have more accurate results it might be necessary to take into account the effects of in-plane load since it can change the natural frequency of plate considerably. To provide a better view of the free vibration behavior of the plate with curvilinear stiffeners subjected to axial/biaxial or shear stresses several numerical examples are studied.

The FEM analysis of curvilinearly stiffened plate is quite computationally expensive, and the meshfree method seems to be a proper substitution to reduce the CPU time. However it will still require many

simulations. Because of the number of simulations may be required in the solution of an engineering optimization problem, many researchers have tried to find approaches and techniques in optimization which can reduce the number of function evaluations. In these problems, surrogate models for analysis and optimization can be very efficient. The basic idea in surrogate model is to reduce computational cost and giving a better understanding of the influence of the design variables on the different objectives and constrains. To use the advantage of both meshfree method and surrogate model in reducing CPU time, the meshfree method is used to generate the sample points and combination of Kriging (a surrogate model) and Genetic Algorithms is used for design of curvilinearly stiffened plate. The meshfree and kriging results and CPU time were compared with those obtained using *EBF3PanelOpt*.

Acknowledgments

I am grateful to all people who encouraged me and supported me throughout my life. I have a number of individuals to thank for helping me to persue my dream and for making my life in Blacksburg so wonderful and memorable.

I would like to express my sincere gratitude to my supervisor, Professor Rakesh K. Kapania, who encourage me, helped me and supported me throughout my thesis with his patience and knowledge. Without him, I would not have the opportunity to work on this interesting subject as a team member. He helped whenever there were problems in my research and I cannot thank him enough for all he taught me.

The work presented here was funded under NASA Subsonic Fixed Wing Hybrid Body Technologies NRA (NASA NN L08AA02C) with Ms. Karen Taminger as the API, Ms. Cynthina Lach as the COTR, and Mr. Richard Bird as the Technical Monitor. I am thankful to Ms. Taminger, Ms. Lach and Mr. Bird for their suggestions. Thanks are also due to Institute for Critical Technologies and Applied Sciences for providing laboratory space and other infrastructure.

I would like to express my sincere thanks to the administrative staff of the Engineering Science and Mechanics Department, especially Professor Muhammad R. Hajj and Ms. Lisa Smith for taking care of all the paper work.

I would like to thank all the members of unitized structure group for their valuable help throughout my studies.

I would like to thank my friends at Virginia Tech for all the fun we had together in the last couple of years during.

Finally, I would like to thank my father, mother, American mom, sister and brother for their love, my uncle for always standing beside me, and lastly, but most importantly Almighty God whom I trust. Thanks for giving more meaning to my life and thanks for your love and support. To them I dedicate this thesis.

Table of Contents

List of Figures

List of Tables

Nomenclature

A	=	area
a_R	=	Rayleigh damping coefficient
b	=	stiffener binormal direction
b_s	=	stiffener width
b_R	=	Rayleigh damping coefficient
C	=	damping
D_p	=	plate stress strain matrix for an isotropic material
D_s	=	stiffener stress strain matrix for an isotropic material
$detJ$	=	Jacobian of the transformation
E	=	elastic modulus
F	=	force vector
h_p	=	plate thickness
h_s	=	stiffener thickness
h	=	impulse response function matrix
H	=	admittance matrix
I	=	second moment of the stiffener cross section area
J	=	L_2 norm
J_t	=	torsional stiffness of the stiffener
K	=	stiffness matrix
K_G	=	shear correction factor
K_{Gp}	=	plate geometric stiffness matrix
K_{Gs}	=	stiffener geometric stiffness matrix
L	=	Lagrangian
M	=	mass matrix
m	=	mass

N_i = shape function

n = stiffener normal direction

p = plate

$p(X)$ = monomial basis

Q = modal force vector

R = correlation function

s = stiffener

S = cross spectral density

T_p = plate kinetic energy

T_s = stiffener kinetic energy

T_{sp} = transformation matrix relating the stiffener nodal displacements and the plate nodal displacements

t_1, t_2 = arbitrary time limits

t = stiffener tangential direction

U_p = plate strain energy

U_s = stiffener strain energy

u = displacement

u_i = nodal displacements

u_{p0} = plate displacement along x direction

v_{p0} = plate displacement along y direction

w_{p0} = plate displacement along z direction

u_{s0} = stiffener displacement along x direction

v_{s0} = stiffener displacement along y direction

w_{s0} = stiffener displacement along z direction

w = weight function

X = mode shape vector

υ = Poisson's ratio

ε_p = plate strain vector

ε_s = stiffener strain vector

ε_{Gp} = plate nonlinear strain vector

ε_{Gs} = stiffener nonlinear strain vector

τ_{Gp} = plate stress vector

$1/R$ = curvature

Λ = coordinate transformation matrix

φ_{px} = plate rotation with respect to y-axis

φ_{py} = plate rotation with respect to x-axis

φ_{sx} = stiffener rotation with respect to y-axis

φ_{sy} = stiffener rotation with respect to x-axis

θ_n = stiffener rotation with respect to t direction

θ_t = stiffener rotation with respect to n direction

α = the angle between the stiffener tangential direction (t) and x-axis

α_p = penalty parameter

r_i = support size

ρ = density

Ω = plate domain

ℓ = stiffener domain

ζ = natural coordinate

$\bar{S}$ = the centroidal distance of the stiffener to plate midsurface

$\bar{u}$ = prescribed displacement

ψ = modal transformation matrix

Γ_t = prescribed tractions boundary

Γ_u = prescribed displacements boundary

λ_b = buckling load factor

λ = buckling parameter

1 Introduction

1.1 Motivation

The aerospace industry continuously looks for reducing the weight of flight vehicle structures. There is an unending quest for both materials and fabrication techniques that can yield structures that are light–weight yet are robust, durable, damage tolerant, and corrosion resistant. Historically, stiffened panels have been used in many engineering applications, *e.g.* in aerospace industries, the wings or fuselage of an aircraft, in ship industries, the hull and the deck and in construction industries, the bridges and offshore structures, to improve the stiffness of a structure while keeping the weight within allowable limits. Researchers in flight vehicle structures also reported (Fig. 1-1) that the use of unitized structure is expected to grow exponentially by the year 2020 [1]. Unitized structures have several benefits including reduce weight by joint elimination techniques, such as rivets, or adhesive bonds between a panel and a stiffener, provide stiffeners that are of varying thickness, height, material, and even curvilinear if the load path so demands for an optimal design, *i.e.* to achieve a composites-like capability to tailor a design to operational needs, can directly connect the fabrication to the actual CAD design thus reducing the fabrication time and cost, and have structures that can be both multifunctional and can be functionally graded depending upon the materials deposited.

These structures usually consist of a base structure and local reinforcement elements called “stiffeners” to improve the static and dynamic characteristics of the base structure. The stiffeners are designed to meet the strength or stiffness requirements of a particular situation. An economical design is achieved through a proper selection of the plate size and the stiffener size and shape while reducing the overall panel weight.

With the advances being made in manufacturing technology, it is now possible to manufacture panels with arbitrary curvilinear stiffeners. The fabrication techniques (*e.g.* Electron Beam Free Form Fabrication (EBF3)) capability in the manufacturing resulted in a new design flexibility toward unitized structures. By using the fabrication techniques, the unitized structures can be formed by adding or building up material as opposed to taking the material away as in machining.

To realize this vision of wide-spread use of unitized structures requires the development of a Computational Design Environment (CDE) and knowledge of fundamental issues of panel fabrication and others namely, optimization, computational structural mechanics including rapid mesh generation as the stiffener shape and location changes. Designing a panel with curvilinear stiffeners of varying physical and geometric properties is a computationally intensive task and requires techniques that are capable of determining global optimization. There is an additional requirement that the constraints used in the design be as realistic as determined by an original aircraft manufacturer and that designs obtained using

computational means be experimentally validated. Only then, would the aerospace industry use such a Computational Design Environment (CDE).

Recently, Kapania *et al*. [2] presented some numerical results for optimal design of curvilinearly-stiffened panels, Fig. 1-2. They have developed an integrated approach and framework in the MATLAB environment to achieve optimal designs of EBF3 stiffened panels under various practical requirements to reduce the structural weight subjected to buckling and stress constraints, *etc*. The codes for several capabilities, such as NURBS (for geometric model), DISTMESH (for mesh generation), 3D display (for visualization of the stiffened panel), and NASTRAN (A finite element commercial sofware), are taken as subroutines or subprograms. Kapania *et al*. demonstrated the feasibility and advantages of the proposed technique for the flat panel with straight and curvilinear blade stiffeners of various layouts and shapes to do trade studies under static in-plane/out-plane loads subjected to buckling and stress displacement constraints. The weight reduction was the first option for the design objective. Later, they developed and evaluated a new response surface approach to find minimal weight by doing sizing and placement optimization. Sizing optimization is done by NASTRAN and placement optimization by Response Surface approach. The final goal was to implement the unified automatic placement and size optimization of both planar and curvilinear stiffened panels. It was shown in their paper that using curvilinear stiffeners, in some cases, may lead to better designs than using straight stiffeners.

The experience towards CPU time of re-meshing of panel, when the location of stiffeners' shape changes, shows that one way to reduce the computer time, is using of meshless approach in modeling unitized structures. Unlike the meshing process in the FEM, in the meshless methods, there is no need of a mesh; the method discretizes the domain of a problem using a set of scattered points, Fig. 1-3. The main advantage of this formulation is that the stiffeners can be placed anywhere within the plate and they need not necessarily follow the nodal lines for the plate. This liberates the user from the rigors of providing a nodal line along every stiffener and the mesh divisions can be chosen according to the resolution sought. This feature results in the placement and shape of a stiffener changing without remeshing the entire domain, which can decrease the CPU time and be very beneficial for performing optimization studies. By using Meshless method, there is no need of connectivity for interpolation, different curves can be used for stiffener and there is no concern of distorted mesh. This capability makes the meshless methods to be flexible in many features, such as for a sharp boundary problem, crack growth with arbitrary and complex paths, and nonlinear problems. In these cases, elements which are used in FEM can encounter difficulties.

In the conducted research, the Element Free Galerkin (EFG) method, which is based on the Moving Least Squares (MLS) approximation, is developed for vibration, random vibration, buckling and static analysis of plate with curvilinear stiffeners. The First Order Shear Deformation Theory (FSDT) was used for modeling the plate and stiffener. Numerical results for different stiffeners configurations and boundary conditions are presented. All results are verified using the commercial finite element software ANSYS®. Excellent agreement is seen in all cases. A comparison of the present formulations with other available

results for stiffened plates is also made. The meshfree approach yields highly accurate results for the plates with curvilinear stiffeners.

In addition, the vibration analysis of plates with curvilinear stiffeners is carried out using Ritz method. The Chebyshev polynomial functions are used as the basic functions in the Ritz method. The major part of this work is concerned with modeling the curvilinear stiffeners and comparing the results with experimental data. In the present method, the geometric properties of curvilinear stiffeners can be modified without changing the plate geometric properties. In the developed formulations, both eccentric and concentric stiffeners were studied. Natural frequencies and mode shapes for plate with straight and curvilinear stiffeners were compared with the results available in the literature and those obtained using ANSYS®. A good agreement was seen. A 24 by 28 in. curvilinear stiffened panel was machined from 2219-T851 aluminum for experimental validation of the Ritz and meshfree methods of vibration mode shape predictions. Results were obtained for this panel mounted vertically to a steel clamping bracket using acoustic excitation and a laser vibrometer. Experimental results appear to correlate well with the meshfree and Ritz method results.

In reality, many engineering structures are subjected to random pressure loads in nature and cannot be assumed to be deterministic quit often. Typical engineering structures include buildings and towers, offshore structures, vehicles and ships, are subjected to random pressure. The vibrations induced from gust loads, engine noise, and other auxiliary electrical system can also produce noise inside aircraft. Consequently, all flight vehicles operate in random vibration environment. These random loads can be modeled by using their statistical properties. The dynamical responses of the structures which are subjected to random excitations are very complicated. To investigate their dynamic responses under random loads, the meshfree method is developed for random vibration analysis of curvilinearly-stiffened plates. The MLS approximation is used to construct the cross spectral density of the nodal force vector. The direct complex matrix inversion method and normal mode method are used to compute the spectral density of displacement.

To study the accuracy of the developed formulation for random vibration, several examples of unstiffened and stiffened plate under white noise and jet noise with different boundary conditions are presented. The results obtained by the present approach are compared with those available in the literature. Also the meshless results of spectral density of displacement and stress for curvilinearly-stiffened plate under white noise are compared with those obtained using ANSYS®, commercially available finite element software. The meshfree results appear to correlate well with other results. In order to study the stiffeners configuration effect on the spectral density of deflection and stress, four models including plate with straight, inclined and curvilinear stiffeners have been considered and the results are compared. Also a number of numerical examples are presented to show the influence of various parameters such as stiffener stiffness ratio, stiffener curvature and in-plane compression on the random response of the plate with curvilinear stiffeners.

Since extensive efforts have been devoted to study the buckling and vibration analysis of stiffened panel to maximize their natural frequencies and critical buckling loads, these structures are subjected to in-plane loading while the vibration analysis is considered. In these cases the natural frequencies calculated by neglecting the in-plane compression are usually overpredicted. In order to have more accurate results it might be necessary to take into account the effects of in-plane load since the in-plane load can change the natural frequency of plate considerably. To provide a better view of the free vibration behavior of the plate with curvilinear stiffeners subjected to axial/biaxial or shear stresses several numerical examples are studied. In these set of examples, various plate aspect ratios, cross sectional area ratios of the stiffener to that of the plate and bending stiffness ratios of the stiffener to that of the plate for the plate with one, two and four stiffeners are studied. It is shown that the in-plane load can change the natural frequency and in some cases the corresponding mode shape of the stiffened plate significantly.

As it was discussed before, since the FEM analysis of curvilinearly stiffened plate is quite expensive, the meshfree method is chosen as the analyzer to reduce the CPU time. However it will still require many simulations and are computationally expensive. In this problem, surrogate models for analysis and optimization can be very efficient. The basic idea in surrogate model is to reduce computational cost and giving a better understanding of the influence of the design variables on the different objectives and constrains. Because of the number of simulations may be required in the solution of an engineering optimization problem which can be computationally expensive, many researchers have tried to find approaches and techniques in optimization which can reduce the number of function evaluations. Matheron [3] brought the word “kriging" into Anglo-Saxon mining terminology for the first time, and he named it in honor of South African mining engineer Danie Krig who first reported this method in his Master's thesis. The Kriging method [4] is a method of spatial prediction that is based on minimizing the mean error of the weighting sum of the sampling values. To use the advantage of both meshfree method and surrogate model in reducing CPU time, the meshfree method is used to generate the sample points and combination of Kriging and Genetic Algorithms (GA), is used for design of curvilinearly stiffened plate. To study the accuracy of the predicted response by Kriging, the cross-validation error is computed.

1.2 Vibration of Stiffened Plate

A number of analytical and numerical models for the analysis of the stiffened plates have been reported in the literature. Earlier researchers simulated stiffened plates with grillage models [5] or orthotropic models [6]. A more accurate model is achieved by representing the plate and stiffeners separately and imposing appropriate continuity between them. Olsen and Hazell [7] presented a theoretical and experimental comparison study on the vibrations of stiffened plates. The finite element method and a real time laser holography were used for the theoretical predictions and the experimental verifications, respectively.

- ***Finite Element Method***

Bhimaraddi *et al*. [8] developed a finite element model for the analysis of orthogonally stiffened shells of revolution. They used shell and curved beam elements in their model. These two elements were isoparametric elements in which the effects of shear deformation and rotary inertia effects were taken into account. A finite element model was introduced for the free vibration analysis of stiffened plates by Holopainen [9]. The main advantage of this plate-bending element as compared with the other finite element models, is that this element is free from shear locking. A stiffened plate element for the analysis of laminated stiffened plates has been developed by Kumar and Mukhopadhyay [10]. The stiffened plate element includes the effects of transverse shear. The element has no restrictions on the mesh division and can include any number of stiffeners.

Gangadhara Prusty and Satsangi [11] presented static analysis of stiffened shells. The shell is analyzed using an eight-noded isoparametric element and the stiffener element is considered as a three-noded isoparametric curved beam element and the stiffness matrix is calculated using the standard principles of finite element analysis. Also a new four-noded stiffened plate bending element was proposed by Barik and Mukhopadhyay [12] for the analysis of both unstiffened and stiffened plates. This element was derived by combining the four-noded rectangular plane stress element having 8 degrees of freedom with the simplest rectangular plate bending element having 12 degrees of freedom. One of the advantages of their approach is that the orientation and the position of the stiffeners inside the plate element are without any restriction and hence need not necessarily be positioned between nodes.

- ***Ritz Method***

The Ritz method was also used for solving free vibration of stiffened plate. Chen *et al*. [13] used Ritz method with B-splines as the trial functions. In their research, the spline compound strip method was used. The spline compound strip method can be considered as a special form of the finite element method. The free vibration analysis of intermediate stiffeners [14] and inclined stiffeners [15] is studied by Liew *et al*. The Mindlin theory was incorporated to derive the formulation; the transverse shear deformation is included in their formulation. Liew *et al*. [14], [15] used the Ritz method with a set of simple polynomials and their approach was able to enforce the different geometric boundary conditions of various plates considered.

Smith *et al*. [16] used the Rayleigh Ritz method, with a polynomial based displacement function, to study the buckling behavior of rectangular plates. They studied different aspect ratios and combinations of clamped, simply- supported and free edges. The simple and classical orthogonal polynomials are used in the Ritz method. The orthogonal polynomials were Chebyshev, Hermite, Legendre and Laguerre. They showed that orthogonal polynomials have better convergence characteristics in plate buckling problems and the simple polynomial is the preferred displacement function for unilateral plate analysis due to its simplicity and computational speed for iterative solution procedures.

Differential Quadrature (DQ) method proposed by Bellman *et al*. [17] has been used in the area of plate analysis and a large number of publications can be found in the literature. Zeng and Bert [18] studied the free vibration of eccentrically stiffened plates by using DQ. The DQ is a numerical technique for initial and boundary value problems. It is based on the approximation of a function and hence its partial derivatives with respect to the space variables, within a domain, by a linear sum of function values at all discrete grid points.

The Discrete Singular Convolution (DSC) method was developed by Wei and his associates [19] and was implemented to analyze the free vibration of a plate. The DSC algorithm is based on the distribution and wavelet theories. Numerical solutions to the differential equations are formulated via the singular kernels of data type. The DSC is able to predict high frequencies of plates (Zhao *et al*. [20]); however the versatility and applicability of the DSC method for more complicated structures have not been reported.

As it has been mentioned earlier, many methodologies have been implemented for various free vibration stiffened plate problems. These methods include analytical and numerical techniques, such as the Ritz method, differential quadrature method, finite strip method, and the finite element method.

- ***Meshfree Method***

In recent decades, meshless methods have attracted much attention due to the need of no elements for interpolation purposes. Belytschko *et al*. [21] developed Element Free Galerkin (EFG) method and used it to model the elasticity and heat conduction problems. Moving Least Square (MLS) is used to construct the shape function. Belytschko *et al*. introduced a background cell structure to find integration by numerical quadrature and Lagrange multipliers is used to enforce essential boundary conditions.

Krysl and Belytschko [22] developed meshless approach for the analysis of the arbitrary Kirchhoff shells by the Element Free Galerkin (EFG) method. The shell theory used was geometrically exact that can be applied to deep shells. The method is based on Moving Least Squares approximation. The Element Free Galerkin (EFG) method is almost identical to the conventional finite element method, as both of them are based on the Galerkin formulation, and employ local interpolation to approximate the trial functions. The key differences lie in the interpolation methods, integration schemes and in the enforcement of essential boundary conditions. Belytschko *et al*. [23] also studied different features of the kernel methods, Moving Least Square methods (MLS), and partition of unity methods. It was shown that these methods can have similar features; especially the MLS method, if certain conditions are imposed, can be similar to the kernel method. Two kinds of meshless methods, collocation methods and Galerkin methods were also considered by using the MLS and partition of unity methods and convergence of these methods for various structures were studied.

Peng *et al*. [24], [25] used Element Free Galerkin (EFG) method for the static and dynamic analysis of plate with straight stiffeners in *x* and *y* directions. It has been shown in their paper that by using the EFG method they avoided the need for remeshing that occurs with FEM because the stiffeners need to be placed along the mesh lines and the change of the stiffener position leads to remeshing of the entire plate domain.

The Moving Least Square (MLS) is a method of reconstructing continuous functions from a set of data. Researchers have applied the MLS technique in the analysis of solid mechanics problems by developing the meshfree method (Peng *et al.* [24]). Recently, the MLS data interpolation technique was utilized to establish the Ritz method for the vibration analysis of plate by Zhou and Zheng [26]. The geometric boundary conditions of the plate can be enforced through a point substitution technique. They studied the convergence, the influence of the MLS mesh size, the MLS support radius and the number of Gaussian integration points.

One of the main issues in numerical analysis is the CPU time and it is obvious that remeshing (e.g. in shape optimization) will increase it. Bobaru and Mukherjee [27] studied the shape optimization of the fillet using Element Free Galerkin (EFG) method and the results were compared with the FEM, BEM and Boundary Counter Method (BCM). They showed that the cost of remeshing, which is required in many shape optimizations using FEM or BEM, can be eliminated by using EFG method.

- ***Random Vibration of Stiffened Plate***

In reality, many engineering structures are subjected to random pressure loads in nature and cannot be assumed to be deterministic quit often. Typical engineering structures, include buildings and towers, offshore structures, vehicles and ships, are subjected to random pressure. The vibrations induced from gust loads, engine noise, and other auxiliary electrical system can also produce noise inside aircraft. Consequently, all flight vehicles operate in random vibration environment. These random loads can be modeled by using their statistical properties. The dynamical responses of the structures which are subjected to random excitations are very complicated. To investigate their dynamic responses under random loads, different approaches have been introduced.

Olson and Lindberg [28] studied the random response of integrally stiffened plates. They used finite element method to model the structure. A particular configuration of a five-bay panel with length to width ratio of 5 to 2 was taken as an example in their study. A triangular plate bending elements and beam bending and torsional elements were used to model the plate and stiffeners, respectively. First, Olson and Lindberg compared the natural frequencies and corresponding mode shapes of the stiffened panel using finite element method with those predicted experimentally. Then they compared the results of the panel to the jet noise excitation with the experimental results. The method was based on the standard modal superposition approach using the mode shapes obtained from finite element solution. To obtain the random response of a stiffened panel, the consistent finite element method is applied in their research for calculating the cross spectral density. To simplify the integrations involved in the cross spectral density of the generalized forces, Olson and Lindberg approximated the cross spectral density over each element by using a polynomial in the local coordinates.

Dey [29] also applied the finite element method to obtain the response of a structure subjected to random loads. The author used two well known methods, direct complex matrix inversion method and normal mode method, to obtain the response of structures. In both methods, Dey assumed that the same

random pressure is acting over the whole contributing area with full correlation. This assumption allowed the lumping of pressure around a node to form a nodal force spectral density matrix. This method was illustrated using a truss, a beam and a plate element.

Yang and Kapania [30] used the finite element method to study the random response of a cooling tower. The authors employed the displacement shape functions of a 48 degree-of-freedom shell element to form the cross spectral density of the nodal force vector. The shape functions were also used to represent the cross spectral density at an arbitrary pair of points located within two different elements. The Gaussian quadrature was used for the integrations involved in the cross spectral density instead of assuming a polynomial form for cross spectral density [28].

Mukherjee and Mukhopadhyay [31] studied the random vibration analysis of stiffened plates using finite element method. In their formulation, the stiffener need not necessarily be connected between the nodes and it can be located anywhere within the plate element. The element is isoparametric quadratic, which has advantages such as accommodating irregular boundaries, laminated materials and accounting for shear deformations, which extends its applicability to both thin and thick plates. The Gaussian quadrature is used for the integration of force cross spectral density matrix. Mukherjee and Mukhopadhyay obtained the random response for straight, curved and skew stiffened plates subjected to white noise and jet noise.

Lyrintzis and Vaicaitis [32] developed an analytical solution to predict dynamic response and noise transmission of discretely stiffened, multilayered composite panels. They obtained the sound pressure levels in the interior of the enclosure by coupling the acoustic field to the sidewall vibrations of the stiffened structure.

In most of the research that has been mentioned earlier, three approaches have been employed to find the integrations involved in the cross spectral density: a) Gaussian quadrature to evaluate double area, b) approximate the cross spectral density over each elements by using a linear function and c) assume that the same random pressure is acting over the whole contributing area with full correlation. Liu *et al.* [33] suggested an efficient formulation of consistent random loads. They approximated the cross spectral density by interpolating the cross spectral density at nodal points to approximate the continuous random pressure field. They applied this method to beam and plate element to find the random response of structures under white noise and jet noise.

Dogan [34] studied the linear and nonlinear vibrations of antisymmetric angle-ply laminated plates subjected to random loads. In their research random pressure is simulated by using the Monte Carlo method. The author obtained the spectral densities for linear and nonlinear responses. It was shown that the linear approach overestimates the displacement for high-random inputs.

Joshi *et al.* [35] studied the optimal design of curvilinearly-stiffened plate subjected to a point excitation. In their research, the objective function was the radiated acoustic power and the constraint was the total mass of structure. The authors considered the shape and sizing optimization to reduce the radiated acoustic power. They used MD NASTRAN®, a commercial software, to obtain the structural response, Rayleigh integral to find the acoustic and VisualDOC®, a commercial software, to find the optimal design.

It was shown that by optimizing the curvilinear stiffeners size and shape, an overall reduction of 7-12db in radiated acoustic power can be achieved.

- ***Stiffened Functionally Graded Plate***

Recently, a new class of materials known as "Functionally Graded Materials" (FGMs) has been introduced to the literature. The concept of functionally-graded materials was first suggested by a group of Japanese scientists in 1984 to address the needs of aggressive environment of thermal shock. The Functionally Graded Material (FGM) is usually made from a mixture of ceramic and metal. The metal rich part can increase mechanical properties, such as toughness and the ceramic rich side can increase the thermal resistance. Due to these properties, the functionally-graded material can have a superior resistance to interfacial failure and may be used in various structures in high speed aircraft and space vehicles applications as a thermal barrier.

Reddy *et al*. [36] and [37] studied the static and dynamic response of the functionally-graded material plates and shells. In both papers the properties are graded in the thickness direction according to a volume fraction power-law distribution.

Yang and Shen [38] studied the free vibration of FGM plate which the material properties are assumed to be temperature dependent, and graded in the thickness direction according to a volume fraction exponent. They used one dimensional differential quadrature and the Galerkin procedure, and mode superposition method to solve the free vibration problem and transient problem, respectively. The FGM plate is assumed to be initially stressed, and the influence of the magnitude of the stress on natural frequency was studied in their paper.

Qian *et al*. [39] applied the Meshless Local Petrov-Galerkin method to study the free and forced vibration problem of thick FGM plate based on higher-order shear and normal deformable plate theory. The plate material is assumed to be made of two isotropic materials with properties varying in the thickness direction.

Zhao *et al*. [40] developed an element-free kp-Ritz method based on the first-order shear deformation plate theory for free vibration analysis of functionally-graded plates. The displacements are approximated using kernel particle functions. They studied the influences of the boundary conditions, volume fraction exponent, and length-to-thickness ratio on the frequency of FGM plates.

He *et al*. [41] presented a finite element formulation based on the classical laminated plate theory for the shape and vibration control of the functionally-graded material (FGM) plates with integrated piezoelectric sensors and actuators. They studied the influence of the volume fraction exponent on the static and dynamic response of FGM plate. They also showed the passive and active control of FGM plate using piezoelectric layers.

Sheng and Wang [42] studied the buckling and vibration of functionally-graded cylindrical shells with ring-stiffener using Ritz method. The temperature distribution is found by solving the heat conduction equation across the shell thickness. The effect of thermal loading on the critical buckling load and natural

frequency of functionally-graded cylindrical shells with ring-stiffener was studied in their research. They also investigated the effects of stiffener's number and size on natural frequency of functionally-graded cylindrical shells.

Birman and Byrd [43] studied the stability and free vibrations of rectangular functionally-graded panels reinforced by a system of parallel stringers. They found the closed-form solution of the problem for large aspect ratio panels with simply-supported long edges, arbitrary boundary conditions along the short edges, and arbitrary spacing between the stringers and the cross sections of individual stringers. They also found the optimized size of stringers and their spacing for the buckling loads or fundamental frequencies.

Najafizadeh *et al*. [44] derived a closed form solution for the critical buckling load of functionally-graded cylindrical shells stiffened by rings and stringers. They studied the effects of the volume fraction exponent and the thickness of shell on the critical buckling load. Chen *et al*. [45] also studied the free vibration and buckling of FGM plates subjected to in-plane loads based on higher-order deformation theory. The initial stresses are assumed to be a combination of a uniaxial extensional stress and a pure bending stress. In their study, the effect of volume fraction on vibration and buckling was examined. Malekzadeh *et al*. ([46], [47]) studied the three dimensional free vibration of FGM annular plates under thermal environment and FGM plates on elastic foundations. They used differential quadrature method (DQM) to solve the thermoelastic equilibrium equations and equations of motion. The results for convergence behavior, the effects of the temperature rise, the geometrical parameters, material graded index, coefficients of elastic foundations and boundary conditions on the frequency parameters are presented in their papers.

1.3 Buckling of Stiffened Plate

The study of stability of stiffened plates has a long history. The wide-spread application of stiffened plates has resulted in different methods for performing an appropriate structural analysis of these plates. A large number of studies on bending, buckling and vibration of stiffened panels are available in the literature.

- ***Semi-Analytical Method***

Timoshenko and Gere [48] presented numerical tables for buckling loads of rectangular plates stiffened by longitudinal and transverse ribs. The effect of eccentricity of the stiffeners on the stress-strain matrix was introduced by modifying the second moment of area of the stiffener by Seide [49]. Kolakowski [50] presented a semi-analytical method for the buckling analysis including modal interaction of prismatic plate structures using trigonometric series. A semi-analytical model for global buckling and postbuckling analysis of stiffened panels was proposed by Byklum *et al.* [51]. In their research, the loads were biaxial inplane compression or tension, shear and lateral pressure. By using the principle of virtual work and

assuming deflections in the form of trigonometric function series, they solved the buckling and postbuckling analysis of stiffened panels. Perturbation methods were used for solving the nonlinear algebraic equilibrium equations which are generated by the principle of virtual work.

Brubak, Hellesland, and Steen [52] presented a semi-analytical model for buckling strength analysis of stiffened plates with arbitrarily oriented stiffeners. By using the proposed model, stiffened plate with different boundary conditions can be modeled. In the strain energy formulations, which are considered in their research, the coupling terms between bending and membrane components for the plate and stiffeners were ignored. Later, Bedair [53] discussed that since there are other several papers on the buckling of stiffened plates available in the literature, Brubak *et al.* should have compared the efficiency of their formulations to some of these methods, since they had claimed that their's is an efficient method. Also Bedair discussed that the authors ignored the contribution of torsional rigidity of the stiffeners in their formulations and pointed out that Brubak *et al.* should have mentioned that this assumption is not valid for the stiffeners with closed sections. The lack of stating the assumptions relating the displacements of the stiffeners to the midplane displacements of the plate, ignoring the coupling terms between bending and membrane components for the plate and stiffeners and comparing the computer speed of their solution to the ANSYS® were also discussed by Bedair.

- ***Finite Element Method***

Several finite element models are developed to analyze buckling of a stiffened plate. Shastry, Venkateswara Rao, and Reddy [54] studied finite element model for the plate and stiffener and applied it to the stability analysis of stiffened plates subjected to arbitrary inplane loading. Mukhopadhyay and Mukherjee [55] applied the finite element model for the buckling analysis of the stiffened plates. The stiffened plate was modeled by using isoparametric bending element. In their formulation, the stiffener nodes need not to be necessarily connected to those of the plate and they can be located anywhere within the plate element. The element developed by Mukhopadhyay and Mukherjee is an isoparametric quadratic element and has the advantages that it can represent irregular boundaries, laminated plates and can account for shear deformations.

Biswal and Ghosh [56] developed a four-noded rectangular element with seven degrees of freedom at each node for a laminated plate. They used a higher-order shear deformation theory which can explain the parabolic distribution of transverse shear stresses and the nonlinearity of the inplane displacements across the thickness. The stiffness of the stiffener is reflected at all four nodes of the plate element in which it is located. However, in Biswal and Ghosh's paper, the stiffener element can be placed parallel to the x or y directions only. The stiffness matrix of a stiffened plate element consists of the contributions of the plate and that of the stiffeners. A nine-noded plate element and a three-noded stiffener element were developed by Sadek and Tawfik [57] to model the stiffened composite plates. The model is based on a higher-order shear deformation theory which is derived out of a power series expansion of the mid-surface displacements. The model is applicable for both moderately thick and thin stiffened composite plates. By

using the transformation matrix, the stiffener nodal parameters transform to the plate nodal parameters. Consequently, the stiffeners can be positioned anywhere within the plate element along lines of constant natural coordinates and need not necessarily be placed on the plate nodes.

- ***Ritz Method***

Guot and Lindner [58] developed a material and geometric nonlinear spline strip method to analyze the stiffened panels subjected to axial compression. They mentioned that since the collapse of stiffened panel made of thin steel plates is often caused by the interaction between the local buckling of the plate and stiffeners and the overall buckling of the whole stiffened panel, they studied the elastic-plastic interaction behavior of the stiffened panel. Kirchhoff hypothesis was used to model both the plate and the beam. The residual stresses and initial geometric imperfections are considered and their effects on the ultimate strength of the stiffened panel were considered.

Kapania and Li [59], [60] studied the geometrically exact finite strain curved twisted beam theory with large displacements/rotations and extended using orthonormal frames and the rigid cross-section assumption. Except for the rigid cross-section assumption, no further approximations were made in the formulations. All reference frames are orthonormal and therefore the geometric aspects become more direct. They used the principle of virtual work to derive the equations for initially curved/twisted beams by considering the first Piola-Kirchhoff stresses. The developed formulation can be used for 3-D natural curved/twisted slender beams with finite strains and rotations. Several examples for slender beam cases were presented to test the developed element formulation. Since the initial curvature correction term is considered by Kapania and Li, especially when long-term dynamic responses are concerned, their formulation may give more accurate results.

- ***Meshfree Method***

To avoid meshing, a tedious and time consuming affair, of a domain using finite elements, meshless methods are increasingly being used to solve problems in solid mechanics. In the meshfree methods, the displacement approximation is defined based on a set of particles in the influence domain. Various approaches have been proposed in the literature. Two of these approaches are the Element Free Galerkin (EFG) [22] using Moving Least Square (MLS) and the Meshless Local Petrov-Galerkin (MLPG) [61] using MLS or Symmetric Smoothed Particle Hydrodynamics (SSPH) [62].

Atluri and Zhu [61] proposed a Meshless local Petrov-Galerkin (MLPG) method, which is a truly meshless method. Remarkable successes of MLPG method have been reported in solving convection diffusion problems, fracture mechanics problems and plate bending problems.

Batra and Zhang [62] proposed a new and simple technique called the Symmetric Smoothed Particle Hydrodynamics (SSPH) method to construct basis functions for meshless methods that use only locations of particles. The idea is based on approximating derivatives of a function without differentiating the basis functions. By using Taylor series the function is related to neighboring nodes. In this method, the

restrictions on the choice of the kernel function are fewer than those for other SPH methods. Consequently, it is possible to use a wider class of kernel functions. They used their proposed basis functions for constructing the strong and a weak form of equations of equilibrium for a 2D elastic problem. Liew *et al*. [63] emploed a meshfree Galerkin method for the elastic analysis of stiffened and un-stiffened folded plates under partial in-plane edge loads. The developed formulations are based on first-order shear deformation theory (FSDT). They compared their results those obtained using ANSYS.

- ***Effect of In-Plane Load on Natural Frequency and Modeshapes***

Smith *et al*. [64] presented analytical and experimental results on the resonant frequencies of vibration of damped stiffened and un-stiffened plate. The effects of point masses and in-plane loading were studied in their research. Kielb and Han [65] developed numerical solutions for the natural frequency and mode shape of a rectangular plate subjected to in-plane hydrostatic forces for different aspect ratios, boundary conditions and load magnitudes. They showed that for some combinations of aspect ratio, boundary conditions and edge loads, the unloaded fundamental mode shape and the mode shape of plate subjected to in-plane loads are completely different.

Attaf and Hollaway [66] studied vibration analysis of un-stiffened and stiffened composite plates. The effect of in-plane load was considered in the frequency response. They discussed the dynamic response of rectangular composite plates subjected to static in-plane compressive loads. The finite element method was used to predict the dynamic behavior and critical buckling loads of in-plane loaded plates. The experimental technique was implemented to verify the analytical analysis; however, the plates were not loaded to their critical load values.

Srivastava *et al*. [67] solved the vibration analysis of rectangular stiffened plates subjected to in-plane partial edge load. They used finite element formulation to solve the buckling load and frequency parameters in various modes with different boundary conditions, aspect ratios and various parameters of stiffened plates. The nine-noded isoparametric quadratic element was used to model the plate. In their formulation, the stiffener may lie anywhere within a plate element. Srivastava *et al*. [68] also solved the same problem for the stiffened plates with cutouts subjected to uni-axial in-plane uniform edge loading at the plate boundaries using the finite element method. They presented the effects of size and location of cutouts, aspect ratios of the plate and cutout, different boundary conditions and stiffener parameters on buckling and vibration characteristics of rectangular stiffened plates with cutouts. It is mentioned in their papers that the developed element can be applied to a structure having irregular boundaries such as curved boundaries.

1.4 Optimization Using Surrogate Model

For shape and size optimization of curvilinear stiffeners, the optimization scheme needs to explore the design variable space. One major issue in this problem is the long running time of the analysis. Since the Finite Element Method (FEM) analysis of curvilinearly stiffened plate is quite expensive, the meshfree method is chosen as the analyzer to reduce the CPU time. Since the remeshing is avoided in meshfree methods, they are faster than FEM when the stiffener shape changes while plate width and height are kept unchanged. This gives a great capability in reducing the CPU time during optimization process.

Because of the number of simulations may be required in the solution of an engineering optimization problem which can be computationally expensive, many researchers have tried to find approaches and techniques in optimization which can reduce the number of function evaluations. Work by Schmit and Farshi [69], for example looked at various approximation concepts to improve the efficiency of structural optimization. They considered the number of independent design variables to reduce it by employing design variable linking, the number of constraints to reduce it by considering only critical and near critical constraints, and the number of structural analyses is reduced by employing first order Taylor series expansion. It was shown in their research that using reciprocal variables also can improve the quality of the linear approximations for displacement and stress response.

In a design process, it frequently occurs that the objective function or constraints are not expressed in a closed-form equation. In these cases, having a simple approximate function (called a surrogate model) will save computational time and could be used by a global optimizer. Some of these surrogate models are shown on the left side of Fig. 1-4. Also some popular global optimizers that are being used in structural shape and size optimization are shown on the right side of Fig. 1-4.

Jones [70] presented a categorization of various approaches for using response surfaces for global optimization. For each method an example were presented to highlight the advantages and disadvantages and show the failure modes of each method, which sometimes is not very obvious. In his research, the response surfaces were categorized as the non-interpolating and interpolating response surfaces. It was reported that non-interpolating surfaces, such as fitted quadratic surfaces, are not reliable because the surface may not sufficiently capture the shape of the function. For example, it was shown that with quadratic surface, which is a non-interpolating surface, adding additional points would not necessarily result in a more accurate surface, however in contrast, for interpolating surface, like natural cubic splines, adding new points will improve the accuracy.

Simpson *et al.* [71] compared second-order response surface and kriging for approximating non random, deterministic computer analyses. They applied both methods to do the multidisciplinary design of an aerospike nozzle. They performed error analysis, graphical comparison, and optimization, using response surface and kriging. It was shown that both methods can predict well and kriging are slightly better than response surface. It was also reported that for aerospike nozzle optimization, response surface

requires fewer analysis and gradient calls than the kriging which can be due to the fact that second-order response surface is a simple second-order polynomial whereas the kriging is more complex.

Neural networks can be also thought as another way of developing response surface. Carpenter *et al*. [72] used neural networks and polynomial approximations to develop response surfaces and compared the performance of two approximations based on the number of function evaluations that each one requires. It was reported in their research that neural networks can be very accurate at sample points, and higher order approximation can be obtained by simply including more nodes. However, they also reported some disadvantages of neural networks versus polynomial response surface. One is the training of the nets which could be very lengthy and cause the computational cost in learning.

The response surfaces generated by using kriging and neural networks were also compared by Sakata *et al*. [73]. It was shown in their paper that neural networks results are closer to the exact results than kriging results. However, it was also reported that the optimum solution of the estimated function using the kriging method is closer to the original than that obtained by using neural networks approximation. They reported that it might be due to the fact that the approximated function using neural networks generates the response surface by minimizing the sum of the approximation errors at the sample points; however kriging generates the response surface by minimizing the average square error at each region. They also described a structural optimization method by using kriging estimation and a gradient optimization and applied it to the eigenfrequency optimization of a stiffened cylinder.

Queipo *et al*. [74] discussed the issues that arise in the surrogate based analysis and optimization such as the design of experiments, surrogate selection and validation, sensitivity analysis, and how to incorporate surrogates in optimization efforts when constraints are present. They presented both parametric (e.g., polynomial regression, kriging) and non-parametric (e.g. radial basis functions) surrogate models. The parametric models assume that the global functional form of the relationship between the response and the design variables is known, while the non-parametric ones use different types of simple, local models in different regions of the data to build up an overall model. Queipo *et al*. also presented the multi-objective optimal design of a liquid rocket injector to illustrate the issues and usefulness of surrogate models for multi-objective optimization.

Building the review conducted by Queipo *et al*., Forrester and Keane [75] took a more in depth look at the range of surrogate modeling methods and infill criteria and presented the advantages and disadvantages of each method. They discussed in their paper that, polynomial models can model simple problem in few dimensions. Moving Least Square (MLS) can be a good surrogate model for more complex analysis, but is still limited to lower dimensions, fixed bases Radial Basis Functions (RBFs) are suitable for higher-dimensional, but simple analysis, and kriging and parametric RBFs, because of the expense of training, can be used for relatively low dimensional problems. However kriging and parametric RBFs have the potential to provide more accurate predictions.

Sakata *et al*. [76] applied the kriging estimation and gradient method to the size optimization of a stiffened plate. They compared their results with those obtained using neural networks approximation. In

their research the eigenfrequency of stiffened plate is maximized while the mass of structure is kept constant. They reported the effectiveness of the kriging and optimization algorithm using gradient method.

Continuing on curvilinearly stiffened panel, Gurav and Kapania [77] developed a framework (*EBF3PanelOpt*) for design optimization of unitized structures in PYTHON programming environment. The finite element commercial software, MD.PATRAN® and MD.NASTRAN®, were used to parametrically create and analyze a detailed finite element model of curvilinearly stiffened plate and VisualDOC®, an optimization commercial software, was used to find the optimal design. While optimizing the mass of the stiffened panel, constraints were placed on critical buckling load, von Mises stress and crippling. The optimization included the shape as well as sizing design variables. With the *EBF3PanelOpt* environment Joshi et al. [35] and Dang et al. [78] studied the optimization of stiffened panels considering various responses, such as structural acoustics and damage tolerance.

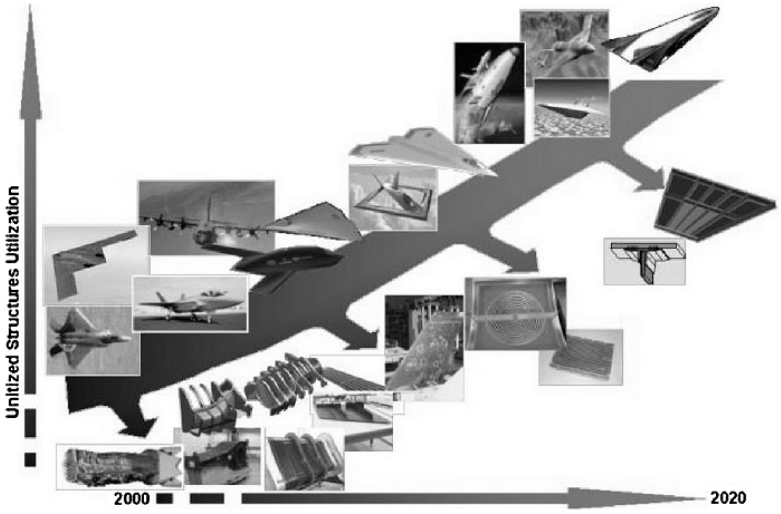

Fig. 1-1 Graphical representation of unitized structure [1]

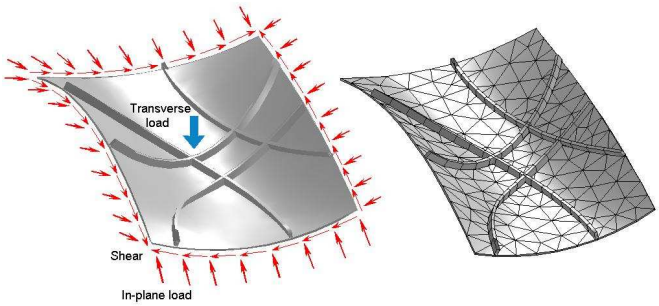

Fig. 1-2 A curved panel with arbitrarily oriented stiffeners and its finite element mesh [2]

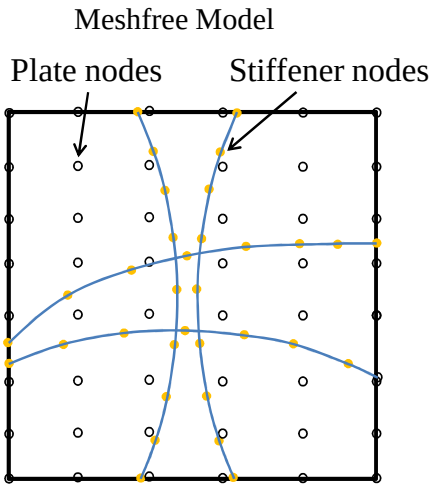

Fig. 1-3 A meshfree model of panel with curvilinear stiffeners

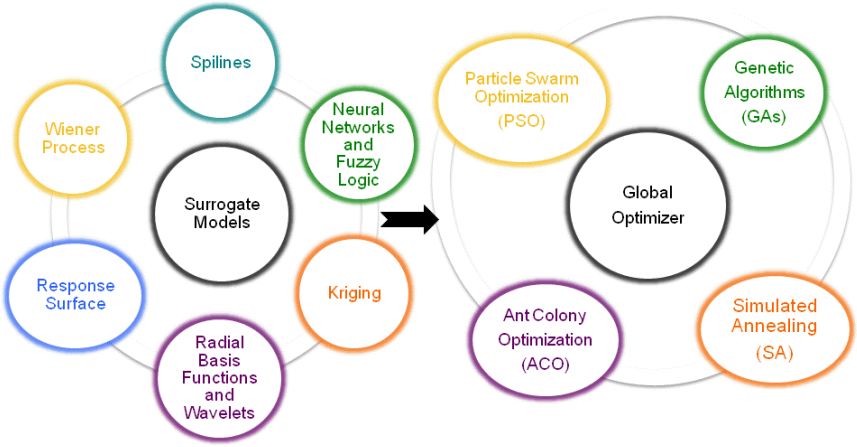

Fig. 1-4 Using surrogate models and global optimizers in design

2 Vibration of Curvilinearly Stiffened Plate Using Element Free Galerkin Method

2.1 Introduction

The Element Free Galerkin (EFG) method, which is based on the Moving Least Squares (MLS) approximation, is developed for vibration analysis of unitized structures, e.g. a plate with curvilinear stiffeners. The plate and stiffeners are modeled using the First Order Shear Deformation Theory (FSDT) and Timoshenko beam theory, respectively. The Moving Least Squares approximation does not satisfy the delta function property. Consequently, an approximation method, e.g. the well-known penalty method, must be used for imposing essential boundary conditions. A key benefit of using EFG for vibration analysis of stiffened panel is that the locations and curvatures of the stiffeners can be changed without modifying the plate nodes. Numerical results for different stiffeners configurations and boundary conditions are presented. All results are verified using the commercial finite element software ANSYS®. Excellent agreement is seen in all cases. A comparison of the present formulations with other available results for stiffened plates is also made. The meshfree approach yields highly accurate results for the plates with curvilinear stiffeners.

2.2 Formulation of the Problem

- ***Strain and Kinetic Energies of the Plate and Stiffener***

Based on the first order shear deformation theory [79], the displacement field of a plate is expressed as:

$$\begin{aligned} u_x(x,y,z,t) &= u_{p_0}(x,y,t) + z\varphi_{px}(x,y,t) \\ v_y(x,y,z,t) &= v_{p_0}(x,y,t) + z\varphi_{py}(x,y,t) \\ w_z(x,y,z,t) &= w_{p_0}(x,y,t) \end{aligned} \tag{2-1}$$

where u_x, v_y and v_y are the displacement components along the x, y and z directions, respectively, φ_{px} and φ_{py} are the rotations with respect to the y and x axis, u_{p_0}, v_{p_0} and w_{p_0} are the midplane displacements and p indicates the plate (Fig. 2-1). The strains associated with these displacement components are [79]

$$\varepsilon_p = \begin{Bmatrix} \varepsilon_{px} \\ \varepsilon_{py} \\ \gamma_{pxy} \\ \gamma_{pxz} \\ \gamma_{pyz} \\ \kappa_{px} \\ \kappa_{py} \\ \kappa_{pxy} \end{Bmatrix} = \begin{Bmatrix} \frac{\partial u_{p_0}}{\partial x} \\ \frac{\partial v_{p_0}}{\partial y} \\ \frac{\partial v_{p_0}}{\partial x} + \frac{\partial u_{p_0}}{\partial y} \\ \frac{\partial w_{p_0}}{\partial x} + \varphi_{px} \\ \frac{\partial w_{p_0}}{\partial y} + \varphi_{py} \\ \frac{\partial \varphi_{px}}{\partial x} \\ \frac{\partial \varphi_{py}}{\partial y} \\ \frac{\partial \varphi_{py}}{\partial x} + \frac{\partial \varphi_{px}}{\partial y} \end{Bmatrix} = \begin{bmatrix} \frac{\partial}{\partial x} & 0 & 0 & 0 & 0 \\ 0 & \frac{\partial}{\partial y} & 0 & 0 & 0 \\ \frac{\partial}{\partial y} & \frac{\partial}{\partial x} & 0 & 0 & 0 \\ 0 & 0 & 1 & 0 & \frac{\partial}{\partial x} \\ 0 & 0 & 0 & 1 & \frac{\partial}{\partial y} \\ 0 & 0 & \frac{\partial}{\partial x} & 0 & 0 \\ 0 & 0 & 0 & \frac{\partial}{\partial y} & 0 \\ 0 & 0 & \frac{\partial}{\partial y} & \frac{\partial}{\partial x} & 0 \end{bmatrix} \begin{Bmatrix} u_{p_0} \\ v_{p_0} \\ \varphi_{px} \\ \varphi_{py} \\ w_{p_0} \end{Bmatrix} = L_p u_p \tag{2-2}$$

The generalized plate stress strain matrix for an isotropic material is:

$$D_p = \frac{E_p h_p}{1-\upsilon^2} \begin{bmatrix} 1 & & & & & & & \\ \upsilon & 1 & & & & & & \\ 0 & 0 & \frac{1-\upsilon}{2} & & & \textit{sym.} & & \\ 0 & 0 & 0 & K_G \frac{1-\upsilon}{2} & & & & \\ 0 & 0 & 0 & 0 & K_G \frac{1-\upsilon}{2} & & & \\ 0 & 0 & 0 & 0 & 0 & \frac{h_p^2}{12} & & \\ 0 & 0 & 0 & 0 & 0 & \frac{\upsilon h_p^2}{12} & \frac{h_p^2}{12} & \\ 0 & 0 & 0 & 0 & 0 & 0 & 0 & \frac{h_p^2(1-\upsilon)}{24} \end{bmatrix} \tag{2-3}$$

where h_p is the thickness of the plate, A is the area of the plate, E_p is Young's modulus, υ is the Poisson's ratio and K_G is the shear correction factor (It is taken as $K_G = \frac{5}{6}$). The strain and kinetic energies of the plate can be written as [79]:

$$U_p = \frac{1}{2} \int_A \varepsilon_p{}^T D_p \varepsilon_p dA$$
$$T_p = \frac{1}{2} \int_A \dot{u}_p^T m_p \dot{u}_p dA \tag{2-4}$$

where the dot represents the differentiation with respect to time, and m_p is

$$m_p = \rho_p \begin{bmatrix} h_p & 0 & 0 & 0 & 0 \\ 0 & h_p & 0 & 0 & 0 \\ 0 & 0 & \frac{h_p^3}{12} & 0 & 0 \\ 0 & 0 & 0 & \frac{h_p^3}{12} & 0 \\ 0 & 0 & 0 & 0 & h_p \end{bmatrix} \tag{2-5}$$

where ρ_p is the density of plate material.

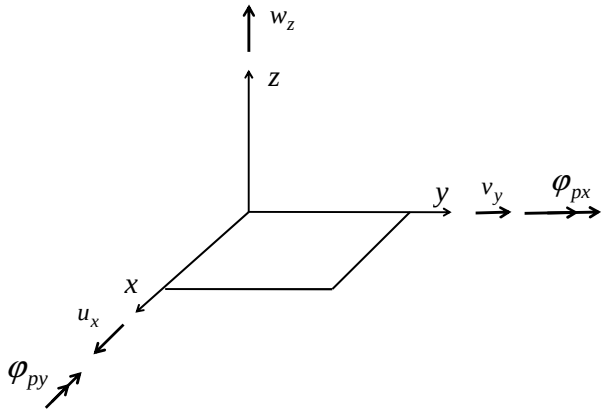

Fig. 2-1 Directions of the generalized displacements of the plate

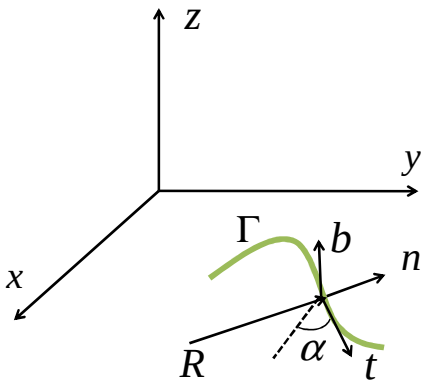

Fig. 2-2 Local and global coordinate systems for curvilinear stiffener

Line Γ in a three dimensional global coordinate system x, y and z is shown in Fig. 2-2. The local coordinates are t, n and b in tangential, normal and binormal directions, respectively. R is the radius of curvature, and the curvature is in the $x-y$ plane, consequently b is in z direction. α is the angle between the t and x axes. The line Γ can be defined by:

$$x = x(\zeta)$$
$$y = y(\zeta) \tag{2-6}$$

in which x and y are global coordinates and ζ is the natural coordinate for parameterizing the curve, as can be seen in Fig. 2-3. The *detJ*, which is the Jacobian of the transformation, may be defined as [80]:

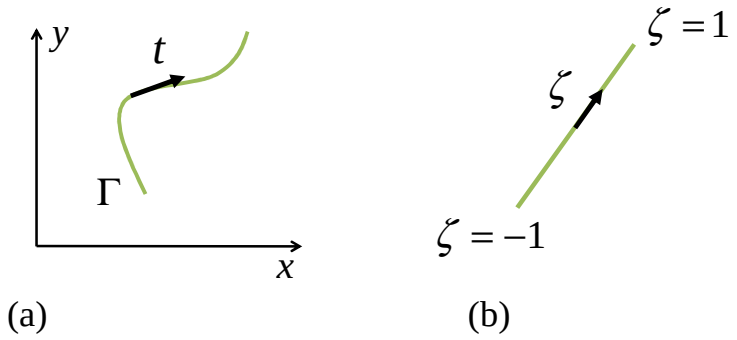

Fig. 2-3 (a) Curved stiffener in *x*–*y* plane; (b) Its transformed plane.

$$\det J = \sqrt{(\frac{dx}{d\zeta})^2 + (\frac{dy}{d\zeta})^2} \tag{2-7}$$

The curvature [80]:

$$\frac{1}{R} = \frac{(\frac{dx}{d\zeta}\frac{d^2y}{d\zeta^2} - \frac{dy}{d\zeta}\frac{d^2x}{d\zeta^2})}{(\det J)^3} \tag{2-8}$$

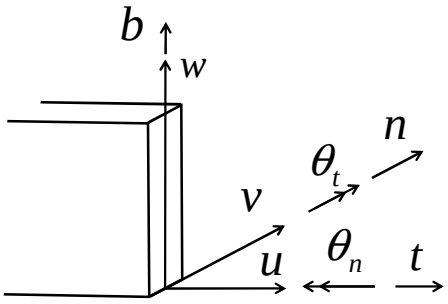

Fig. 2-4 Directions of the generalized displacements of the stiffener

The strain vector can be written as [80]

$$\varepsilon_s = \begin{Bmatrix} \varepsilon_t \\ \gamma_b \\ \gamma_n \\ \kappa_t \\ \kappa_n \end{Bmatrix} = \begin{bmatrix} \frac{1}{\det J}\frac{d}{d\zeta} & \frac{1}{R} & 0 & 0 & 0 \\ -\frac{1}{R} & \frac{1}{\det J}\frac{d}{d\zeta} & 0 & 0 & 0 \\ 0 & 0 & 1 & 0 & \frac{1}{\det J}\frac{d}{d\zeta} \\ 0 & 0 & \frac{1}{\det J}\frac{d}{d\zeta} & \frac{1}{R} & 0 \\ 0 & 0 & -\frac{1}{R} & \frac{1}{\det J}\frac{d}{d\zeta} & 0 \end{bmatrix} \begin{Bmatrix} u_t \\ v_n \\ \theta_t \\ \theta_n \\ w_b \end{Bmatrix} = L_s u_s' \qquad (2\text{-}9)$$

where u_t, v_n and w_b are the reference plane (which in this research is placed in the mid-plane of the plate) displacements along the t, n and b directions, respectively and θ_t and θ_n are the rotations with respect to the n and t-axis (Fig. 2-4). The displacement fields in terms of the global coordinate system are (Fig. 2-2)

$$u_s' = \begin{Bmatrix} u_t \\ v_n \\ \theta_t \\ \theta_n \\ w_s \end{Bmatrix} = \begin{bmatrix} \cos\alpha & \sin\alpha & 0 & 0 & 0 \\ -\sin\alpha & \cos\alpha & 0 & 0 & 0 \\ 0 & 0 & \cos\alpha & \sin\alpha & 0 \\ 0 & 0 & -\sin\alpha & \cos\alpha & 0 \\ 0 & 0 & 0 & 0 & 1 \end{bmatrix} \begin{Bmatrix} u_{s_0} \\ v_{s_0} \\ \varphi_{sx} \\ \varphi_{sy} \\ w_{s_0} \end{Bmatrix} = \Lambda u_s \qquad (2\text{-}10)$$

where u_{s_0}, v_{s_0} and w_{s_0} are the reference plane displacements along the x, y and z directions, respectively and φ_{sx} and φ_{sy} are the rotations with respect to the y and x axis. By using Eq. (2-9), the strain in global coordinate system can be written as:

$$\varepsilon_s = L_s \Lambda u_s \qquad (2\text{-}11)$$

The matrix L_s is defined by Eq. (2-9). The strain energy can be defined as:

$$U_s = \frac{1}{2}\int_{-1}^{1} \varepsilon_s^T D_s \varepsilon_s \det J d\zeta \qquad (2\text{-}12)$$

where the generalized stiffener stress strain matrix for an isotropic material is:

$$D_s = \begin{bmatrix} E_s A_s & 0 & 0 & E_s A_s \bar{S} & 0 \\ 0 & G_s A_n & 0 & 0 & G_s A_s \bar{S} \\ 0 & 0 & G_s A_b & 0 & 0 \\ E_s A_s \bar{S} & 0 & 0 & E_s I_n & 0 \\ 0 & G_s A_s \bar{S} & 0 & 0 & G_s J_t \end{bmatrix} \qquad (2\text{-}13)$$

In the above equation, E_s is Young's modulus, G_s is shear's modulus, $A_s = b_s h_s$, where b_s and h_s are the width and height of stiffener, is the stiffeners cross-sectional area, $\bar{S}$ is the centroidal distance of the

stiffener to plate midsurface, $A_n = k_n A_s$ and $A_b = k_b A_s$, where k_n and k_b are the shear correction factors and A_n and A_b are the shear areas, I_n is the second moment of the stiffener cross section area about *n*-axis, and J_t is torsional constant of stiffener which an approximate $J_t \approx \frac{1}{3} h_s b_s^3$ is used. For concentric stiffener and eccentric stiffener we have $\bar{S} = 0$, $I_n = \frac{1}{12} b_s h_s^3$ and $\bar{S} = \frac{h_p}{2} + \frac{h_s}{2}$, $I_n = \frac{1}{12} b_s h_s^3 + A_s \bar{S}^2$, respectively. The kinetic energy can be written as:

$$T_s = \frac{1}{2} \int_{-1}^{1} (\Lambda \dot{u}_s)^T m_s (\Lambda \dot{u}_s) \det J d\zeta \tag{2-14}$$

where

$$m_s = \rho_s \begin{bmatrix} A_s & 0 & A_s \bar{S} & 0 & 0 \\ 0 & A_s & 0 & A_s \bar{S} & 0 \\ A_s \bar{S} & 0 & I_n & 0 & 0 \\ 0 & A_s \bar{S} & 0 & I_n + I_t & 0 \\ 0 & 0 & 0 & 0 & A_s \end{bmatrix} \tag{2-15}$$

where ρ_s is the density of stiffener material and I_t is the second moment of the stiffener cross section area about *t*-axis.

- ***Description of the MLS Approximation***

In the following section, we provide a brief description of the MLS approximation and also introduce the notation and some definitions. Consider a subdomain Ω_x, the neighborhood of a point X and denoted as the domain of definition of the MLS approximation for the trial function at X, which is located in the problem domain Ω. To approximate the distribution of function u in Ω_x, over a number of local nodes, the Moving Least Squares approximant $u^h(X)$ of u; $\forall x \in \Omega_x$, can be defined by:

$$u^h(X) = p^T(X) a(X) \qquad \forall x \in \Omega_x \tag{2-16}$$

where $p^T(X) = [p^1(X) ..... p^m(X)]$ is a complete monomial basis of order m; and $a(X)$ is a vector containing coefficients $a_j(X)$ which are functions of the space coordinates $X = [x, y]$. In this research the quadratic basis $p^T = [1, x, x^2]$ in *1 D, m=3,* and $p^T = [1, x, y, x^2, xy, y^2]$ in *2 D, m=6* is used.

The unknown coefficients $a_j(X)$ are obtained by the minimization of a weighted discrete L_2 norm:

$$J(X)=\sum_{i=1}^{n} w(X_i)(p^T(X_i)a(X)-\hat{u}_i)^2 \tag{2-17}$$

where $w(X_i)$ is the weight function that is associated with Node i, $w(X_i)=0$ outside Ω_x, n is the number of nodes in Ω_x and $\hat{u}_i$ are the nodal parameters. In this research the spline weight function is used:

$$w(X_i)=\begin{cases} 1-6\ (\frac{d_i}{r_i})^2+8\ (\frac{d_i}{r_i})^3-3\ (\frac{d_i}{r_i})^4 & 0\le d_i<r_i \\ 0 & d_i\ge r_i \end{cases} \qquad d_i=|X-X_i| \tag{2-18}$$

where r_i is the size of the support for the weight function, $w(X_i)$, and it determines the size of the support for node X_i. If the domain of influence is a circle, r_i is the radius of the circle, and if the domain of influence is rectangular the weight function can be written in the tensor product form $w(X_i)=w(x_i)w(y_i)$ [23], and r_i can be dx_i and dy_i, the lengths of the rectangular support in the *x* and *y* directions (see Fig. 2-5). The minimization of $J(x)$ in Eq. (2-17) with respect to $a(X)$ leads to the following system of linear equations for the determination of $a(X)$:

$$A(X)a(X)=B(X)\hat{u} \tag{2-19}$$

where

$$\begin{aligned} A(X)&=\sum_{i=1}^{n} w(X_i)p(X_i)p^T(X_i) \\ B(X)&=[w(X_1)p(X_1)\quad ....\quad w(X_n)p(X_n)] \end{aligned} \tag{2-20}$$

Substituting Eq. (2-19) in Eq. (2-16):

$$u^h=\sum_{i=1}^{n} N_i(X)\hat{u}_i \tag{2-21}$$

where the shape function $N_i(X)$ is defined as :

$$N_i(X)=\sum_{j=1}^{m} p_j(X)(A^{-1}(X)B(X))_{ji} \tag{2-22}$$

- ***Discrete Equations of the EFG Method***

In order to obtain the discrete equations of the EFG method, the equations are rewritten by using MLS basis function. As can be seen in Fig. 2-5, the supports of weights for plate's nodes and stiffener's nodes are rectangular (Ω_i) and one dimensional domain (ℓ_i), respectively. dx_i and dy_i are the lengths of the rectangular support in the *x* and *y* directions. By using the shape function that has been introduced in Eq. (2-22), u_p and u_s, the plate and stiffener displacements vector, respectively, can be prescribed as:

$$
\begin{aligned}
u_p &= N_p \delta_p \\
u_s &= N_s \delta_s \\
\delta_s &= [u_{s1} \quad v_{s1} \quad \varphi_{sx1} \quad \varphi_{sy1} \quad w_{s1} \quad \dots \quad u_{sN} \quad v_{sN} \quad \varphi_{sxN} \quad \varphi_{syN} \quad w_{sN}]^T \\
\delta_p &= [u_{p1} \quad v_{p1} \quad \varphi_{px1} \quad \varphi_{py1} \quad w_{p1} \quad \dots \quad u_{pn} \quad v_{pn} \quad \varphi_{pxn} \quad \varphi_{pyn} \quad w_{pn}]^T
\end{aligned}
\tag{2-23}
$$

where N_p and N_s are the shape functions (Eq. (2-22)) related to the plate and stiffener, respectively. Substituting Eq. (2-23) in Eqs. (2-2) and (2-11):

$$
\begin{aligned}
\varepsilon_p &= B_p \delta_p \\
\varepsilon_s &= B_s \Lambda \delta_s
\end{aligned}
\tag{2-24}
$$

where the B matrices used or defining the strains in terms of nodal displacements are:

$$
\left[B_p\right]_i = \begin{bmatrix}
\frac{\partial N_{pi}}{\partial x} & 0 & 0 & 0 & 0 \\
0 & \frac{\partial N_{pi}}{\partial y} & 0 & 0 & 0 \\
\frac{\partial N_{pi}}{\partial y} & \frac{\partial N_{pi}}{\partial x} & 0 & 0 & 0 \\
0 & 0 & N_{pi} & 0 & \frac{\partial N_{pi}}{\partial x} \\
0 & 0 & 0 & N_{pi} & \frac{\partial N_{pi}}{\partial y} \\
0 & 0 & \frac{\partial N_{pi}}{\partial x} & 0 & 0 \\
0 & 0 & 0 & \frac{\partial N_{pi}}{\partial y} & 0 \\
0 & 0 & \frac{\partial N_{pi}}{\partial y} & \frac{\partial N_{pi}}{\partial x} & 0
\end{bmatrix}
\tag{2-25}
$$

$$
[B_s]_i = \begin{bmatrix}
\frac{1}{\det J}\frac{dN_{si}}{d\zeta} & \frac{N_{si}}{R} & 0 & 0 & 0 \\
-\frac{N_{si}}{R} & \frac{1}{\det J}\frac{dN_{si}}{d\zeta} & 0 & 0 & 0 \\
0 & 0 & N_{si} & 0 & \frac{1}{\det J}\frac{dN_{si}}{d\zeta} \\
0 & 0 & \frac{1}{\det J}\frac{dN_{si}}{d\zeta} & \frac{N_{si}}{R} & 0 \\
0 & 0 & -\frac{N_{si}}{R} & \frac{1}{\det J}\frac{dN_{si}}{d\zeta} & 0
\end{bmatrix}
\tag{2-26}
$$

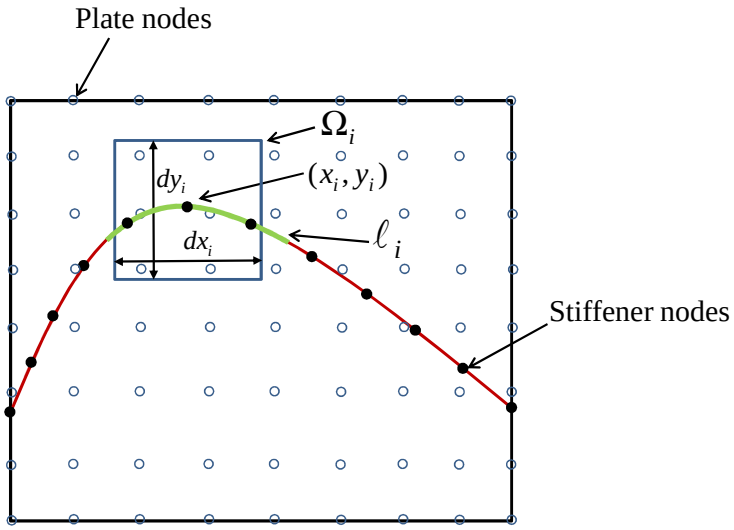

Fig. 2-5 Plate and stiffener nodes for a plate with a curvilinear stiffener

- ***Transformation Equations***

Two approaches for employing the displacement compatibility conditions at the contact surface between the plate and the stiffener have been reported in the literature. In the first approach [61], the reference axis of the stiffener is considered on the neutral axis of the stiffener and the stress-strain matrix (Eq. (2-13)) is calculated based on this assumption. By using this approach, $\bar{S}$, the distance between the neutral axis of the plate to the neutral axis of the stiffener, as can be seen in Fig. 2-6, can change the transformation matrix, which transforms the node parameters of the stiffener to the node parameters of the plate. In the second approach [19], which is used in the current research, the reference plane of the stiffener is placed in the mid-plane of the plate. Consider node i of stiffener, located at (x_i, y_i), see in Fig. 2-5. For this node, the displacement compatibility at the contact surface between the plate and the stiffener impose that:

$$\begin{aligned} u_p(x_i, y_i, z)\big|_{z=h_p/2} &= u_s(x_i, y_i, z)\big|_{z=h_p/2} \\ v_p(x_i, y_i, z)\big|_{z=h_p/2} &= v_s(x_i, y_i, z)\big|_{z=h_p/2} \\ w_{p_0}(x_i, y_i) &= w_{s_0}(x_i, y_i) \end{aligned} \tag{2-27}$$

By using Eq. (2-1), Eq. (2-27) can be written as

$$
\begin{aligned}
u_{p_0}(x_i, y_i) &= u_{s_0}(x_i, y_i) \\
v_{p_0}(x_i, y_i) &= v_{s_0}(x_i, y_i) \\
w_{p_0}(x_i, y_i) &= w_{s_0}(x_i, y_i) \\
\varphi_{px}(x_i, y_i) &= \varphi_{sx}(x_i, y_i) \\
\varphi_{py}(x_i, y_i) &= \varphi_{sy}(x_i, y_i)
\end{aligned}
\tag{2-28}
$$

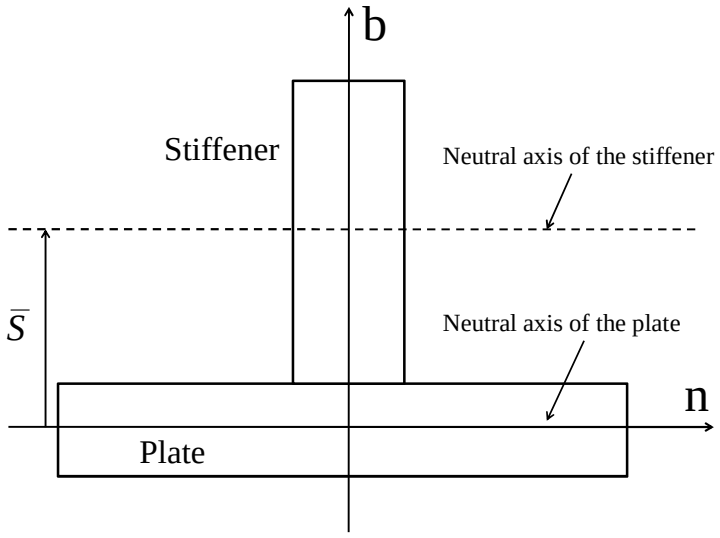

Fig. 2-6 The cross section of plate and stiffener

The square domain related to this node is Ω_i which includes plate's *n* nodes. The one dimensional domain related to this node is ℓ_i which contains stiffeners' *N* nodes. The domain and nodes are shown in Fig. 2-5. By using the discrete equations and the shape functions that have been introduced in Eq. (2-23), Eq. (2-28) is rewritten as

$$
\begin{aligned}
&\sum_{I=1}^{n} N_{pI}(x_i, y_i)\delta_{puI} = \sum_{J=1}^{N} N_{sJ}(x_i, y_i)\delta_{suJ} \qquad I = 1,....,n \\
&\sum_{I=1}^{n} N_{pI}(x_i, y_i)\delta_{pvI} = \sum_{J=1}^{N} N_{sJ}(x_i, y_i)\delta_{svJ} \qquad J = 1,....,N \\
&\sum_{I=1}^{n} N_{pI}(x_i, y_i)\delta_{pwI} = \sum_{J=1}^{N} N_{sJ}(x_i, y_i)\delta_{swJ} \\
&\sum_{I=1}^{n} N_{pI}(x_i, y_i)\delta_{p\varphi xI} = \sum_{J=1}^{N} N_{sJ}(x_i, y_i)\delta_{s\varphi xJ} \\
&\sum_{I=1}^{n} N_{pI}(x_i, y_i)\delta_{p\varphi yI} = \sum_{J=1}^{N} N_{sJ}(x_i, y_i)\delta_{s\varphi yJ}
\end{aligned}
\tag{2-29}
$$

Rewriting Eq. (2-29) in matrix form

$$
\begin{aligned}
T_{su}\delta_{su} &= T_{pu}\delta_{pu} \\
T_{sv}\delta_{sv} &= T_{pv}\delta_{pv} \\
T_{sw}\delta_{sw} &= T_{pw}\delta_{pw} \\
T_{s\varphi x}\delta_{s\varphi x} &= T_{p\varphi x}\delta_{p\varphi x} \\
T_{s\varphi y}\delta_{s\varphi y} &= T_{p\varphi y}\delta_{p\varphi y}
\end{aligned}
\tag{2-30}
$$

The transformation matrices can be written as:

$$
\begin{aligned}
T_{pu} &= \begin{bmatrix} N_{p1}(x_1,y_1) & N_{p2}(x_1,y_1) & \dots & N_{pn}(x_1,y_1) \\ \vdots & \vdots & \ddots & \vdots \\ N_{p1}(x_N,y_N) & N_{p2}(x_N,y_N) & \dots & N_{pn}(x_N,y_N) \end{bmatrix} \\
T_{su} &= \begin{bmatrix} N_{s1}(x_1,y_1) & N_{s2}(x_1,y_1) & \dots & N_{sN}(x_1,y_1) \\ \vdots & \vdots & \ddots & \vdots \\ N_{s1}(x_N,y_N) & N_{s2}(x_N,y_N) & \dots & N_{sN}(x_N,y_N) \end{bmatrix}
\end{aligned}
\tag{2-31}
$$

From Eq. (2-30), we get:

$$
\begin{aligned}
\delta_{su} &= T_{su}^{-1}T_{pu}\delta_{pu} \\
\delta_{sv} &= T_{sv}^{-1}T_{pv}\delta_{pv} \\
\delta_{sw} &= T_{sw}^{-1}T_{pw}\delta_{pw} \\
\delta_{s\varphi x} &= T_{s\varphi x}^{-1}T_{p\varphi x}\delta_{p\varphi x} \\
\delta_{s\varphi y} &= T_{s\varphi y}^{-1}T_{p\varphi y}\delta_{p\varphi y}
\end{aligned}
\tag{2-32}
$$

All the nodal displacements (δ_{su}, δ_{pu}, …) vectors for the stiffener and for the plate can be written in one vector, respectively. The transformation matrix relating the stiffener nodal displacements and the plate nodal displacements can be defined as:

$$
\delta_s = T_{sp}\delta_p \tag{2-33}
$$

in which T_{sp} is the $5N \times 5n$ matrix which transforms the node parameters of the stiffener to the node parameters of the plate.

- ***Enforcement of Essential Boundary Conditions***

As in the standard FEM, the EFG method uses the weak form of the problem to describe the equations of motion. The essential boundary conditions are accounted for by means of a penalty method. By using the principle of minimum potential energy, the Lagrangian can be defined:

$$
L = T_p + T_s - U_p - U_s + \int_{\Gamma_t} u^T f \, d\Gamma - \frac{\alpha_p}{2}\int_{\Gamma_u} (u-\bar{u})^T (u-\bar{u})\, d\Gamma \tag{2-34}
$$

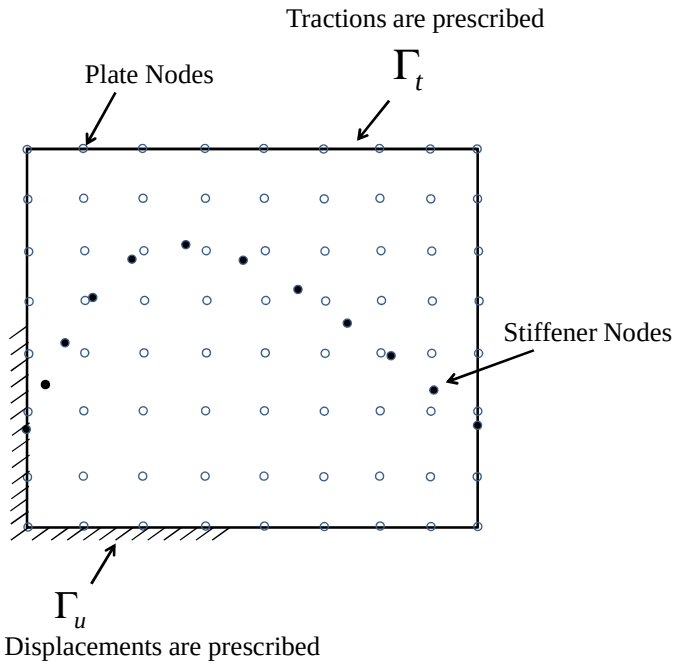

Fig. 2-7 The prescribed boundaries of the plate with a curvilinear stiffener

The boundary conditions are shown in Fig. 2-7; and $\bar{u}$ and f are prescribed displacement and traction on the boundaries.

An important consideration for using the penalty method is the choice of an appropriate penalty parameter α_p. We should note that the penalty terms will not only affect the diagonal entries of the system stiffness matrix but also the off diagonal entries of the system matrix. The system stiffness matrix may become ill conditioned when the off diagonal entries are multiplied by a very large number. Hence the main issue in using the penalty method is proper choosing of penalty parameter. From the literature review [81], the penalty parameter (α_p) can be chosen as $(10^3 - 10^7) \times E$, where E is the Young's modulus of the material under consideration.

- ***Derivation of the Stiffness and Mass Matrices and the Force Vector***

In the formulation of linear Element Free Galerkin method, it is assumed that deformations remain small so that linear relations can be used to represent the strain as a function of the displacements in a body. The emphasis of the present work is on developing a formulation for the vibration analysis of the stiffened plates. Strain and kinetic energy expressions were derived. Then, by using transformation equation (Eq. (2-33)), transform the node parameters of the stiffener to the node parameters of the plate, by considering their positions within the plate. Consequently, the displacements are expressed only in terms of the plate nodes degrees of freedom. In implementing the EFG method, first the basis function was defined. As it was

mentioned, in this research, Moving Least Squares (MLS) basis function is used. The size of support for weight function should be large enough to provide a sufficient number of nodes in the domain of definition of the MLS to warrant a reasonable accuracy. As has been reported by Zhu and Atluri [81], while using the MLS basis, the shape functions and their derivatives become strongly nonpolynomial. Consequently, the Gauss quadrature method in such a case may give a relatively large error. After finding the basis function and defining the shape function by considering the nodes, the background cell, as can be seen in Fig. 2-8, should be defined for integration. It should be noted that the background cells are independent of the structure's nodes and domain of influence. From the above discussion, it is clear that the EFG method does not need elements, but it does need a cell structure to evaluate integrals.

By substituting Eqs. (2-23) and (2-24) in Eq. (2-4)

$$\begin{aligned} U_p &= \frac{1}{2}\delta_p^T \int_A {B_p}^T D_p B_p dA \delta_p \\ T_p &= \frac{1}{2}\dot{\delta}_p^T \int_A N_p^T m_p N_p dA \dot{\delta}_p \end{aligned} \tag{2-35}$$

also first transform the displacements of the stiffener to the displacements of the plate by substituting Eq. (2-33) in Eqs. (2-23) and (2-24) then substituting the results in the Eqs. (2-12) and (2-14)

$$\begin{aligned} U_s &= \frac{1}{2}\delta_p^T T_{sp}^T \int_{-1}^{1} \Lambda^T {B_s}^T D_s B_s \Lambda \det J d\zeta \, T_{sp} \delta_p \\ T_s &= \frac{1}{2}\dot{\delta}_p^T T_{sp}^T \int_{-1}^{1} \Lambda^T N_s^T m_s N_s \Lambda \det J d\zeta \, T_{sp} \dot{\delta}_p \end{aligned} \tag{2-36}$$

According to the Hamilton's principle:

$$\delta \int_{t_1}^{t_2} L dt = 0 \tag{2-37}$$

where L is the Lagrangian function of stiffened plate and t_1 and t_2 are the arbitrary time limits. By substituting Eqs. (2-35) and (2-36) in (2-34) and then substitute it in Eq. (2-37), the mathematical model for the stiffened plate is found to be

$$\begin{aligned} &\delta \int_{t_1}^{t_2} [\frac{1}{2}\dot{\delta}_p^T (\int_A N_p^T m_p N_p dA + T_{sp}^T \int_{-1}^{1} \Lambda^T N_s^T m_s N_s \Lambda d\zeta \, T_{sp}) \dot{\delta}_p - \delta_p^T (\frac{1}{2}(\int_A B_p^T D_p B_p dA + \\ &T_{sp}^T \int_{-1}^{1} \Lambda^T B_s^T D_s B_s \Lambda \det J d\zeta \, T_{sp} + \alpha_p \int_{\Gamma_u} N_p^T N_p d\Gamma) \delta_p - \alpha_p \int_{\Gamma_u} N_p^T \bar{u} d - \int_{\Gamma_t} N_p^T f d\Gamma)] dt = 0 \end{aligned} \tag{2-38}$$

Taking the variation of the above equation will result in equations of motion

$$\left(M_p + M_s\right)\ddot{\delta}_p + \left(K_p + K_s\right)\delta_p = F \tag{2-39}$$

where M_p, M_s, K_p, K_s and F are:

$$
\begin{aligned}
K_p &= \int_A B_p^T D_p B_p dA + \alpha_p \int_{\Gamma_u} N_p^T N_p d\Gamma \\
K_s &= T_{sp}^T \int_{-1}^{1} \Lambda^T B_s^T D_s B_s \Lambda \det J d\zeta T_{sp} \\
M_p &= \int_A N_p^T m_p N_p dA \\
M_s &= T_{sp}^T \int_{-1}^{1} \Lambda^T N_s^T m_s N_s \Lambda \det J d\zeta T_{sp} \\
F &= \int_{\Gamma_t} N_p^T f d\Gamma + \alpha_p \int_{\Gamma_u} N_p^T \bar{u} d\Gamma
\end{aligned}
\tag{2-40}
$$

The damping matrix is assumed to be given as:

$$C = a_R(M_p + M_s) + b_R(K_p + K_s) \tag{2-41}$$

where a_R and b_R are Rayleigh's coefficients.

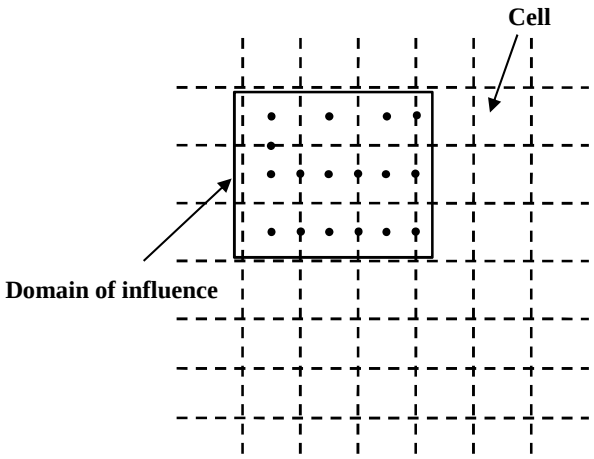

Fig. 2-8 Domain of influence and background cell structures

2.3 Results and Discussion

To check the accuracy of the present meshless formulation and behavior of the stiffened plate under various circumstances, a number of numerical examples are given. The size of rectangular support domain is discussed in details by Peng *et al*. [24], [25] for buckling and free vibration analysis of plate with straight stiffeners in *x* and *y* directions. It is suggested in these references that satisfactory convergence and computational cost can be achieved by using the scaling factor ($d_{max}=dx_i/dp$ and $d_{max}=dy_i/dp$, d_p : the distance between neighboring nodes) in the range of 3-4. In this research, the rectangular support domain is considered and the scaling factor is 4 in both *x* and *y* directions. In order to evaluate integrations involved in stiffness and mass matrices over each cell, our experience suggests that 16 integration points in each cell can be sufficient to obtain accurate results with relatively less computational cost.

- ***A Simply-Supported Plate with a Single Stiffener***

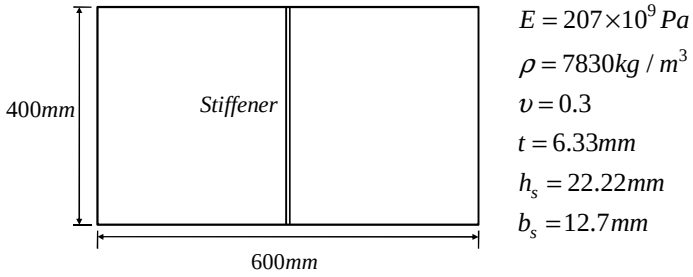

Fig. 2-9 A stiffened plate with single stiffener

Free vibration of a rectangular plate simply-supported on all four edges and with one central stiffener, as shown in Fig. 2-9, has been considered. Plate and stiffener properties are also given in this figure. Chen *et al.* [13] solved this problem by using Ritz-Galerkin method with B-spline as trial functions. In their paper, the results are compared with results given by other different researchers. However, in their study, the formulation is restricted to stiffeners that are placed in *x* or *y* direction. Bhimaraddi *et al.* [8] studied the same problem by using the finite element model. They used shell element and beam element for modeling the plate and stiffener, respectively. In their research, the effect of shear deformation and rotary inertia was taken in to account.

Zeng and Bert [18] have also studied this problem. They used Differential Quadrature (DQ) method for solving the problem. In addition to the meshfree method, the problem is also modeled in ANSYS® by using 600 SHELL63 elements for modeling the plate and 20 BEAM 188 elements for modeling the stiffener. In the meshless code, 24×16 uniform locations are considered for modeling the plate and 16 locations of nodes are considered for modeling the stiffener. Table 2-1 shows the first ten natural frequencies. It can be seen that there is a good agreement between the results of the present meshfree analysis and those available in the literature and those obtained by using ANSYS®. The mode shapes of the stiffened plate which are calculated by using the present code and ANSYS® are shown in Fig. 2-10. The results are in good agreement.

The accuracy of the present meshfree formulation can be evaluated by considering the convergence. In this method, it is mentioned that there is no need of matching the nodes of a stiffener and the nodes of the plate. The relative difference in the results given by this code with respect to a meshfree scheme with 30×20 nodes for the plate and 20 nodes for the stiffeners is calculated. Also, a convergence study for the ANSYS® results has been carried out. The relative difference of the ANSYS® is with respect to 30×20 nodes and *h* is the distance between two nodes in meshfree and ANSYS®, respectively. As can be seen in Fig. 2-11, convergence occurred for all four natural frequencies; however, contrary to the intuition, the relative difference of the fourth natural frequency is less than the third natural frequency. By comparing two figures, it can be observed that for the higher frequencies, meshfree results converge faster than the FEM.

Table 2-1 Ten Natural frequencies (Hz) for simply-supported plate with single stiffener

Mode	Ritz(B-splines) [13]	FEM [8]	DQ [18]	ANSYS®	Meshfree
1	245	247	252	251	247
2	277	274	275	273	273
3	511	513	523	512	506
4	-	-	-	559	557
5	-	-	-	575	565
6	-	-	-	778	777
7	-	-	-	1028	1014
8	-	-	-	1039	1018
9	-	-	-	1060	1036
10	-	-	-	1094	1081

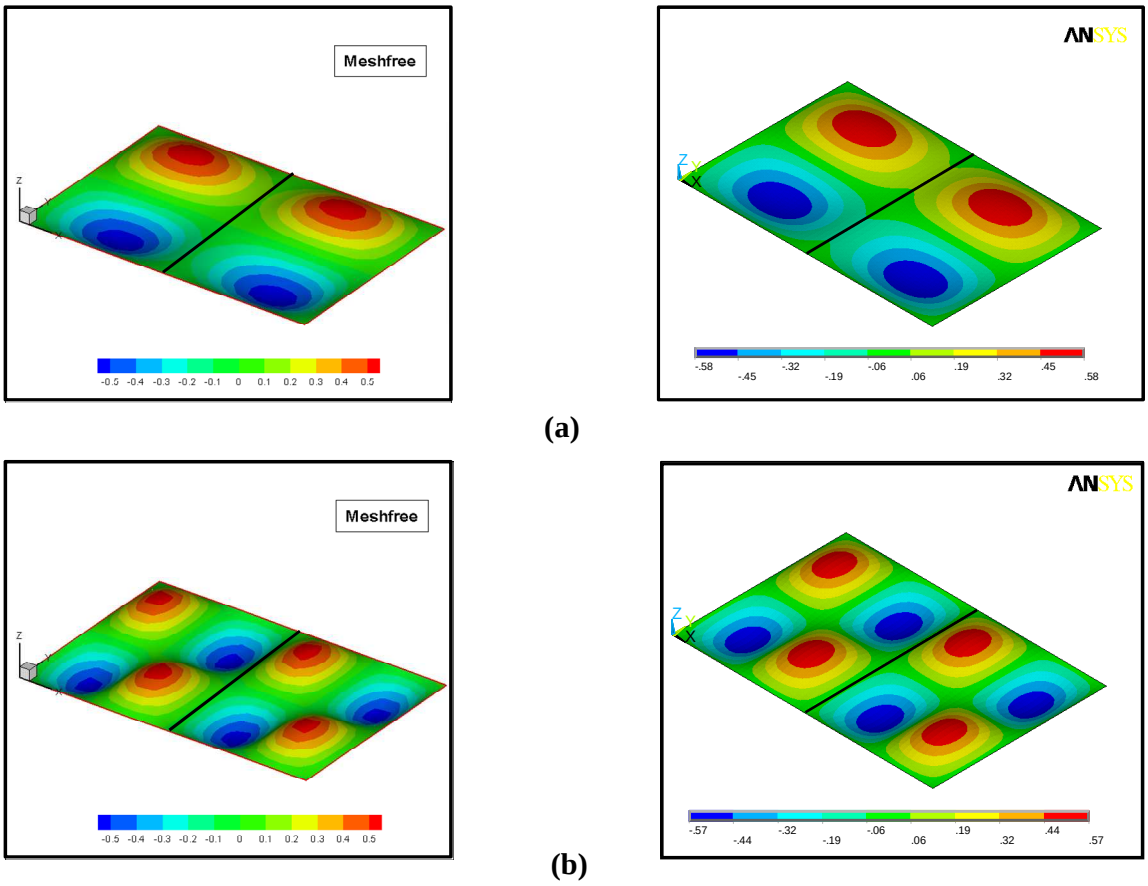

Fig. 2-10 The mode shapes obtained for a stiffened plate using a meshfree method (left) and ANSYS®, a commercial available software (right) (a) The Fifth mode shape (b) The Tenth mode shape

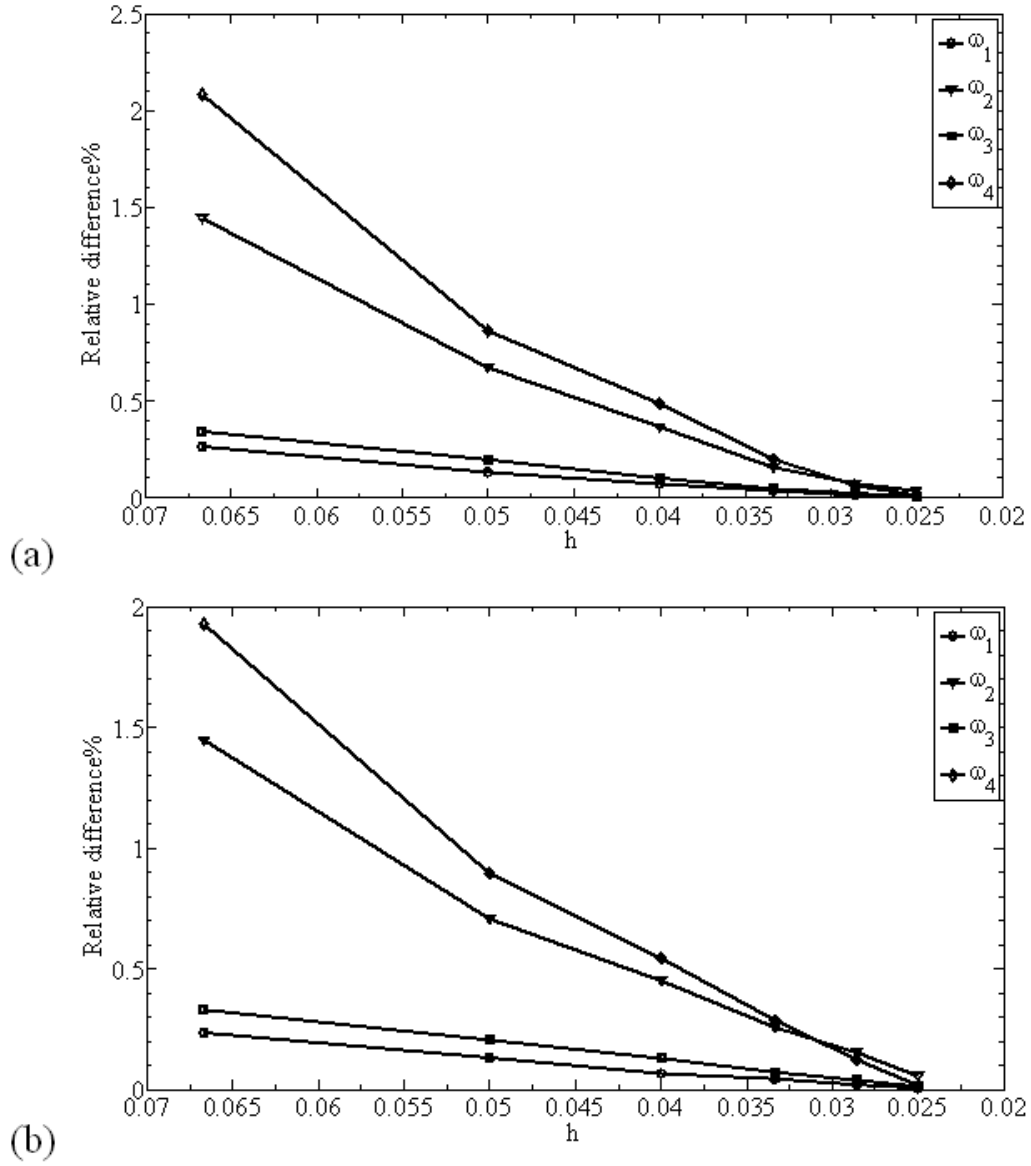

Fig. 2-11 Relative difference in natural frequencies for the four modes (a) Meshfree (b) ANSYS®

- ***Plate Having Two Stiffeners and Clamped On All Sides***

The double stiffeners plate with all edges clamped, analyzed by Olson and Hazell [7] theoretically and experimentally, by Chen *et al.* [13] using the Ritz method, by Holopainen [9] using the finite element model, by Bhimaraddi *et al.* [8] implement finite element method by using shell and beam element and by Zeng and Bert [18] using DQ, is selected as the second example.

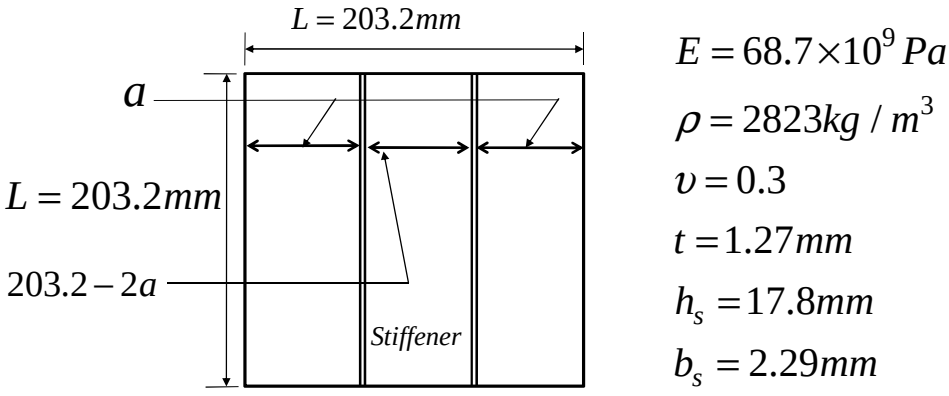

Fig. 2-12 A square plate with double stiffeners

The geometry and material properties of the plate and stiffeners ($a = 67.73mm$) are shown in Fig. 2-12. The first ten natural frequencies are demonstrated in Table 2-2. It can be seen that the results of the present analysis and those that can be found in the literature and also those obtained by ANSYS® are close. When using ANSYS®, 1225 SHELL63 elements were used for modeling the plate and 70 BEAM188 elements were used for modeling each stiffener. For meshfree domain, 18×18 nodes were considered for the plate and 18 nodes were considered for each stiffener. The fifth and tenth mode shapes of the stiffened plate which is obtained by ANSYS® and the developed meshless code are shown in Fig. 2-13.

In Fig. 2-14, the effect of location of the stiffeners is studied. It can be seen that as the distance between the two stiffeners decreases, the ratio of natural frequency (the natural frequency of stiffened plate to the corresponding natural frequency of unstiffened plate) first increases and then decreases. As a simple check, one can see that as the distance of the stiffener from the nearby edge becomes zero, the fundamental frequency of the stiffened plate approaches that of the clamped unstiffened plate.

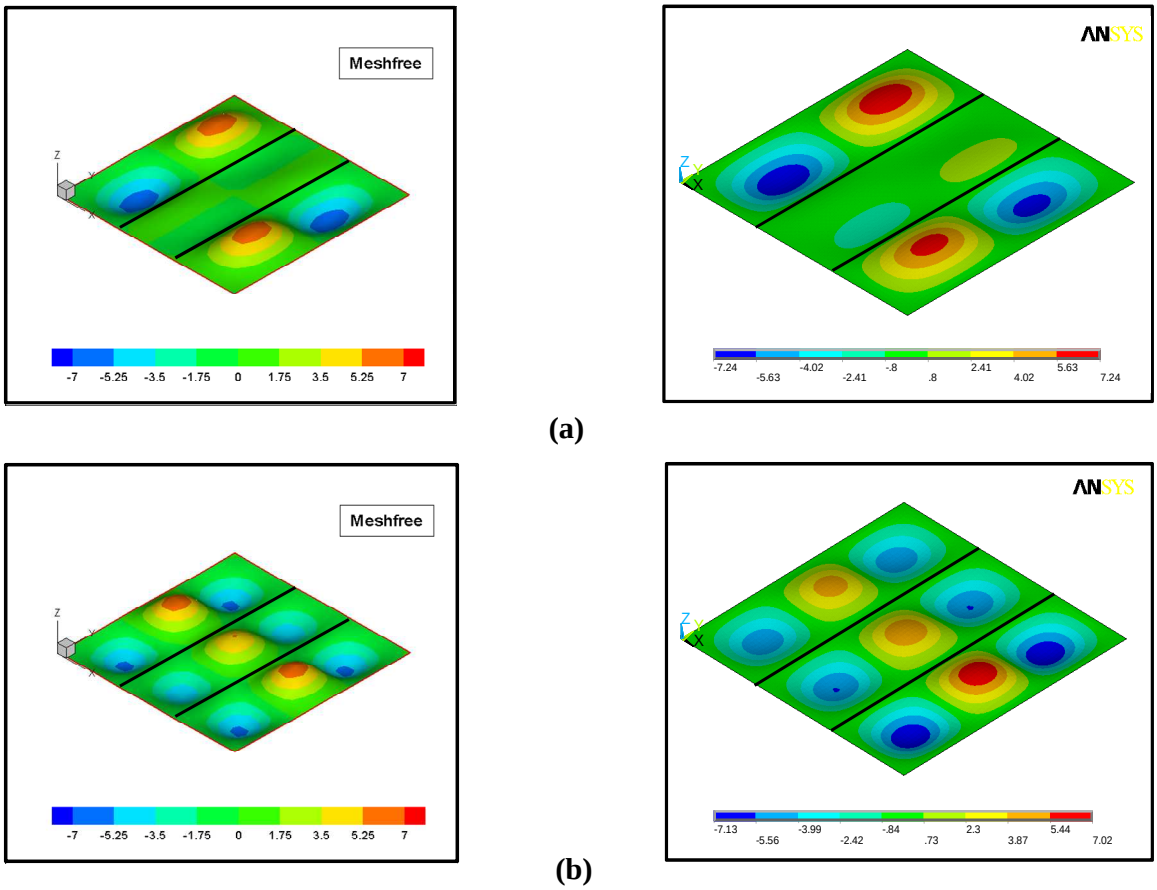

Fig. 2-13 The mode shapes obtained for a plate with two stiffeners, using a meshfree method (left) and ANSYS®, a commercial available software (right). (a) The fifth mode shape (b) The tenth mode shape

Table 2-2 Ten Natural frequencies (Hz) for clamped plate with double stiffeners

Mode	Experimental [7]	Theoretical [7]	Ritz(B-splines) [13]	FEM [9]	FEM [8]	DQ [18]	ANSYS®	Meshfree
1	909	965	978	943	911	915	909	909
2	1204	1282	1283	1237	1198	1242	1209	1201
3	1319	1364	1371	1331	1293	1344	1296	1301
4	1506	1418	1435	1361	1400	1414	1360	1380
5	1560	1602	1592	1561	1512	-	1530	1543
6	1693	1757	1719	1706	1648	-	1680	1693
7	1807	1854	1861	1808	1763	-	1776	1795
8	1962	2015	1997	1962	1908	-	1931	1984
9	2052	2109	2055	2057	1989	-	2023	2016
10	2097	2253	2459	2163	-	-	2090	2072

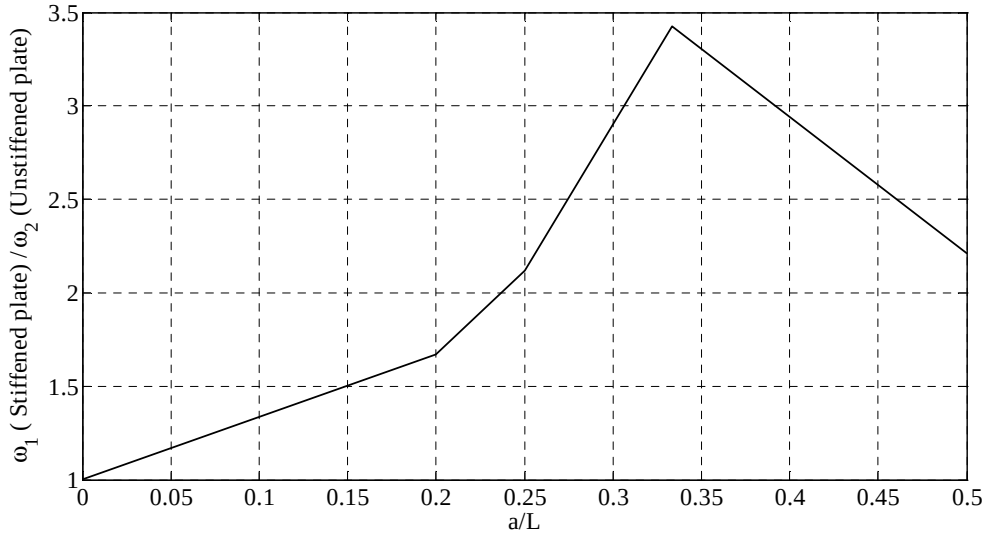

Fig. 2-14 The effect of stiffeners position on the natural frequency of stiffened plate

- ***A Simply-Supported Plate with Arbitrarily Inclined Stiffeners***

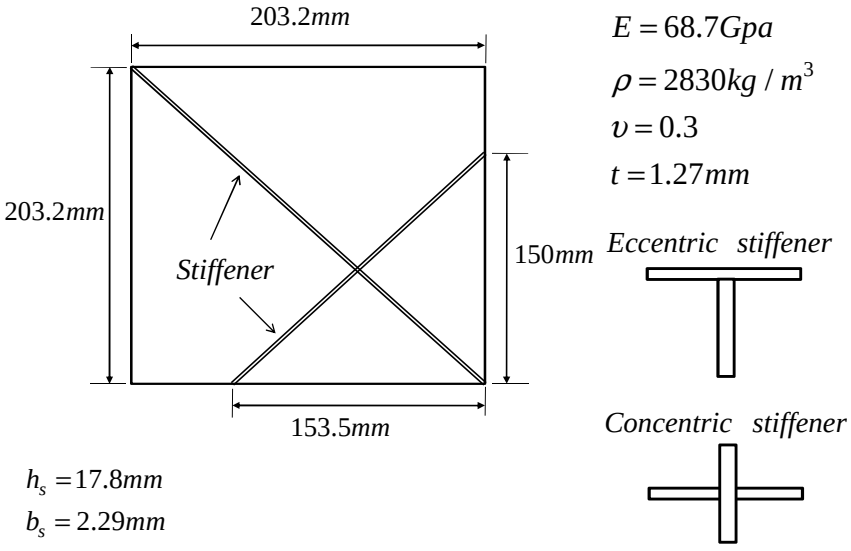

Fig. 2-15 A square plate with two arbitrary orientated stiffeners

In order to validate the applicability of the proposed EFG formulation for the analysis of plates with arbitrary orientated stiffeners, a new example is suggested. This example studies the free vibration of a simply-supported plate with stiffeners placed at arbitrary orientations. Both the concentric and eccentric

stiffener configurations are studied. The dimensions and material properties of the panel are presented in Fig. 2-15. For comparison purposes, the complete stiffened plate was modeled in ANSYS® with an irregular mesh composed of 1600 SHELL63 elements for modeling the plate and 80 BEAM188 elements for modeling the stiffeners. The meshless scheme is chosen to be 18×18 nodes for the plate and 40 nodes for the stiffeners. It is important to note that, in ANSYS®, the mesh is determined by the position and orientation of the stiffener within the plate which limits the flexibility of the plate mesh. In Table 2-3, the natural frequencies for the eccentric and concentric inclined stiffeners are given. Also the mode shapes can be observed in Fig. 2-16. As can be seen in Table 2-3, a close agreement of results using the present formulation and ANSYS® has been achieved for all the natural frequencies. Also by comparison of the results of eccentric and concentric inclined stiffeners, it can be concluded that considering the eccentricity affects some modes considerably, but it does not influence some other modes very much. The reason is that in some of the modes the stiffener deforms only slightly. Hence, the inclusion of eccentricity does not influence these modes appreciably. This fact can be used to place the stiffeners in a way to impact modes with specific frequencies (e.g. for desired dynamic response under known excitation frequencies).

Table 2-3 Ten Natural frequencies (Hz) for simply-supported plate with inclined stiffeners

	Eccentric stiffeners		Concentric stiffeners	
Mode	ANSYS®	Meshfree	ANSYS®	Meshfree
1	565	561	401	409
2	577	578	562	561
3	946	951	767	770
4	1035	1037	1019	1025
5	1169	1170	1058	1057
6	1397	1371	1393	1396
7	1506	1492	1406	1400
8	1562	1530	1491	1489
9	1639	1634	1573	1564
10	1658	1656	1708	1706

- ***A Simply-Supported Plate with a Curvilinear Stiffener***

The free vibration analysis of a simply-supported plate with a curvilinear stiffener is considered. Two stiffener configurations are considered. The geometry and the material properties are shown in Fig. 2-17. The natural frequencies of plate with stiffener 1 are shown in Table 2-4. In order to check the accuracy of the present formulation, analysis has been carried out using the present formulation and also using the ANSYS® software. In the meshfree method, 18×18 nodes are used for the plate and 24 nodes are used for the stiffener. In the ANSYS® modeling, 2120 SHELL63 elements were used for the plate and 50 BEAM188 elements were used for the curvilinear stiffener. In Table 2-4, a good agreement of results is observed between the ANSYS® and the present EFG solution. The fifth and tenth mode shapes of the

stiffened plate which are given by meshfree and ANSYS® are shown in Fig. 2-18. It was found that the ANSYS® results were all in excellent agreement with the present predictions. It is also of interest to compare the CPU time of ANSYS® and meshfree method. As can be seen in Table 2-4, ANSYS® is 20% more efficient in terms of CPU time than the meshfree code. However it can be observed in Table 2-5, which shows the natural frequencies of plate with stiffener 2, that as the stiffener shape changes while plate geometry properties are kept unchanged, the meshfree code is 40% more efficient in terms of CPU time than ANSYS®.

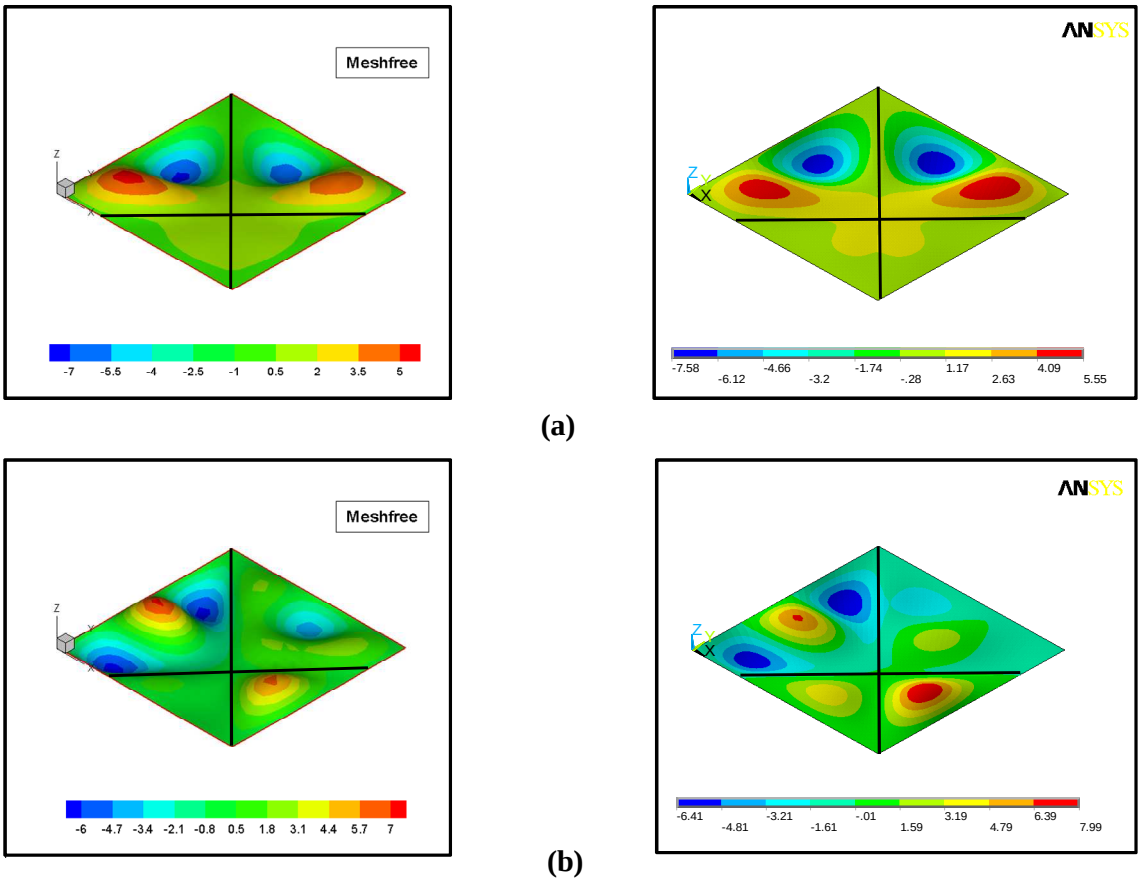

Fig. 2-16 The mode shapes obtained for a plate with inclined stiffeners using a meshfree method (left) and ANSYS®, a commercial available software (right) (a) The fifth mode shape (b) The tenth mode shape

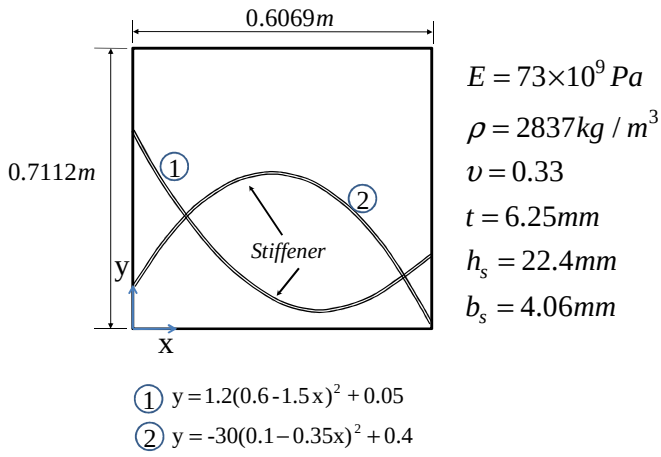

Fig. 2-17 A curvilinearly-stiffened plate

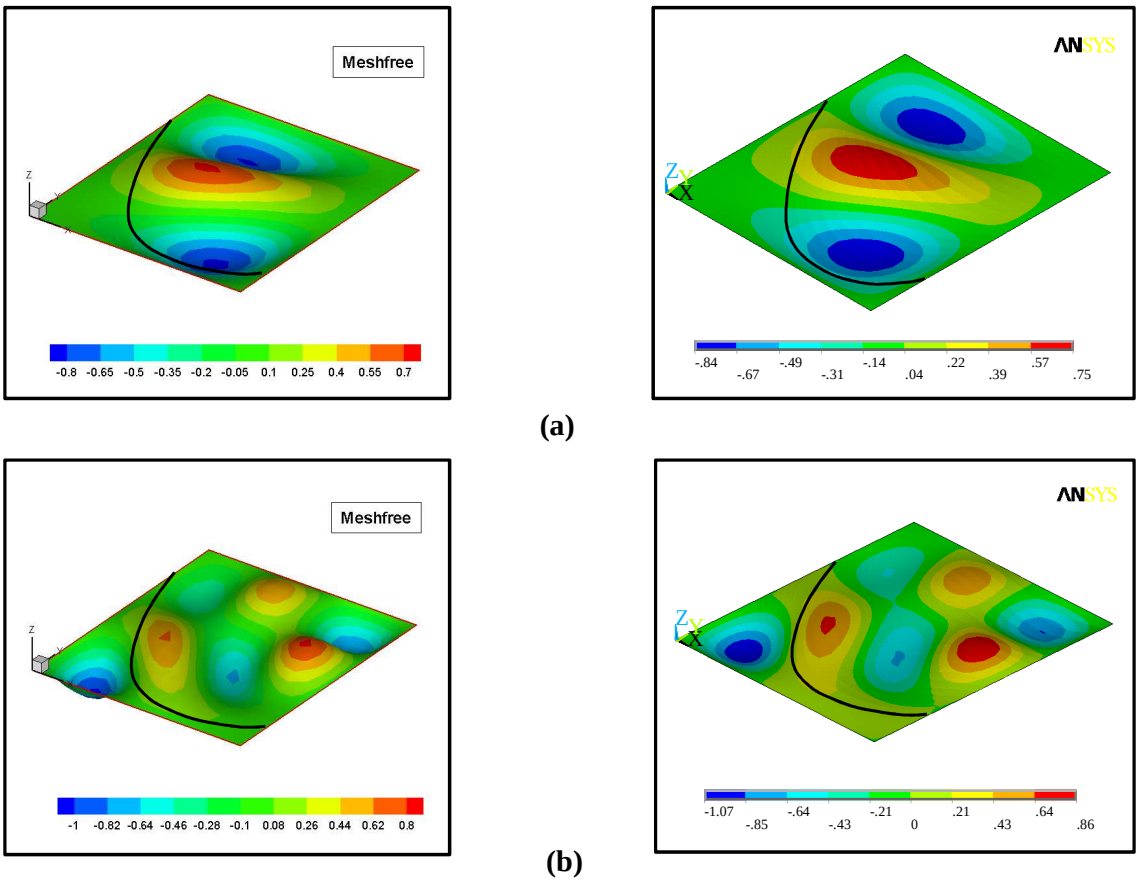

Fig. 2-18 The mode shapes obtained for a plate with a curvilinear stiffener using a meshfree method (left) and ANSYS®, a commercial available software (right) (a) The fifth mode shape (b) The tenth mode shape

Table 2-4 Ten Natural frequencies (Hz) for simply-supported plate with a curvilinear stiffener (Stiffener 1)

Mode	ANSYS®	Meshfree
1	84	83
2	183	175
3	213	217
4	316	319
5	347	327
6	417	421
7	485	489
8	536	521
9	567	561
10	662	661
CPU Time*	1.0	1.2
*Time is normalized.		

Table 2-5 Ten Natural frequencies (Hz) for simply-supported plate with a curvilinear stiffener (Stiffener 2)

Mode	ANSYS®	Meshfree
1	83	85
2	190	184
3	229	241
4	316	314
5	331	327
6	454	457
7	485	500
8	538	526
9	558	561
10	688	680
CPU Time*	1.4	1.0
*Time is normalized.		

- ***Frequency Response of a Plate with Curvilinear Stiffeners***

In this section, the harmonic response of a plate with curvilinear stiffeners is considered. The geometry of the stiffeners is defined in Fig. 2-17. Harmonic excitation $P = |P|e^{iwt}$ ($|P| = 10kN/m^2$) is imposed on the plate along the transverse direction to study the harmonic response. The frequency of excitation covers the first nine mode shapes. The aim is to seek the effect of curvilinear stiffeners on the harmonic response. The damping ratio for this particular example is 2% and the mass of the plate is 7.69kg. The mass of curvilinear stiffener can be defined by:

$$m_s = \int_{\ell} \rho_s A_s d\ell \tag{2-42}$$

The total mass of the plate with one stiffener and two stiffeners is 7.91kg and 8.16kg, respectively. As can be seen, the stiffener does not change the mass of the structure considerably. However, as can be seen in Fig. 2-19, adding stiffeners can increase the natural frequencies of structure and also it can decrease the average deflection of the stiffened plate. It can be concluded that the stiffener contributes to the stiffness matrix significantly. By using the contribution of the stiffener to the stiffness matrix, a desired level of the natural frequency and the peak of average deflection ($w_{ave} = \sqrt{\frac{1}{n}\sum_{i=1}^{n} w_i^2}$, *n*: number of nodes) corresponding to a given excitation frequency can be achieved by adjusting the curvature and the location of one or more stiffeners.

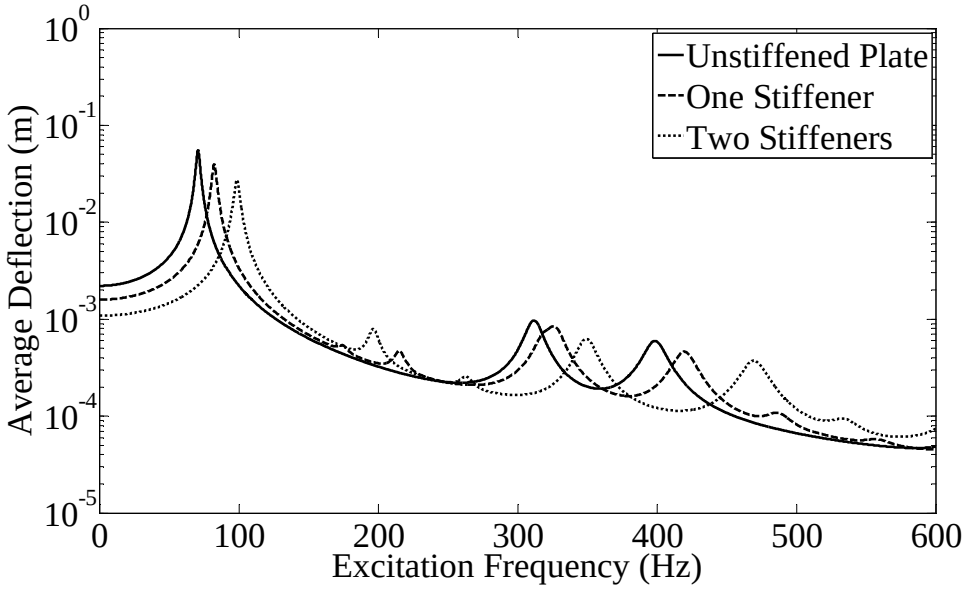

Fig. 2-19 Effects of the stiffener on the harmonic responses

2.4 Functionally Graded Stiffened Plate

For an FGM plate of uniform thickness, Fig. 2-20, the properties of the plate are assumed to vary only through the thickness. The variation of the elastic modulus, density and Poisson ratio of the plate is assumed to be in terms of power law distributed given as [37]:

$$E_p = (E_c - E_m)(\frac{2z + h_p}{2h})^n + E_m$$
$$\rho_p = (\rho_c - \rho_m)(\frac{2z + h_p}{2h})^n + \rho_m \quad (2\text{-}43)$$
$$\upsilon_p = (\upsilon_c - \upsilon_m)(\frac{2z + h_p}{2h})^n + \upsilon_m$$

where E_p, ρ_p and υ_p are the elastic modulus, density, and poison ratio of the plate, E_c, ρ_c and υ_c are the elastic modulus, density, and poison ratio of the ceramic, E_m, ρ_m and υ_m are the elastic modulus, density, and poison ratio of the metal, and *n* is the volume fraction exponent.

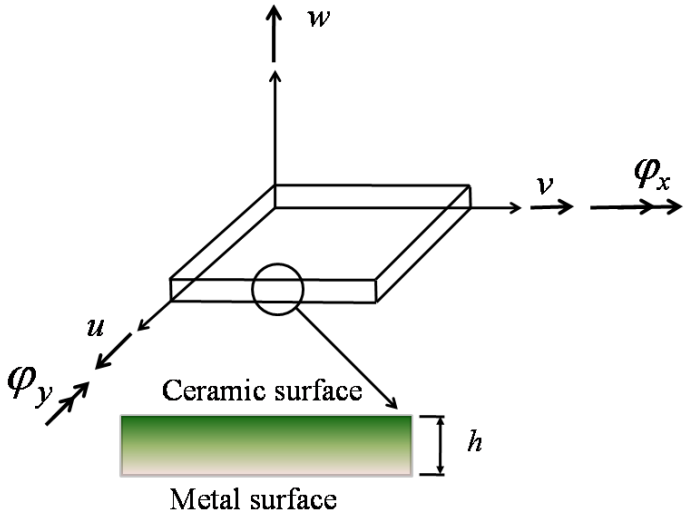

Fig. 2-20 Directions of the generalized displacements of the plate

- ***Comparison Study***

In order to verify the presented Element Free Galerkin model, the results of unstiffened FGM plate are compared with those available in the literature for various cases. He *et al*. [41] developed a finite element model based on the Classical Laminated Plate Theory (CLPT) for the shape and vibration control of FGM plates with piezoelectric sensors and actuators. The influence of the constituent volume fraction of Ti-6A1-4V/aluminum oxide was also studied for the static deflection, natural frequency and dynamic response of the FGM plate. Zhao *et al*. [40] developed the element-free kp-Ritz method for the free vibration of FGM plate with arbitrary boundary conditions. They examined the influences of the boundary conditions, volume fraction exponent, and length-to- thickness ratio on the natural frequencies of FGM plate. Four types of functionally-graded material, Al/Al_2O_3, Al/ZrO_2, Ti–6Al–4V/Aluminum oxide, and $SUS304/Si_3N_4$ were studied in their research. In this section, the results for three types of functionally-graded material,

Al/Al_2O_3, Al/ZrO_2, and Ti–6Al–4V/Aluminum oxide are chosen and the results for various constituent volume fractions and boundary conditions are compared with those reported by Zhao *et al*. [40] and He *et al*. [41].

For the first example, a square simply-supported plate consists of Aluminum (Al) and Alumina (Al_2O_3), studied earlier by Zhao *et al*. [40], is considered. The properties of Aluminum (Al) and Alumina (Al_2O_3) are presented in Table 2-6. A total of 289 nodes are used to model the plate. The results of the FGM plate with the length-to-thickness ratios (*a/h*) 5 and 10 for different volume fractions are shown in Table 2-7. In this table, $\bar{\omega}$ represents the frequency parameter ($\bar{\omega} = \omega h\sqrt{\rho_c / E_c}$). The maximum difference between the results is 1.7%. Table 2-8 compares the first ten natural frequencies of the plate with volume fraction exponents *n=1* and 2000, with the results presented by Zhao *et al*. [40] and He *et al*. [41]. The plate is a square with the length set at 0.4m and the FGM layer of thickness 5mm. The FGM plate consists of Ti–6Al–4V and Aluminum oxide, their properties are shown in Table 2-6. As can be observed in Table 2-8, the present results agree well with results available in the literature.

Zhao *et al*. [40] also examined the natural frequencies of FGM plates consisting of four types of FGM material, Al/Al_2O_3, Al/ZrO_2, Ti–6Al–4V/Aluminum oxide, and $SUS304/Si_3N_4$. In this section, two material systems are chosen, Al/Al_2O_3 and Al/ZrO_2 and the results are compared with those presented by Zhao *et al*. [40]. The properties of these materials are given in Table 2-6. The volume fractions between 0 to 10 are chosen. Three different boundary conditions, all edges simply-supported (SSSS), cantilever (CFFF) and all edges clamped (CCCC), are chosen. The plate is a square, the thickness of the plates is *h=0.01m* and the length-to-thickness ratios is 10. Table 2-9 shows the first four frequency parameters with various volume fraction exponents for the Al/Al_2O_3 plates. The frequency parameter is defined as:

$$\Omega = \omega a^2 \Big/ h\sqrt{\rho_c / E_c} \tag{2-44}$$

As can be seen in Table 2-9, there is a good agreement between the results obtained by the presented code and Zhao *et al*. [40] for three boundary conditions. Also, it can be observed, for all boundary conditions, the frequency parameters decreases as the volume fraction exponent increases. This variation is due to the change of FGM volume fraction which is modeled by varying the value of the power law exponent *n* in Eq. (2-43). As is clear from Eq. (2-43), when the power law exponent is set to zero, the FGM plate consists only of the ceramic material, which is Alumina in this work. When *n* tends to infinity, the FGM plate consists only of the metal, which is aluminum here.

Table 2-10 shows the first four frequency parameters of the plates made of Al/ZrO_2. Similar trends, which were seen in Table 2-10, are also observed for the SSSS, CFFF and CCCC boundary conditions.

- ***FGM Plates with Curvilinear Stiffeners***

The geometric properties of the plate and stiffeners are shown in Fig. 2-21. The plate was clamped at one end during testing to a steel bracket bolted to a heavy steel frame table. Notches at either end of this boundary condition were designed to mechanically separate the main plate from the clamped extra material.

In this research the plate is assumed to consist of Al/ZrO_2, which their properties are shown in Table 2-6. The stiffeners are also made of ZrO_2.

The first ten frequency parameters for various volume fraction exponents between 0 to 10 are presented in Table 2-11. As is expected, all frequency parameters are decreased by increasing the volume fraction exponent.

Effect of Stiffener Stiffness Ratio

The ratio of the cross-sectional area of the stiffener to that of the plate is defined by $\delta = b_s h_s / a h_p$ where b_s and h_s are the width and the height of the stiffener. The ratio of the bending stiffness of the stiffener to that of the plate is defined by $\gamma = E_s I_s / aD$ where E_s, I_s, a and D are elastic modulus of stiffener, second moment of the stiffener cross section area, width of the plate and flexural rigidity of the plate.

A comparison of the first frequency parameter of the unstiffened plate, stiffened plate when stiffener rigidity stiffness is 2, and stiffened plate when stiffener rigidity stiffness is 5, is shown in Fig. 2-22, where Ω_0 is the frequency parameter for $n=0$. It can be seen that for all three cases, the frequency parameter decreases by increasing the volume fraction exponent. Also it can be observed that adding stiffeners can increase the frequency parameter. From Fig. 2-22, it is seen that the effect of volume fraction exponent on frequency parameter for unstiffened plate is more than that for the stiffened plate. This is because the stiffness of structure increases due to stiffeners; the stiffness may be thus influenced less by the FGM plates' volume fraction exponents.

As can be seen in Fig. 2-23 and Fig. 2-24, similar trends are also observed for the second and third frequency parameters.

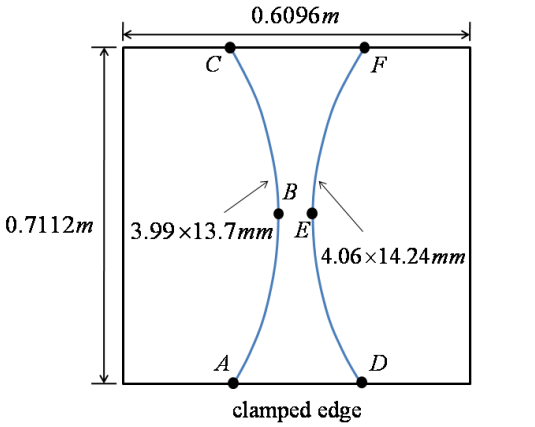

Fig. 2-21 Cantilever Curvilinearly-stiffened plate

Effect of Number of Stiffeners

Here consideration is given to the effect of number of stiffeners on the frequency parameters of FGM plates. The same plate as above, in this example is chosen, but now different number of curvilinear stiffeners is considered. The plate with one, two, three, and four curvilinear stiffeners are shown in Fig, 2-25. The plate is assumed to consist of Al/ZrO2, with their properties shown in Table 2-6. The stiffeners are also made of ZrO2. The variation of the first frequency parameters with the volume fraction exponents for different number of stiffeners is shown in Fig. 2-26. The frequencies for all number of stiffeners decreases as the volume fraction exponent increases, while this trend is becoming gentler for volume fraction exponents higher than 2. This is expected, because the plate has a smaller stiffness for a larger volume fraction exponent. As can be seen in Fig. 2-27 and Fig. 2-28, the same pattern can be observed for the second and third frequency parameters.

Table 2-6 Properties of the FGM components [Zhao *et al*. [40]], used under fair use guidelines, 2011

Material	Properties		
	E (N/m^2)	υ	ρ (kg/m^3)
Aluminum (Al)	70×10^9	0.3	2707
Alumina (Al2O3)	380×10^9	0.3	3800
Zirconia (ZrO2)	151×10^9	0.3	3000
Ti–6Al–4V	105.7×10^9	0.298	4429
Aluminum oxide	320.21×10^9	0.26	3750

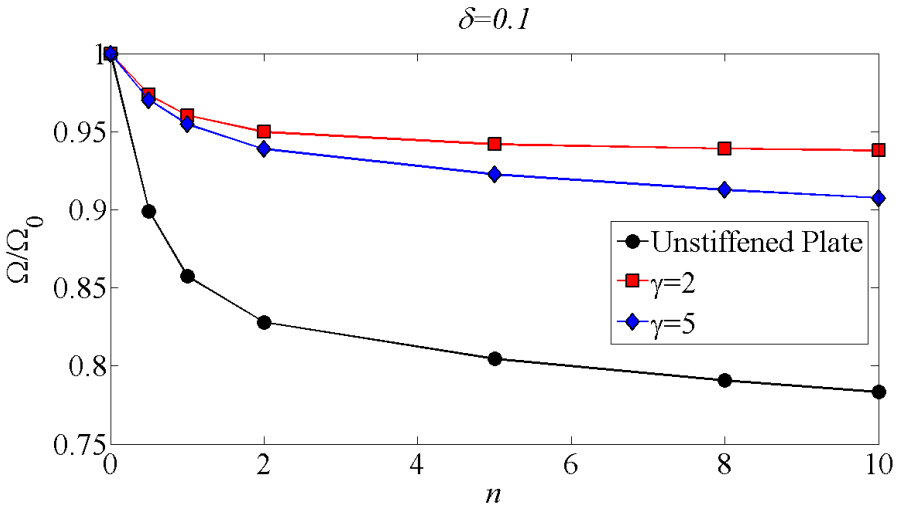

Fig. 2-22 First frequency parameter vs. the volume fraction exponents

Table 2-7 The frequency parameters ($\bar{\omega}$) for square FGM plates with varying volume fractions

$a/h=5$					
	n=0	n=0.5	n=1	n=4	n=10
Present Code	0.2089	0.1786	0.1614	0.1379	0.1305
Zhao *et al.* [40]	0.2055	0.1757	0.1587	0.1356	0.1284
$a/h=10$					
	n=0	n=0.5	n=1	n=4	n=10
Present Code	0.0576	0.0489	0.0441	0.0382	0.0365
Zhao *et al.* [40]	0.0567	0.0482	0.0435	0.0376	0.0359

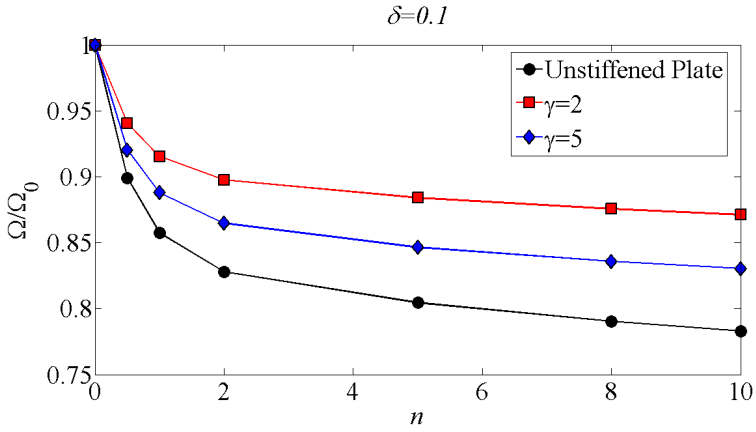

Fig. 2-23 Second frequency parameter vs. the volume fraction exponents

Table 2-8 The first ten natural frequencies (Hz) of FGM plates

	$n=0$			$n=2000$		
Mode	Zhao *et al.* [40]	He *et al.* [41]	Present Code	Zhao *et al.* [40]	He *et al.* [41]	Present Code
1	144.66	145.04	143.23	268.92	271.23	270.91
2	360.53	362.61	358.78	669.4	678.06	678.63
3	360.53	362.61	358.78	669.4	678.06	678.63
4	569.89	580.18	572.61	1052.49	1084.9	1083.1
5	720.57	725.22	718.18	1338.52	1356.1	1358.5
6	720.57	725.22	718.18	1338.52	1356.1	1358.5
7	919.74	942.79	930.24	1695.23	1763	1759.6
8	919.74	942.79	930.24	1695.23	1763	1759.6
9	1225.72	1233.00	1220.40	2280.95	2305.4	2308.4
10	1225.72	1233.00	1220.40	2280.98	2305.4	2308.4

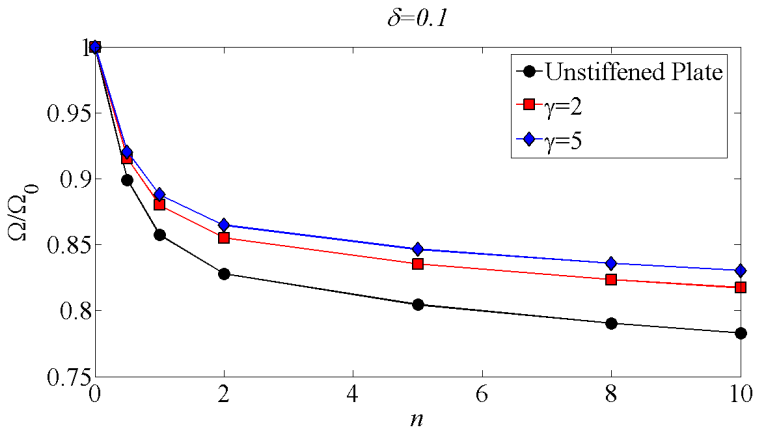

Fig. 2-24 Third frequency parameter vs. the volume fraction exponents

Table 2-9 The first four frequency parameters of square Al/Al_2O_3 FGM plates

SSSS								
Zhao *et al.* [40]					Present Code			
Mode	1	2	3	4	1	2	3	4
$n=0$	5.6763	13.5370	13.5370	20.6330	5.7622	13.7380	13.7380	21.0660
$n=0.5$	4.8209	11.5390	11.5390	17.6390	4.8928	11.7050	11.7050	18.0010
$n=1$	4.3474	10.4160	10.4160	15.9360	4.4125	10.5670	10.5670	16.2650
$n=2$	3.9474	9.4435	9.4435	14.4310	4.0075	9.5851	9.5851	14.7380
$n=5$	3.7218	8.8448	8.8448	13.4450	3.7806	8.9869	8.9869	13.7500
$n=8$	3.6410	8.6264	8.6264	13.0820	3.6993	8.7689	8.7689	12.9350
$n=10$	3.5923	8.5037	8.5037	12.8870	3.6501	8.6453	8.6453	12.7420
CFFF								
Mode	1	2	3	4	1	2	3	4
$n=0$	1.0298	2.3907	6.0047	7.6356	1.0380	2.4401	6.0778	7.7155
$n=0.5$	0.8728	2.0313	5.1061	5.8932	0.8797	2.0734	5.1675	5.9037
$n=1$	0.7867	1.8324	4.6048	5.4609	0.7929	1.8708	4.6615	5.4725
$n=2$	0.7150	1.6639	4.1769	4.9331	0.7207	1.6991	4.2303	4.9437
$n=5$	0.6768	1.5678	3.9273	4.2625	0.6823	1.6012	3.9803	4.2713
$n=8$	0.6633	1.5332	3.8382	3.9916	0.6687	1.5658	3.8909	3.9997
$n=10$	0.6547	1.5125	3.7861	3.8852	0.6601	1.5447	3.8383	3.8931
CCCC								
Mode	1	2	3	4	1	2	3	4
$n=0$	9.6329	18.3130	18.3130	25.4990	9.8135	18.7050	18.7050	26.1850
$n=0.5$	8.2388	15.7420	15.7420	21.9790	8.3851	16.0590	16.0590	22.5440
$n=1$	7.4533	14.2650	14.2650	19.9350	7.5833	14.5490	14.5490	20.4440
$n=2$	6.7629	12.9240	12.9240	18.0420	6.8829	13.1870	13.1870	18.5130
$n=5$	6.3060	11.9460	11.9460	16.5970	6.4292	12.2170	12.2170	17.0680
$n=8$	6.1314	11.5670	11.5670	16.0370	6.2568	11.8430	11.8430	16.2430
$n=10$	6.0375	11.3770	11.3770	15.7630	6.1626	11.6520	11.6520	15.8140

Table 2-10 The first four frequency parameters of square Al/ZrO_2 FGM plates

SSSS								
	Zhao *et al.* [40]				Present Code			
Mode	1	2	3	4	1	2	3	4
$n=0$	5.6763	13.5370	13.5370	20.6330	5.7622	13.7380	13.7380	21.0660
$n=0.5$	5.1105	12.2070	12.2070	18.6300	5.1869	12.3840	12.3840	19.0130
$n=1$	4.8713	11.6330	11.6330	17.7480	4.9445	11.8020	11.8020	18.1160
$n=2$	4.6977	11.1990	11.1990	17.0630	4.7692	11.3660	11.3660	17.4250
$n=5$	4.5549	10.8280	10.8280	16.4620	4.6256	10.9970	10.9970	16.8250
$n=8$	4.4741	10.6320	10.6320	16.1570	4.5437	10.7980	10.7980	16.5150
$n=10$	4.4323	10.5330	10.5330	16.0080	4.5012	10.6970	10.6970	16.3620
CFFF								
Mode	1	2	3	4	1	2	3	4
$n=0$	1.0299	2.3908	6.0046	7.6356	1.0380	2.4401	6.0778	7.7155
$n=0.5$	0.9263	2.1528	5.4090	6.0506	0.9336	2.1971	5.4739	6.0612
$n=1$	0.8832	2.0521	5.1549	5.7604	0.8901	2.0944	5.2171	5.7706
$n=2$	0.8526	1.9787	4.9675	5.4439	0.8593	2.0197	5.0288	5.4536
$n=5$	0.8280	1.9181	4.8115	5.0955	0.8346	1.9580	4.8729	5.1045
$n=8$	0.8135	1.8839	4.7255	4.9709	0.8200	1.9232	4.7861	4.9797
$n=10$	0.8058	1.8663	4.6816	4.9245	0.8123	1.9052	4.7415	4.9332
CCCC								
Mode	1	2	3	4	1	2	3	4
$n=0$	9.6354	18.3050	18.3050	25.5060	9.8135	18.7050	18.7050	26.1850
$n=0.5$	8.7011	16.5670	16.5670	23.1110	8.8576	16.9170	16.9170	23.7100
$n=1$	8.2925	15.7830	15.7830	22.0140	8.4422	16.1190	16.1190	22.5870
$n=2$	7.9756	15.1470	15.1470	21.0990	8.1235	15.4790	15.4790	21.6650
$n=5$	7.6959	14.5630	14.5630	20.2470	7.8449	14.8990	14.8990	20.7600
$n=8$	7.5521	14.2820	14.2820	19.8490	7.6995	14.6140	14.6140	20.2540
$n=10$	7.4815	14.1490	14.1490	19.6660	7.6454	14.5400	14.5400	20.3420

Table 2-11 First ten frequency parameters of curvilinearly-stiffened plate vs. the volume fraction

Mode	$n=0$	$n=0.5$	$n=1$	$n=2$	$n=5$	$n=8$	$n=10$
1	1.018	0.95606	0.93137	0.91571	0.90823	0.90458	0.90245
2	2.4154	2.2128	2.1289	2.0706	2.0276	2.0028	1.9896
3	5.7555	5.2927	5.0983	4.9631	4.8647	4.8069	4.7754
4	8.0324	7.2961	6.99	6.7754	6.6103	6.5139	6.4627
5	8.2114	7.4951	7.2027	7.0021	6.8571	6.7744	6.7304
6	14.326	12.978	12.42	12.029	11.728	11.552	11.459
7	17.159	15.552	14.881	14.409	14.041	13.826	13.712
8	17.55	16.191	15.617	15.214	14.922	14.756	14.666
9	19.498	17.579	16.783	16.222	15.778	15.514	15.374
10	26.055	23.528	22.478	21.737	21.152	20.809	20.627

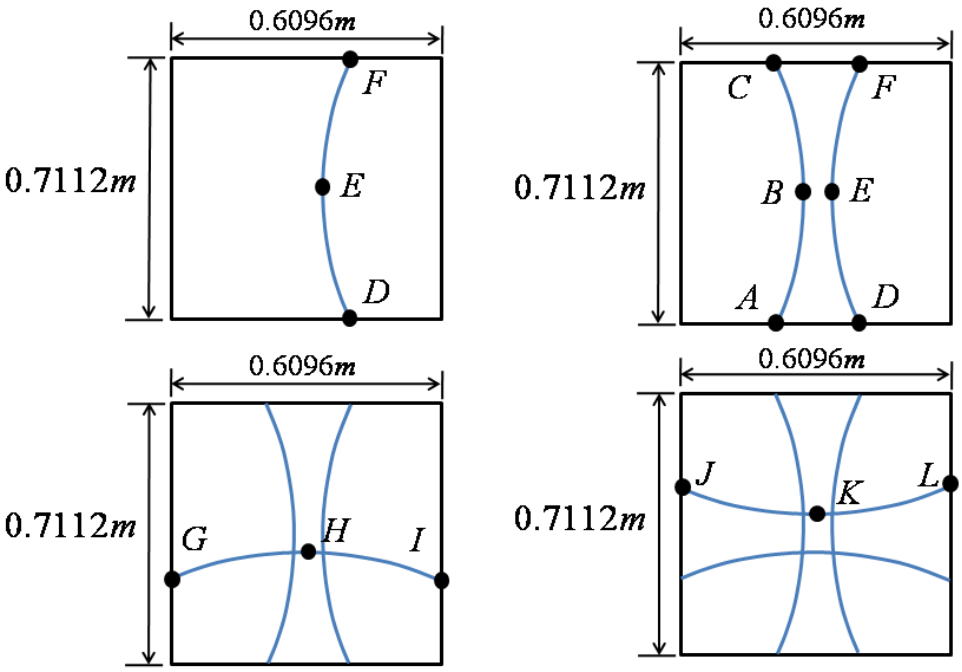

Fig, 2-25 Plate with one, two, three and four curvilinear stiffeners

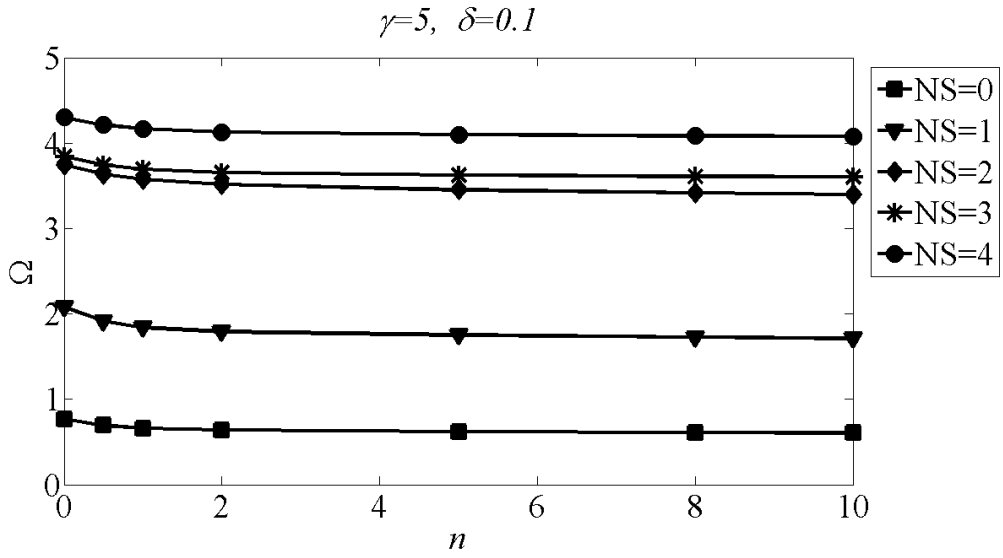

Fig. 2-26 First frequency parameter vs. the volume fraction exponent for plate with different number of curvilinear stiffeners (NS: Number of Stiffeners)

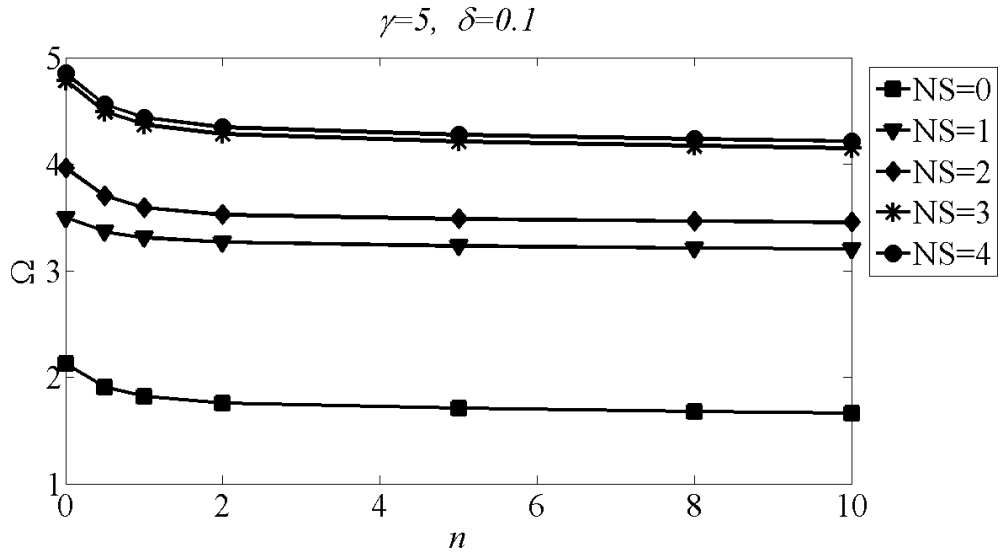

Fig. 2-27 Second frequency parameter vs. the volume fraction exponent for plate with different number of curvilinear stiffeners (NS: Number of Stiffeners)

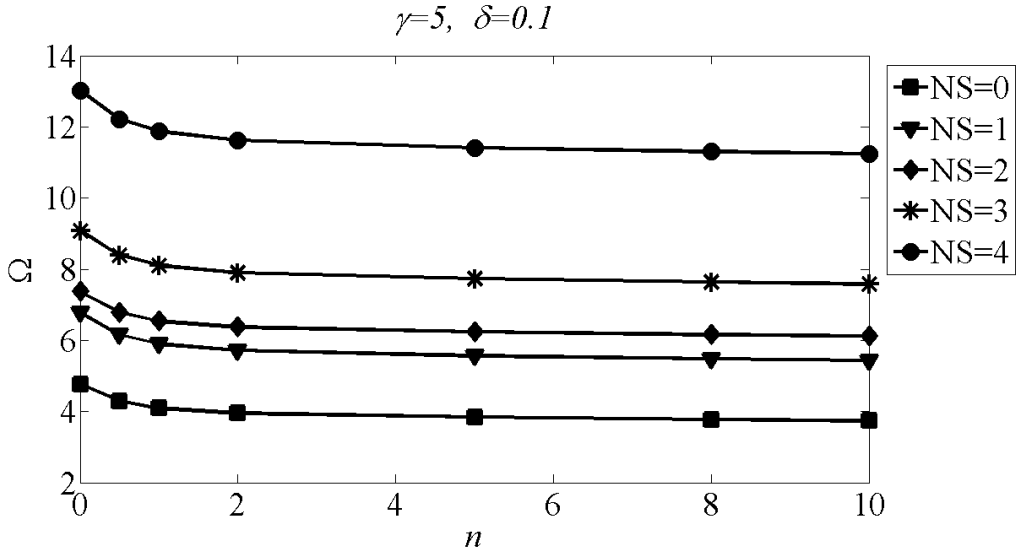

Fig. 2-28 Third frequency parameter vs. the volume fraction exponent for plate with different number of curvilinear stiffeners (NS: Number of Stiffeners)

2.5 Conclusions

The Element Free Galerkin method has been successfully used for vibration analysis of the plate with straight, arbitrary oriented as well as curvilinear stiffeners. By employing the displacement compatibility conditions at the contact surface between the plate and the stiffener, the displacement field of the stiffener

is expressed in terms of the displacements of the plate. The essential boundary conditions are imposed by using the penalty method. Numerical examples with different boundary conditions and different stiffener location and curvature have been solved to verify the feasibility of the presented meshless method for solving the problems, and the results show that the accuracy is comparable with that of the other methods. Because there is no mesh in the meshless method to construct the shape function, the formulation allows the positioning of stiffener anywhere within the plate which gives a greater flexibility in the choice of the number of nodes used both for representing the plate as well as the stiffeners. This capability can be used in the topological placement of stiffeners using EFG method, by updating the stiffness and mass matrices of stiffeners while the stiffness and mass matrices of plate are kept unchanged.

3 Free Vibration Analysis of Curvilinearly-Stiffened Plates Using Chebyshev Ritz and Experimental Validation

3.1 Introduction

Ritz method is applied while stiffeners are considered as discrete elements. The First Order Shear Deformation Theory (FSDT) is used to represent the plate and stiffener. The Chebyshev polynomial functions are used as the basic functions in the Ritz method. The major part of this work is concerned with modeling the curvilinear stiffeners and comparing the results with experimental data. By considering the curvilinear stiffeners, the curvature, the continuous variation in orientation, can be used in controlling different mode shapes in addition to the associated frequencies. It can provide a mechanism to passively control the dynamic response under certain excitations. In the present method, the geometric properties of curvilinear stiffeners can be modified without changing the plate geometric properties. In the developed formulations, both eccentric and concentric stiffeners were studied. Natural frequencies and mode shapes for plate with straight and curvilinear stiffeners were compared with the results available in the literature. A good agreement was seen. A 24 by 28 *in.* curvilinear stiffened panel was machined from 2219-T851 aluminum for experimental validation of the Ritz and meshfree method of vibration mode shape predictions. Results were obtained for this panel mounted vertically to a steel clamping bracket using acoustic excitation and a laser vibrometer. Experimental results appear to correlate well with theoretical predictions.

3.2 Mathematical Formulation for Stiffened Plate

In the present formulation, it is assumed that the deformations remain small so that linear relations can be used to represent the strain in the plate and the stiffeners. The emphasis of the present work is on developing a Ritz method based on Chebyshev polynomials for the analysis of an isotropic plate with curvilinear stiffeners. Using the Ritz method and developing the equations for the plate and stiffeners separately will give us the capability to evaluate the mass and stiffness matrices of the stiffener independently of those of the plate.

- ***Strain and Kinetic Energy of the Plate***

Based on FSDT, the in-plane and transverse displacements in the plate are assumed in the following form:

$$\begin{aligned} u_p(\bar{x},\bar{y},z,t) &= z\phi_x(\bar{x},\bar{y},t) \\ v_p(\bar{x},\bar{y},z,t) &= z\phi_y(\bar{x},\bar{y},t) \\ w_p(\bar{x},\bar{y},z,t) &= w_p(\bar{x},\bar{y},t) \end{aligned} \tag{3-1}$$

here ϕ_{px}, and ϕ_{py} are the rotations normal to the midsurface about the *y* and *x* axes, respectively, and w_p implies the transverse displacement of a point in the midsurface.

For free vibration of the plate with curvilinear stiffeners, one has

$$\begin{aligned} \phi_x(\bar{x},\bar{y},t) &= \varphi_x(\bar{x},\bar{y})e^{i\omega t} \\ \phi_y(\bar{x},\bar{y},t) &= \varphi_y(\bar{x},\bar{y})e^{i\omega t} \\ w_p(\bar{x},\bar{y},t) &= w(\bar{x},\bar{y})e^{i\omega t} \end{aligned} \tag{3-2}$$

where $\varphi_x(\bar{x},\bar{y})$, $\varphi_y(\bar{x},\bar{y})$ and $w(\bar{x},\bar{y})$ are the amplitude of $\phi_x(\bar{x},\bar{y},t)$, $\phi_y(\bar{x},\bar{y},t)$ and $w_p(\bar{x},\bar{y},t)$, respectively. Also ω is the natural frequency of the structure. Form the displacement field, defined in Eq. (3-1), strain components are defined as:

$$\varepsilon_p = \begin{Bmatrix} \gamma_{pxz} \\ \gamma_{pyz} \\ \kappa_{px} \\ \kappa_{py} \\ \kappa_{pxy} \end{Bmatrix} = \begin{bmatrix} 1 & 0 & \frac{1}{a}\frac{\partial}{\partial\bar{x}} \\ 0 & 1 & \frac{1}{b}\frac{\partial}{\partial\bar{y}} \\ \frac{1}{a}\frac{\partial}{\partial\bar{x}} & 0 & 0 \\ 0 & \frac{1}{b}\frac{\partial}{\partial\bar{y}} & 0 \\ \frac{1}{b}\frac{\partial}{\partial\bar{y}} & \frac{1}{a}\frac{\partial}{\partial\bar{x}} & 0 \end{bmatrix} \begin{Bmatrix} \varphi_x \\ \varphi_y \\ w \end{Bmatrix} \tag{3-3}$$

The strain and kinetic energies of the plate can be, respectively, expressed as [15]

$$\begin{aligned} U_p &= \frac{1}{2}\int_0^1 \int_0^1 [D((\frac{1}{a}\frac{\partial\varphi_x}{\partial\bar{x}})^2 + (\frac{1}{b}\frac{\partial\varphi_y}{\partial\bar{y}})^2 + 2\upsilon(\frac{1}{ab}\frac{\partial\varphi_x}{\partial\bar{x}}\frac{\partial\varphi_y}{\partial\bar{y}}) + \\ &\frac{1-\upsilon}{2}(\frac{1}{b}\frac{\partial\varphi_x}{\partial\bar{y}} + \frac{1}{a}\frac{\partial\varphi_y}{\partial\bar{x}})^2) + K_G G h_p((\varphi_x + \frac{1}{a}\frac{\partial w}{\partial\bar{x}})^2 + (\varphi_y + \frac{1}{b}\frac{\partial w}{\partial\bar{y}})^2)]ab d\bar{x}d\bar{y} \\ T_p &= \frac{1}{2}\rho\omega^2\int_0^1 \int_0^1 [h_p w^2 + \frac{1}{12}h_p{}^3(\varphi_x^2 + \varphi_y^2)]ab d\bar{x}d\bar{y} \end{aligned} \tag{3-4}$$

where $D,\ K_G,\ G,\ E,\ h_p, a$ and b are the flexural rigidity, shear correction factor, shear modulus, elastic modulus, thickness, width and height of the plate, respectively.

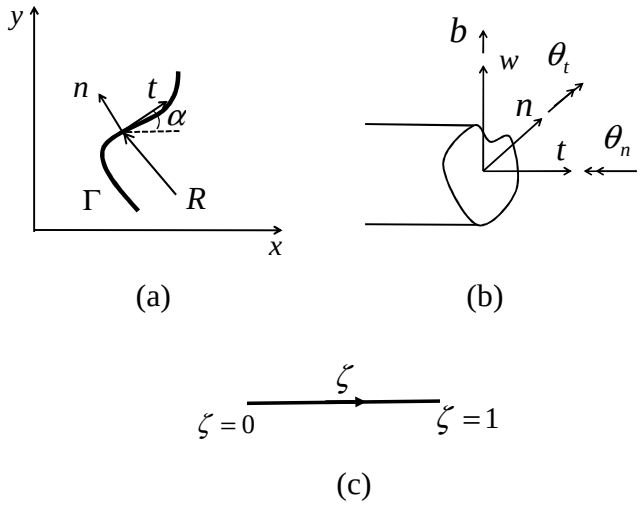

Fig. 3-1 (a) Local and global coordinate systems for the curvilinear stiffener (b) Directions of the generalized displacements of the stiffener (c) The transformed plane of curvilinear stiffener

- ***Strain and Kinetic Energy of the Stiffener***

The arbitrary shape of the curvilinear stiffener is mapped to a region [0, 1] in the ζ coordinate (Fig. 3-1c) with the help of η_i shape functions [80]:

$$\begin{aligned} \overline{x} &= \sum_{i=1}^{np} \eta_i(\zeta)\overline{x}_i \\ \overline{y} &= \sum_{i=1}^{np} \eta_i(\zeta)\overline{y}_i \end{aligned} \tag{3-5}$$

where $(\overline{x}_i, \overline{y}_i)$ are the coordinates of the *i*th point on the curvilinear stiffener in the $\overline{x} - \overline{y}$ plane, *np* is the number of points and ζ is the natural coordinate for parameterization of the curve (Fig. 3-1c). The stiffener strain vector is [80]:

$$\begin{cases} \gamma_n = \dfrac{dw_s}{ds} + \theta_t \\ \kappa_t = \dfrac{d\theta_t}{ds} + \dfrac{\theta_n}{R} \\ \kappa_n = \dfrac{d\theta_n}{ds} - \dfrac{\theta_t}{R} \end{cases} \qquad \begin{aligned} s(\zeta) &= \int_0^{\zeta} \det J d\zeta \\ \det J &= \sqrt{(a\frac{d\overline{x}}{d\zeta})^2 + (b\frac{d\overline{y}}{d\zeta})^2} \end{aligned} \tag{3-6}$$

here *detJ* is the Jacobian of the transformation and *R* is the radius of curvature (Fig. 3-1a). θ_t, θ_n and w_s, which are the rotations about normal (*n*) and tangential (*t*) directions, respectively, and the deflection along binormal direction (*b*), are shown in Fig. 3-1b. Using Eq. (3-5), the rotations and deflection can be expressed as:

$$\begin{cases} \theta_t = \theta_t(\bar{x}(\zeta), \bar{y}(\zeta)) \\ \theta_n = \theta_n(\bar{x}(\zeta), \bar{y}(\zeta)) \\ w_s = w_s(\bar{x}(\zeta), \bar{y}(\zeta)) \end{cases} \tag{3-7}$$

The strain and kinetic energy of the stiffener can be defined as

$$\begin{aligned} U_s &= \frac{1}{2}\int_\Gamma [G_s A_b(\theta_t + \frac{dw_s}{ds})^2 + G_s J_s(\frac{d\theta_n}{ds} - \frac{\theta_t}{R})^2 + E_s I_n(\frac{d\theta_t}{ds} + \frac{\theta_n}{R})^2]ds \\ T_s &= \frac{1}{2}\rho_s \omega^2 \int_\Gamma [A{w_s}^2 + I_n{\theta_t}^2 + (I_n + I_t){\theta_n}^2]ds \end{aligned} \tag{3-8}$$

where A_b, A, I, J_s, G_s, E_s and h_s are the shear area, area, second moment of the stiffener cross section area about the reference axis, torsional stiffness of the stiffener (using St Venant's torsion constant), shear modulus, elastic modulus and thickness of stiffener, respectively.

As a general case, a curved stiffener having eccentricity with respect to the midplane of the plate, and placed anywhere on the plate, is considered as shown in Fig. 3-1a. Since the stiffener is curvilinear, its direction changes from point to point, and hence a local axis (*t*) is considered along the tangent to the stiffener at the Gaussian integration point, making an angle α with the global axis (*x*) (Fig. 3-1a), which is defined by:

$$u_s' = \begin{Bmatrix} \theta_t \\ \theta_n \\ w_s \end{Bmatrix} = \begin{bmatrix} \cos\alpha & \sin\alpha & 0 \\ -\sin\alpha & \cos\alpha & 0 \\ 0 & 0 & 1 \end{bmatrix} \begin{Bmatrix} \varphi_x \\ \varphi_y \\ w \end{Bmatrix} = \Lambda u_s \tag{3-9}$$

where Λ is the coordinate transformation matrix.

- ***Parameterization of Deflections and Rotations***

It is known that a choice of admissible functions is very important to the accuracy and efficiency of the solutions obtained by the Ritz method; there are several types of functions such as beam characteristic functions, simple polynomials, orthogonal characteristic polynomials which were employed when dealing with free vibration problems successfully [82], [83], [84]. In this research, a set of Chebyshev polynomials is selected for the Ritz method. Each of the displacement and rotations functions can be written as double series of Chebyshev polynomials multiplied by boundary functions:

$$\begin{cases} \varphi_x(\bar{x},\bar{y}) = \sum_{m=1}^{p_1}\sum_{n=1}^{q_1} c_{mn}\psi_{xmn}(\bar{x},\bar{y}) \\ \varphi_y(\bar{x},\bar{y}) = \sum_{m=1}^{p_2}\sum_{n=1}^{q_2} d_{mn}\psi_{ymn}(\bar{x},\bar{y}), \\ w(\bar{x},\bar{y}) = \sum_{m=1}^{p_3}\sum_{n=1}^{q_3} e_{mn}\varphi_{mn}(\bar{x},\bar{y}) \end{cases} \quad \begin{cases} \psi_{xmn}(\bar{x},\bar{y}) = \psi_{bx}(\bar{x},\bar{y})X_m(\bar{x})Y_n(\bar{y}) \\ \psi_{ymn}(\bar{x},\bar{y}) = \psi_{by}(\bar{x},\bar{y})X_m(\bar{x})Y_n(\bar{y}) \\ \varphi_{mn}(\bar{x},\bar{y}) = \varphi_b(\bar{x},\bar{y})X_m(\bar{x})Y_n(\bar{y}) \end{cases} \tag{3-10}$$

where c_{mn}, d_{mn} and e_{mn} are the unknown coefficients and p_s and q_s (s=1,2 and 3) are the degrees of the Chebyshev polynomials in the $\bar{x}$ and $\bar{y}$ directions, respectively. $X_m(\bar{x})$ and $Y_n(\bar{y})$ are one dimensional Chebyshev polynomials $P_i(\chi)$

$$P_i(\chi) = \cos[(i-1)\arccos(\chi)],\ i = 1,\ 2,\ ....;\ \chi = \bar{x},\ \bar{y} \tag{3-11}$$

Also, $\psi_{bx}(\bar{x},\bar{y})$, $\psi_{by}(\bar{x},\bar{y})$ and $\varphi_b(\bar{x},\bar{y})$ are polynomial expressions describing the boundary conditions that are functions of the plate geometry and kinematics. The non-dimensionalized boundary polynomial expressions for a rectangular plate with varying boundary conditions are [Liew *et al*. [14]]:

$$\psi_{bx}(\bar{x},\bar{y}),\ \psi_{by}(\bar{x},\bar{y}) \text{ and } \varphi_b(\bar{x},\bar{y}) = \prod_{j=1}^{4}\left[\Gamma_j(\bar{x},\bar{y})\right]^{\Omega_j} \tag{3-12}$$

where Γ_j is the boundary equation of the *jth* supporting edge and Ω_j, depending on the support edge condition, is shown in Table 3-1.

Table 3-1 Plate boundary equations

	φ_x	φ_y	w
$\Omega_i = 0$	If the *jth* edge is free; or simply supported in the *y* direction	If the *jth* edge is free; or simply supported in the *x* direction	If the *jth* edge is free
$\Omega_i = 1$	If the *jth* edge is clamped; or simply supported in the *x* direction	If the *jth* edge is clamped; or simply supported in the *y* direction	If the *jth* edge is clamped; or simply supported

- ***Natural Frequencies and Mode Shapes of the Plate with Curvilinear Stiffener***

The Lagrangian L of the stiffened plate is defined as:

$$L = T_p + T_s - U_p - U_s \tag{3-13}$$

By substituting Eq. (3-10) in Eq. (3-4)

$$\begin{cases} U_p = \frac{1}{2} C^T \int_0^1 \int_0^1 B_p^T D_p B_p abd\bar{x}d\bar{y}\, C \\ T_p = \frac{1}{2} \omega^2 C^T \int_0^1 \int_0^1 N_p^T m_p N_p abd\bar{x}d\bar{y}\, C \end{cases}, \; C = \begin{Bmatrix} \boldsymbol{c} \\ \boldsymbol{d} \\ \boldsymbol{e} \end{Bmatrix}$$

$$D_p = \frac{Eh_p}{1-\upsilon^2} \begin{bmatrix} \frac{h_p^2}{12} & & & & \\ \frac{\upsilon h_p^2}{12} & \frac{h_p^2}{12} & & sym. & \\ 0 & 0 & \frac{h_p^2(1-\upsilon)}{24} & & \\ 0 & 0 & 0 & K_G \frac{1-\upsilon}{2} & \\ 0 & 0 & 0 & 0 & K_G \frac{1-\upsilon}{2} \end{bmatrix}, \; m_p = \rho \begin{bmatrix} \frac{1}{12} h_p^3 & & sym. \\ 0 & \frac{1}{12} h_p^3 & \\ 0 & 0 & h_p \end{bmatrix} \tag{3-14}$$

where B_p, N_p, D_p and m_p are :

$$\left[B_p \right]_{mn}^T = \begin{bmatrix} \frac{1}{a} \frac{\partial \psi_{xmn}}{\partial \bar{x}} & 0 & \frac{1}{b} \frac{\partial \psi_{xmn}}{\partial \bar{y}} & \psi_{xmn} & 0 \\ 0 & \frac{1}{b} \frac{\partial \psi_{ymn}}{\partial \bar{y}} & \frac{1}{a} \frac{\partial \psi_{ymn}}{\partial \bar{x}} & 0 & \psi_{ymn} \\ 0 & 0 & 0 & \frac{1}{a} \frac{\partial \varphi_{mn}}{\partial \bar{x}} & \frac{1}{b} \frac{\partial \varphi_{mn}}{\partial \bar{y}} \end{bmatrix} \tag{3-15}$$

$$\left[N_p \right]_{mn} = \begin{bmatrix} \psi_{xmn} & & sym. \\ 0 & \psi_{ymn} & \\ 0 & 0 & \varphi_{mn} \end{bmatrix}$$

By using Eq. (3-9) and (3-10), Eq. (3-8) can be written as

$$\begin{cases} U_s = \frac{1}{2} C^T \int_0^1 B_s^T D_s B_s \det J d\zeta\, C \\ T_s = \frac{1}{2} \omega^2 C^T \int_0^1 N_s^T m_s N_s \det J d\zeta\, C \end{cases} \tag{3-16}$$

where B_s, N_s, D_s and m_s are:

$$D_s = \begin{bmatrix} EI & & sym. \\ 0 & GJ & \\ 0 & 0 & GA_b \end{bmatrix},\ m_s = \rho_s \begin{bmatrix} I_n & & sym. \\ 0 & I_t + I_n & \\ 0 & 0 & A \end{bmatrix}$$

$$[N_s]_{mn} = \begin{bmatrix} \psi_{xmn}\cos\alpha & \psi_{ymn}\sin\alpha & 0 \\ -\psi_{xmn}\sin\alpha & \psi_{ymn}\cos\alpha & 0 \\ 0 & 0 & \varphi_{mn} \end{bmatrix}$$

$$[B_s]_{mn} = \begin{bmatrix} B_{11mn} & B_{12mn} & 0 \\ B_{21mn} & B_{22mn} & 0 \\ B_{31mn} & B_{32mn} & B_{33mn} \end{bmatrix}$$

$$\begin{cases} B_{11mn} = \dfrac{1}{a}\dfrac{\partial \psi_{xmn}}{\partial \bar{x}}\cos\alpha^2 + \dfrac{1}{b}\dfrac{\partial \psi_{xmn}}{\partial \bar{y}}\cos\alpha\sin\alpha - \dfrac{\sin\alpha}{R}\psi_{xmn} \\ B_{12mn} = \dfrac{1}{a}\dfrac{\partial \psi_{ymn}}{\partial \bar{x}}\sin\alpha\cos\alpha + \dfrac{1}{b}\dfrac{\partial \psi_{ymn}}{\partial \bar{y}}\sin\alpha^2 + \dfrac{\cos\alpha}{R}\psi_{ymn} \\ B_{21mn} = -\dfrac{1}{a}\dfrac{\partial \psi_{xmn}}{\partial \bar{x}}\sin\alpha\cos\alpha - \dfrac{1}{b}\dfrac{\partial \psi_{xmn}}{\partial \bar{y}}\sin\alpha^2 - \dfrac{\cos\alpha}{R}\psi_{xmn} \\ B_{22mn} = \dfrac{1}{a}\dfrac{\partial \psi_{ymn}}{\partial \bar{x}}\cos\alpha^2 + \dfrac{1}{b}\dfrac{\partial \psi_{ymn}}{\partial \bar{y}}\cos\alpha\sin\alpha - \dfrac{\sin\alpha}{R}\psi_{ymn} \\ B_{31mn} = \psi_{xmn}\cos\alpha \qquad B_{32i} = \psi_{ymn}\sin\alpha \\ B_{33mn} = \dfrac{1}{a}\dfrac{\partial \varphi_{mn}}{\partial \bar{x}}\cos\alpha + \dfrac{1}{b}\dfrac{\partial \varphi_{mn}}{\partial \bar{y}}\sin\alpha \end{cases} \tag{3-17}$$

Minimization of the maximum strain and kinetic energies of the stiffened plate with respect to the c_{mn}, d_{mn} and e_{mn} leads to a set of linear eigenvalue equations [14], [15]:

$$\left((K_p + K_s) - \omega^2 (M_p + M_s)\right) C = 0 \tag{3-18}$$

where the plate and stiffener stiffness (K_p and K_s) and mass (M_p and M_s) matrices are:

$$\begin{aligned} K_p &= \int_0^1 \int_0^1 B_p^T D_p B_p ab d\bar{x} d\bar{y} \\ M_p &= \int_0^1 \int_0^1 N_p^T m_p N_p ab d\bar{x} d\bar{y} \\ K_s &= \int_0^1 B_s^T D_s B_s \det J d\zeta \\ M_s &= \int_0^1 N_s^T m_s N_s \det J d\zeta \end{aligned} \tag{3-19}$$

3.3 Convergence and Comparison Studies

As is known, the Ritz method can provide accurate solutions. However, its convergence depends on the choice of global admissible functions. The natural frequencies obtained by the Ritz method converge as upper bounds to the exact values. These upper bound estimates could be improved by increasing the number of terms in functions. Using different kinds of functions can increase or decrease the number of terms for which the results converge. To illustrate the versatility of the current method, numerical examples have been performed by using MatLab®. In order to decide upon the number of terms to be used in the assumed expansion, the convergence of the solutions with increasing numbers of terms being used in the assumed approximations was examined for the natural frequency parameters of the stiffened plate. As expected, it is seen that the convergence using the present approximate method is monotonic. The results are provided for the plate with straight and curvilinear stiffeners with different boundary conditions. The validity of the formulation is shown by comparing the results with the available results in the literature.

- ***A Plate with a Single Stiffener***

The problem which is selected as the first example to validate the present method is a square plate with a centrally placed stiffener as shown in Fig. 3-2. Both plate and stiffener are made of the same isotropic material with $\nu = 0.3$. This problem is previously reported by Liew *et al.* [14]. They studied the application of Ritz method for this problem by using simple polynomials. The results presented by Liew *et al*. were obtained for eccentric stiffener. In order to make comparison, this problem was analyzed for an eccentric stiffener using Chebyshev polynomials. The frequency parameter is defined as:

$$\lambda = (\omega b^2 / \pi^2)\sqrt{\rho h_p / D} \tag{3-20}$$

In this example, the plate with $a/b = 1$, $h_p/b = 0.05$, $b_s/b = 0.05$ and $h_s/h_p = 1.5$ are considered. The results for the simply-supported and clamped on all edges, as shown in Table 3-2, show that acceptable convergence has been achieved for the first six frequencies. Also the results are in good agreement with the previously published results. The convergence of all six natural frequencies in Table 3-2 indicates the suitability of the Chebyshev polynomials as the basis functions in the Ritz analysis of the stiffened plate.

- ***A Plate with Two Stiffeners***

As shown in Fig. 3-3, a plate, simply-supported on all edges, with cross stiffeners is considered. The natural frequencies are compared with those of Liew *et al* [15]. They developed Ritz method by using simple polynomials based on Mindlin-Engesser model. The convergence of the first six frequency

parameters for the plates with different a/b and h_p/b ratios are presented in Table 3-3. it can be seen that the solutions generated in both studies are in close agreement. The same convergence trend as shown in Table 3-2 has been observed when more stiffeners are used in the computation.

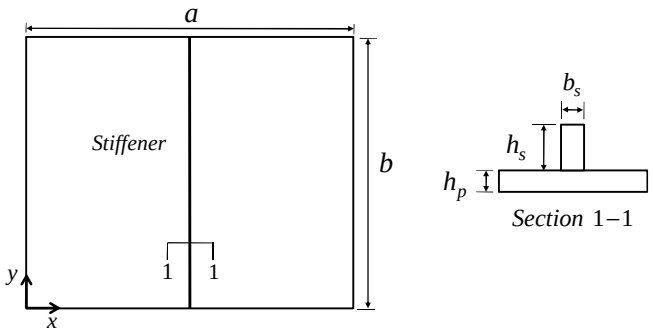

Fig. 3-2 A Plate with central stiffener

Table 3-2 Frequency parameters for a square plate with a central stiffener

Clamped plate (CCCC)								
Mode	Simple polynomials (Liew *et al.* [14])				Chebyshev polynomials			
	10*	12	13	14	10	12	13	14
1	4.674	4.654	4.640	4.639	4.643	4.629	4.629	4.616
2	7.139	7.138	7.138	7.138	7.025	7.025	7.025	7.025
3	9.758	9.678	9.669	9.628	9.640	9.594	9.594	9.555
4	10.401	10.399	10.398	10.398	10.258	10.258	10.258	10.258
5	11.967	11.964	11.960	11.960	11.947	11.943	11.943	11.940
6	15.422	15.417	15.416	15.414	15.240	15.239	15.239	15.239
Simply-supported plate (SSSS)								
Mode	Simple polynomials (Liew *et al.* [14])				Chebyshev polynomials			
	10	12	13	14	10	12	13	14
1	2.391	2.389	2.388	2.388	2.384	2.383	2.383	2.381
2	4.948	4.948	4.948	4.948	4.897	4.897	4.897	4.897
3	6.851	6.822	6.822	6.801	6.798	6.775	6.773	6.757
4	7.866	7.865	7.864	7.864	7.791	7.791	7.791	7.791
5	9.107	9.105	9.104	9.104	9.091	9.089	9.089	9.088
6	12.482	12.397	12.334	12.333	12.312	12.263	12.257	12.229
*The degree of polynomial considered in the expansion								

Table 3-3 Frequency parameters for a rectangular plate with cross stiffeners

$a/b=1$	$h_p/b=0.05$			$b_s/b=0.01$		$h_s/h_p=1.5$	
Mode	Simple polynomials (Liew *et al.* [15])				Chebyshev polynomials			
	10*	12	13	14	10	12	13	14
1	2.463	2.460	2.458	2.458	2.456	2.452	2.450	2.450
2	5.915	5.907	5.906	5.896	5.890	5.878	5.875	5.868
3	5.916	5.908	5.908	5.897	5.890	5.878	5.875	5.868
4	9.323	9.290	9.256	9.255	9.241	9.199	9.187	9.167
5	10.213	10.201	10.194	10.193	10.194	10.182	10.177	10.175
6	11.930	11.870	11.840	11.840	11.833	11.780	11.753	11.740
$a/b=2$	$h_p/b=0.001$			$b_s/b=0.01$		$h_s/h_p=1.5$	
Mode	Simple polynomials (Liew *et al.* [15])				Chebyshev polynomials			
	10	12	13	14	10	12	13	14
1	1.463	1.461	1.459	1.459	1.458	1.456	1.455	1.455
2	2.563	2.558	2.558	2.557	2.555	2.552	2.551	2.550
3	4.322	4.309	4.302	4.302	4.296	4.287	4.282	4.282
4	4.930	4.922	4.922	4.906	4.909	4.895	4.890	4.886
5	5.903	5.877	5.850	5.850	5.843	5.814	5.814	5.796
6	6.582	6.543	6.543	6.524	6.523	6.498	6.494	6.483
*The degree of polynomial considered in the expansion								

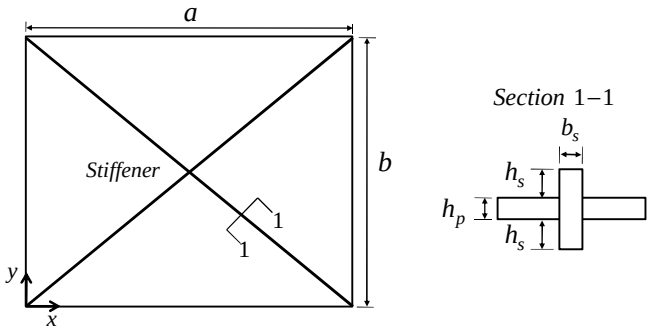

Fig. 3-3 A plate with cross stiffeners

- ***A Plate with Multiple Stiffeners***

The plate with multiple stiffeners, simply-supported on all edges, is analyzed for free vibrations (see Fig. 3-4). The convergence and comparison study with different values of the plate aspect ratio a/b and that of h_p/b are tabulated in Table 3-4. The natural frequencies, as expected, converge from above and reach acceptable upper bound values. As noted from Tables 2, 3 and 4, the convergence of the orthogonal

polynomials is superior to that of the simple polynomials. The procedure presented here can be used to generate very accurate results for the natural frequencies of rectangular plates with various types of boundary conditions and curvilinear stiffeners.

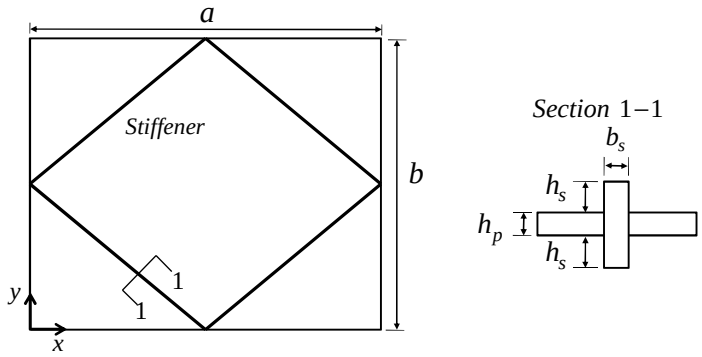

Fig. 3-4 A plate with multiple stiffeners

Table 3-4 Frequency parameters for a rectangular plate with multiple stiffeners

$a/b=1$	$h_p/b=0.05$			$b_s/b=0.01$		$h_s/h_p=1.5$	
Mode	Simple polynomials (Liew *et al.* [15])			Chebyshev polynomials			
	10*	12	13	14	10	12	13	14
1	2.545	2.542	2.540	2.540	2.539	2.537	2.536	2.535
2	5.923	5.909	5.909	5.903	5.900	5.888	5.884	5.878
3	5.924	5.910	5.910	5.904	5.900	5.888	5.884	5.878
4	9.327	9.289	9.273	9.273	9.257	9.217	9.204	9.186
5	9.777	9.771	9.763	9.763	9.767	9.758	9.754	9.752
6	12.370	12.320	12.280	12.280	12.293	12.230	12.204	12.192
$a/b=2$	$h_p/b=0.001$			$b_s/b=0.01$		$h_s/h_p=1.5$	
Mode	Simple polynomials (Liew *et al.* [15])			Chebyshev polynomials			
	10	12	13	14	10	12	13	14
1	1.521	1.519	1.518	1.518	1.518	1.517	1.516	1.516
2	2.563	2.561	2.561	2.558	2.558	2.555	2.554	2.552
3	4.143	4.136	4.131	4.131	4.139	4.128	4.123	4.123
4	4.909	4.918	4.918	4.909	4.915	4.900	4.895	4.889
5	5.910	5.877	5.860	5.860	5.856	5.827	5.827	5.808
6	6.572	6.531	6.531	6.521	6.536	6.498	6.493	6.482

*The degree of polynomial considered in the expansion

3.4 Experimental Design

Experimental work was used to validate the ability of Ritz and meshfree. methods to realistically predict natural frequencies and mode shapes of curvilinear-stiffened plates. A design for a 24 by 28 *in.* plate with two curvilinear stiffeners was chosen. For testing the plate was bolted to a steel bracket to create a clamped condition on one end, while the remaining edges were allowed to remain free. The Virginia Tech Department of Aerospace and Ocean Engineering (AOE) Structures and Engineering Lab's single point Polytec laser vibrometer was used to sense vibration response of the plate to acoustic excitation. MatLab® and STAR Modal® [85] were used for data collection and data analysis, respectively.

- ***Experiment Models and Equipment***

A 24 by 28 *in.* curvilinear-stiffened plate was fabricated from 2219 – T851 Aluminum in the AOE Machine Shop. The geometric and material properties [86] of the plate are shown in Fig. 3-5. The plate had thickness near a quarter of an inch, and identically shaped curvilinear stiffeners, each about one half inch tall and one eighth inch wide. The plate was clamped at one end during testing to a steel bracket bolted to a heavy steel frame table. Notches at either end of this boundary condition were designed to mechanically separate the main plate from the clamped extra material. Also, the stiffeners of this plate were shortened by approximately one half inch on either end and beveled at either end at an angle of 30 degrees.

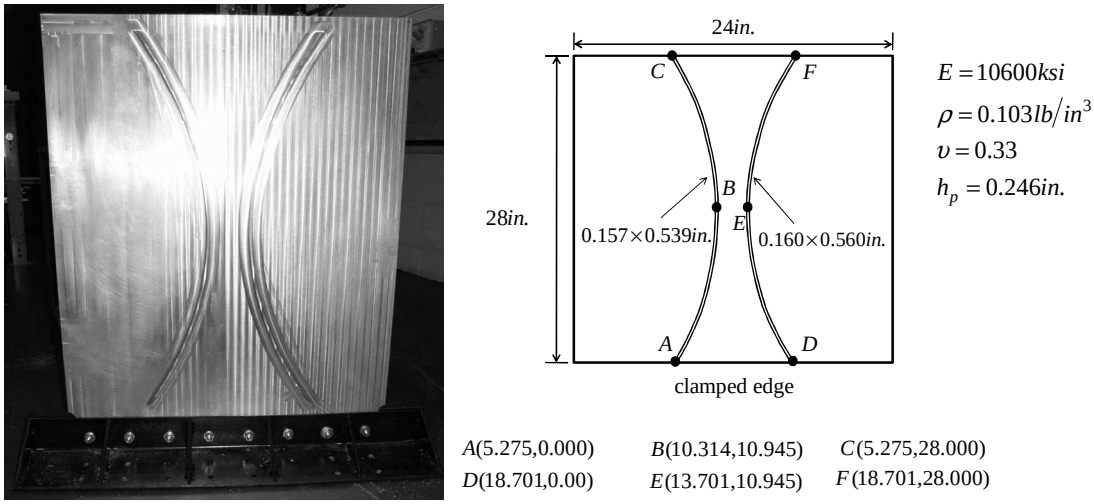

Fig. 3-5 Curvilinear-stiffened plate bolted to mounting bracket for experimental testing.

Electronic interfaces were handled with a dSpace PPC Controller Board. An analog signal was sent from a PC through a generic Crown signal amplifier to a Cerwin-Vega! 3-in-1 public address speaker which was used for excitation. Single point measurements were taken by a Polytec OFV-505 Laser Vibrometer, which was positioned using Newport linear motion stages. The analog signal from the Vibrometer was sent through a Multimetrics, Inc. AF-4201 high-pass filter before being converted to a

digital signal and stored in the same PC as above. Through MatLab® and dSpace Control Desk, the experiment was controlled, including signal creation, stage motion and positioning, data collection, pre-processing and storage. The lab setup can be seen in Fig. 3-6. The experimental procedure is detailed in the following section.

Fig. 3-6 Laser vibrometer and support equipment in place for testing, photo taken by author, 2011.

- ***Experimental Procedure***

A MatLab® Graphical User Interface (GUI) was created to automate the experiment and control each of the components linked through the dSpace control board. A 24 by 24 point square grid with 1 *in.* spacing was used to locate the laser at each measurement point. The 23 by 23 *in.* measured area of the plate was determined by the limitations of the linear motion stages length. Once the vibrometer was positioned, the plate was excited by 3 sign pulse waves in the range 0 to 300 Hz. The recorded response for each of the five excitation iterations was averaged. The Frequency Response Function (FRF) was calculated from the averaged response information for each point and stored in local memory until all measurements were complete. After all the measurements were taken at all the 576 points, they were written in Universal File Format (UFF) and saved to the hard drive of a PC.

Following the initial measurements, experimentation was completed by post-analysis done with STAR Modal® software. A model was created to mimic the grid of measurement points discussed above. Once the correct relationships between the measurement points was established, the UFF file containing the FRF was

loaded and assigned to the model. With this information, STAR graphically constructs the plate vibration shape at each frequency within the measurement spectrum. Use of curve fitting is necessary to identify the frequencies of the modal peaks in the FRF. These frequencies and the corresponding mode shapes are the experimental natural frequencies and mode shapes of vibration and are presented in the next section.

- ***Results and Discussion***

The analytic predictions and experimental results for the vibration mode shapes and frequencies of the curvilinear-stiffened plate are presented in Fig. 3-7. In the Ritz method Chebyshev polynomials up to fourteenth order are used and in the meshfree, 22×22 particles and 60 particles are considered for the plate and stiffeners, respectively. The mode shapes in Fig. 3-7 are ordered numerically with respect to the corresponding frequency in Hz. All of the mode shapes are presented with the clamped side at the bottom of the curvilinear-stiffened rectangle. Although the experimental plate was 24 by 28 in. and the analytic plates were also dimensioned to represent the same area, only a 23 by 23 in. area was picked to represent each mode shape in Fig. 3-7. This is to represent the 23 by 23 in. area that was measured experimentally. A reduced area was measured from the full plate size due to movement limitations of the linear actuation stages. Rather than reposition the stages and overlay the results, a 23 by 23 in. area was picked in the center of the plate to represent the plate response. From the results, this area appears to be sufficient. Overall, the mode shapes correspond well with the appropriate Ritz and meshfree predictions with a few discrepancies. These discrepancies and other interesting characteristics are noted in the following section.

It can be noted that the analytical frequencies were consistently predicted to be higher than the experimental results shown. The discrepancy varied between 5% and 12% for all of the experimental modes that were successfully documented from the experimental results. The lone mode shape which was not predicted with error in this range was the fundamental mode. The larger error present in the analytic prediction of this mode can be attributed to its location below the lower limit of the operating range of the speaker used for excitation, which was 25 Hz. Also, since this discrepancy is fairly uniform, perhaps an estimation method for reducing this error or the cause could be found and removed although that cause is unknown at this time.

It is also of interest to compare the CPU time of the Ritz and meshfree methods. The algorithms for both methods are coded in MatLab® and run on a same computer and it is found that the meshfree code is 15% more efficient in terms of CPU time than the Ritz code. However it should be noted that the Ritz method code is simpler, more understandable and easier to debug than the meshfree code.

First mode = 13.34 **Meshfree**

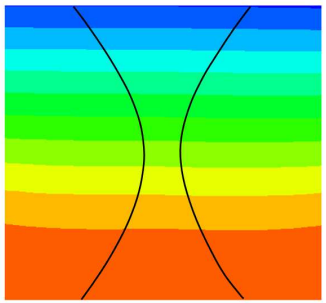

First mode = 13.18 **Ritz Method**

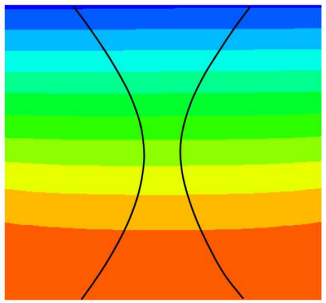

First mode = 8.98 **Experimental**

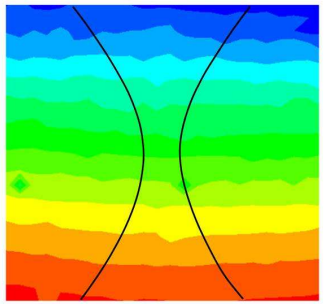

Second mode = 29.80 **Meshfree**

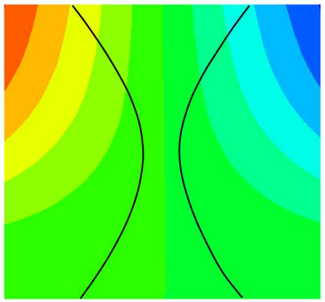

Second mode = 29.68 **Ritz Method**

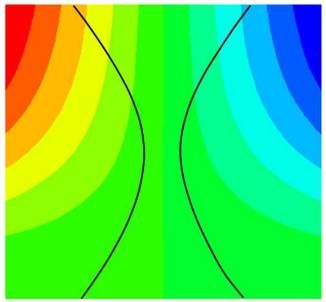

Second mode = 26.91 **Experimental**

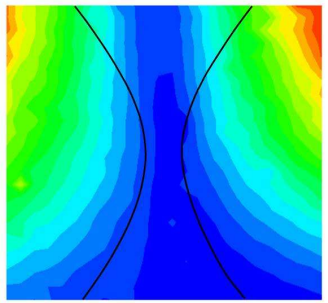

Third mode = 79.96 **Meshfree** Third mode = 80.34 **Ritz Method** Third mode = 70.81 **Experimental**

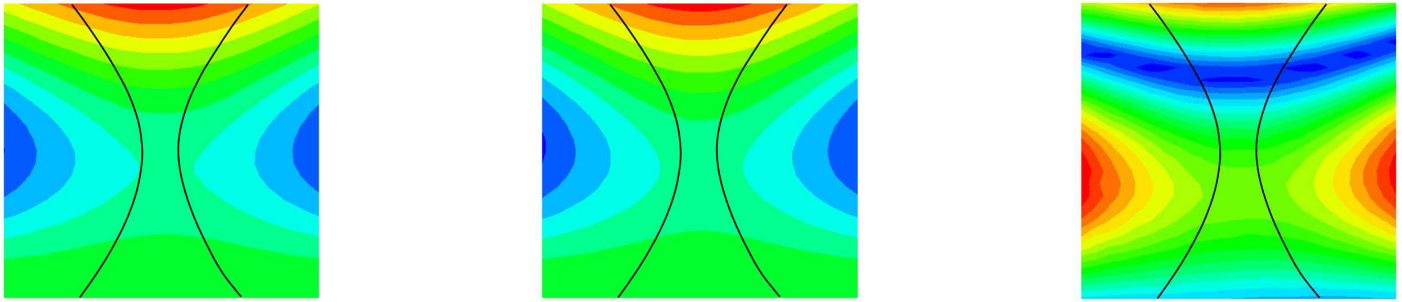

Fourth mode = 108.85 **Meshfree** Fourth mode = 109.18 **Ritz Method** Fourth mode = 103.34 **Experimental**

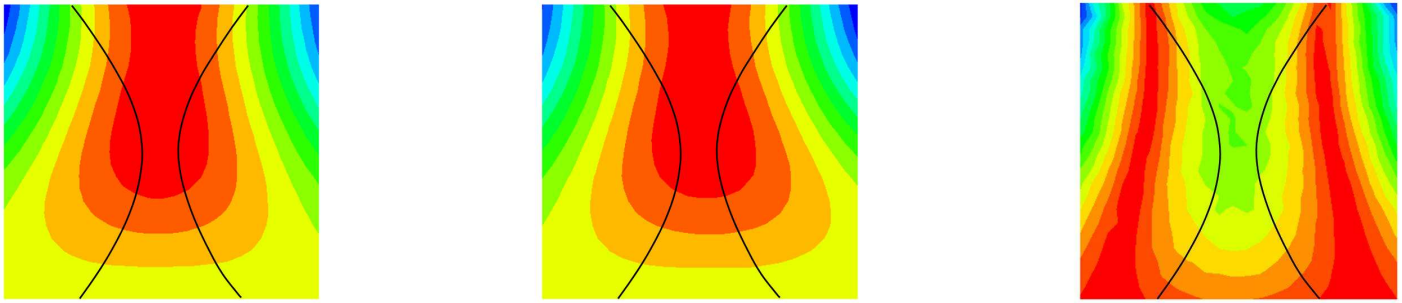

Fig. 3-7 Comparison of analytic and experimental mode shapes

The fifth mode is indeed missing from the experimental results. Noting that the frequency difference between the fourth and fifth modes is less than 1 percent, a likely cause is that the amplitude of the fourth mode response is higher in magnitude. For the precision that these measurements were taken with, the fourth mode response may mask the fifth mode.

Some other discrepancies in the results are as follows. The experimentally found second mode has the same general shape as the two analytic predictions, but the resulting shape is symmetric rather than asymmetric with respect to the free corners. A similar pattern is seen in the third mode where the free side displacements in the experimental result are all in the same direction, whereas the analytic mode shapes feature opposite displacement directions on the vertical free sides than the horizontal free side. Also, in the fifth mode, the maximum displacement region in the center is split into a "U"-shaped region by a medium amplitude region. Finally, this same phenomenon is present in the sixth mode.

It is believed that any other imperfections or asymmetries are present only due to material and plate imperfections inherent in any real plate. Furthermore, the boundary conditions at the clamped edge may not be perfectly clamped. This can explain a lower value of the natural frequencies obtained in the experimental results. Overall, the experimental predictions appear to correlate well with the meshfree and Ritz analytic predictions for a plate with curvilinear stiffeners.

3.5 Conclusions

The formulation of plate with curvilinear stiffeners using Ritz method based on First Order Shear Deformation Theory (FSDT) is presented. The Chebyshev polynomials are used in the Ritz method. Since the stiffness and mass matrices of the stiffened plate are obtained by superimposing the stiffness and mass matrices of the plate and stiffeners, for modifying the stiffener geometric the plate geometry does not need to be changed. The boundary conditions are imposed by using a set of polynomials which gives us the capability to impose different kinds of boundary conditions. The developed formulation can be applied to arbitrary curvilinear stiffeners. The accuracy of the present formulation was verified through several comparisons with other results available in the literature. The numerical examples indicate that using Chebyshev polynomials up to fourteenth order as the basis functions in the Ritz method can estimate the first six natural frequencies with a good convergence. From the experimental studies, the following conclusions can be made. A 23 by 23 *in.* experimentally measured area of a 24 by 28 *in.* curvilinear-stiffened plate seems to validate the analytical predictions accomplished using Ritz and meshfree methods. Overall, the frequencies are over-predicted, but in a seemingly consistent manner (experimental results are lower than the analytical results) that would suggest a relationship (e.g. the clamped edge not being perfectly clamped) could be established for the difference between analytic and experimental frequencies. The fifth mode was not found experimentally, most likely due to its proximity to the stronger fourth mode.

Other discrepancies were either minor shape or symmetry differences. Overall the experiment results seem to correspond well to the predictions, both in terms of mode shape and placement in the frequency domain.

4 Buckling and Static Analysis of Curvilinearly Stiffened Plates Using Meshfree Method

4.1 Introduction

In this section, the Element Free Galerkin (EFG) method is employed for buckling and static analysis of stiffened plates. The formulation allows the placement of any number of arbitrarily curvilinear stiffeners within a plate. The First Order Shear Deformation Theory (FSDT) is used to model the behavior of the plate and the stiffener. Moving Least Squares (MLS) approximation is used to construct the shape functions. One of the major difficulties in the implementation of some meshfree methods is the imposition of essential boundary conditions as the approximations do not pass through the nodal parameter values. In this research, the penalty method is used for satisfying the boundary conditions. A meshfree method frees the user from providing a nodal line on the plate along every stiffener. This is very beneficial for performing optimization studies. Several numerical examples using both straight and curvilinear stiffeners are obtained and compared with those available in the literature and those obtained using ANSYS®. This demonstrates the validity of the presented approach.

4.2 Formulation of the Problem

- ***Potential Energy of the Plate***

For the buckling analysis, the bending moments developed due to the action of inplane loads are considered. Thus the nonlinear terms in strain-displacement relations are considered. Inplane displacements have not been taken into account for the formation of geometric stiffness matrices, as they would increase the complexity of the formulation without any significant improvement in results [55]. The nonlinear terms in the plate strain terms are [55]

$$\varepsilon_{Gp}=\begin{Bmatrix} \frac{1}{2}\left(\frac{\partial w}{\partial x}\right)^2+\frac{z^2}{2}\left(\frac{\partial \varphi_{px}}{\partial x}\right)^2+\frac{z^2}{2}\left(\frac{\partial \varphi_{py}}{\partial x}\right)^2 \\ \frac{1}{2}\left(\frac{\partial w}{\partial y}\right)^2+\frac{z^2}{2}\left(\frac{\partial \varphi_{px}}{\partial y}\right)^2+\frac{z^2}{2}\left(\frac{\partial \varphi_{py}}{\partial y}\right)^2 \\ \left(\frac{\partial w}{\partial x}\right)\left(\frac{\partial w}{\partial y}\right)+z^2\left(\frac{\partial \varphi_{px}}{\partial x}\right)\left(\frac{\partial \varphi_{px}}{\partial y}\right)+z^2\left(\frac{\partial \varphi_{py}}{\partial x}\right)\left(\frac{\partial \varphi_{py}}{\partial y}\right) \end{Bmatrix} \tag{4-1}$$

where w is the displacement components along the z directions, φ_{px} and φ_{py} are the rotations with respect to the y and x axis and p indicates the plate. Eq. (4-1) can be written as

$$\varepsilon_{Gp}=\frac{1}{2}[A_p][H_p]\{\varepsilon_{Np}\} \tag{4-2}$$

where

$$\left[A_p\right]=\begin{bmatrix} \frac{\partial w}{\partial x} & 0 & z\frac{\partial \varphi_{px}}{\partial x} & 0 & z\frac{\partial \varphi_{py}}{\partial x} & 0 \\ 0 & \frac{\partial w}{\partial y} & 0 & z\frac{\partial \varphi_{py}}{\partial y} & 0 & z\frac{\partial \varphi_{px}}{\partial y} \\ \frac{\partial w}{\partial y} & \frac{\partial w}{\partial x} & z\frac{\partial \varphi_{px}}{\partial y} & z\frac{\partial \varphi_{py}}{\partial x} & z\frac{\partial \varphi_{py}}{\partial y} & z\frac{\partial \varphi_{px}}{\partial x} \end{bmatrix} \quad [H_p]=\begin{bmatrix} 1 & & & & & \\ 0 & 1 & & & \textit{sym.} & \\ 0 & 0 & z & & & \\ 0 & 0 & 0 & z & & \\ 0 & 0 & 0 & 0 & z & \\ 0 & 0 & 0 & 0 & 0 & z \end{bmatrix} \tag{4-3}$$

and

$$\varepsilon_{Np}=\begin{bmatrix} \frac{\partial w}{\partial x} & \frac{\partial w}{\partial y} & \frac{\partial \varphi_{px}}{\partial x} & \frac{\partial \varphi_{py}}{\partial y} & \frac{\partial \varphi_{py}}{\partial x} & \frac{\partial \varphi_{px}}{\partial y} \end{bmatrix}^T \tag{4-4}$$

The potential of the membrane forces in the plate is given by:

$$W_p=-\int_V \varepsilon_{Gp}^T\tau_{Gp}\,dV \tag{4-5}$$

where

$$\tau_{Gp}=\begin{Bmatrix} \sigma_x \\ \sigma_y \\ \tau_{xy} \end{Bmatrix} \tag{4-6}$$

It can be shown that the potential of the membrane force can be written as [87]:

$$W_p=-\frac{1}{2}\int_A \varepsilon_{Np}^T\sigma_p\varepsilon_{Np}dA \tag{4-7}$$

where

$$\sigma_p = \begin{bmatrix} \sigma_x h & & & & & \\ \tau_{xy} h & \sigma_y h & & & & \\ 0 & 0 & \frac{h^3}{12}\sigma_x & & sym. & \\ 0 & 0 & 0 & \frac{h^3}{12}\sigma_y & & \\ 0 & 0 & 0 & \frac{h^3}{12}\tau_{xy} & \frac{h^3}{12}\sigma_x & \\ 0 & 0 & \frac{h^3}{12}\tau_{xy} & 0 & 0 & \frac{h^3}{12}\sigma_y \end{bmatrix} \tag{4-8}$$

By using MLS basis function and Eq. (4-4) can be written as

$$\varepsilon_{Np} = B_{Np}\delta_p \qquad [B_{Np}]_i = \begin{bmatrix} 0 & 0 & 0 & 0 & \frac{\partial N_{pi}}{\partial x} \\ 0 & 0 & 0 & 0 & \frac{\partial N_{pi}}{\partial y} \\ 0 & 0 & \frac{\partial N_{pi}}{\partial x} & 0 & 0 \\ 0 & 0 & 0 & \frac{\partial N_{pi}}{\partial y} & 0 \\ 0 & 0 & 0 & \frac{\partial N_{pi}}{\partial x} & 0 \\ 0 & 0 & \frac{\partial N_{pi}}{\partial y} & 0 & 0 \end{bmatrix} \tag{4-9}$$

By substituting Eq. (4-9) in (4-7)

$$W_p = -\frac{1}{2}\delta_p{}^T \int_A B_{Np}^T \sigma_p B_{Np} dA \delta_p \tag{4-10}$$

- ***Potential Energy of a Stiffener***

The nonlinear part of the stiffener strain is:

$$\varepsilon_{Gs} = \frac{1}{2}\left(\frac{1}{\det J}\frac{dw}{d\zeta}\right)^2 + \frac{z^2}{2}\left(\frac{1}{\det J}\frac{d\theta_t}{d\zeta} + \frac{\theta_n}{R(\zeta)}\right)^2 + \frac{z^2}{2}\left(\frac{1}{\det J}\frac{d\theta_n}{d\zeta} - \frac{\theta_t}{R(\zeta)}\right)^2 \tag{4-11}$$

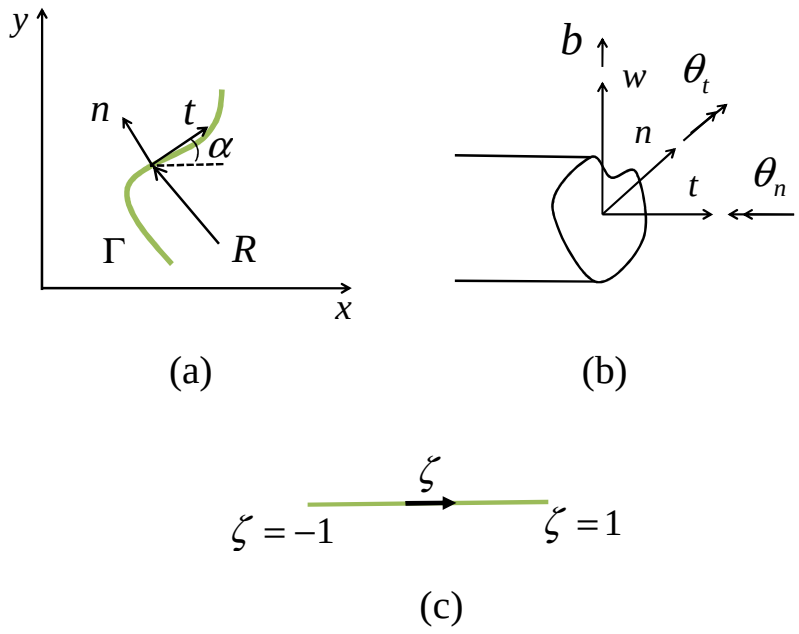

Fig. 4-1 (a) Local and global coordinate systems for curvilinear stiffener (b) Directions of the generalized displacements of the stiffener (c) The transformed plane of curvilinear stiffener

where *detJ* is the Jacobian of the transformation, $R(\zeta)$ is radius of curvature (Fig. 4-1a) and ζ is the natural coordinate for parameterizing the curve (Fig. 4-1c), which they are described in [36], θ_t, θ_n and w, which are the rotations and deflection, are shown in Fig. 4-1b. Eq. (4-11) can be written as

$$\varepsilon_{Gs} = \frac{1}{2}[A_s][H_s]\{\varepsilon_{Ns}\} \tag{4-12}$$

where

$$[A_s] = \left[\frac{1}{\det J}\frac{dw}{d\zeta} \quad z\left(\frac{1}{\det J}\frac{d\theta_t}{d\zeta} + \frac{\theta_n}{R(\zeta)}\right) \quad z\left(\frac{1}{\det J}\frac{d\theta_n}{d\zeta} - \frac{\theta_t}{R(\zeta)}\right)\right] \quad [H_s] = \begin{bmatrix} 1 & & sym. \\ 0 & z & \\ 0 & 0 & z \end{bmatrix} \tag{4-13}$$

and

$$\varepsilon_{Ns} = \begin{bmatrix} 0 & 0 & \frac{1}{\det J}\frac{d}{d\zeta} \\ \frac{1}{\det J}\frac{d}{d\zeta} & \frac{1}{R(\zeta)} & 0 \\ -\frac{1}{R(\zeta)} & \frac{1}{\det J}\frac{d}{d\zeta} & 0 \end{bmatrix} \begin{Bmatrix} \theta_t \\ \theta_n \\ w \end{Bmatrix} = L_{Ns}u_s' \tag{4-14}$$

The potential of the membrane forces in the stiffener is given by:

$$W_s = -\int_V \varepsilon_{Gs}\sigma_t \, dV \tag{4-15}$$

where σ_t is the axial stress of the stiffener. It can be shown that [87]

$$W_s = -\frac{1}{2}\int_{-1}^{1} \varepsilon_{Ns}^T \sigma_s \varepsilon_{Ns} \det J d\zeta \tag{4-16}$$

where

$$\sigma_s = \begin{bmatrix} \sigma_t A & 0 & 0 \\ 0 & \sigma_t I_n & 0 \\ 0 & 0 & \sigma_t I_n \end{bmatrix} \tag{4-17}$$

In the above equation, A is the cross sectional areas; I_n = second moment of the stiffener cross section area about the reference axis. The displacement fields in terms of global coordinate system are:

$$u_s' = \begin{Bmatrix} u_t \\ v_n \\ \theta_t \\ \theta_n \\ w_s \end{Bmatrix} = \begin{bmatrix} \cos\alpha & \sin\alpha & 0 & 0 & 0 \\ -\sin\alpha & \cos\alpha & 0 & 0 & 0 \\ 0 & 0 & \cos\alpha & \sin\alpha & 0 \\ 0 & 0 & -\sin\alpha & \cos\alpha & 0 \\ 0 & 0 & 0 & 0 & 1 \end{bmatrix} \begin{Bmatrix} u_{s_0} \\ v_{s_0} \\ \varphi_{sx} \\ \varphi_{sy} \\ w_{s_0} \end{Bmatrix} = \Lambda u_s \tag{4-18}$$

where u_{s_0}, v_{s_0} and w_{s_0} are the midplane displacements along the x, y and z directions, respectively, φ_{sx} and φ_{sy} are the rotations with respect to the y and x axis, respectively and α is the angle between the t and x axes (Fig. 4-1a). Eqs. (4-14) and (4-18), the strain in global coordinate system can be written as:

$$\varepsilon_{Ns} = B_{Ns}\Lambda\delta_s \quad [B_{Ns}]_i = \begin{bmatrix} 0 & 0 & 0 & 0 & \frac{1}{\det J}\frac{dN_{si}}{d\zeta} \\ 0 & 0 & \frac{1}{\det J}\frac{dN_{si}}{d\zeta} & \frac{N_{si}}{R} & 0 \\ 0 & 0 & -\frac{N_{si}}{R} & \frac{1}{\det J}\frac{dN_{si}}{d\zeta} & 0 \end{bmatrix} \tag{4-19}$$

Substituting Eq. (4-19) in (4-16), the potential of the membrane forces of a stiffener can be written as

$$W_s = -\frac{1}{2}\delta_s^T \int_{-1}^{1} \Lambda^T B_{Ns}^T \sigma_s B_{Ns} \Lambda \det J d\zeta \, \delta_s \tag{4-20}$$

The stiffener particles parameters can be presented as the plate particles parameters by using a transformation matrix.

$$\delta_s = T_{sp}\delta_p \tag{4-21}$$

- ***Derivation of the Stiffness Matrices and the Force Vector for Static Analysis***

In the formulation of linear Element Free Galerkin method for static analysis, it is assumed that deformations remain small so that linear relations can be used to represent the strain in a body. The emphasis of this section is on developing a formulation for the static analysis of the stiffened plates. Since the nonlinear part of strain is neglected in the static analysis, the total potential energy can be rewritten as:

$$\Pi_{st} = U_p + U_s - \int_{\Gamma_t} u^T f \, d\Gamma + \frac{\alpha_p}{2} \int_{\Gamma_u} (u-\bar{u})^T (u-\bar{u}) \, d\Gamma \tag{4-22}$$

By substituting the strain energy of plate and stiffener in Eq. (4-22) and using the variation of the potential energy (Π_{st}), the mathematical model for the static analysis stiffened plate is found to be

$$\begin{aligned} &\delta(\delta_p^T(\frac{1}{2}(\int_A B_p^T D_p B_p dA + T_{sp}^T \int_{-1}^{1} \Lambda^T B_s^T D_s B_s \Lambda \det J d\zeta T_{sp} + \\ &\alpha_p \int_{\Gamma_u} N_p^T N_p d\Gamma)\delta_p - \alpha_p \int_{\Gamma_u} N_p^T \bar{u} d\Gamma - \int_{\Gamma_t} N_p^T f d\Gamma)) = 0 \end{aligned} \tag{4-23}$$

Solving the above equation will result in equilibrium equation

$$\begin{aligned} &\left(K_p + K_s\right)\delta_p = F \\ &F = \int_{\Gamma_t} N_p^T f d\Gamma + \alpha_p \int_{\Gamma_u} N_p^T \bar{u} d\Gamma \end{aligned} \tag{4-24}$$

- ***Derivation of the Geometric Stiffness Matrices for Buckling Analysis***

For conducting the buckling analysis, the nonlinear terms in the strain will be considered. The equation for the stability problem can be obtained by defining the total potential energy as:

$$\Pi_G = U_p + U_s + W_p + W_s + \frac{\alpha_p}{2} \int_{\Gamma_u} (u-\bar{u})^T (u-\bar{u}) \, d\Gamma \tag{4-25}$$

By using the variation of the potential energy (Π_G)

$$\begin{aligned} &\delta(\delta_p^T((\frac{1}{2}(\int_A B_p^T D_p B_p dA + T_{sp}^T \int_{-1}^{1} \Lambda^T B_s^T D_s B_s \Lambda \det J d\zeta T_{sp} + \alpha_p \int_{\Gamma_u} N_p^T N_p d\Gamma) - \\ &\int_A B_{Np}^T \sigma_p B_{Np} dA - T_{sp}^T \int_{-1}^{1} \Lambda^T B_{Ns}^T \sigma_s B_{Ns} \Lambda \det J d\zeta T_{sp})\delta_p - \alpha_p \int_{\Gamma_u} N_p^T \bar{u} d\Gamma)) = 0 \end{aligned} \tag{4-26}$$

The above equation will give the linear eigenvalue problem

$$K_p + K_s - \lambda_b (K_{Gp} + K_{Gs}) = 0 \tag{4-27}$$

where K_{Gs} and K_{Gp} are the assembled geometric stiffness matrices for stiffeners and plate, respectively:

$$\begin{aligned} K_{Gp} &= \int_A B_{Np}^T \sigma_p B_{Np} dA \\ K_{Gs} &= T_{sp}^T \int_{-1}^{1} \Lambda^T B_{Ns}^T \sigma_s B_{Ns} \Lambda \det J d\zeta T_{sp} \end{aligned} \tag{4-28}$$

4.3 Results and Discussion

To demonstrate the versatility and to validate the method, buckling analysis of several plates with different stiffeners, both straight and curvilinear, are carried out and the results are compared with the existing ones or with those obtained using ANSYS, a commercially available software. Generally speaking, this method is applicable to plates with different kinds of stiffeners. The selected examples are for comparison purpose only and do not represent the full capabilities of the proposed method. A rectangular domain is considered and the scaling factor of 4, in both *x* and *y* directions, for all examples is used (see [24] for details). To evaluate the integrals in all equations over each cell, the Gauss integration rule with 16 integration points in each cell are used.

- ***A Simply-Supported Plate with a Single Stiffener***

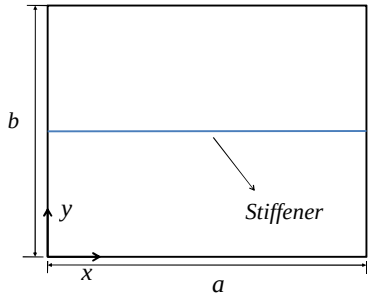

Fig. 4-2 Plate with a single stiffener

First, the buckling analysis of a series rectangular plate simply supported on all four edges and with one central stiffener has been considered as shown in Fig. 4-2. The plate is under uniaxial inplane compression in the *x* direction. The results are compared with those available in Timoshenko and Gere [77] [48]. Mukhopadhyay and Mukherjee [55] solved this problem by using isoparametric stiffened plate bending element. In their research, the stiffener can be positioned anywhere within the plate element. The plate and the stiffener are made of the same material, with Poisson's ratio $\upsilon = 0.3$. The buckling parameter is defined as:

$$\lambda = \frac{\sigma_{cr} b^2 h_p}{\pi^2 D} \tag{4-29}$$

where σ_{cr} and D are the critical stress and the flexural rigidity of the plate. The ratio of the cross sectional area of the stiffener to that of the plate is defined by $\delta = b_s h_s / b h_p$ where b_s and h_s are the width and

the height of the stiffener. The ratio of the bending stiffness of the stiffener to that of the plate is defined by $\gamma = E_s I_s / bD$.

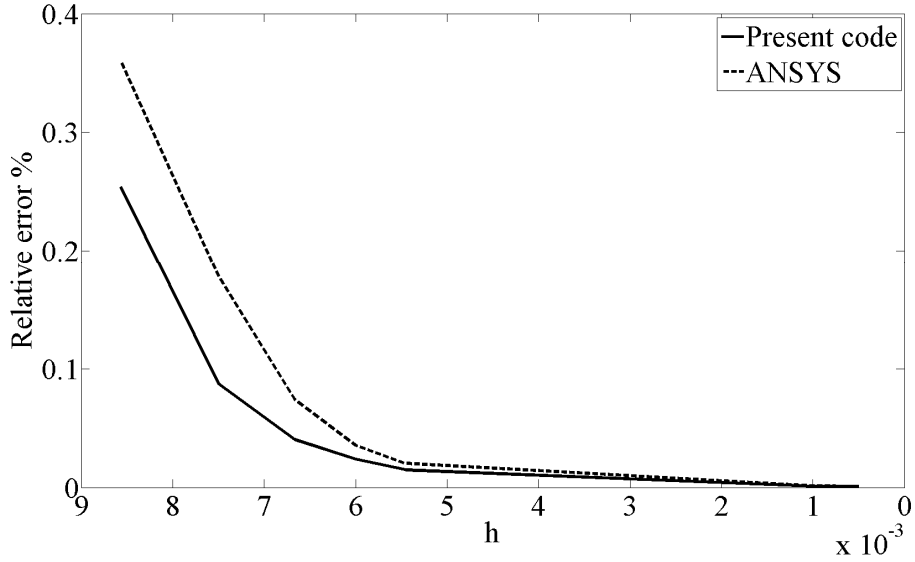

Fig. 4-3 Relative error in buckling parameter using meshfree and ANSYS®

The accuracy of the present code is evaluated by considering the relative error and investigating the convergence. In ANSYS® the nodes of stiffener should match the nodes of plate, however, as has been mentioned before, in a meshfree method, there is no need of having the particles of a stiffener and those of the plate to coincide. The relative error in the results given by this code with respect to a meshfree scheme with 24×24 particles for the plate and 24 particles for the stiffeners is calculated. Also, convergence for the ANSYS® results has been carried out. The relative error of the ANSYS® is with respect to 24×24 nodes and *h* is the distance between two particles and nodes in meshfree and ANSYS®, respectively. For comparison, the numerically obtained convergence curve of meshfree and ANSYS® are compared and plotted in Fig. 4-3. From this figure, it can be seen that the meshfree method has a better rate of convergence. Also the accuracy of meshfree, as can be observed from the same figure, is slightly better than ANSYS®.

Table 4-1 shows the buckling parameter compared with the other results which are available in the literature (aspect ratio (a/b)=1, $GJ/Db_s = 0$). It can be seen that there is a good agreement between the results of the present analysis and those that can be found in the literature. It is observed from this table that γ has an important effect on the buckling of the stiffened plate.

In the next step, the static analysis of the simply supported square plate with one stiffener at the center as shown in Fig. 4-4, is considered. The plate is subjected to a uniformly distributed load of 1.0 psi. The elastic modulii of both the plate and stiffener materials are same, 17×10^6psi. The Poisson ratio for both is 0.3.

Table 4-1 The buckling parameters for rectangular stiffened plates with varying stiffener rigidity

$\gamma = 5$			
δ	Timoshenko and Gere [77]	Mukhopadhyay and Mukherjee [55]	Meshfree
0.05	12	11.72	11.71
0.1	11.1	10.93	10.94
0.2	9.72	9.7	9.61
$\gamma = 10$			
δ	Timoshenko and Gere [77] [48]	Mukhopadhyay and Mukherjee [55]	Meshfree
0.05	16	16	15.85
0.1	16	16	15.86
0.2	15.8	15.44	15.37
$\gamma = 15$			
δ	Timoshenko and Gere [77] [48]	Mukhopadhyay and Mukherjee [55]	Meshfree
0.05	16	16	15.86
0.1	16	16	15.86
0.2	16	16	15.87

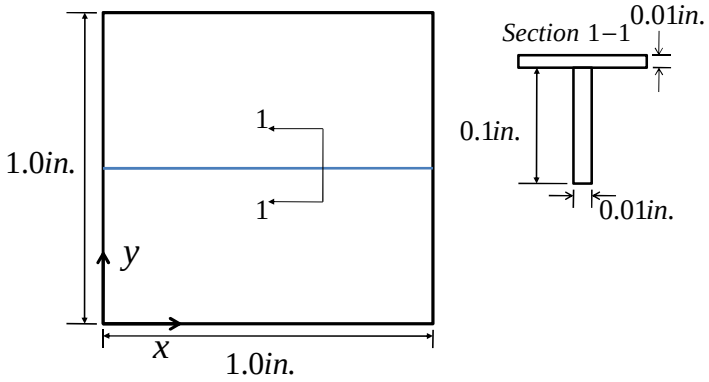

Fig. 4-4 Simply supported square plate stiffened centrally by one stiffener.

This example was solved by Peng *et al.* [24]. They solved the problem by using EFG, however in their formulation the stiffeners must be in *x* or *y* directions. This problem also has been solved by Rossow and Ibrahimkhail [88] and McBean [89] using the FEM. In the present formulation, since the stiffeners can posses any direction or curvature, it has more degrees of freedom than what Peng *et al*. [24] considered in their formulation. The results for eccentrically and concentrically stiffened plate are provided in Fig. 4-5. As can be seen in this figure, the results are close to what are available in the literature.

- ***A Simply-Supported Plate with Two Stiffeners***

A plate with two stiffeners and all edges simply supported analyzed by Timoshenko and Gere [77] and by Peng *et al.* [25] is selected as the second example. The geometry of the plate and the stiffeners are shown in Fig. 4-6. The plate is under uniaxial inplane compression along the *x* direction. Parametric studies were conducted for plate aspect ratios (a/b). The buckling parameters obtained using meshfree for $\delta = 0.05$ and $\gamma = 10/3$ are compared with other results in Fig. 4-7. As can be seen in this figure, the results are in good agreement with other available results.

The static analysis of the plate with orthogonal stiffeners has been conducted by considering the stiffeners in both concentric and eccentric configuration. The geometric and material properties of the stiffeners and the plate are shown in Fig. 4-8. The plate is subjected to a uniformly distributed load of 10.0psi. The boundary conditions are taken to be simply supported. Peng *et al.* [24] solved this problem using EFG by considering straight stiffeners in the *x* or *y* directions. The problem was also solved by Rossow and Ibrahimkhail [88] and Chang [90]. The deflection along *x*=7.5*in.* for concentric stiffeners and *x*=15*in.* for eccentric stiffeners are shown in Fig. 4-9. Also the moment Mx for concentric and eccentric stiffeners along *y*=30*in.* are demonstrated in this figure. The deflection and moment agree closely with other available results. As can be seen, the agreement between the two sets of results for the concentric stiffeners is closer than that for eccentric stiffeners. This difference arises due to the differences between the plate and beam deformation theories, the method used in considering the effect of stiffener eccentricity in the stiffness matrix, and the differences in the shape functions used in the mentioned references and in this research.

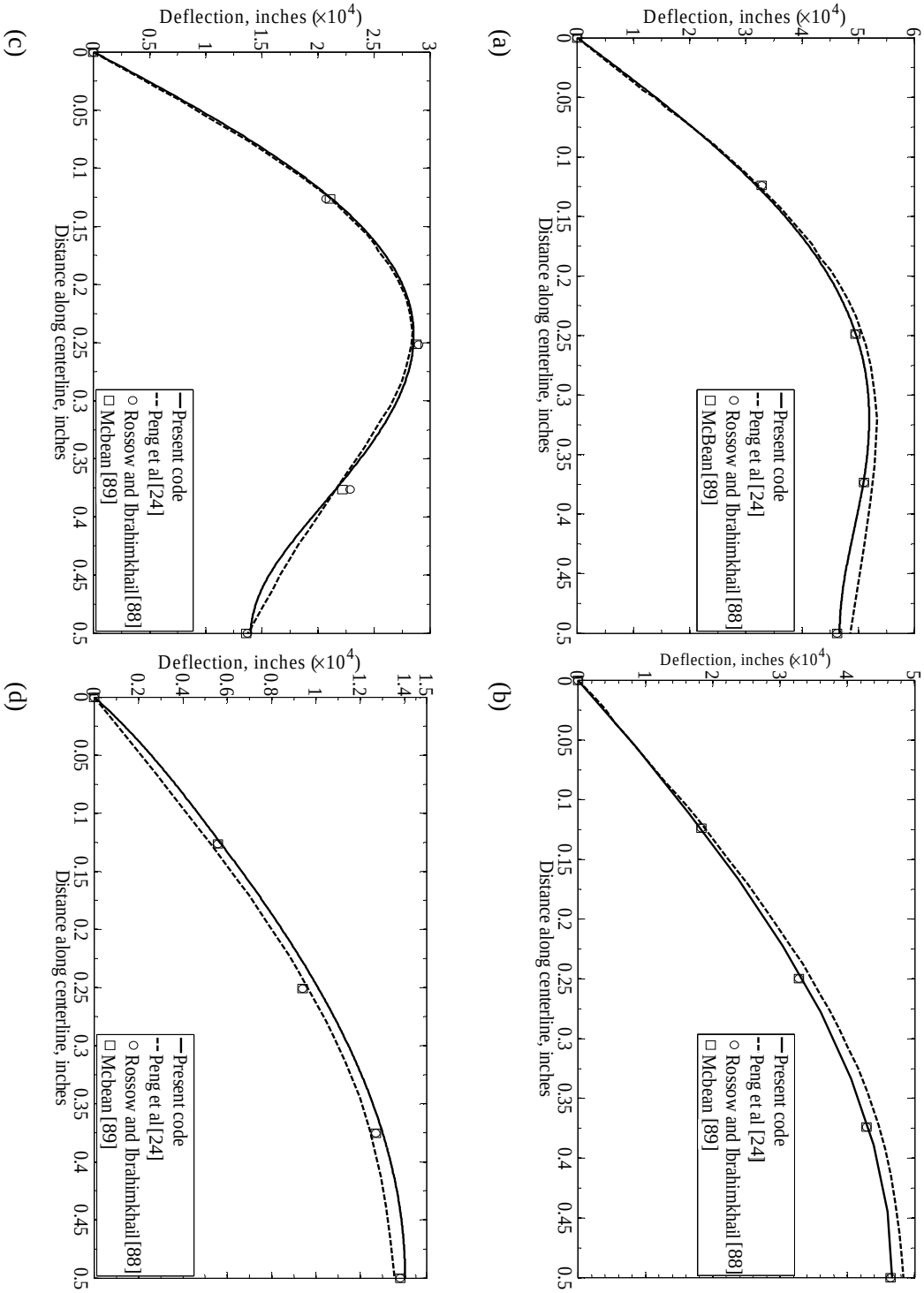

Fig. 4-5 (a) Deflection along centerline (x=0.5 in) (b) Deflection along centerline (y=0.5 in) of the concentrically stiffened plate (c) Deflection along centerline (x=0.5 in) (d) Deflection along centerline (y=0.5 in) of the eccentrically stiffened plate

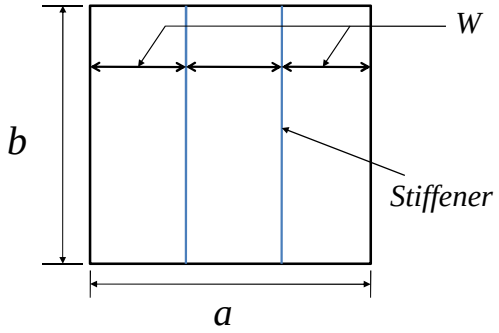

Fig. 4-6 A square plate with double stiffeners

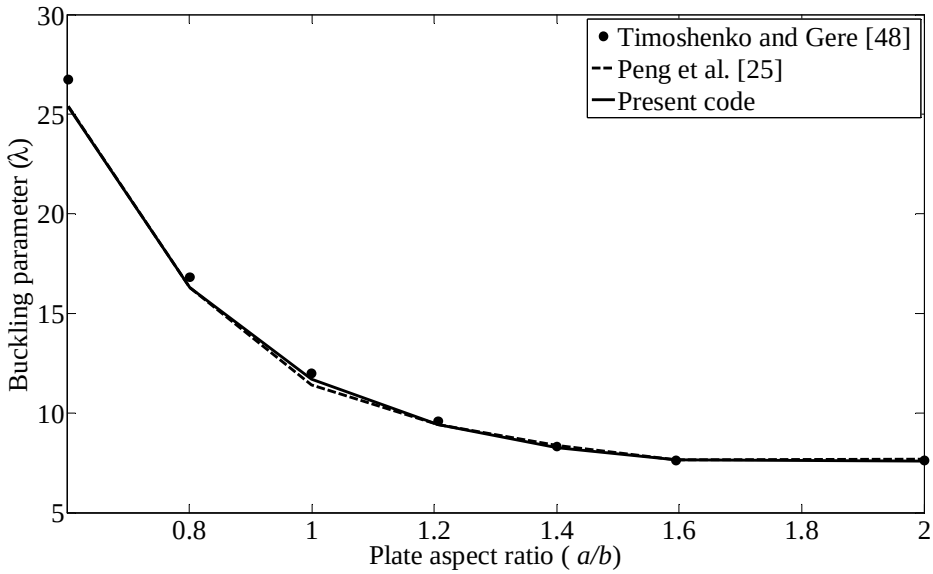

Fig. 4-7 Buckling parameter of plate stiffened by two stiffeners for different plate aspect ratios

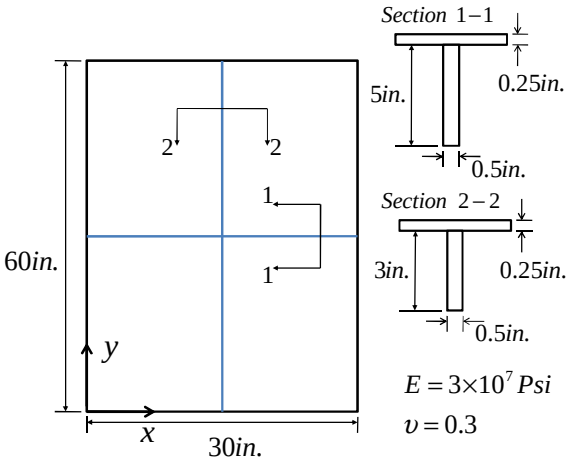

Fig. 4-8 Rectangular plate stiffened by two stiffeners

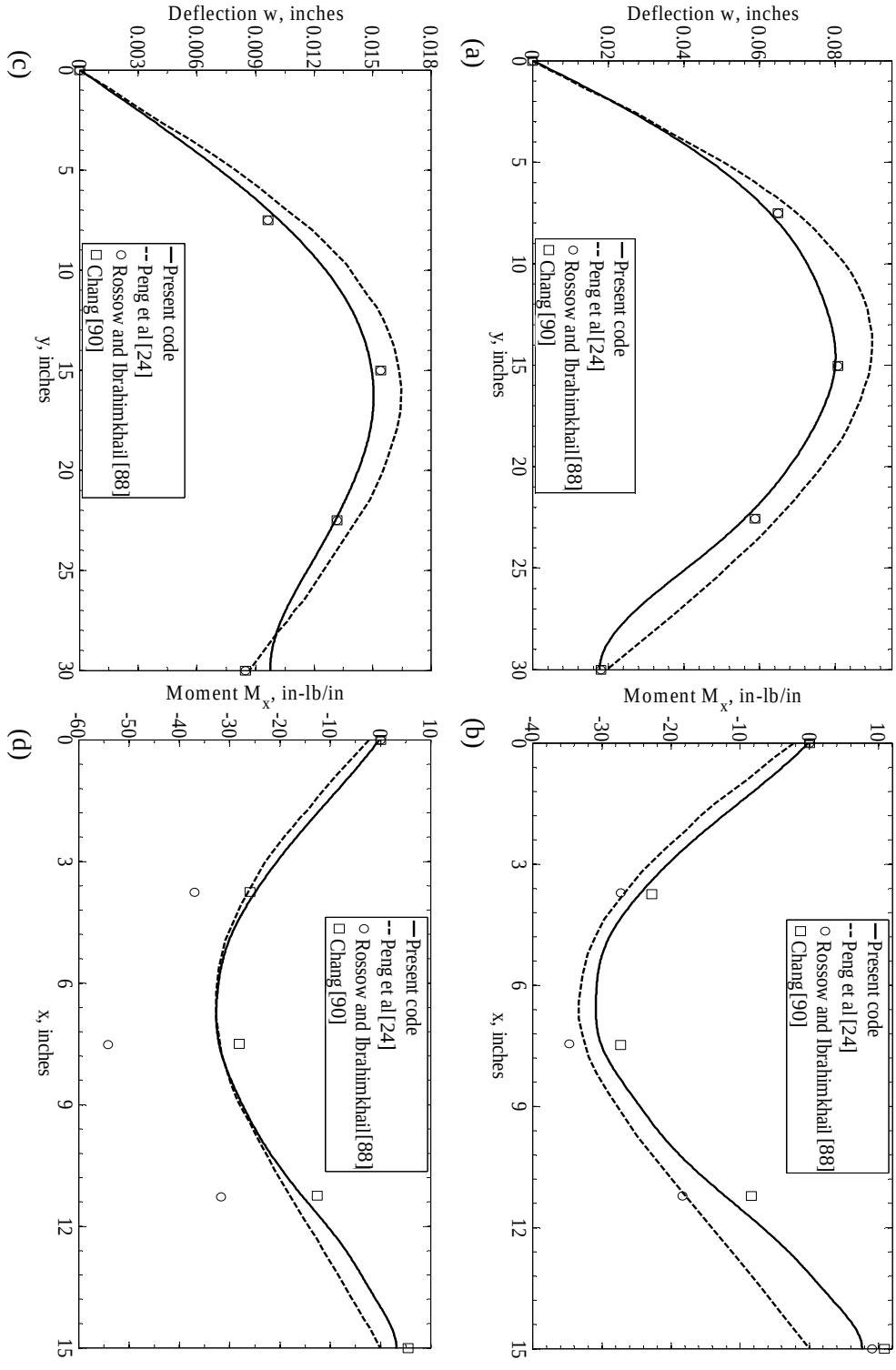

Fig. 4-9 (a) Deflection at *x*=7.5*in.* (b) Moment Mx at *y*=30*in.*: Plate under distributed load is stiffened by concentric stiffeners (c) Deflection at *x*=15*in.* (b) Moment Mx at *y*=30*in.*: Plate under distributed load is stiffened by eccentric stiffeners

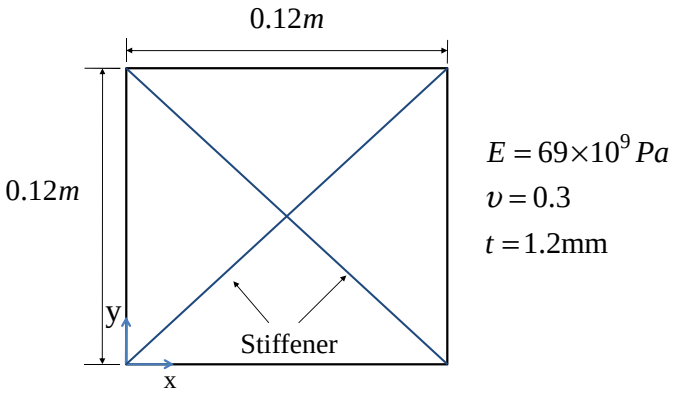

Fig. 4-10 A square plate with inclined stiffeners

- ***A Simply-Supported Plate Having Two Inclined Stiffeners***

In this example, an eigenvalue analysis for determining buckling load is performed for the plate with inclined stiffeners subjected to biaxial compression. To check the accuracy of the present meshfree code, results for inclined stiffeners are compared with those obtained using ANSYS®. From the ANSYS® library, 2250 SHELL63 and 100 BEAM188 are chosen for modeling the plate and stiffeners, respectively. The geometric and material properties of the stiffened plate are demonstrated in Fig. 4-10. In the meshfree code, 22×22 particles and 60 particles are considered for the plate and stiffeners, respectively. The buckling parameters obtained for $\delta=0.1$ and $\gamma=10$ related to eccentric and concentric stiffeners. Accurate estimates of buckling parameters are achieved and the results are presented in Fig. 4-11.

In Fig. 4-12, deflections and bending moments per unit length are plotted along the centerline of the same plate when subjected to the distributed load of 10kPa. Both concentric and eccentric stiffeners are considered in this example. Excellent agreement is observed. As might be expected, the eccentric stiffener can decrease both the stresses and the deflection of the plate.

- ***A Simply-Supported Plate with a Curvilinear Stiffener***

The next example considered in this study is the stability of a square plate with curvilinear stiffener subjected to biaxial compression. The stiffener configuration, plate geometry and material properties are described in Fig. 4-13 ($\delta=0.1$ and $\gamma=10$). For comparison purposes, the complete stiffened plate was modeled in ANSYS® with an irregular mesh composed of 2850 SHELL63 elements for modeling the plate and 60 BEAM188 elements for modeling each stiffener. Modeling a plate stiffened by curvilinear stiffeners in ANSYS® needs a significant care in defining the stiffener geometry, since the stiffener elements must be placed along the mesh lines. In the meshfree formulation, 24×24 particles and 40 particles are used to discretize the plate and the stiffener, respectively. In Fig. 4-14, it is clear that there is a good agreement between the buckling parameters for a stiffened panel subjected to biaxial compression. The buckling mode

shapes obtained using the meshfree approach are similar to the buckling mode shapes obtained using ANSYS®.

For static analysis, the simply supported plate with curvilinear stiffener, subjected to 10kPa, is considered. The deflection results obtained using meshfree, as can be seen in Fig. 4-15, agree well with those calculated using ANSYS®. In ANSYS®, the curvilinear stiffener is modeled by straight beam element and the stiffener nodes follow the plate nodes. Also the MLS shape function used in EFG method enable us to predict more accurate results. The difference in the moment results, especially for the eccentric stiffeners, may be due to the above reasons.

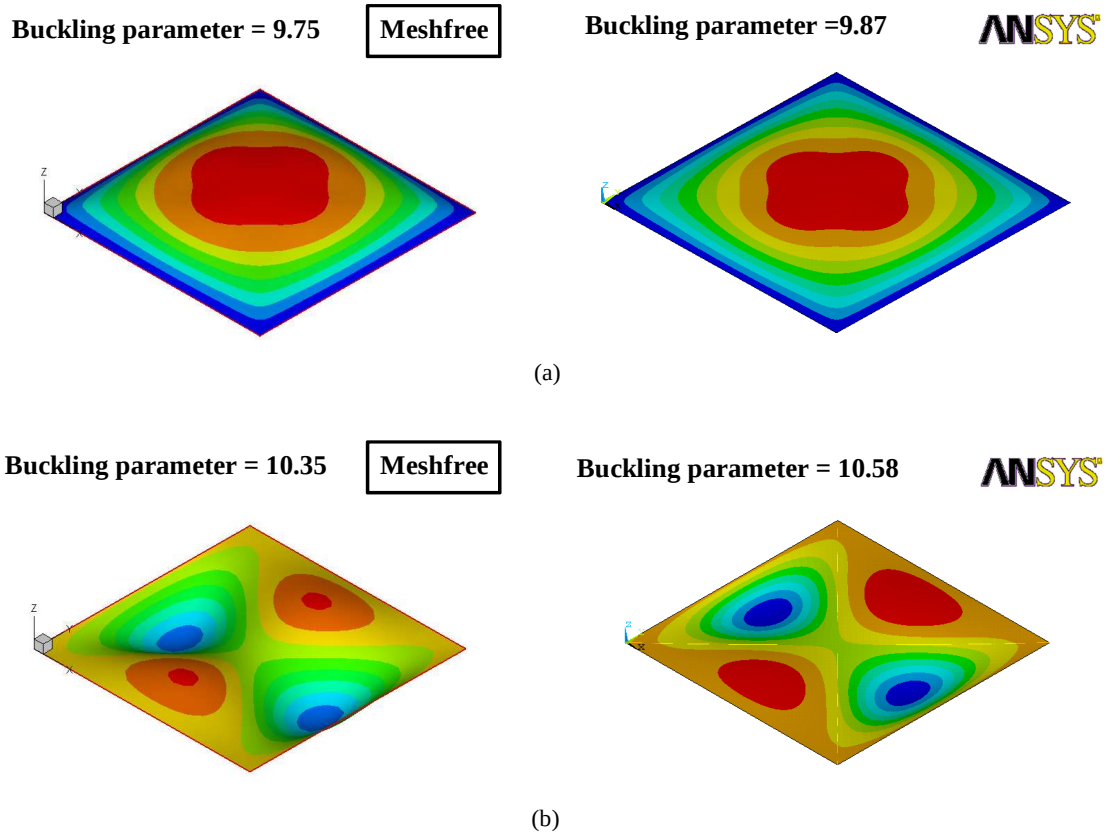

Fig. 4-11 Buckling mode shape for a plate with inclined stiffeners in biaxial compression using a meshfree method (left) and ANSYS®, a commercial available software (right) (a) The concentric stiffeners (b) The eccentric stiffeners

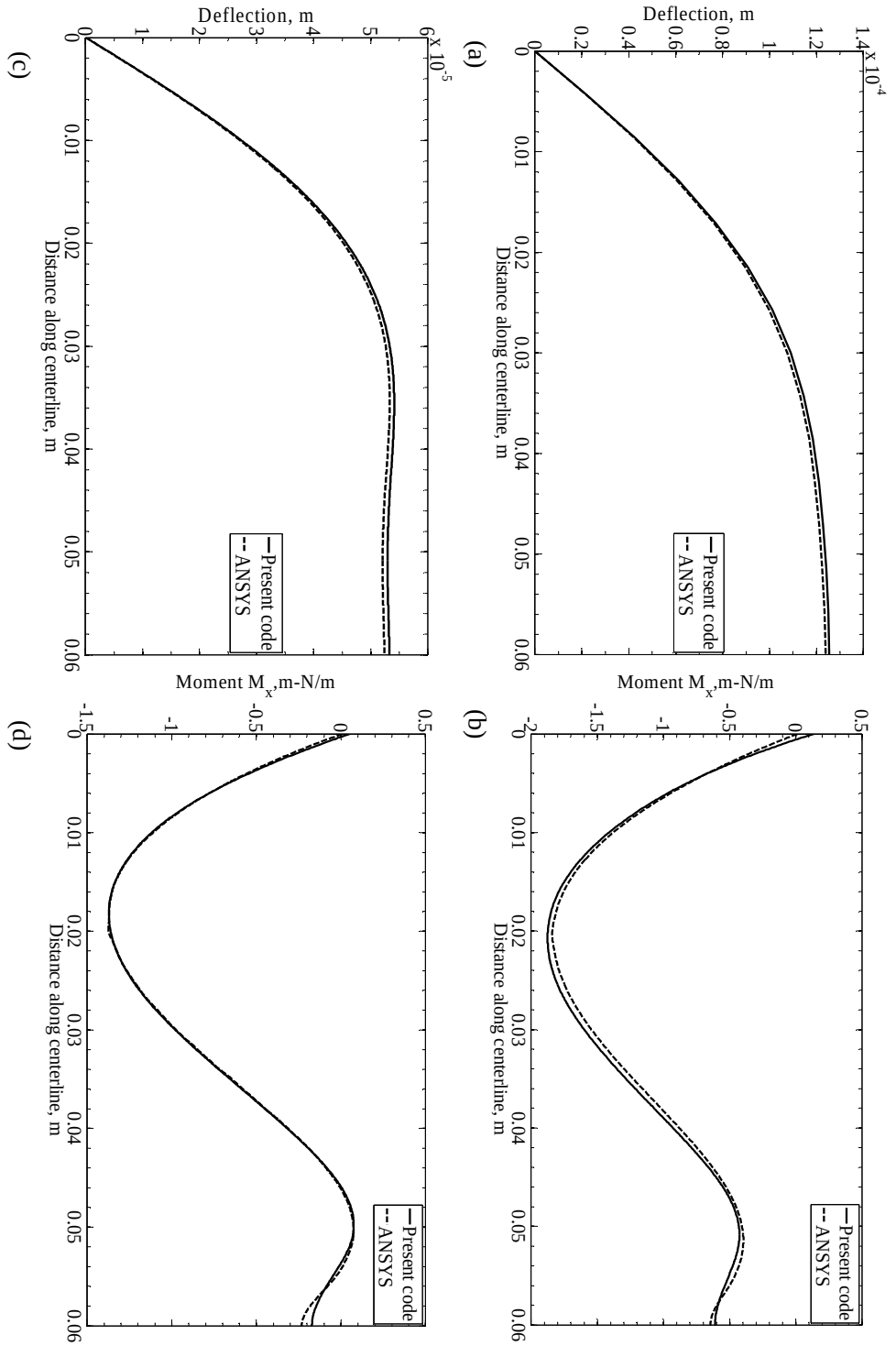

Fig. 4-12 (a) Deflection at *x*=0.06m (b) Moment Mx at *y*=0.06m: Plate under distributed load is stiffened by inclined concentric stiffeners (c) Deflection at *x*=0.06m (b) Moment Mx at *y*=0.06m: Plate under distributed load is stiffened by inclined eccentric stiffeners

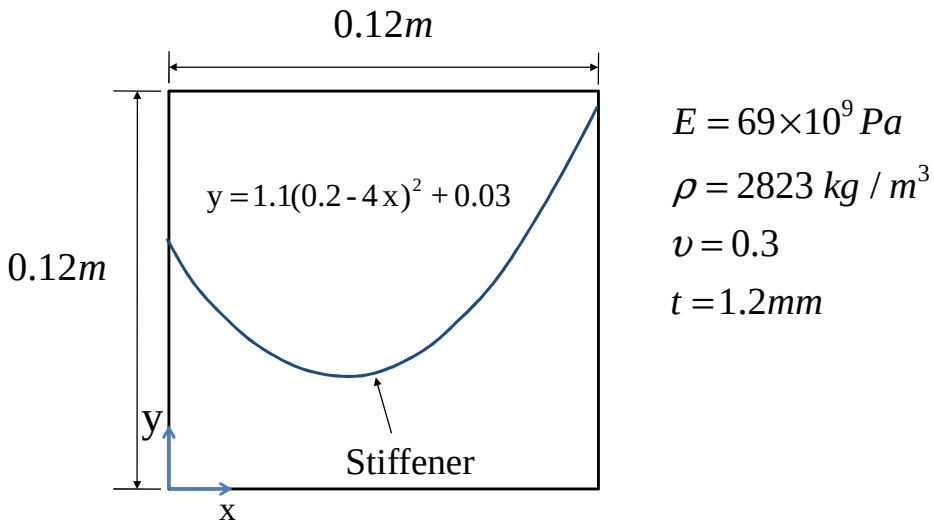

Fig. 4-13 A square plate with curvilinear stiffener

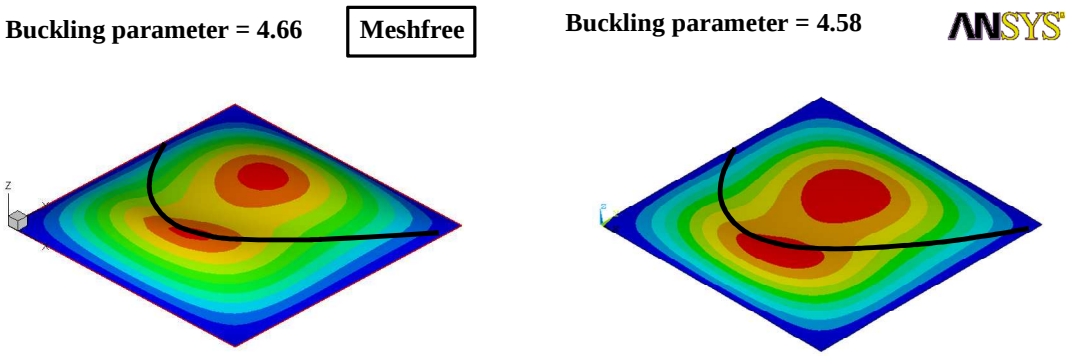

(a)

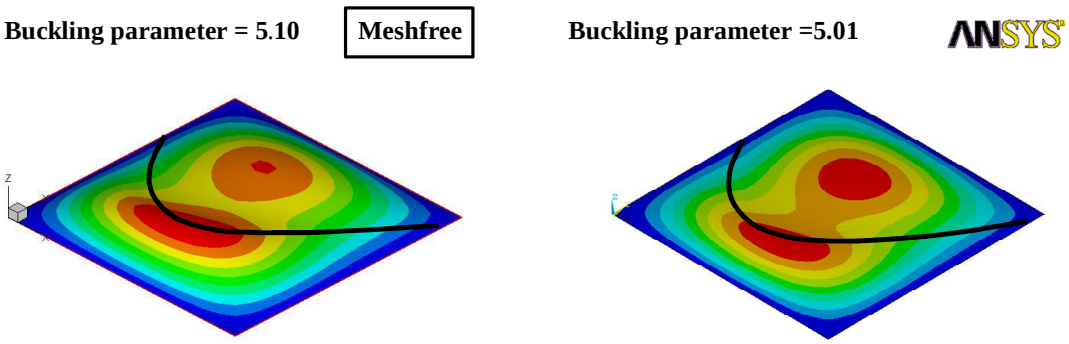

(b)

Fig. 4-14 Buckling mode shape for a plate with curvilinear stiffener in biaxial compression using a meshfree method (left) and ANSYS®, a commercial available software (right) (a) The concentric stiffeners (b) The eccentric stiffeners

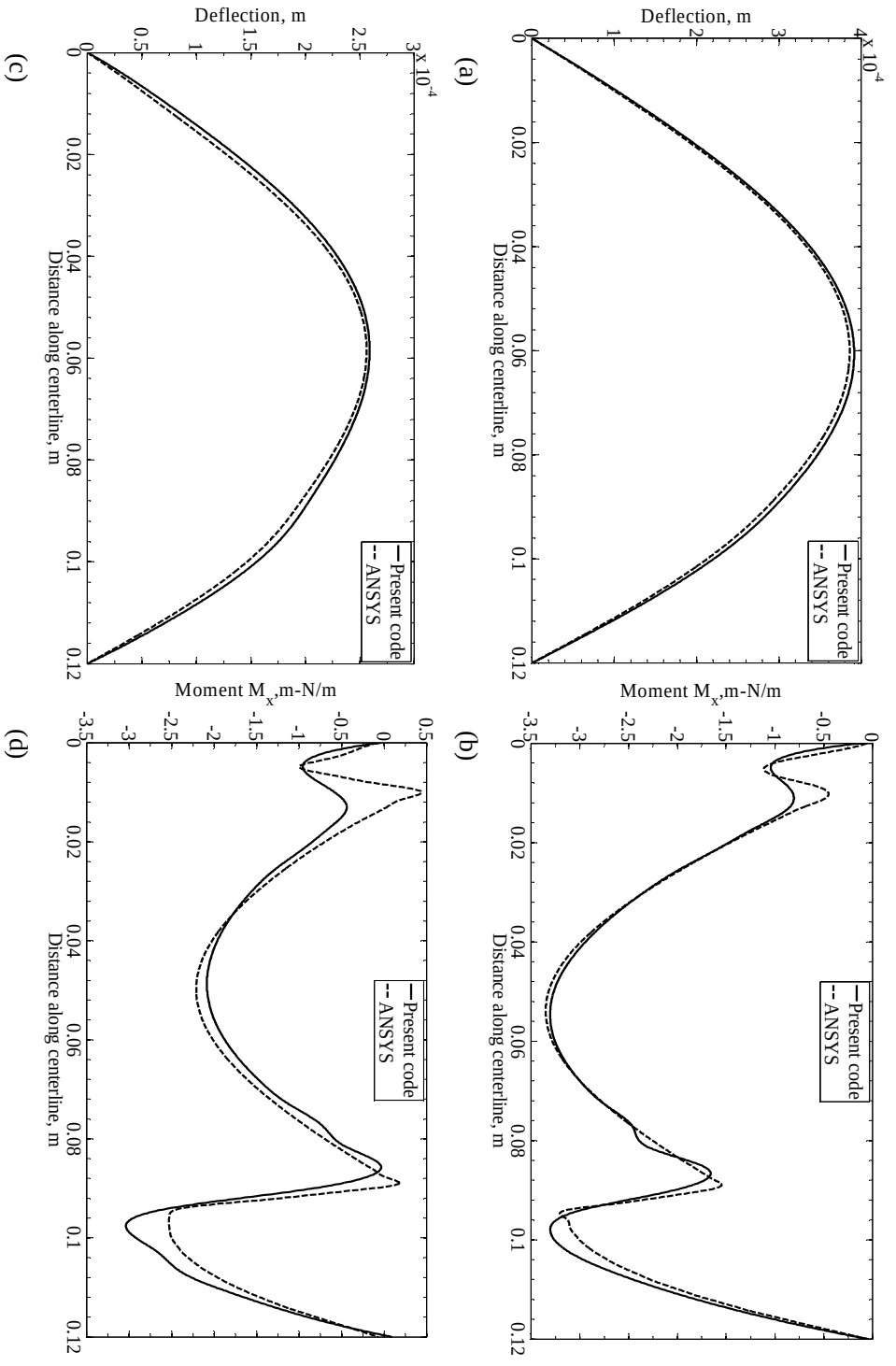

Fig. 4-15 (a) Deflection at *x*=0.06m (b) Moment Mx at *y*=0.06m: Plate under distributed load is stiffened by a concentric curvilinear stiffener (c) Deflection at *x*=0.06m (b) Moment Mx at *y*=0.06m: Plate under distributed load is stiffened by an eccentric curvilinear stiffener

- ***Simply-Supported Plates with Different Stiffener Configurations***

Square simply-supported plates with different stiffener configurations are considered (Fig. 4-16) next. The plate is under a biaxial compressions and the material and the geometric properties are same as in previous example. Three stiffener configurations are considered in this example; straight, inclined and curvilinear. In previous examples, the results for these three configurations are compared with other methods. As we are interested in a high buckling parameter while having a low total mass, in this example, using the meshfree method, both the buckling parameters and the masses of the ustiffened and the stiffened plates are compared. As can be seen in Table 4-2, the curvilinear stiffener can increase the buckling parameter ($\frac{\lambda_{stiffened}-\lambda_{unstiffened}}{\lambda_{unstiffened}}\times 100=165\%$) while the total mass increases by a relatively small amount ($\frac{m_{stiffened}-m_{unstiffened}}{m_{unstiffened}}\times 100=10\%$). As can be seen in Table 4-2, ANSYS® is more efficient in terms of CPU time than the meshfree code for the first analysis. However it can be observed that as the stiffener shape changes while plate geometry properties are kept unchanged, the meshfree code is more efficient in terms of CPU time than ANSYS®. The final optimal design can be found by using optimization tools. As the stiffener configuration changes, the plate particles' locations in optimization' process need not to be modified. This gives a great capability in reducing the CPU time during optimization process.

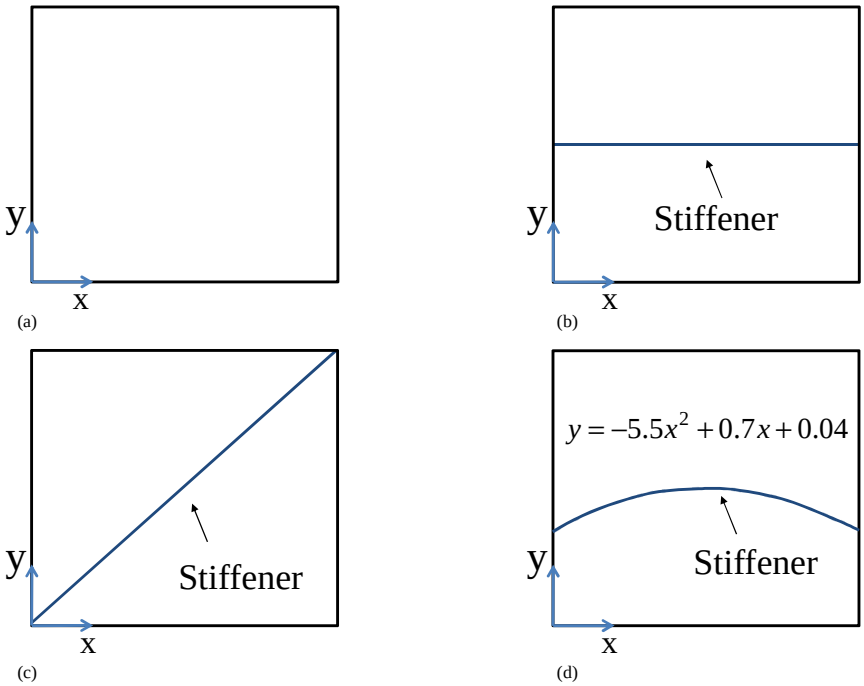

Fig. 4-16 (a) Unstiffened plate (b) Plate with straight stiffener (c) Plate with inclined stiffener (d) Plate with curvilinear stiffener

Table 4-2 Mass and buckling parameter of unstiffened and stiffened plates

	Unstiffened plate (a)	Plate with straight stiffener (b)	Plate with inclined stiffener (c)	Plate with curvilinear stiffener (d)
Mass (kg)	0.0488	0.0537	0.0557	0.0540
Buckling parameter (Meshfree)	1.98	5.07	5.05	5.25
Buckling parameter (ANSYS)	1.98	5.06	5.01	5.16
Time (Meshfree)*	1.6	1	1.1	1.1
Time (ANSYS)*	1.3	1.4	1.5	1.6
* Time is normalized.				

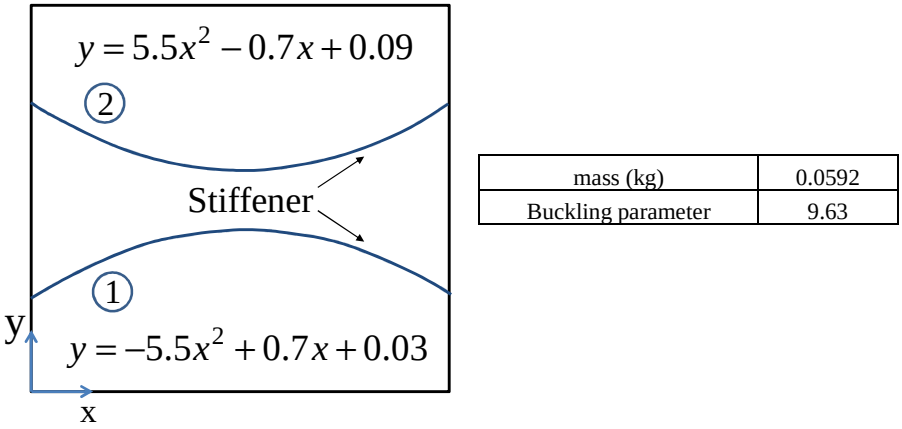

mass (kg)	0.0592
Buckling parameter	9.63

Fig. 4-17 Plate with two curvilinear stiffeners

In addition to changing the location or curvature of stiffener, adding another stiffener can increase the buckling parameter to a desire level while keeping the mass as minimum as possible. The buckling parameter and the mass of the plate with two stiffeners are shown in Fig. 4-17. By comparing Fig. 4-17 and Table 4-2, it can be seen that the buckling parameter increases significantly by adding the second stiffener. Consequently, the developed method can give the user the capability of changing the location, orientation, curvature and number of stiffeners to find the buckling parameter while the plate particles do not change.

4.4 Conclusion

The main objective of this study is to develop a meshfree approach to analyze plates with arbitrary curvilinear stiffeners, and compare the accuracy with the results available in the literature. In the EFG method, employing the MLS basis functions, because the actual nodal values differ from the nodal

parameters used in the MLS basis functions, boundary conditions cannot be imposed directly. The penalty method is used in this research to satisfy the boundary conditions. In this research linear buckling and static analysis are considered. The stiffener cross section is assumed to be symmetric about the stiffener binormal axis; however the formulation accepts eccentric and concentric stiffeners. Accurate numerical results are obtained which not only are close to the results available in the literature but also to ANSYS® results. In engineering design of stiffened plates, changing the stiffener properties and monitoring the structural behavior is one of the most important objects. In FEM modifying the stiffener location or curvature would lead to remeshing of the both plate and the stiffeners. However in the present meshless formulation, because no mesh is required, remeshing the entire structure is avoided.

5 A Chebyshev Ritz Approach to Buckling and Vibration of Curvilinearly-Stiffened Plate

5.1 Introduction

In this section, the free vibration of plates with curvilinear stiffeners subjected to in-plane loading is studied. The First Order Shear Deformation Theory (FSDT) is used to model both the plate and stiffeners. The transverse deflection and rotations of the plate and stiffener are expressed in terms of Chebyshev polynomials. The stiffness and geometric stiffness matrices of the curvilinearly-stiffened plate are obtained by superimposing the strain energy and potential of the membrane force for both the curvilinear stiffeners and the plate. Results are computed for unstiffened and stiffened plate with straight and curvilinear stiffeners using different boundary conditions. The effect of in-plane loading, increasing from zero to the buckling load, on the natural frequencies is studied. Several numerical examples are compared with the other results available in the literature and meshfree results, illustrating the accuracy of the present approach. It is also shown that the in-plane load can lead to a significant change in the natural frequency and also in some cases the corresponding mode shapes of plate with curvilinear stiffeners. Numerical results are presented for a range of plate aspect ratios, bending stiffness ratios of the stiffener to that of the plate and area ratios of the stiffener to that of the plate. The effect of these parameters on the natural frequencies of the plate with different number of curvilinear stiffeners under in-plane loads is studied. For studying the influence of the in-plane load on natural frequency, both axial/biaxial and shear in-plane loads are considered. Numerical results show that the vibration behavior of stiffened plate in the presence of in-plane loads is influenced by different parameters such as the plate aspect ratio, the stiffener area ratio, the stiffener stiffness ratio and the number of stiffeners in the panel.

5.2 Curvilinear Stiffened Plate Formulation

The configuration of a rectangular plate is shown in Fig. 5-1 (a).The plate has length a, width b and has a uniform thickness h_p. The potential of the in-plane loads (W_p) acting on the plate can be expressed as:

$$W_p = -\frac{1}{2}\int_0^1 \int_0^1 [\sigma_x (h_p (\frac{1}{a}\frac{\partial w}{\partial \bar{x}})^2 + \frac{{h_p}^3}{12}(\frac{1}{a}\frac{\partial \varphi_x}{\partial \bar{x}})^2 + \frac{{h_p}^3}{12}(\frac{1}{a}\frac{\partial \varphi_y}{\partial \bar{x}})^2) +$$
$$\sigma_y (h_p (\frac{1}{b}\frac{\partial w}{\partial \bar{y}})^2 + \frac{{h_p}^3}{12}(\frac{1}{b}\frac{\partial \varphi_x}{\partial \bar{y}})^2 + \frac{{h_p}^3}{12}(\frac{1}{b}\frac{\partial \varphi_{py}}{\partial \bar{y}})^2) + \tag{5-1}$$
$$\sigma_{xy} (h_p (\frac{1}{ab}\frac{\partial w}{\partial \bar{x}}\frac{\partial w}{\partial \bar{y}}) + \frac{{h_p}^3}{12}(\frac{1}{ab}\frac{\partial \varphi_{px}}{\partial \bar{x}}\frac{\partial \varphi_{px}}{\partial \bar{y}}) + \frac{{h_p}^3}{12}(\frac{1}{ab}\frac{\partial \varphi_{py}}{\partial \bar{x}}\frac{\partial \varphi_{py}}{\partial \bar{y}}))] ab d\bar{x} d\bar{y}$$

where φ_x, and φ_y are the rotations normal to the mid-surface about the *y* and *x* axes, respectively, and w is transverse displacement of a point in the mid-surface in the *z* direction; σ_x and σ_y are axial stresses in the *x* and *y* directions, respectively, and σ_{xy} is shear stress in the *x-y* plane; and D, K_G, G, E and ω are the flexural rigidity, shear correction factor, shear modulus, elastic modulus and natural frequency of the plate, respectively. Also non-dimensionalized $\bar{x}$ and $\bar{y}$ are defined as $\bar{x} = x/a$ and $\bar{y} = y/b$, respectively.

The rotations and displacement functions, using Chebyshev polynomials, and multiplied by a boundary function that ensures the displacement and rotation components satisfy the essential geometric boundary conditions of the plate, are given as:

$$\begin{cases} \varphi_x(\bar{x},\bar{y}) = \sum_{m=0}^{p_1}\sum_{n=0}^{q_1} c_{mn}\psi_{xmn}(\bar{x},\bar{y}) \\ \varphi_y(\bar{x},\bar{y}) = \sum_{m=0}^{p_2}\sum_{n=0}^{q_2} d_{mn}\psi_{ymn}(\bar{x},\bar{y}), \\ w(\bar{x},\bar{y}) = \sum_{m=0}^{p_3}\sum_{n=0}^{q_3} e_{mn}\varphi_{mn}(\bar{x},\bar{y}) \end{cases} \quad \begin{cases} \psi_{xmn}(\bar{x},\bar{y}) = \psi_{bx}(\bar{x},\bar{y}) X_m(\bar{x}) Y_n(\bar{y}) \\ \psi_{ymn}(\bar{x},\bar{y}) = \psi_{by}(\bar{x},\bar{y}) X_m(\bar{x}) Y_n(\bar{y}) \\ \varphi_{mn}(\bar{x},\bar{y}) = \varphi_b(\bar{x},\bar{y}) X_m(\bar{x}) Y_n(\bar{y}) \end{cases} \tag{5-2}$$

here c_{mn}, d_{mn} and e_{mn} are the unknown coefficients and p_s and q_s (*s*=1,2 and 3) are the highest degrees of the Chebyshev polynomials in the $\bar{x}$ and $\bar{y}$ directions, respectively. Also, $\psi_{bx}(\bar{x},\bar{y})$, $\psi_{by}(\bar{x},\bar{y})$ and $\varphi_b(\bar{x},\bar{y})$ are polynomial expressions describing the boundary conditions that are functions of the plate geometry and kinematics. These are defined by Liew *et al.* [14].

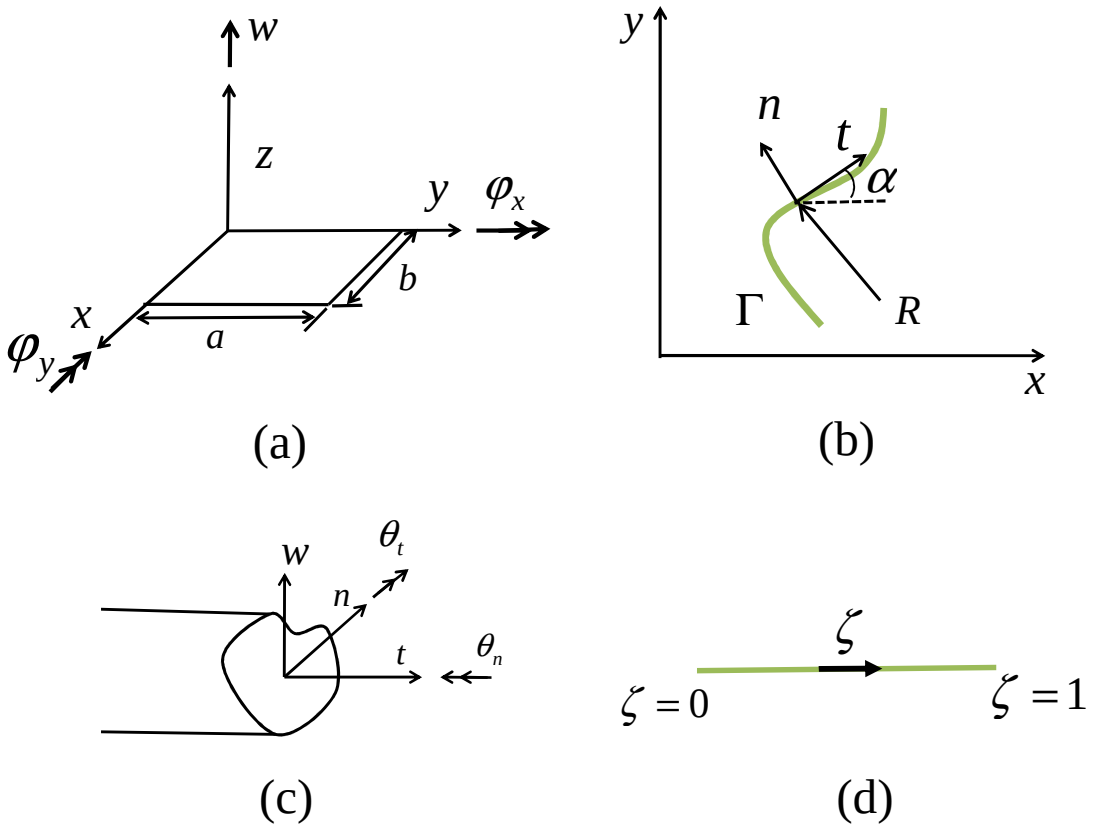

Fig. 5-1 (a) Directions of the generalized displacements of the plate (b) Local and global coordinate systems for the curvilinear stiffener (c) Directions of the generalized displacements of the stiffener (d) The transformed plane of curvilinear stiffener

The curvilinear stiffener is shown in Fig. 5-1(b). The curvilinear stiffener is mapped to natural coordinate (ζ) extending from ($\zeta = 0$) to ($\zeta = 1$) in one direction as illustrated in Fig. 5-1(d).

The potential of the membrane force acting in the curvilinear stiffener is defined as:

$$W_s = -\frac{1}{2}\int_0^1 \int_0^1 [\sigma_t (A(\frac{\partial w_s}{\partial s})^2 + I_n(\frac{d\theta_t}{ds} + \frac{\theta_n}{R})^2 + I_n(\frac{d\theta_n}{ds} - \frac{\theta_t}{R})^2)]ds \tag{5-3}$$

where σ_t is the tangential stress in the curvilinear stiffener.

The Lagrangian of the curvilinear stiffened plate is

$$L = T_p + T_s - U_p - U_s - W_p - W_s \tag{5-4}$$

The governing equation for the free vibration of the curvilinear stiffeners, subjected to in-plane load, by using the Lagrangian equation can be obtained as:

$$[(K_p + K_s) - (K_{Gp} + K_{Gs})] - \omega^2[M_p + M_s] = 0 \tag{5-5}$$

K_p, K_{Gp} and M_p are the elastic stiffness, geometric stiffness and mass matrices of plate and K_s, K_{Gs} and M_s are the elastic stiffness, geometric stiffness and mass matrices of stiffener. The integrations in elastic stiffness, geometric stiffness and mass matrices are carried out by using the Gaussian quadrature, and Gauss points are also used to evaluate the α, the angle between the t and x axes (please see Fig. 5-1).

As can be seen in Eq. (5-5), the total structure stiffness decreases as the in-plane compressive load increases, resulting in a reduction in natural frequency. The relationship between the in-plane load and natural frequencies is discussed in details in the next section.

5.3 Convergence and Validation

For obtaining the exact solution of Eq. (11) infinite series should be considered. Depending upon the accuracy required, the upper limit of the summation is truncated at a finite number. The convergence properties of the numerical solutions according to the order of approximation in the Chebyshev polynomials as applied to our problem are examined here. Numerical examples on buckling analysis of stiffened plates are solved in this section by using the Ritz method. In order to verify the present results, they are compared with those available in the literature for various cases with straight stiffeners. Also in order to illustrate the applicability of the Chebyshev Ritz method in analyzing the curvilinearly-stiffened plate, the results are compared with those obtained using meshfree method.

- ***A Simply-Supported Plate with a Single Stiffener***

For the first example, the buckling analysis of a series rectangular plate simply-supported on all four edges and with one central stiffener is considered (Fig. 5-2). The plate is under axial compression in the *x* direction. This problem was investigated by Timoshenko and Gere [77] using the classical plate theory for the out-of-plane displacement. Also, Mukhopadhyay and Mukherjee [55] solved the same problem by using finite element method based on First Order Shear Deformation Theory (FSDT). In their research, the stiffener can be positioned anywhere within the plate element. The plate and the stiffener are made of the same material, with Poisson's ratio $\upsilon = 0.3$. The buckling load parameter is defined as:

$$\lambda_{cr} = \frac{\sigma_{cr} a^2 h_p}{\pi^2 D} \tag{5-6}$$

where σ_{cr} and *D* are the critical stress and the flexural rigidity of the plate. The ratio of the cross sectional area of the stiffener to that of the plate is defined by $\delta = b_s h_s / a h_p$ where b_s and h_s are the width and

the height of the stiffener. The ratio of the bending stiffness of the stiffener to that of the plate is defined by $\gamma = E_s I_s / aD$.

In the Ritz method, it is important to have the convergence studies to estimate the order of polynomial which is required for the numerical solution. The convergence studies have been carried out for buckling analysis for stiffened plate with various δ and γ subjected to axial compression. Table 4-1 shows the convergence of the present method results with increasing the order of approximation. As it was expected, the convergence is monotonic. Also as can be seen in the Table 4-1, the convergence property of the developed formulations for the buckling load is shown to be very satisfactory.

- ***A Simply-Supported Plate Having Two Inclined Stiffeners***

The buckling analysis of a simply-supported square plate with inclined stiffeners ($\delta = 0.1$ and $\gamma = 10$) subjected to in-plane biaxial compression is considered. Both the concentric and eccentric stiffener configurations are studied (Fig. 5-3). The buckling parameters and mode shapes obtained using Ritz method are presented with meshfree method results in Fig. 5-4 for both eccentric and concentric stiffeners. It was seen in Table 4-1 that the acceptable convergence has been achieved for the buckling parameter by using fourteenth-order Chebyshev polynomial. Consequently, in the Ritz method fourteenth-order Chebyshev polynomial is used for modeling the plate with inclined stiffeners. In the meshfree code, 24×24 particles and 70 particles are considered for the plate and stiffeners, respectively. Excellent agreement between the two methods' results can be observed in Fig. 5-4.

- ***A Simply-Supported Plate with a Curvilinear Stiffener***

The buckling analysis of a simply supported square plate with curvilinear stiffener subjected to in-plane biaxial loading is studied in this example. The stiffener configuration is described in Fig. 5-5. The buckling parameters obtained for $\delta = 0.1$ and $\gamma = 10$ related to eccentric and concentric stiffeners. For comparison purposes, the complete stiffened plate was modeled using meshfree formulation. In the meshfree formulation, 24×24 particles and 40 particles are used to discretize the plate and the stiffener. Also, in the Ritz method, fourteenth-order Chebyshev polynomial is used to model the plate with a curvilinear stiffener. The mode shapes with corresponding buckling parameters obtained by meshfree and Ritz methods are presented in Fig. 5-6. The figure shows a good agreement between the results obtained by the two methods.

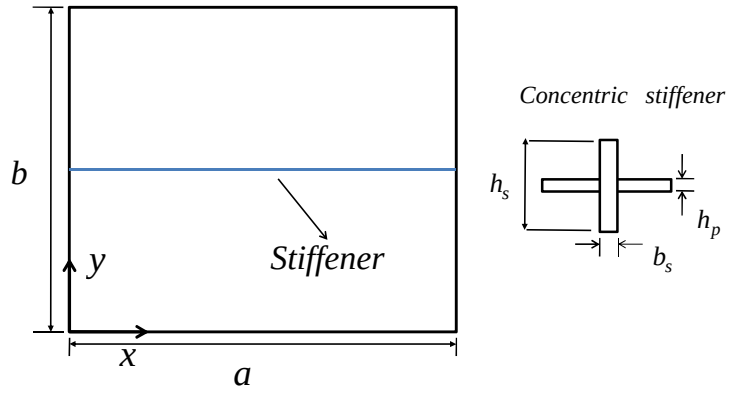

Fig. 5-2 Plate with a single stiffener

Table 5-1 The buckling parameters for rectangular stiffened plates with varying stiffener rigidity

$\gamma = 5$							
δ	Timoshenko and Gere [48]	Mukhopadhyay and Mukherjee [55]	Meshfree	Chebyshev Ritz method			
				8*	10	12	14
0.05	12	11.72	11.71	11.85	11.80	11.78	11.77
0.1	11.1	10.93	10.94	11.05	11.02	11.00	10.99
0.2	9.72	9.7	9.61	9.67	9.65	9.64	9.63
$\gamma = 10$							
δ	Timoshenko and Gere [48]	Mukhopadhyay and Mukherjee [55]	Meshfree	Chebyshev Ritz method			
				8	10	12	14
0.05	16	16	15.85	15.95	15.95	15.95	15.95
0.1	16	16	15.86	15.95	15.95	15.95	15.95
0.2	15.8	15.44	15.37	15.57	15.50	15.46	15.44
$\gamma = 15$							
δ	Timoshenko and Gere [48]	Mukhopadhyay and Mukherjee [55]	Meshfree	Chebyshev Ritz method			
				8	10	12	14
0.05	16	16	15.86	15.95	15.95	15.95	15.95
0.1	16	16	15.86	15.95	15.95	15.95	15.95
0.2	16	16	16.87	15.95	15.95	15.95	15.95

*The highest degree of Chebyshev polynomials considered in the expansion.

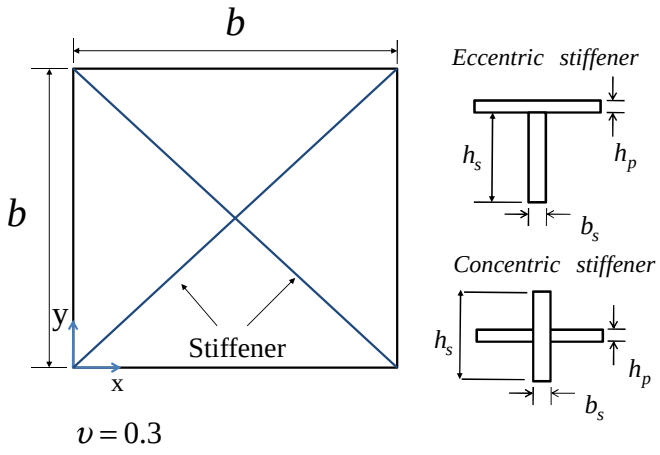

Fig. 5-3 A square plate with inclined stiffeners

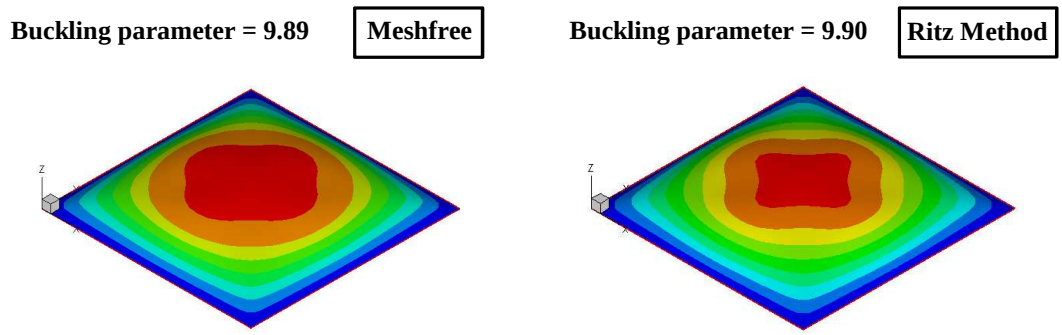

(a)

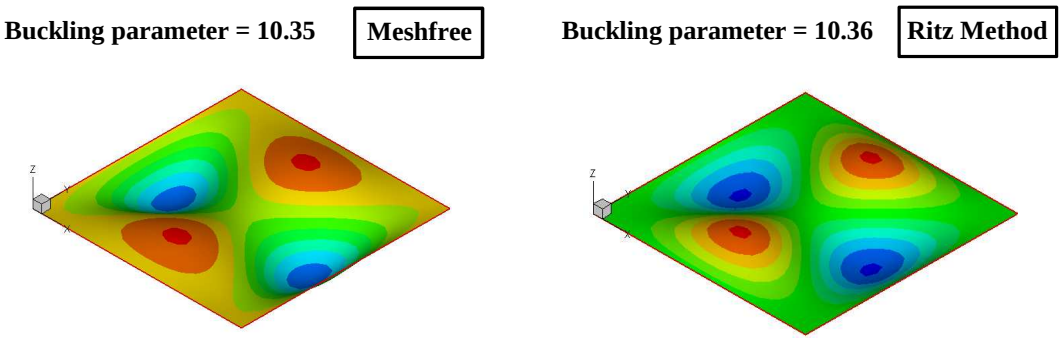

(b)

Fig. 5-4 Buckling mode shape for a plate with inclined stiffeners in biaxial compression using a meshfree method (left) and Ritz method (right) (a) The concentric stiffeners (b) The eccentric stiffeners

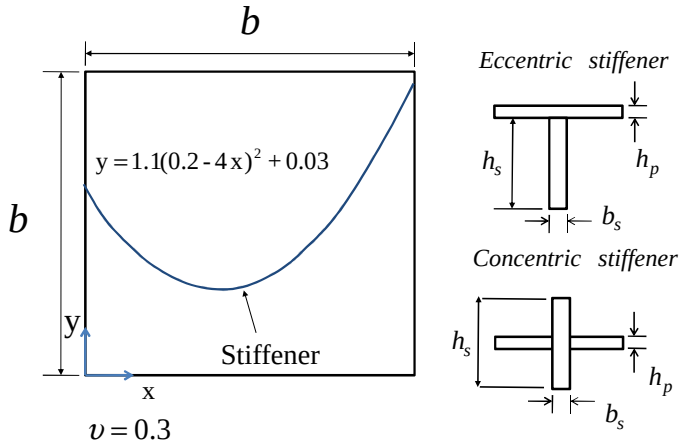

Fig. 5-5 A square plate with curvilinear stiffener

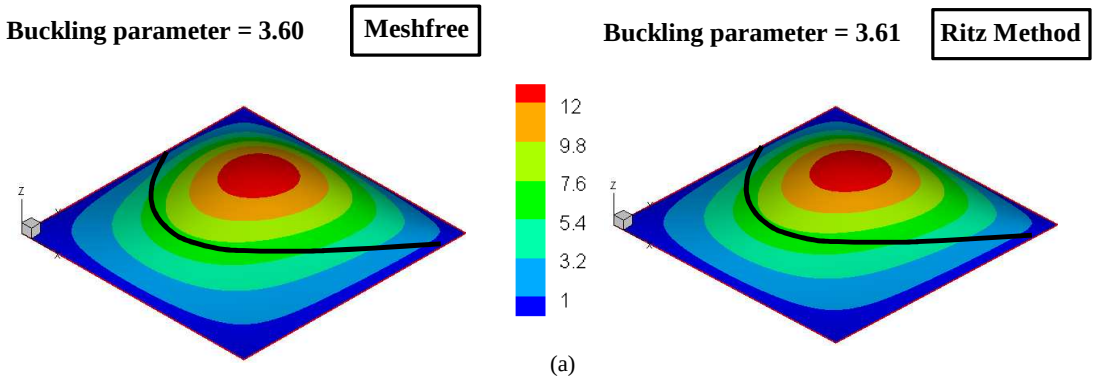

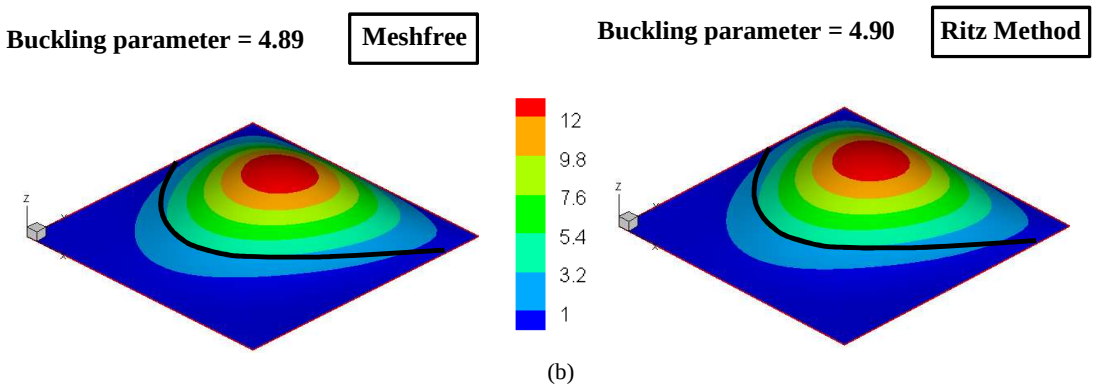

Fig. 5-6 Buckling mode shape for a plate with curvilinear stiffener in biaxial compression using a meshfree method (left) and Ritz method (right) (a) The concentric stiffener (b) The eccentric stiffener

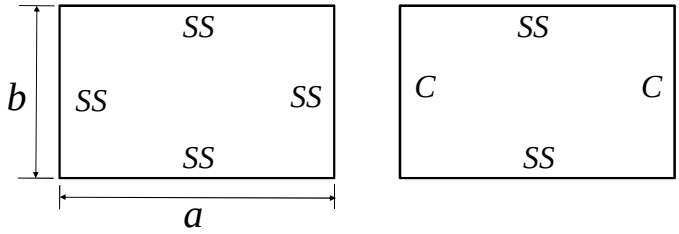

Fig. 5-7 Plate geometry and boundary conditions

5.4 Plates Subjected to Biaxial In-Plane Loading

Plates subjected to biaxial in-plane load are considered in this example. The Poisson ratio is 0.3 and two types of boundary conditions are imposed on the plates (see Fig. 5-7). Both compression and tension loads are considered in this example. In case of in-plane compressive load, first the critical buckling parameter is calculated and then a fraction of this critical load is applied to study the free vibration response. Since the nonlinear analysis was not considered, the compression load is restricted to less than critical buckling loads to avoid the post-buckling. The natural frequency parameter and in-plane load parameter are defined as:

$$\lambda_n = (\omega b^2)^2 (\rho h_p / D)$$
$$\lambda_b = \frac{\sigma_{ap} a^2 h_p}{\pi^2 D} \tag{5-7}$$

where ω and σ_{ap} are natural frequency and applied in-plane stress, respectively.

Natural frequency parameter for different in-plane load, aspect ratios and boundary conditions are obtained and compared with the results of Kielb and Han [65]. Kielb and Han solved the same problem by using the classical plate theory. In the Ritz method, fourteenth-order Chebyshev polynomial is used. The variation of frequency parameter with in-plane load parameter is shown in Fig. 5-8. It can be seen that the results are in good agreement with the previously published results. As can be seen in Fig. 5-8, by applying a compression load in *x* direction, the natural frequency decreases and by applying tension load it increases. It should be noted that the natural frequency parameter varies linearly with the buckling parameter in this figure.

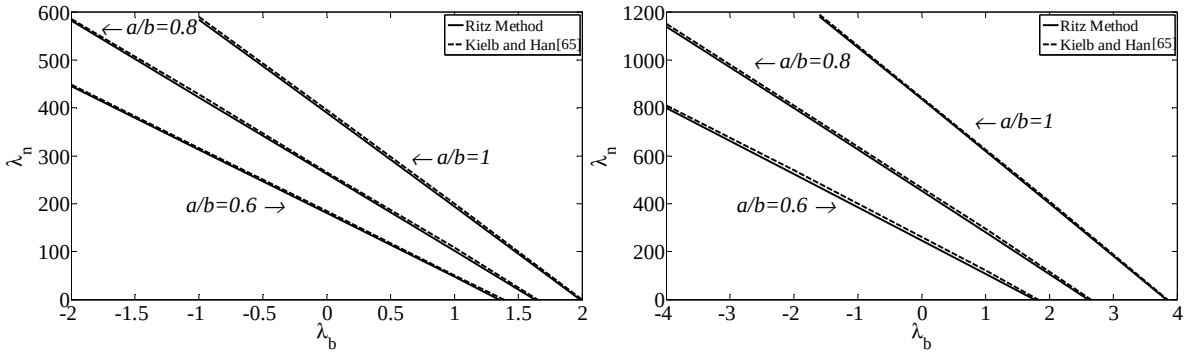

Fig. 5-8 Frequency versus in-plane load parameter for (a) all edges simply supported plates and (b) two edges clamped and two edges simply supported plates (b)

5.5 Curvilinear Stiffened Plate subjected to in-plane loading

In this section, plates with one, two and four curvilinear stiffeners are considered. The plates are subjected to in-plane shear or axial/biaxial compression. The behavior of stiffened plate subjected to in-plane load is studied for different cross sectional area ratios of the stiffener to that of the plate, bending stiffness ratios of the stiffener to that of the plate and plate aspect ratios. The in-plane compression and shear load may have two main effects on the free vibration of the stiffened plate: it can change the natural frequency and it may change the corresponding mode shape. In all cases, both effects are studied and as expected, it will be shown that the increase in magnitude of the in-plane loads reduces the natural frequency, which will become zero when the in-plane load is equal to the critical buckling load of the stiffened plate.

- ***Plate with a curvilinear stiffener***

A plate, simply supported on all edges, with a curvilinear stiffener, as shown in Fig. 5-9, is considered in this section. The plate is subjected to axial in-plane compression. To find the behavior of curvilinear stiffened plates under in-plane compressive loading, various plate aspect ratios and stiffener parameters are considered.

The stiffened square plate with one curvilinear stiffener is chosen to study the variation of first four frequencies with ratios of in-plane load parameter (λ_b) to the buckling load parameter (λ_{cr}). The results for $\delta = 0.1$ and $\gamma = 5$ are shown in Fig. 5-10. It can be seen in this figure that as the in-plane load increases, the natural frequencies, for all modes, decrease. Also the mode shapes for two values of the applied load ($\lambda_b = 0$ and $\lambda_b = 0.75\lambda_{cr}$) are shown in this figure and it is observed that there is not a significant change in the first mode shape. As shown in Fig. 5-10, the relationship between the first frequency parameter and in-plane load parameter is linear; however it does not happen for the second, third and fourth frequency parameter. Since the first mode shape does not change with the in-plane load

parameter, the relationship between the first frequency parameter and in-plane load parameter is expected to be linear. However, due to the intersection between the second and third mode, as can be seen in Fig. 5-10, the second mode switches to the third mode and the third mode switches to the second mode.

In some cases, by changing the plate aspect ratio, stiffener bending stiffness ratio, in-plane loading condition or by adding stiffeners, the relationship between the frequency parameter and the in-plane load parameter might become nonlinear.

Effect of Plate Aspect Ratio:

To provide a better view of the behavior of the stiffened plate for various plate aspect ratios, the effects of the in-plane load on the first frequency parameter are studied for four plate aspect ratios ($b/a = 0.25,\ 0.5,\ 0.75,\ 1$) and results obtained are shown in Fig. 5-11. In order to study the effect of aspect ratio (*b/a*) of a stiffened plate on its free vibration behavior under axial in-plane load, the height (b) of the plate is varied while the other parameters of stiffened plate are kept unchanged. As is expected, the natural frequency and buckling load are both increasing when the plate aspect ratio is decreasing. It appears that reducing the plate aspect ratio changes the relationship between the frequency parameter and the in-plane load parameter. As can be seen in Fig. 5-11, the frequency parameter decreases linearly by increasing the in-plane load parameter for all plate aspect ratios except for $b/a = 0.25$. The mode shape for $b/a = 0.25$ at $\lambda_b = 0$ and $\lambda_b = 0.75\lambda_{cr}$ are both shown in Fig. 5-11, where λ_{cr} is the critical buckling load parameter for $b/a = 0.25$. Since the mode shape varies drastically with λ_b, the deviation from linearity of λ_n versus λ_b becomes significant.

Effect of Stiffener Area Ratio:

The effect of stiffener area on the natural frequency for simply-supported square curvilinear stiffened plates for the same in-plane load as described above are examined here. Except for the stiffener area, other parameters of stiffened plate are kept unchanged. The study on the natural frequency has been done for various stiffener area ratios ($\delta = 0.5,\ 0.1,\ 0.2$) and the results are shown in Fig. 5-12(a). As can be seen in this figure, the frequency parameters decrease as δ is increased. However, it is seen that the buckling load parameters do not change as much as the frequency parameters change. The variation in the area of stiffener can have an effect on the stiffness, geometric stiffness and mass matrices of a stiffener. The results imply that when the area is increased, the mass matrix effect increases more than the geometric stiffness matrix effect and because of it, the frequency parameter decreases more than the buckling parameter. Also it is observed in Fig. 5-12(a) that the predicted frequency parameters for different stiffener area ratios change linearly with the in-plane load parameter.

Effect of Stiffener Stiffness Ratio:

A square curvilinear stiffened plate with all edges simply supported is analyzed with various stiffener stiffness ratios while other corresponding parameters are similar to the previous example. The torsional stiffness of the stiffener is neglected and the ratio of the bending stiffness (γ) has been varied from 5 to 15.

The effect of bending stiffness rigidity of the stiffened plates having fixed stiffener area ratio ($\delta = 0.1$) on the frequency parameters is shown in Fig. 5-12(b). As can be seen in this figure, the frequency parameter and the buckling load parameter increases by increasing the stiffener bending stiffness while its area is fixed which implies that the structure is becoming more stable as the stiffener stiffness ratio increases. When the area of the stiffener is assumed to be constant, the mass of the stiffener will be constant and by increasing the second moment of the stiffener cross section area, the stiffener will be more stiff which results in a higher natural frequency. Also, it should be noted that the relationship between λ_n and λ_b is, for all cases, linear.

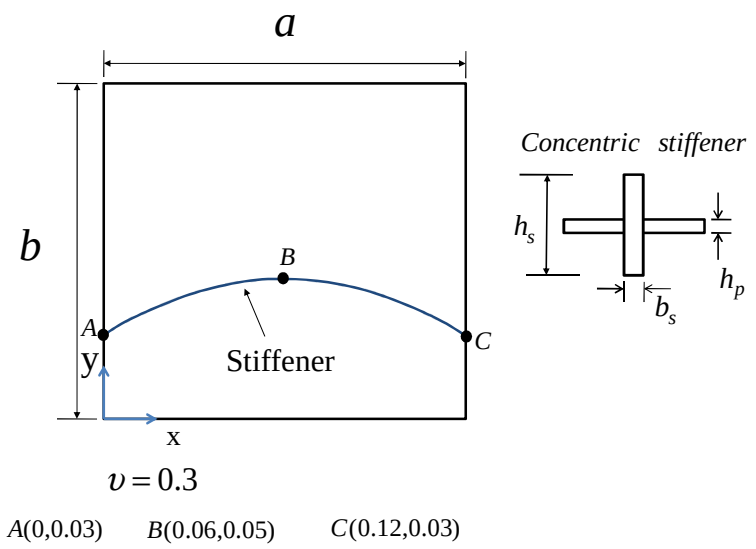

Fig. 5-9 Plate with one curvilinear stiffener

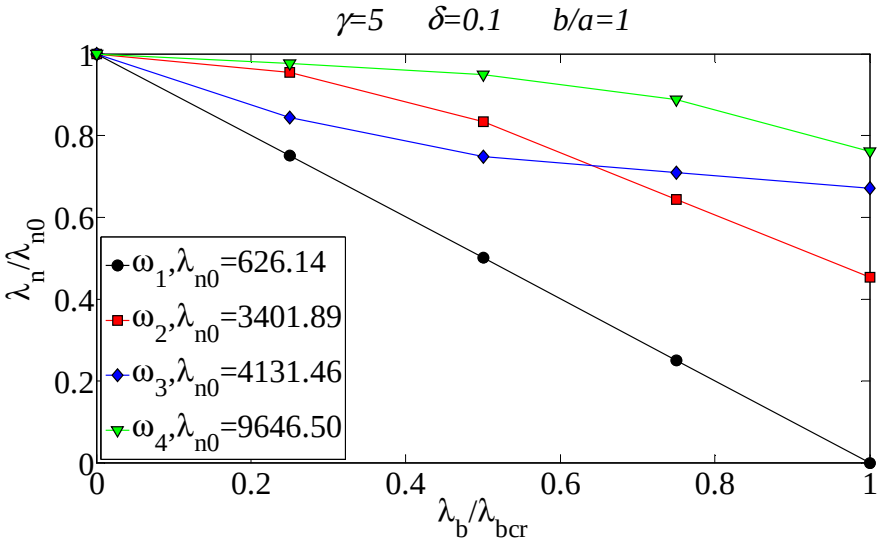

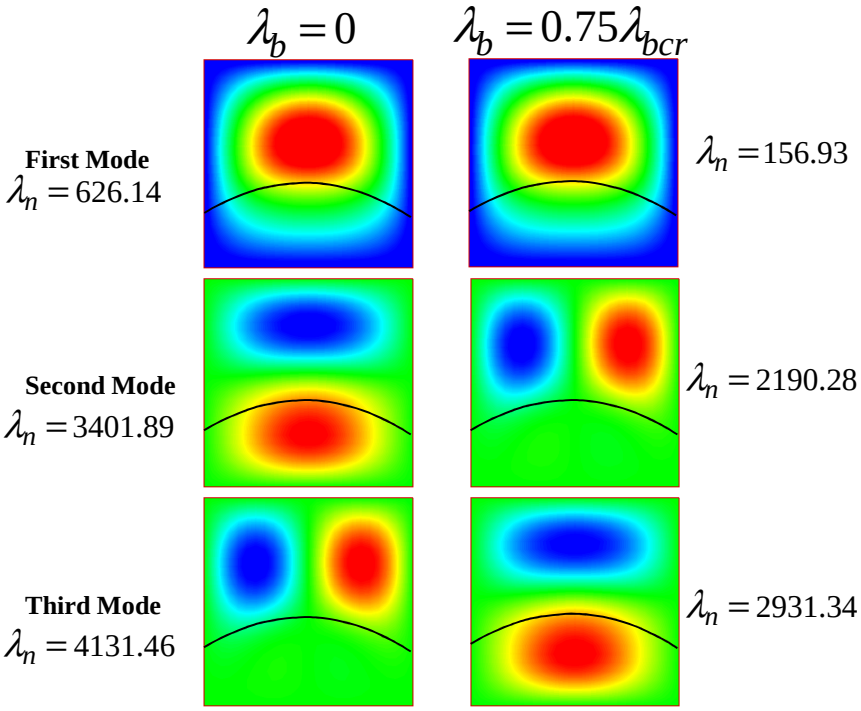

Fig. 5-10 Variation of first four frequency parameters of plate with one curvilinear stiffener ($\delta = 0.1$ and $\gamma = 5$) vs. in-plane load (axial compression) parameter ($\lambda_{bcr} = 6.61$)

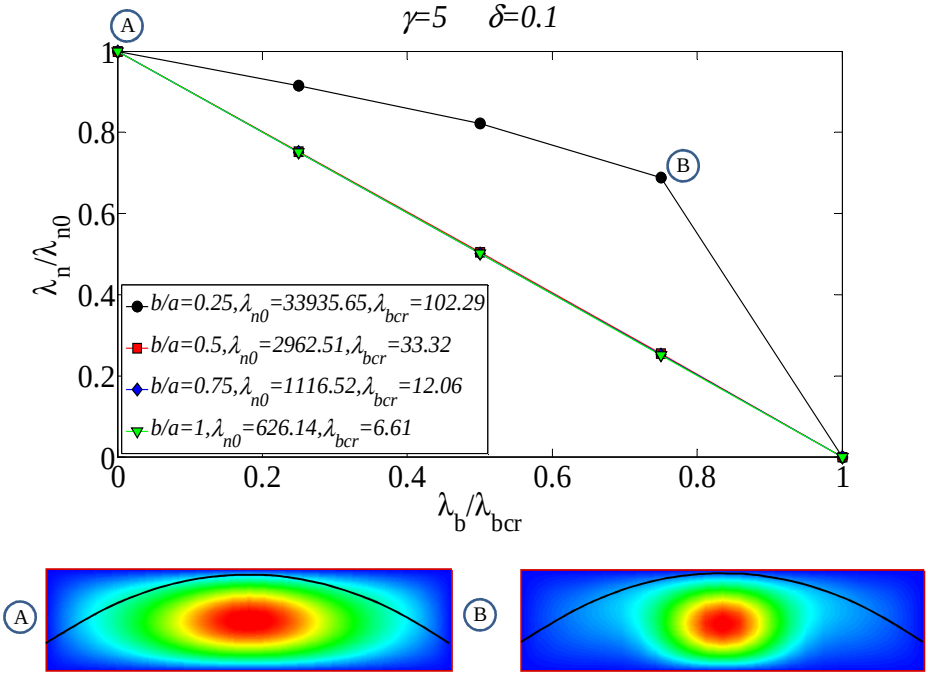

Fig. 5-11 Variation of first frequency parameters of plate with one curvilinear stiffener ($\delta = 0.1$ and $\gamma = 5$) for different plate aspect ratios vs. in-plane load (axial compression) parameter

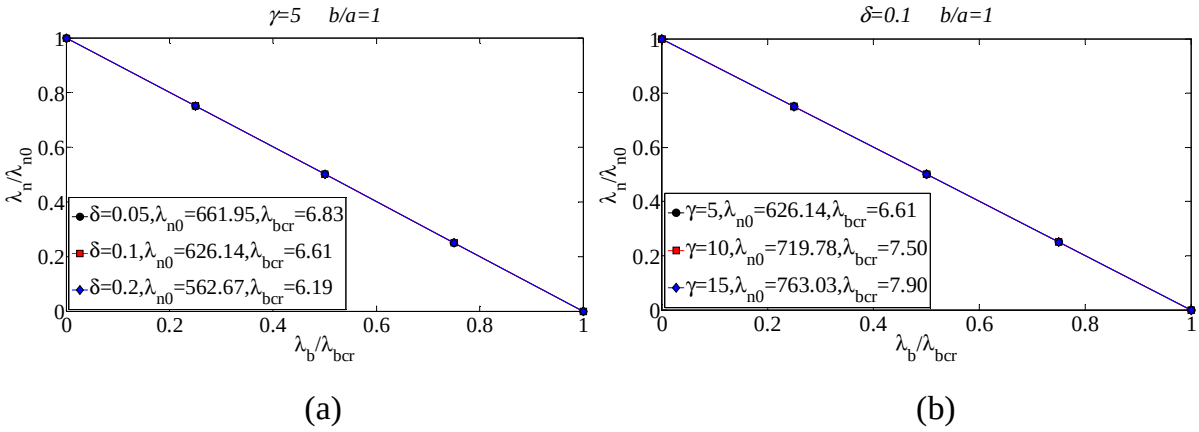

Fig. 5-12 Variation of first frequency parameters vs. in-plane load (axial compression) parameter for (a) different stiffener cross sectional area ratios (δ) (b) different stiffener bending stiffness ratios (γ)

- ***Plate with two curvilinear stiffeners***

In the following section, numerical results for frequency parameters for curvilinear stiffened plate, simply supported on all edges, are studied. The plate and stiffener geometry is shown in Fig. 5-13. The in-plane load in this example is biaxial compression in *x* and *y* directions. The effects of plate aspect ratio (b/a), stiffeners area ratio (δ) and stiffeners stiffness ratio (γ) on the vibration performance of stiffened plate under in-plane load are studied.

As a first case, the effect of in-plane loads is investigated for a square plate with two stiffeners. In this case, the stiffeners area ratio (δ) and stiffeners rigidity ratio (γ) are 0.1 and 5, respectively. The frequency parameter (λ_n) of the first four modes for various ratios of in-plane load parameter (λ_b) to the buckling load parameter (λ_{cr}) are plotted in Fig. 5-14. As can be seen in this figure, the frequency parameter related to the first mode decreases linearly with the increasing of in-plane load parameter. By comparing Fig. 5-14 with Fig. 5-11, it is observed that in addition to the frequency parameter corresponding to the first mode, frequency parameters related to the second, third and fourth modes decrease almost linearly with an increase in the in-plane load parameter. However, in Fig. 5-11, which shows a different mode shape behavior with respect to the in-plane load for the plate with one curvilinear stiffener under axial in-plane load, the relationship deviates from a linear variation between λ_n and λ_b for higher modes. The mode shape corresponding to the first natural frequency for two in-plane load values ($\lambda_b = 0$ and $\lambda_b = 0.75\lambda_{cr}$) are shown in Fig. 5-14. As expected, the mode shapes are very close in this example.

Effect of Plate Aspect Ratio:

As a second case, numerical results for frequency parameters are presented for a simply supported curvilinear stiffened plate with various aspect ratios. The aspect ratio is an important geometric parameter in the design of curvilinear stiffened plates and can change the natural frequency and buckling load significantly. In this example, stiffened plates with aspect ratios of between 0.25 and 1 were selected. While varying the aspect ratio, the other stiffener and plate geometries were kept constant. In this particular case, the stiffener area ratio (δ) is 0.1 and the stiffener stiffness ratio (γ) is 5. The frequency parameters versus in-plane load parameters are shown in Fig. 5-15. The results presented in Fig. 5-15 show that an increase in the aspect ratio of a plate, results in a reduction in the natural frequency and buckling load of stiffened plate. Also, it is observed that the relationship between the frequency parameter (λ_n) and the in-plane load parameter (λ_b) is very close to linear for all values of plate aspect ratio. The mode shape for $b/a = 0.5$ at $\lambda_b = 0$ and $\lambda_b = 0.75\lambda_{cr}$ are presented in Fig. 5-15, where λ_{cr} is the critical buckling load parameter for $b/a = 0.5$. As can be seen, the mode shape does not vary considerably with λ_b in this particular example. It is also observed in Fig. 5-11 for one curvilinear stiffener and in Fig. 5-15 for two curvilinear stiffeners that the frequency parameters are found to increase, for all cases, with higher number of stiffeners. Also, by comparing these two figures, it can be concluded that the relationship between λ_n and λ_b is not always nonlinear for some aspect ratios and it depends on the other parameters like the number of stiffeners and in-plane loads.

Effect of Stiffener Area Ratio:

The variation of the frequency parameters with respect to the in-plane load is studied here for various stiffener area ratios ($\delta = 0.5,\ 0.1,\ 0.2$) while keeping the bending stiffness rigidity of the stiffener unchanged ($\gamma = 5$). The effect of stiffener area ratios on the frequency parameter is presented in Fig. 5-16 (a). It is evident from this figure that raising the stiffener area ratio increases stiffeners' mass matrix more than stiffeners' geometric stiffness matrix. Hence the natural frequency is reduced more than the buckling load. Due to this effect, the frequency parameter of the stiffened plate under the in-plane load decreases less than the frequency parameter of the stiffened plate not subject to in-plane load. This effect can be observed more clearly for the plate with two curvilinear stiffeners (Fig. 5-16 (a)) than the plate with one curvilinear stiffener (Fig. 5-12(a)). From Fig. 5-16 (a), it is found that λ_n varies linearly with λ_b for all stiffener area ratios.

Effect of Stiffener Stiffness Ratio:

The effect of stiffener stiffness rigidity ratio (γ) can be evaluated by keeping the stiffener area ratio unchanged ($\delta = 0.1$). In this case, since the flexural rigidity of the stiffener is increased, the natural frequency and buckling load is increased as shown in Fig. 5-16 (b). Again, it can be seen that the relationship between frequency parameter (λ_n) and in-plane load parameter (λ_b) is linear for all values of

the stiffener stiffness rigidity ratios (γ).The diagram showing the frequency parameter for plate with a curvilinear stiffener for various stiffener stiffness rigidity ratios was previously presented in Fig. 5-12(b). By comparing Fig. 5-12(b) and Fig. 5-16 (b), it can be found that the amount of the increase in frequency parameter for plate with two stiffeners is more than plate with one stiffener. In other words, raising the stiffness rigidity ratios (γ) for two stiffeners can make the stiffened plate to have better vibration performance than plate with one stiffeners.

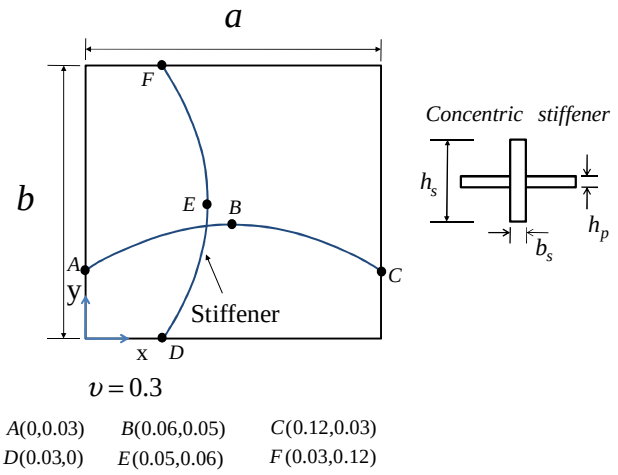

Fig. 5-13 Plate with two curvilinear stiffeners

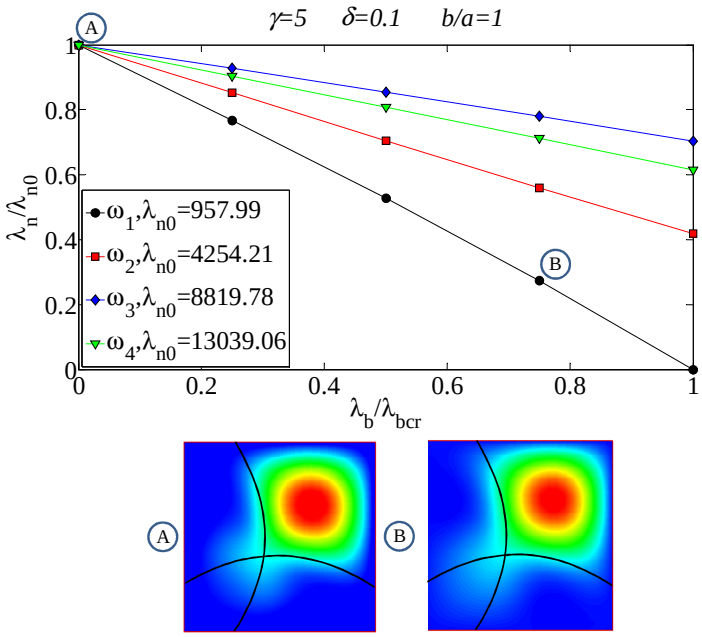

Fig. 5-14 Variation of first four frequency parameters of plate with two curvilinear stiffeners ($\delta = 0.1$ and $\gamma = 5$) vs. in-plane load (biaxial compression) parameter

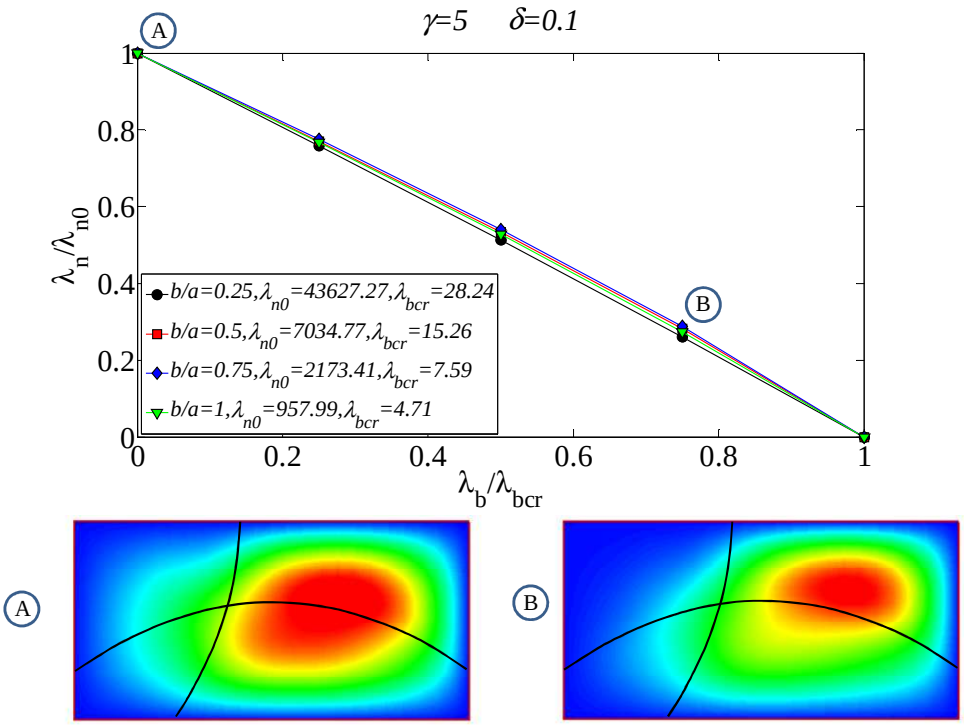

Fig. 5-15 Variation of first frequency parameters of plate with two curvilinear stiffeners ($\delta = 0.1$ and $\gamma = 5$) for different plate aspect ratios vs. in-plane load (biaxial compression) parameter

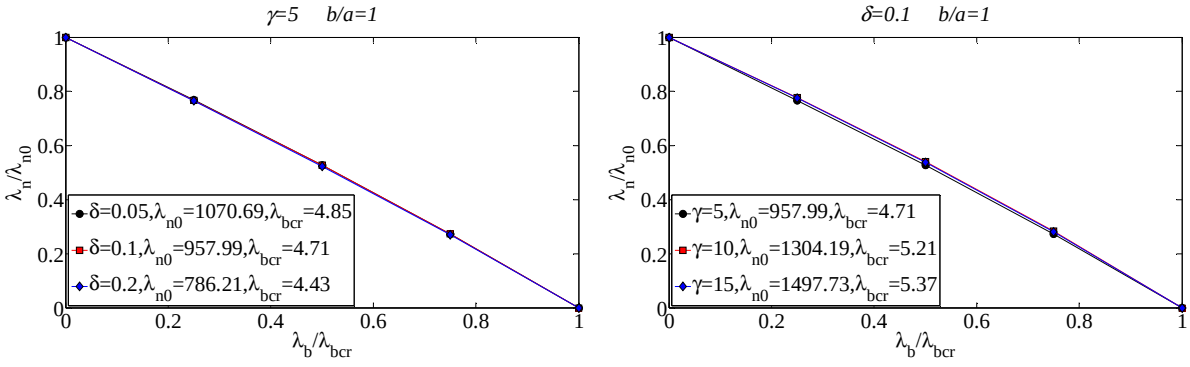

Fig. 5-16 Variation of first frequency parameters of plate with two curvilinear stiffeners vs. in-plane load (biaxial compression) parameter for (a) different stiffeners cross sectional area ratios (δ) (b) different stiffeners bending stiffness ratios (γ)

- ***Plate with four curvilinear stiffeners under biaxial Compression***

The objectives in considering a plate with four stiffeners are: a) to study the behaviour of plate with higher number of stiffeners and b) to compare the performance of this structure with the plate with one or

two curvilinear stiffeners. Specific attention is given to the influence of stiffener parameters on the vibration performance of stiffened plate under in-plane load. It will be shown in the following discussion that in addition to the plate aspect ratio and load condition, the number of stiffener and stiffener parameters can also change the relationship between the frequency parameter and the in-plane load parameter. The stiffened plate is simply supported along all its edges and is subjected to in-plane compression. The stiffener geometric properties are shown in Fig. 5-17. As can be seen in this figure, stiffeners are arranged symmetric with respect to the plate midline in *x* and *y* directions.

To investigate the effect of in-plane load on different modes, a square plate with four curvilinear stiffeners is considered. The stiffeners area ratio (δ) and stiffeners rigidity ratio (γ) are assumed to be 0.1 and 5, respectively. The variation of the frequency parameter of the stiffened plate for the first four modes versus in-plane load parameter is shown in Fig. 5-18. As can be seen in this figure, the frequency parameter for the first three modes varies linearly with the in-plane load parameter. Also, the mode shapes corresponding to the first natural frequency for loaded ($\lambda_b = 0.75\lambda_{cr}$) and unloaded ($\lambda_b = 0$) stiffened plate are shown in Fig. 5-18. Since the plate is square and also the stiffeners are arranged to be symmetric, see Fig. 5-18, the second and third natural frequencies are found to be the same.

Effect of Plate Aspect Ratio:

The behavior of the curvilinear stiffened plate with aspect ratios in the range $0.25 \le b/a \le 1$ is studied here. The results are carried out assuming that, except for the plate aspect ratio, all stiffener and plate geometric properties were kept unchanged. In this case, the stiffener area ratio (δ) is 0.1 and the stiffener stiffness ratio (γ) is 5. The variation of frequency parameter with in-plane load for plate having four stiffeners is shown in Fig. 5-19. It is observed that the variations are linear for all aspect ratios. The figure also indicates that, in general, a decrease of plate aspect ratio increases the stiffened plate's natural frequency and the buckling load.

Effect of Stiffener Area Ratio:

Now, by fixing both the stiffener stiffness ratio ($\gamma = 5$) and the plate aspect ratio ($b/a = 1$), the effect of the stiffener area ratio (δ) is studied. It can be observed in Fig. 5-20 that the frequency parameter variations for four stiffeners are similar to the plate with one stiffener and two stiffeners as shown in Fig. 5-12(a) and Fig. 5-16(a). In all of these figures, it can be seen that λ_n changes linearly with λ_b. Consequently, it can be concluded that changing the stiffener area ratio (δ) while the stiffener stiffness ratio (γ) is fixed will result in a linear relationship between λ_n and λ_b for a plate with various number of stiffeners under axial/biaxial compressive load.

Effect of Stiffener Stiffness Ratio:

Parametric studies are also conducted for various stiffener stiffness ratio (γ) to find the behavior of frequency parameter as the in-plane load varies. The plate aspect ratio and the stiffener area ratio are kept 1 and 0.1, respectively. In contrast with plate with one stiffener and two stiffeners, it can be observed in Fig.

5-21 that the relationship between frequency parameter and in-plane load parameter is not linear for $\gamma = 15$. Hence, it is evident from Fig. 5-12, Fig. 5-16 and Fig. 5-21 that the stiffener stiffness ratio (γ) can have different effect on the frequency parameter behavior with in-plane load parameter depending upon the number of stiffeners. The free vibration mode shape of loaded ($\lambda_b = 0.75\lambda_{cr}$) and unloaded ($\lambda_b = 0$) stiffened plate is also presented in Fig. 5-21. As expected, the mode shape changed by applying the in-plane compression.

- ***Plate with four curvilinear stiffeners under shear load***

The second loading case considered in this section is the uniformly distributed shear loads applied along the middle plane on all edges. The plate is simply supported on all edges and is stiffened by four stiffeners (Fig. 5-17). For studying the vibration behavior of the curvilinear stiffened plate under shear loads, various values for different parameters such as the plate aspect ratio (b/a), stiffeners' area ratio (δ) and stiffeners' rigidity ratio (γ) are considered.

Effect of Plate Aspect Ratio:

In order to obtain the influence of the plate aspect ratio on the relationship of the natural frequency and buckling load, the stiffeners area ratio (δ) and stiffeners rigidity ratio (γ) are fixed to be 5 and 0.1, respectively. The results of variation of frequency parameters with in-plane load parameter are shown in Fig. 5-22. The results indicate that, as expected, larger the aspect ratio, the smaller the critical shear buckling loads. As can be seen in Fig. 5-15, the relationship between λ_b and λ_n for stiffened plate under biaxial compression is close to being linear for all aspect ratios, however, as presented in Fig. 5-22, this relationship for stiffened plate under shear load is, for all cases, nonlinear. Hence, it can be concluded that in addition to the plate aspect ratio, number of stiffeners and the stiffeners' rigidity ratio, the load condition can also change the variation of λ_b with λ_n. The mode shapes for two load cases, loaded ($\lambda_b = 0.75\lambda_{cr}$) and unloaded ($\lambda_b = 0$), are shown in Fig. 5-22. It can be seen that the mode shapes are different for these two load cases.

Effect of Stiffener Area Ratio:

To evaluate the effects of stiffener area ratio (δ) on the curvilinear stiffened plate, the stiffeners rigidity ratio (γ=5) and plate aspect ratio ($b/a = 1$) are fixed. The results for different δ are presented in Fig. 5-23 (a). As it was seen before, although the frequency parameter is decreased considerably by raising δ, the buckling load did not change.

Effect of Stiffener Stiffness Ratio:

Finally, the variation of frequency parameter with in-plane shear load is studied for various stiffeners rigidity ratios (γ) while keeping the stiffener area ratio ($\delta = 0.1$) constant. It can be observed in Fig. 5-23(b) that by increasing the stiffeners rigidity ratio, both buckling and natural frequency are increased. Also, it can be seen that the relationship between λ_b and λ_n, for all cases, is nonlinear. It can be concluded

from present results that the relationship between frequency parameter and shear load parameter is nonlinear for different parameters.

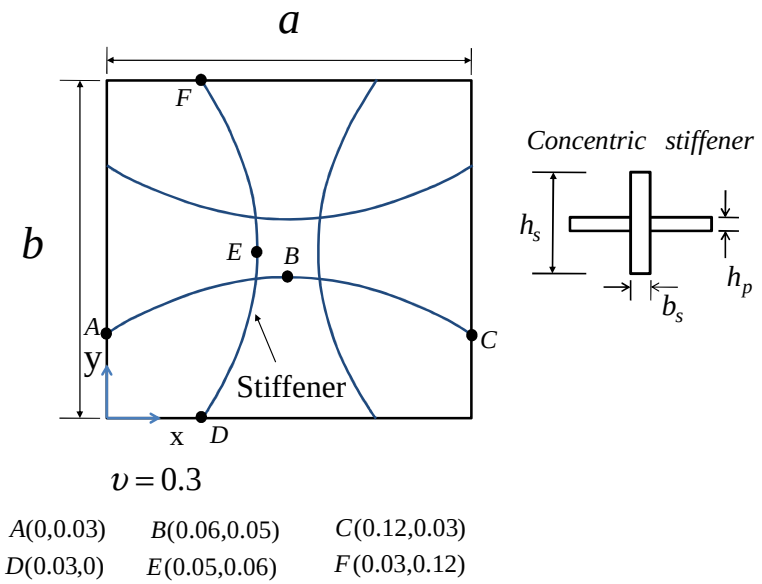

Fig. 5-17 Plate with four curvilinear stiffeners

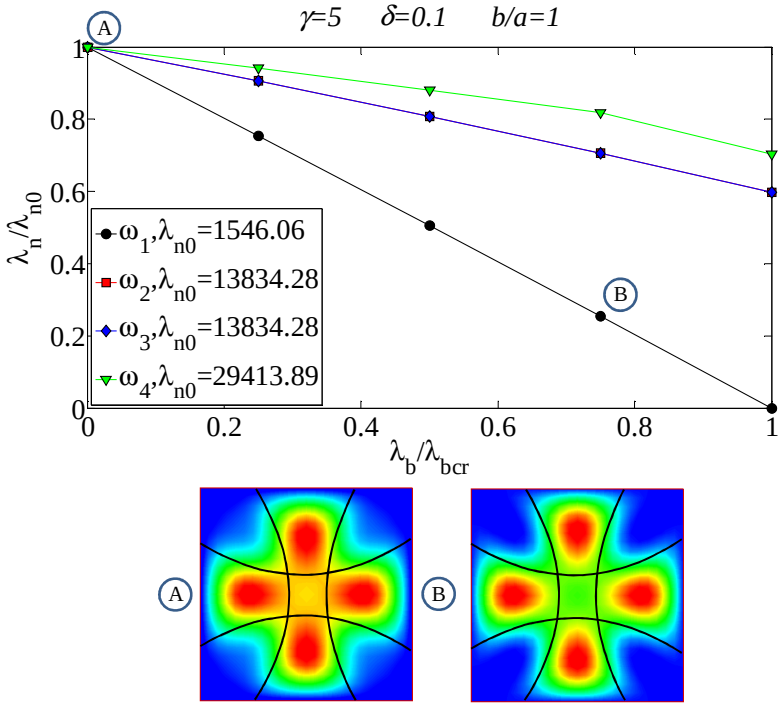

Fig. 5-18 Variation of first four frequency parameters of plate with four curvilinear stiffeners vs. in-plane load (biaxial compression) parameter

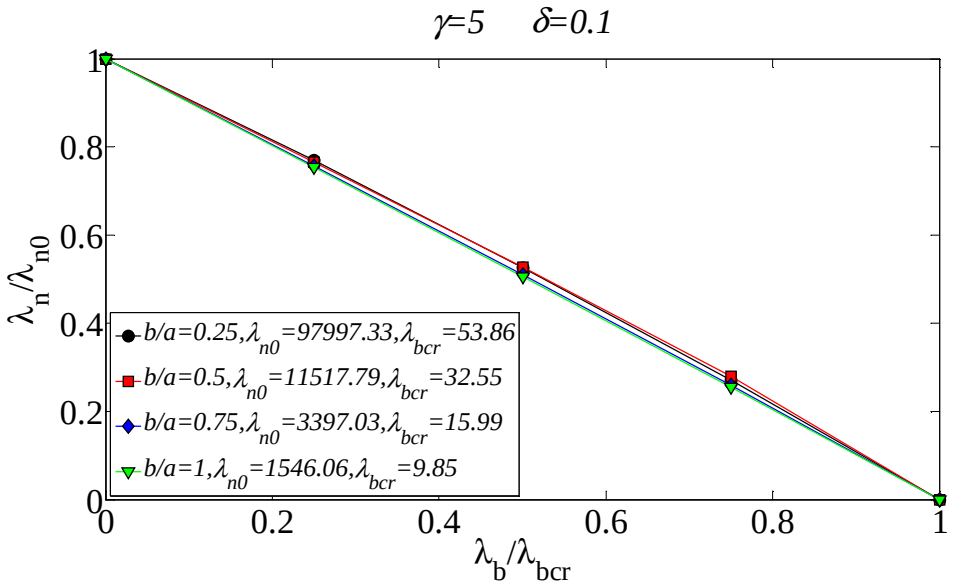

Fig. 5-19 Variation of first frequency parameters of plate with four curvilinear stiffeners ($\delta = 0.1$ and $\gamma = 5$) for different plate aspect ratios vs. in-plane load (biaxial compression) parameter

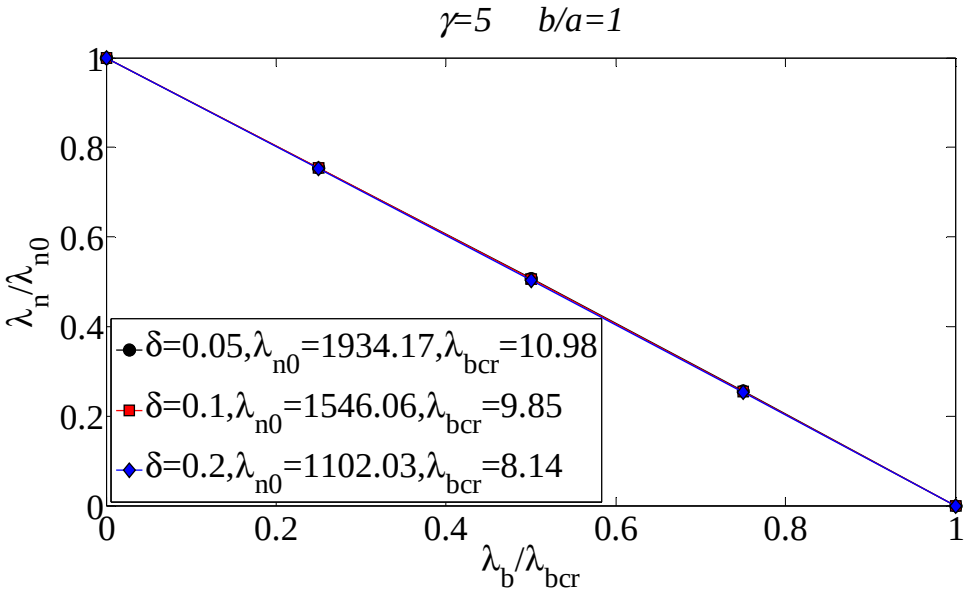

Fig. 5-20 Variation of first frequency parameters of plate with four curvilinear stiffeners ($\gamma = 5$) vs. in-plane load (biaxial compression) parameter for different stiffeners cross sectional area ratios (δ)

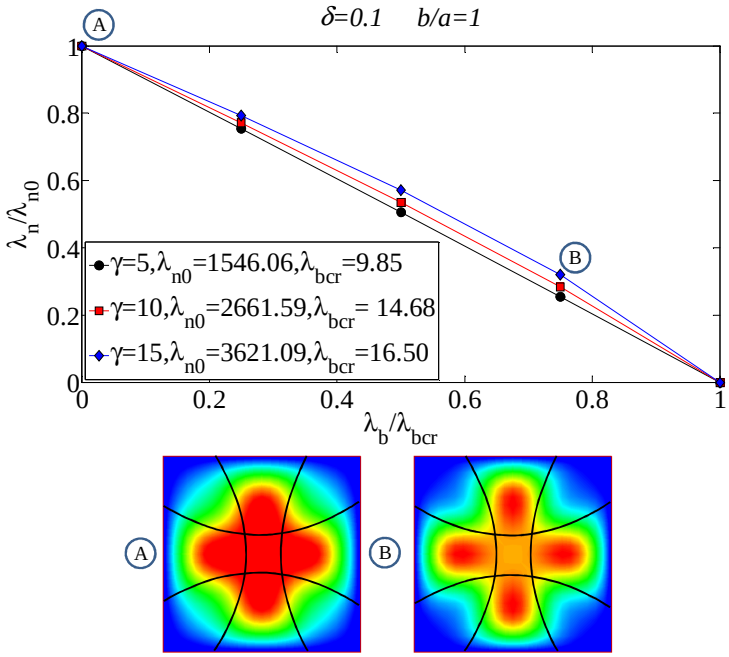

Fig. 5-21 Variation of first frequency parameters of plate with four curvilinear stiffeners ($\delta = 0.1$) vs. in-plane load (biaxial compression) parameter for different stiffeners bending stiffness ratios (γ)

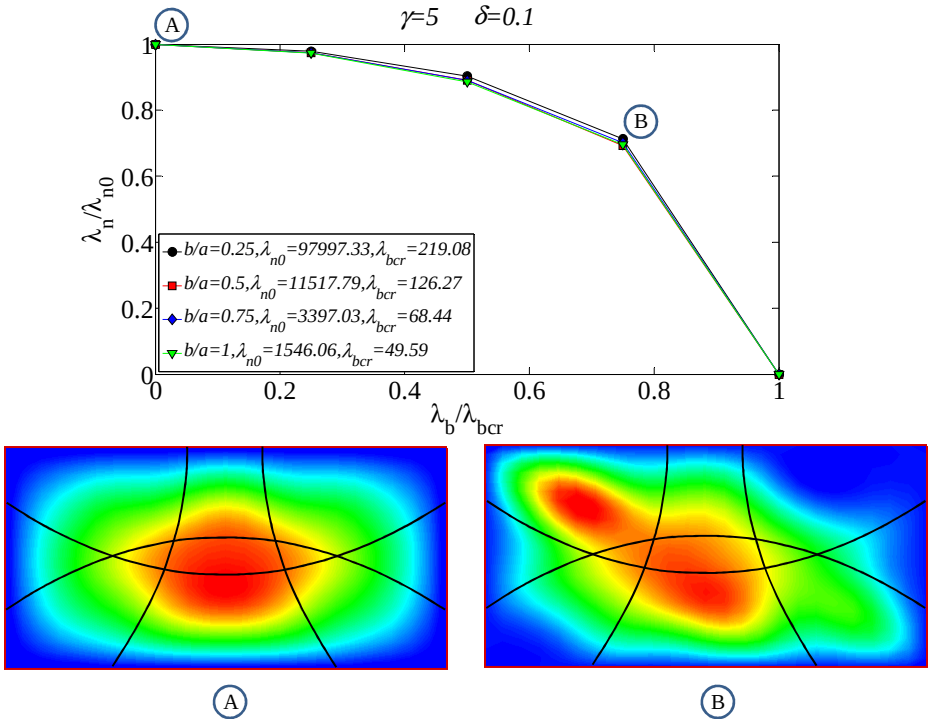

Fig. 5-22 Variation of first frequency parameters of plate with four curvilinear stiffeners ($\delta = 0.1$ and $\gamma = 5$) for different plate aspect ratios vs. in-plane load (shear load) parameter

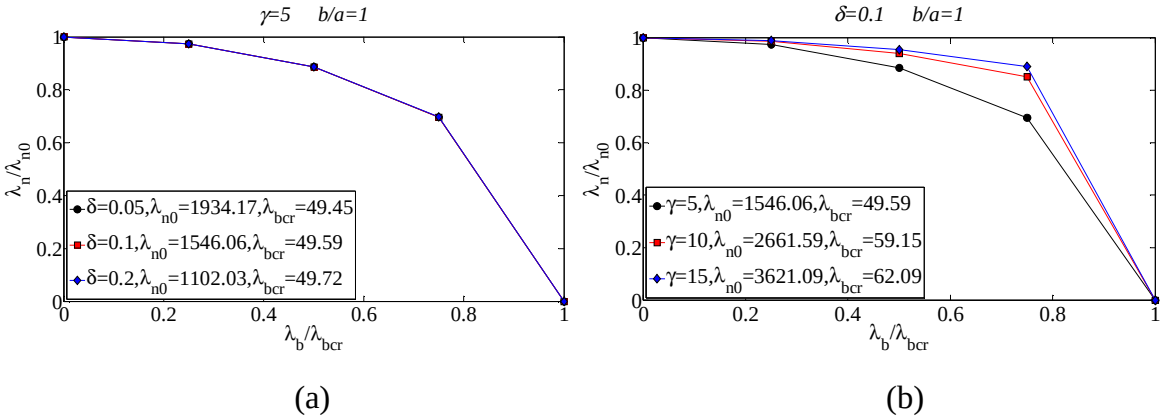

(a) (b)

Fig. 5-23 Variation of first frequency parameters of plate with four curvilinear stiffeners vs. in-plane load (shear load) parameter for (a) different stiffeners cross sectional area ratios (δ) (b) different stiffeners bending stiffness ratios (γ)

5.6 Conclusions

The Ritz method using Chebyshev polynomials is developed for the buckling analysis of curvilinearly-stiffened plate. The results of presented method are compared with those available in the literature as well as our earlier meshfree method. The good agreement between different sets of results was observed.

The vibration behavior of curvilinear stiffened plate subjected to in-plane load is studied. It was shown that the relationship between the natural frequency parameter and in-plane load parameter is a function of the number of stiffeners, the in-plane load condition, the plate aspect ratio and the stiffener stiffness ratio. The influence of these parameters on the vibration and buckling behavior is investigated. It is shown that increasing the stiffener area ratio does not change the critical buckling load considerably; however it can alter the natural frequency of a stiffened plate. Also, it was observed that variation in the stiffener stiffness ratio can make the relationship between frequency parameter and load parameter nonlinear. The stiffened plate under various in-plane load cases was considered. It was presented that for shear load, the frequency parameter changes nonlinearly with in-plane shear load parameter for different set of aspect ratios, stiffener area ratios and stiffener stiffness ratios.

The mode shapes for loaded and unloaded stiffened plate are presented. It is observed that when the frequency parameter changes nonlinearly with the in-plane load parameter, the mode shape can change significantly.

6 Random Response Analysis of Curvilinearly-Stiffened Plate Using Element Free Galerkin Method

6.1 Introduction

An Element Free Galerkin (EFG) formulation is presented for studying the random response of curvilinearly-stiffened plates. The structure is subjected to stationary random stochastic loading. The random loads are assumed as stationary in time but can be nonhomogeneous in space. The spectral density of the nodal force vector is formulated using the displacement shape functions. The direct complex matrix inversion method and modal superposition method are used to obtain the random response of structures. The spectral density of displacement for un-stiffened plate under white noise and plate with straight stiffeners subjected to jet noise are compared with those available in the literature. The power spectral density of displacement and stress of curvilinearly-stiffened plate under white noise are also verified using the commercial finite element software ANSYS®. Excellent agreement is seen in all cases. The effect of stiffener configuration, stiffness and curvature and in-plane load on spectral density is also investigated.

6.2 Theoretical Formulations

The equation of motion for a curvilinearly-stiffened plate can be expressed in matrix form as:

$$\begin{aligned} &[M]\{\ddot{u}\}+[C]\{\dot{u}\}+[K]\{u\}=\{f\} \\ &[M]=[M_p]+[M_s] \\ &[K]=[K_p]+[K_s]-[K_{Gp}]-[K_{Gs}] \end{aligned} \tag{6-1}$$

where $[K_p]$, $[K_{Gp}]$ and $[M_p]$ are the elastic stiffness, geometric stiffness and mass matrices of plate, $[K_s]$, $[K_{Gs}]$ and $[M_s]$ are the elastic stiffness, geometric stiffness and mass matrices of stiffener, and $[C]$ is damping matrix. $\{f\}$ is the time-dependent nodal forcing vector and $\{u\}$ is the nodal displacement vector.

To obtain the spectral density of displacement, first the admittance matrix $[H(\omega)]$ needs to be calculated. The admittance matrix can be found using the direct complex matrix inversion method or modal superposition method.

- ***Direct Complex Matrix Inversion Method***

Taking the Fourier transform of Eq. (6-1)

$$(-\omega^2[M]+i\omega[C]+[K])\{U\}=\{F\} \tag{6-2}$$

here ω is the excitation frequency, and $\{U\}$ and $\{F\}$ are the Fourier transforms of $\{u\}$ and $\{f\}$. $\{U\}$ can be obtained by using the admittance matrix

$$[H(\omega)]=(-\omega^2[M]+i\omega[C]+[K])^{-1}$$
$$[H(\omega)]=\begin{bmatrix} H_{11}(\omega) & \cdots & H_{1n}(\omega) \\ \vdots & \ddots & \vdots \\ H_{n1}(\omega) & \cdots & H_{nn}(\omega) \end{bmatrix} \tag{6-3}$$

where *n* is the number of degrees of freedom. This approach is applicable for non-proportional damping; however due to the need of matrix inversion at each step of the frequency, it requires a very high computation time. An alternative method, which avoids matrix inversion but is just applicable for specific form of damping which uncouples the equation of motion, is modal superposition method.

- ***Modal Superposition Method***

In the modal superposition method, first the free vibration problem in which there is no damping should be solved:

$$([K]-\omega_r^2[M])\{X_r\}=0 \tag{6-4}$$

By solving the above eigenvalue equation, the natural frequencies (ω_r) and mode shapes $\{X_r\}$ can be found. Using the transformation matrix containing the modal vectors as its columns ($[\psi]$), the nodal displacement $\{u\}$ can be transformed to the generalized nodal displacement $\{\eta\}$:

$$[\psi]=\begin{bmatrix} \{X_1\} & \cdots & \{X_i\} & \cdots & \{X_{nm}\} \end{bmatrix}$$
$$\{u\}=[\psi]\{\eta\} \tag{6-5}$$

where *nm* is the number of eigenvectors. By considering the proportional damping and using Eq. (6-5), Eq. (6-1) can be written as

$$\ddot{\eta}_r+2\zeta_r\omega_r\dot{\eta}_r+\omega_r^2\eta=Q_r \quad r=1,2,...nm \tag{6-6}$$

here Q_r, ζ_r and ω_r are the modal forces, modal viscous damping factors, and natural frequency, respectively. Taking Fourier transform of Eq. (6-6) for unit impulse applied for all degrees of freedom:

$$\eta_r = (-\omega^2 + i2\zeta_r\omega_r\omega + \omega_r^2)^{-1}\{X_r\}^T = \hat{H}(\omega_r)\{X_r\}^T \tag{6-7}$$

By substituting Eq. (6-7) in Eq. (6-5), the admittance matrix can be written as:

$$[H(\omega)] = [\psi][\hat{H}(\omega)][\psi]^T \quad \text{diag} \tag{6-8}$$

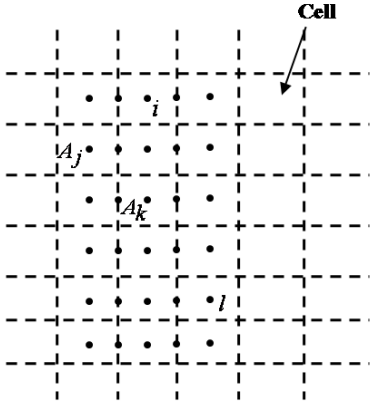

Fig. 6-1 Background cell structures

- ***Response Cross-Spectral Density***

The response at the point *i* of a structure due to a force applied at point *j* is (Fig. 6-1)

$$u_{ij}(t) = \int_{-\infty}^{\infty} h_{ij}(\tau_1) f_j(t-\tau_1) d\tau_1 \tag{6-9}$$

The cross spectral density matrix for displacements for an ergodic process can be written as [91]

$$S_{u_i u_k}(\omega) = [H(\omega)][S_{FF}(\omega)][\bar{H}(\omega)] \tag{6-10}$$

where $[S_{FF}(\omega)]$ is the cross spectral density matrix of the generalize force and $[\bar{H}(\omega)]$ is the complex conjugate of $[H(\omega)]$. For a homogeneous pressure cross spectral density, it can be assumed to be fully correlated over the contributing area. However for nonhomogeneous pressure cross spectral density, double area integrals in Eq. (6-10) need to be evaluated [31].

The relationship between the nodal displacements and stresses can be written as:

$$\{\sigma\} = [D][B]\{u\} \tag{6-11}$$

By using Eq. (6-10) and (6-11), the cross spectral density matrix for stress can be obtained:

$$[S_{\sigma\sigma}(\omega)] = [D][B][S_{uu}(\omega)][B]^T [D] \tag{6-12}$$

6.3 Numerical Results

Numerical results have been obtained for unstiffned plate under white noise, plate with straight stiffeners under jet noise, and plate with curvilinear stiffeners under white noise and jet noise. For unstiffened plate, both the direct complex matrix inversion method and the normal mode approach are used and it is shown that the results agree well. For stiffened plate, the normal mode approach is applied to obtain the admittance. The results for unstiffned plate and plate with straight stiffeners are compared with other available results in the literature. Also the results of curvilinearly-stiffened plate are compared with ANSYS® results. For all examples in this research the proportional damping is considered, however by using the direct complex matrix inversion method, we also are able to apply the non-proportional damping.

- ***Simply-Supported Square Plate under White Noise***

The plate is excited by white noise. The pressure power spectral density is

$$S_{pp} = \frac{1}{\pi}\int_{-\infty}^{\infty} \frac{\sin\omega_c\tau}{\tau} e^{-i\omega\tau} d\tau = \begin{cases} 1 & \text{for } |\omega| \le \omega_c \\ 0 & \text{for } |\omega| > \omega_c \end{cases} \tag{6-13}$$

where ω_c is the cut-off frequency. In this example, the random force acting on the area is assumed to be fully correlated. The plate is square and simply-supported on all edges. The plate geometric and material properties are given in Fig. 6-2. The random response is computed by applying the direct complex matrix inversion method and the normal mode approach using the eigenvalues and eigenvectors of the undamped system. First the nodal force spectral density is computed and then the displacement spectral density is obtained by substituting the nodal force spectral density in Eq. (6-10). The ten lowest modes are considered and the eigenvalues and eigenvectors for those modes are used in Eq. (6-8) to find the admittance. A 11×11 uniform locations are considered for modeling the plate.

The power spectral density for displacement at center of plate is presented in Table 6-1. The results are compared with those of [29], [31] and [33]. As can be seen, there is a good agreement between the results obtained by the proposed method and others' results. The non-dimensional displacement spectral density for the centre of plate versus non-dimensional excitation frequency is presented in Fig. 6-3 along with the results reported by Liu *et al*. [33].

Because the present direct method and normal mode method yielded the same results, for the stiffened plate only the normal mode method, which is more efficient than direct method, is applied to calculate the random response.

Table 6-1 Comparison of PSD for displacement at center of plate at $\omega = 0$ and $\omega = 20$

$\omega = 0$						
Dey [29] (Finite Element)	Dey [29] (Analytical Solution)	Mukherjee and Mukhopadhyay [31]	Liu *et al*. [33] (Lumped-Load)	Liu *et al*. [33] (Consistent-Load)	Present code (Direct Method)	Present code (Normal Mode)
1.56×10^{-5}	1.71×10^{-5}	1.69×10^{-5}	1.61×10^{-5}	1.75×10^{-5}	1.67×10^{-5}	1.67×10^{-5}
$\omega = 20$						
1.54×10^{-3}	1.73×10^{-3}	1.66×10^{-3}	NA	NA	1.61×10^{-3}	1.61×10^{-3}

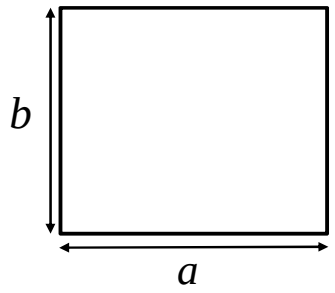

$a = 1 \quad D = 1$

$b = 1 \quad \upsilon = 0.3$

$\rho = 1$

Structural damping $= 0.1$

Fig. 6-2 Simply-supported square plate

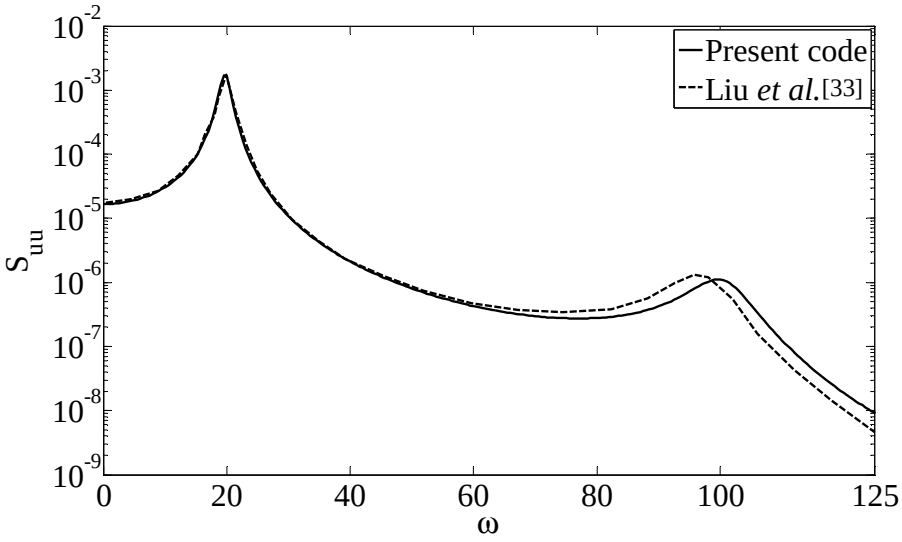

Fig. 6-3 Displacement spectral density at centre of plate

- ***Plate with Straight Stiffeners under Jet Noise***

As was mentioned, the developed method has the ability to accommodate for plate with straight or curvilinear stiffeners. The response of the stiffened plate subjected to jet noise excitation, which is described by Olson and Lindberg [28] and Mukherjee and Mukhopadhyay [31], is considered here. The cross spectral density function for the pressure is [28]

$$S_{pp} = p_0^2 \frac{4500/\pi[4500^2 + 80002 + \omega^2]}{[4500^2 + (\omega - 8000)^2][4500^2 + (\omega + 8000)^2]} e^{[-0.05|\bar{x}| - 0.037|\bar{y}| - i\omega\bar{x}/14000]} \tag{6-14}$$

where p_0 is the mean square pressure, which is assumed to be constant over the plate area, $\omega(rad/\sec)$ is the excitation frequency, and $\bar{x}$ and $\bar{y}$ are $x_i - x_j$ and $y_i - y_j$, respectively (Shown in Fig. 6-1). Since the cross spectral density is not homogenous, the double area integrals in Eq. (6-10) are evaluated by using the Gauss quadrature method. The geometry and material properties of the plate and stiffeners are given in Fig. 6-4. The plate is clamped on all edges.

The natural frequencies of the stiffened plate are shown in Table 6-2. It can be seen that the results of the present method, those available in the literature and those obtained by ANSYS® are all close to each other. In ANSYS®, 1000 SHELL63 elements were used for modeling the plate and 20 BEAM188 elements were used for modeling each stiffener. For the meshfree modeling, 40×16 particles were considered for the plate and 16 particles were considered for each of the stiffeners. For calculating the displacement spectral density, first the admittance matrix is obtained using the normal mode approach. Forty modes are considered to find the admittance and displacement spectral density.

The obtained spectral density of deflection at the center of bay 1, bay 2, and bay 3 using meshfree method are compared with those reported by Olson and Lindberg [28] and Mukherjee and Mukhopadhyay [31] in Fig. 6-5, Fig. 6-6, Fig. 6-7, respectively. Olson and Lindberg [28] and Mukherjee and Mukhopadhyay [31] employed 80 and 14 modes, respectively, to obtain the random response of structure.

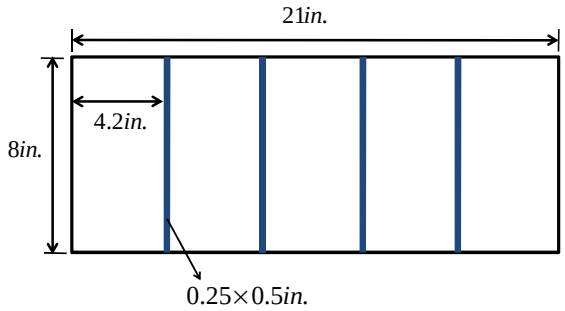

$t = 0.05in.$ $\quad \upsilon = 0.3$

$E = 10^7\ psi$ $\quad \zeta = 0.002$

$\rho = 0.000262\ lb\ \sec^2/in.^4$

Fig. 6-4 A clamped plate with straight stiffeners

Table 6-2 Natural frequencies (Hz) of stiffened panel

Mode	Olson and Lindberg [28]	Olson and Lindberg [28]	Mukherjee and Mukhopadhyay [31]	Present code	ANSYS
1	609	623	619	597	585
2	634	630	629	611	600
3	651	638	629	629	618
4	669	673	659	646	637
5	682	673	660	648	640
6	897	915	898	876	856
7	910	920	901	876	860
8	917	917	905	878	865
9	928	928	910	880	871
10	945	945	910	880	871
11	1175	1175	1160	1267	1250
12	1245	1245	1263	1269	1251
13	1330	1330	1270	1271	1253
14	1429	1429	1265	1272	1255

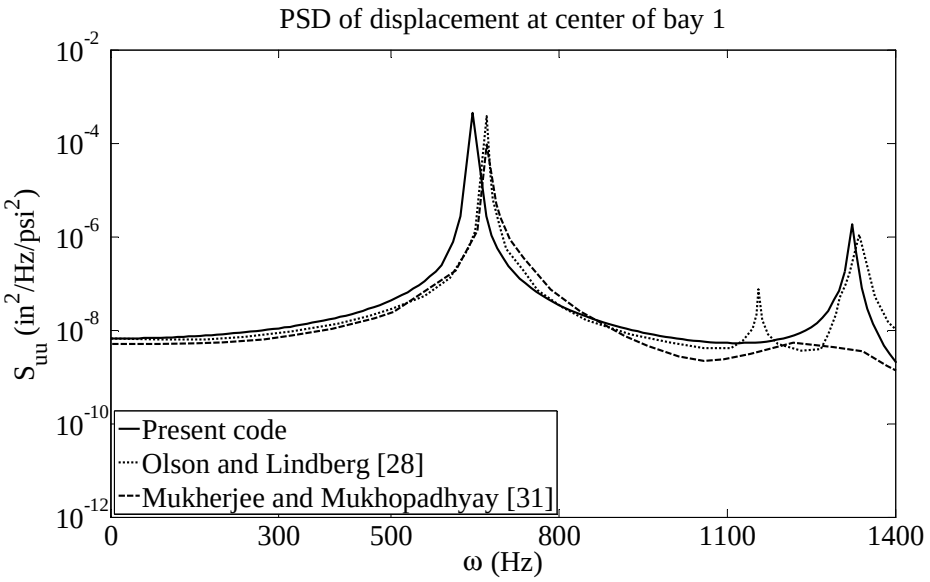

Fig. 6-5 Spectral density of displacement at center of bay 1

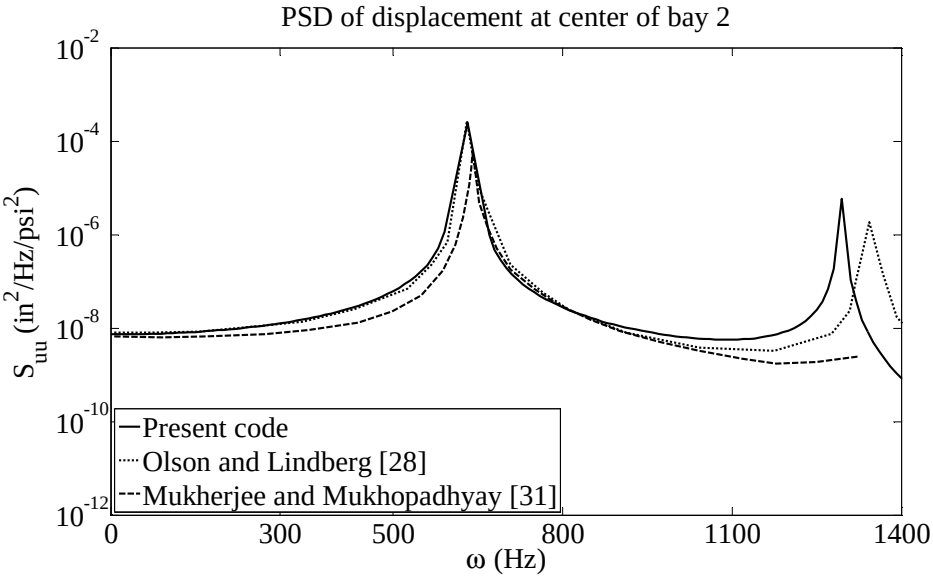

Fig. 6-6 Spectral density of displacement at center of bay 2

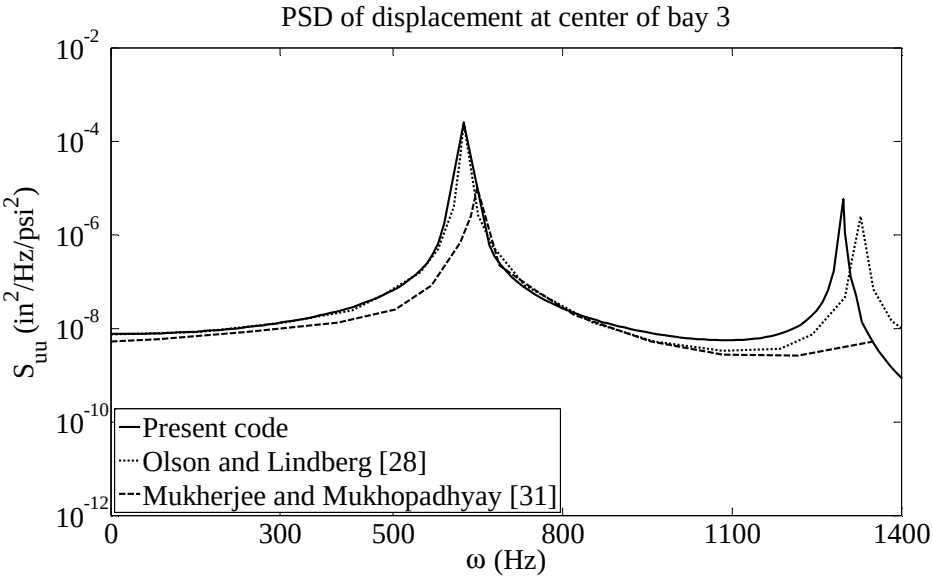

Fig. 6-7 Spectral density of displacement at center of bay 3

- ***Plate with Curvilinear Stiffeners***

A 24 by 28 *in.* curvilinear stiffened panel was machined from 2219-T851 aluminum for experimental validation of the Ritz and meshfree methods. Experimental results appeared to agree well with the meshfree and Ritz method results.

Here the same curvilinearly-stiffened plate and boundary conditions (Fig. 6-8) are considered. The stiffened plate is excited by white noise. The pressure power spectral density is defined in Eq. (6-13). To

check the accuracy of the present meshfree code, results for curvilinearly-stiffened plate under white noise are compared with those obtained using ANSYS®. From the ANSYS® library, 1256 SHELL63 and 60 BEAM188 are chosen for modeling the plate and stiffeners, respectively. In the meshfree code, 20×20 particles and 50 particles are considered for the plate and stiffeners, respectively.

The modal approach is adopted by using the first ten mode shapes obtained from meshfree and ANSYS®. The spectral density of the deflection at the point Q obtained using meshfree, as can be seen in Fig. 6-9, agree well with those calculated using ANSYS®. The spectral density of the stress at the point Q is shown in Fig. 6-10, which is close to the result obtained using ANSYS®.

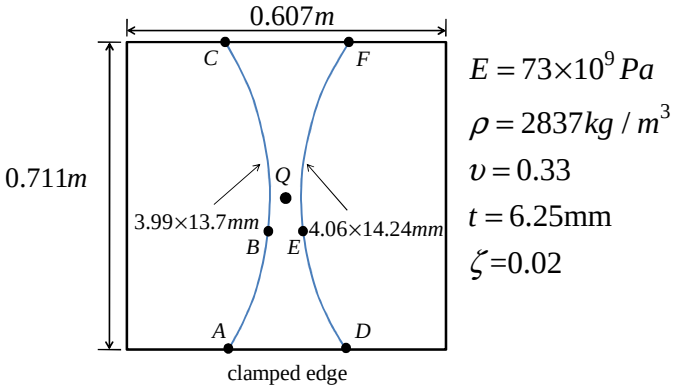

Fig. 6-8 Curvilinearly-stiffened plate

- ***Cantilever Plates with Different Stiffener Configurations***

The behavior of the unstiffened plate and stiffened plate with different stiffener configurations is studied here. Three stiffener configurations are considered in this example; straight, inclined and curvilinear, as can be seen in Fig. 6-11. In the previous example, the spectral density of the deflection of curvilinearly-stiffened plate is calculated. The same curvilinearly-stiffened plate is considered as the fourth model. As we are interested to obtain low spectral density while keeping the mass constant, the average spectral density of deflection ($S_{ave}=\sqrt{\frac{1}{n}\sum_{i=1}^{n}S_{uui}^2}$, n: number of nodes) is carried out assuming that the total mass of structures are kept unchanged. It is also assumed that the structure is under jet noise excitation which is given as:

$$S_{pp}=p_0^2e^{(-i\omega\bar{x}/340)} \tag{6-15}$$

Deflection spectral densities were obtained using Eq. (6-10) by considering the first 10 modes. The spectral density of stress is also calculated using (6-12). The average spectral density of the deflection and

stress for different models are shown in Fig. 6-12 and Fig. 6-13, respectively. It can be observed that the spectral density of deflection and stress can vary by changing the stiffeners' configuration while the total mass is kept unchanged. The final optimal design can be found by using optimization tools.

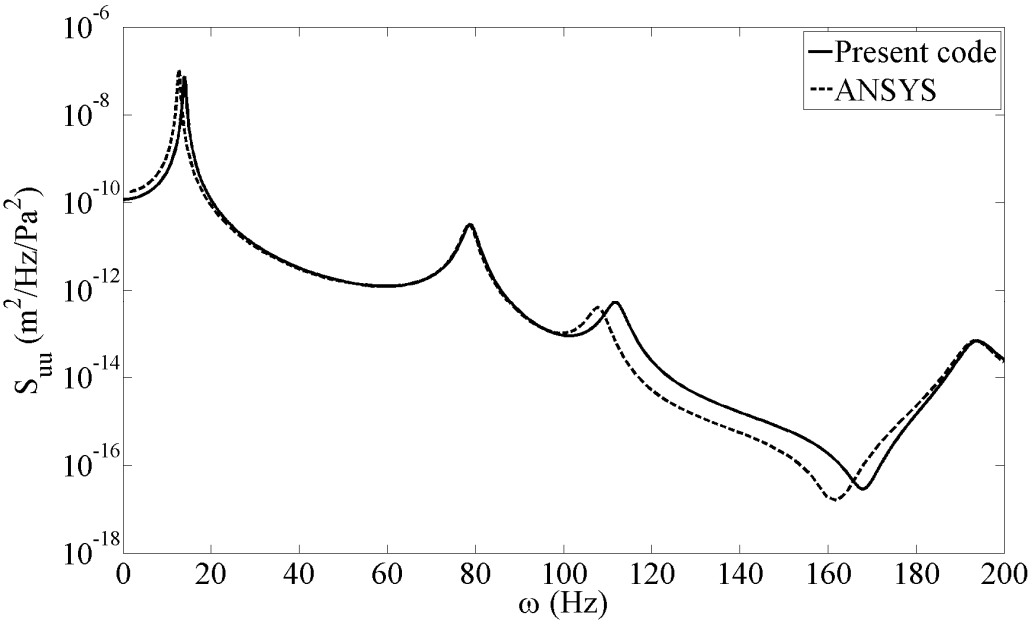

Fig. 6-9 Spectral density of displacement at point Q

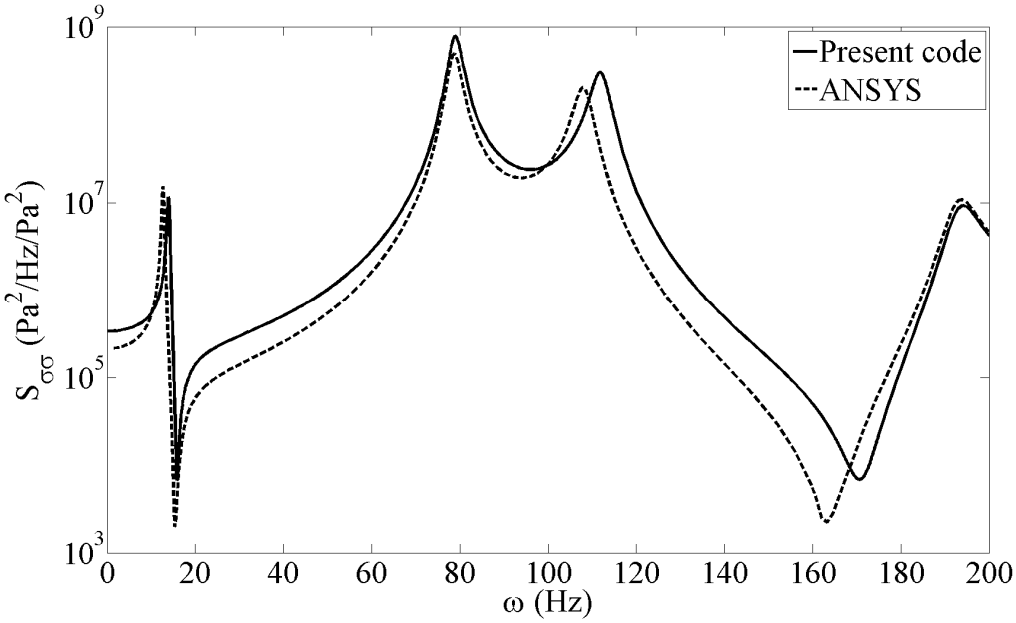

Fig. 6-10 Spectral density of stress at point Q

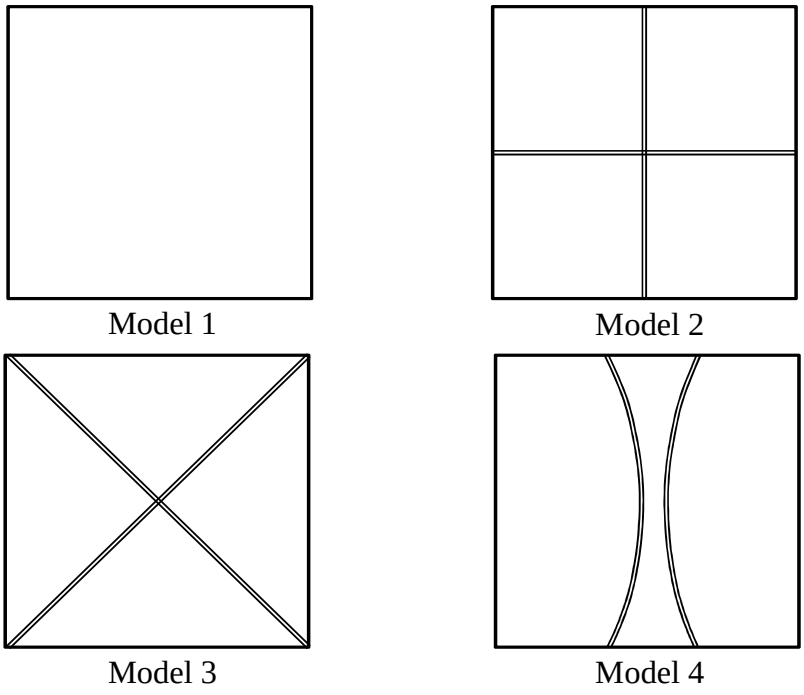

Fig. 6-11 Unstiffened and stiffened plate with straight, inclined and curvilinear stiffeners

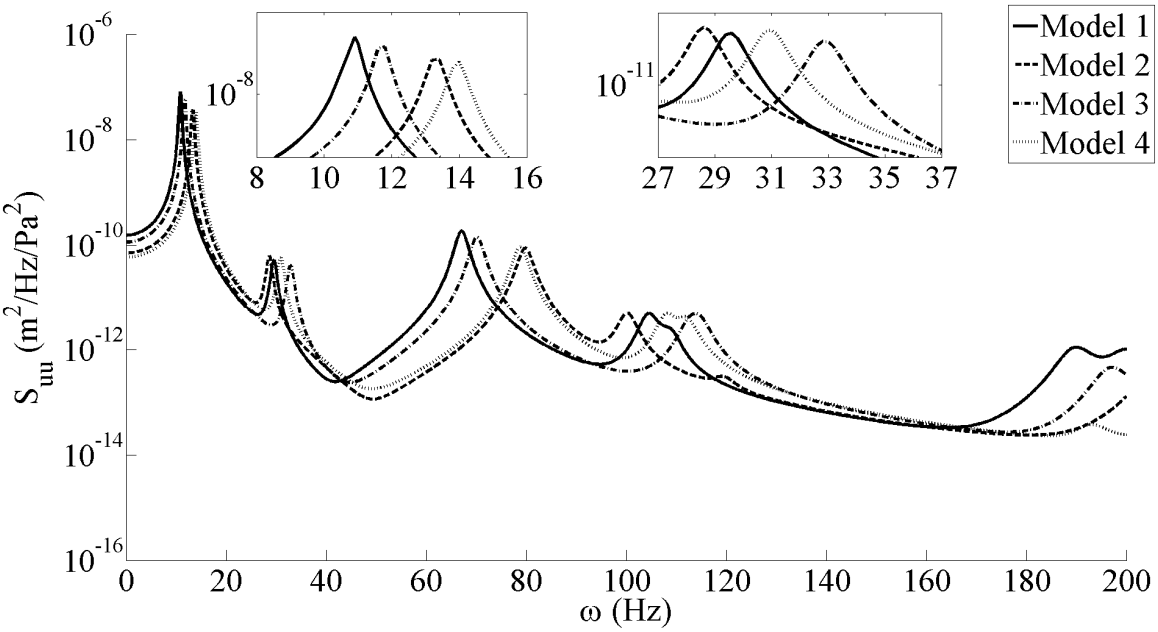

Fig. 6-12 Average spectral density of displacement of unstiffened and stiffened plates

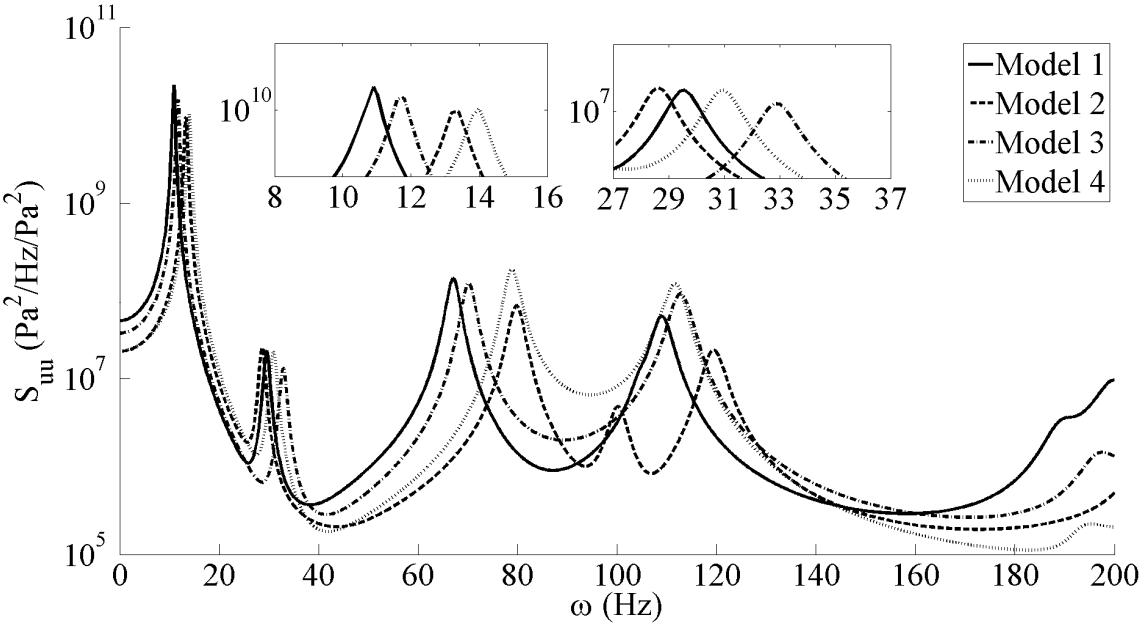

Fig. 6-13 Average spectral density of stress of unstiffened and stiffened plates

- ***Effect of Stiffener Stiffness Ratio***

The effect of stiffener stiffness on spectral density of deflection of a simply-supported square plate with a curvilinear stiffener subjected to jet noise is considered. The properties of the plate and the stiffener are shown in Fig. 6-14. The configuration of stiffener is determined by using three points. The starting and ending points are shown in Fig. 6-14, and the third point was calculated by using curvature. In this example the radius of curvature is $R = 0.23m$.

For simplicity and generality, cross sectional area ratio and bending stiffness ratio of the stiffener are introduced. The ratio of the cross sectional area of the stiffener to that of the plate is defined by $\delta = b_s h_s / a h_p$ where b_s, h_s, a and h_p are the width of the stiffener, height of the stiffener, width of the plate and thickness of the plate, respectively. The ratio of the bending stiffness of the stiffener to that of the plate is defined by $\gamma = E_s I_s / aD$ where E_s, I_s and D are the elastic modulus of the stiffener, second moment of the stiffener cross section area with respect to the stiffener neutral axis and flexural rigidity of the plate, respectively.

The Root Mean Square (RMS) of average spectral density of deflection obtained for $\delta = 0.1$ related to eccentric curvilinear stiffener. The Root Mean Square (RMS) of average spectral density of deflection can be defined as:

$$R(S_{ave}) = \frac{1}{\omega_2 - \omega_1} \int_{\omega_1}^{\omega_2} S_{ave}(\omega) d\omega \tag{6-16}$$

To provide a better view of the behavior of the stiffened plate for various stiffener stiffness ratio, the effect of bending stiffness rigidity of the stiffened plates having fixed stiffener area ratio ($\delta = 0.1$) on the RMS of spectral density of deflection is shown in Fig. 6-15. As it expected, the RMS of spectral density of deflection increases when the stiffener stiffness ratio is increasing. Since the stiffener area ratio is fixed, the mass of stiffener does not change (The stiffener mass is 0.8kg for all cases).

- ***Effect of Stiffener Curvature***

The effect of stiffener curvature on the RMS of spectral density of deflection for simply-supported square curvilinear stiffened plate with $\delta = 0.1$ and $\gamma = 5$, subjected to jet noise, is examined here. The results presented in Fig. 6-16 imply that increasing the curvature may decrease the deflection; however it will always increase the mass of stiffener. The optimal curvature can be found by using optimization tools.

- ***Effect of Axial Compression***

In the following section, the behavior of curvilinear stiffened plate ($\delta = 0.1$, $\gamma = 5$ and $R = 0.23m$), simply supported on all edges, under axial in-plane compressive loading are studied. The structure is subjected to jet noise excitation and the RMS of spectral density of deflection for various ratios of in-plane load is plotted in Fig. 6-17. P_{cr} in this figure is the buckling load of curvilinearly-stiffened plate. As expected, it is shown in Fig. 6-17 that an increase in the in-plane axial compression, results in an increase in the RMS of spectral density of deflection of stiffened plate.

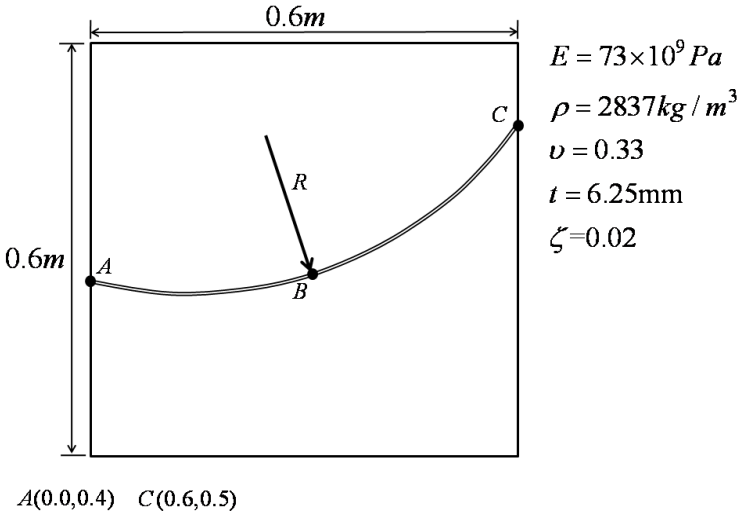

Fig. 6-14 Simply-supported plate with one curvilinear stiffener

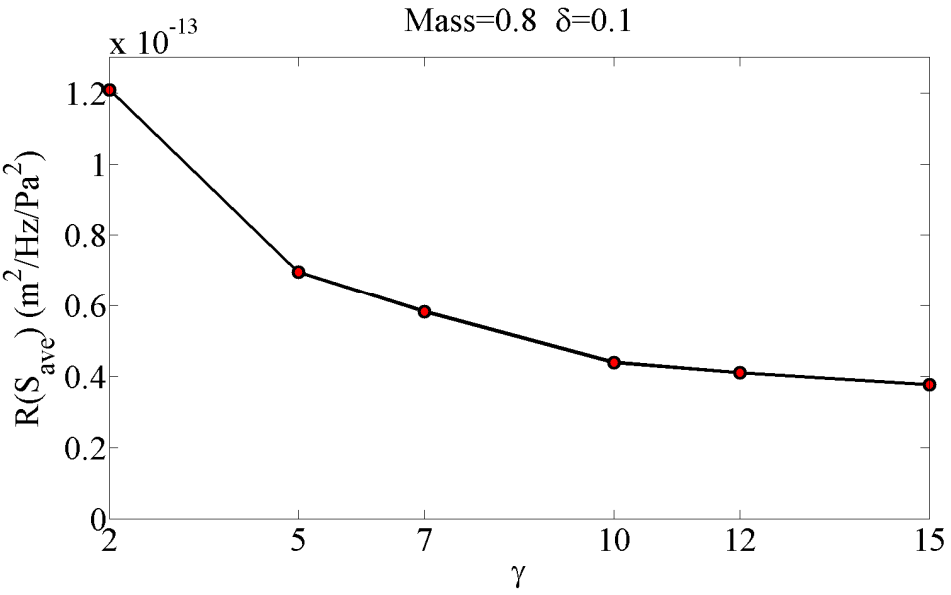

Fig. 6-15 Variation of r.m.s of spectral density of deflection of curvilinearly-stiffened plate ($\delta = 0.1$) vs. stiffeners bending stiffness ratios (γ)

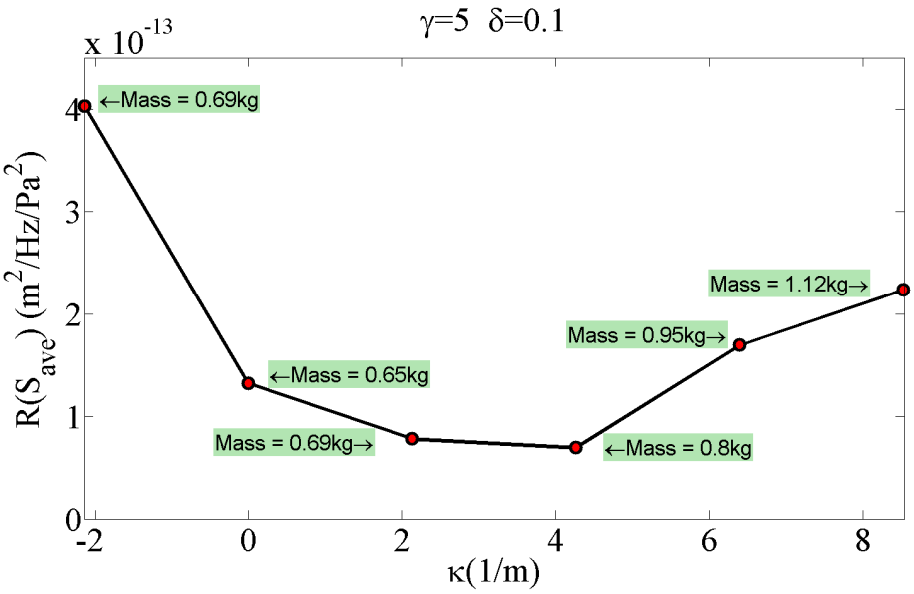

Fig. 6-16 Variation of r.m.s of spectral density of deflection of curvilinearly-stiffened plate ($\gamma = 5$ and $\delta = 0.1$) vs. curvature of stiffener (κ)

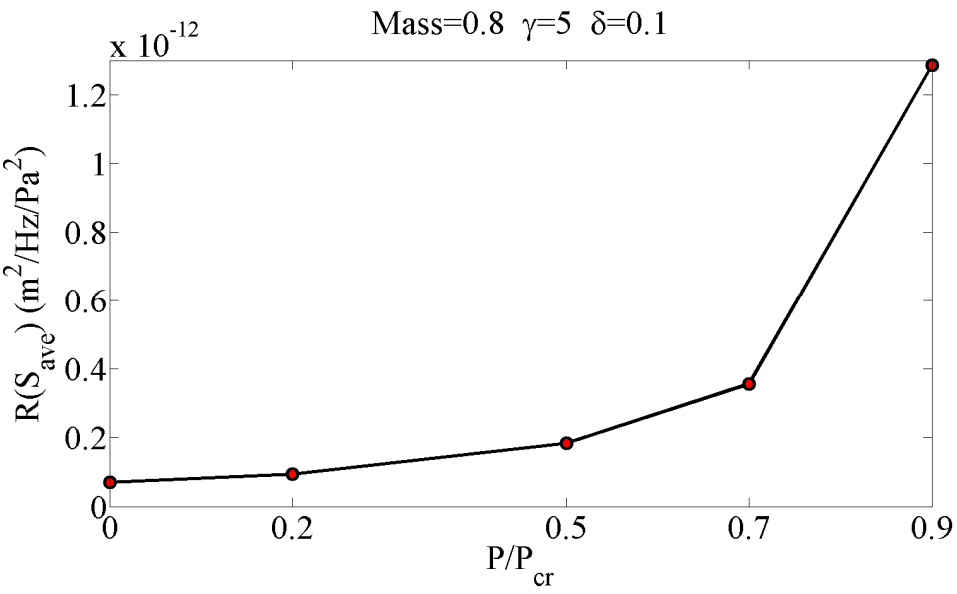

Fig. 6-17 Variation of r.m.s of spectral density of deflection of curvilinearly-stiffened plate ($\delta = 0.1$ and $\gamma = 5$) vs. in-plane load (axial compression)

6.4 Conclusions

This section presents a meshfree formulation for calculating the random response of curvilinearly-stiffened plate. The random load is stationary in time but can be homogeneous or nonhomogeneous in space. Examples are given for unstiffened plate and plate with straight and curvilinear stiffeners. The results of developed method for unstiffened plate and plate with straight stiffeners under white or jet noise are compared with those available in the literature. Also the spectral density of deflection for curvilinearly-stiffened plate is compared with those obtained using ANSYS®. A good agreement was seen in all cases.

Different stiffeners configuration's spectral densities were compared and it was shown that changing the stiffeners' configuration while keeping the total mass constant would change the spectral density of deflection and stress. However the final optimal design can only be found by using optimization tools.

Also, a detailed study of random response of curvilinearly-stiffened plate under jet noise is performed. It was shown that by using the stiffness and curvature of a stiffener, the spectral density of deflection can be impacted. The influence of the in-plane compression on the random vibration behavior of stiffened plate is also investigated.

7 Optimization of Curvilinearly Stiffened Plate Using Meshfree Method and Kriging Estimation

7.1 Introduction

As discussed earlier, since the FEM analysis of curvilinearly stiffened plate is quite expensive, the meshfree method is chosen as the analyzer to reduce the CPU time. However it will still require many simulations. In the optimization of curvilinearly stiffened problem, surrogate models for analysis and optimization can be very efficient. As is discussed, one of the powerful and popular surrogate models in structures and structural dynamics is kriging approximation. To use the advantage of both meshfree method and a surrogate model in reducing CPU time of optimization, the meshfree method is used to generate the sample points and the combination of kriging and Genetic Algorithms (GA) is then used for design of curvilinearly stiffened plate. In this research, optimization process is decomposed into two parts, the first part involves calculation of the best stiffener curve that would give the maximum buckling load, and the second step involves a sizing optimization while keeping the stiffener curve constant to minimize the mass and satisfy the buckling constrain. The meshfree and kriging results and CPU time are compared with those obtained using MD.PATRAN®, MD.NASTRAN®, and kriging, as well as *EBF3PanelOpt*. The readers are referred to the paper by Gurav and Kapania [77] for details of the *EBF3PanelOpt* framework.

7.2 Kriging Approximation

In the following section, we provide a brief description of the kriging approximation and also introduce the notation and some definitions (Please see [70] for more details). kriging is a method that interpolate a set of scattered data using a linear combination of polynomial terms and special ‘basis function’ terms:

$$\hat{y}(x) = \underline{f}^T(x)\underline{a} + Z(x)$$
$$\underline{f}(x) = [\, f_1(x) \quad ..... \quad f_k(x)]^T \tag{7-1}$$
$$\underline{a} = [a_1 \quad ..... \quad a_k]^T$$

where $\underline{f}^T(x)\underline{a}$ and $Z(x)$ are a linear regression and a random process which is centered around one of the sampled points. Let us assume that we have *n* sample points. Eq. (7-1), the predictor at a new point x^* can be written as [70]:

$$\hat{y}(x^*) = \sum_{i=1}^{m} f_i(x^*)a_i + \sum_{j=1}^{n} \varphi_j(x^* - x_j)b_j \tag{7-2}$$

There are different choices for the basis function (φ), e.g. linear, cubic, spline, Gaussian, spherical and etc. One of the most popular choices is Gaussian which we also used in our research:

$$\varphi(\underline{z}) = \exp\ (-\sum_{l=1}^{d} \theta_l |z_l|^2) \tag{7-3}$$

where $\|z_l\|$ is the Euclidean norm, *d* is dimension of *z*, and parameter θ_l is assumed to satisfy $\theta_l \geq 0$. As can be seen in Eq. (7-3), the function is 1 when $x^* = x_j$, it tends to zero when $\|x^* - x_j\| \to \infty$, and The θ_l parameter controls how fast the function moves.

By using the kriging approximation we can also find the predicted mean squared error [92]:

$$MSE(\hat{y}(x)) = \sigma^2 \left[1 - \begin{bmatrix} \underline{f}^T(x) & \underline{r}^T(x) \end{bmatrix} \begin{bmatrix} 0 & F^T(x) \\ F(x) & R \end{bmatrix}^{-1} \begin{bmatrix} \underline{f}^T(x) \\ \underline{r}^T(x) \end{bmatrix} \right] \tag{7-4}$$

where σ^2 is the process variance, *R* is the matrix of correlation between random variables, $\underline{F}$ is the random response vector, and *r* denotes the vector of correlations of $F(x^*)$ and $F(x_i)$.

7.3 Optimization Using Kriging

The design optimization of curvilinearly stiffened plate is obtained using kriging method. The geometry of the structure is defined by the cross sectional dimensions of the plate and stiffeners and the shape of the stiffener curves. The optimization is carried out in two stages. In the first stage, the most effective stiffener curves are obtained in the shape variable subspace by solving a bound unconstrained optimization problem for maximization of the buckling eigenvalue. Only the stiffener curve shape variables are allowed to

change, while the stiffener and plate cross sections are held constant. In the second stage, the stiffener shape is kept constant, and the cross-sectional dimensions are obtained for minimum mass subject to constraint on buckling eigenvalue.

Previous work on unitized structures by Kapania *et al*. [15-17] dealt with size and shape optimization of curvilinear stiffeners using MD.PATRAN®, MD.NASTRAN®, and VisualDOC®. They developed a framework, *EBF3PanelOpt*, for creating interfaces between parametric modeling, FEA, and Optimizer. Although the framework was well developed for various analysis, such us buckling, static, acoustic, and damage tolerance analysis, it was computationally expensive.

The work in this research is an effort to optimize the curvilinearly stiffened plate in less CPU time. There are thirteen design variables in this problem, as listed in Table 7-1 and shown in Fig. 7-1. Two new approaches are introduced toward optimal size and shape of stiffeners for minimum mass design of a stiffened panel under buckling constraint. The first approach, by using MD.PATRAN® and MD.NASTRAN®, kriging method is developed to fit a response surface for mass and buckling estimation of curvilinearly stiffened plate. In the second approach, sample points are obtained by using meshfree method and kriging response is developed for mass and buckling eigenvalue.

Table 7-1 Description of the thirteen design variables

Variable No.	**Meaning**	**Lower Limit**	**Upper limit**
1	Starting point of first stiffener	0	1
2	Shape parameter (x) for first stiffener	0	1
3	Shape parameter (y) for first stiffener	0	1
4	Ending point of first stiffener	0	1
5	Starting point of second stiffener	0	1
6	Shape parameter (x) for second stiffener	0	1
7	Shape parameter (y) for second stiffener	0	1
8	Ending point of second stiffener	0	1
9 & 10	Height of Stiffener 1 and 2	20 cm	60 cm
11,12 & 13	Thickness of Stiffener 1, 2 and Panel	2 mm	6 mm

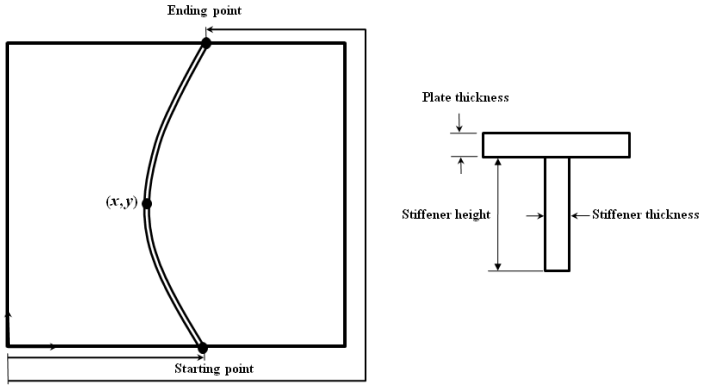

Fig. 7-1 Description of the design variables

- ***Two-Step Optimization Technique***

Because of the noisy response surface, the optimization process was divided into two steps. In the first step, the size and thickness of the plate and the stiffeners are kept fixed and the variables describing the shape of stiffeners are taken as the design variables to build a kriging model and to find the optimum combination of those variables to maximize the buckling using the genetic algorithm. In the second step, the size and thickness of the plate and the stiffeners are considered as the design variables, the shape of stiffeners are kept unchanged, and minimum mass subject to constraint on buckling eigenvalue is obtained.

In order to develop the kriging response for buckling parameter, a set of sample points (training sets) are created using a random statistical data sampling technique called the Latin Hypercube Sampling (LHS). With these sample points, the kriging response is constructed. Then the mean square of estimated error can be calculated at different points in the training sets. As will be discussed in greater detail later, by using the estimated errors, new set of sample points from the previous sample points and the design points that have large estimated error can be created. Using this new set of sample points the kriging response is reconstructed. This process is continued till a desired accuracy is obtained. After developing the kriging model, GA optimization technique is applied to find a set of optimum design variables. The general scheme of kriging based design optimization as used in this paper is shown in Fig. 7-2.

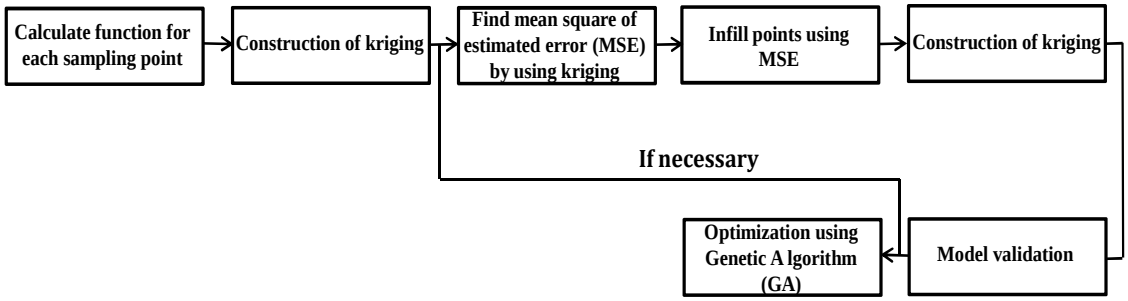

Fig. 7-2 Framework for kriging based design optimization

- ***Enhanced Kriging Model with Additional Design Points***

Since having a large number of sample points to develop an accurate kriging model is costly, and it is unlikely that the kriging model, will, initially, be sufficiently accurate by using a limited number of sample points, we need to develop an algorithm to use the minimum number of sample points while having the desired accuracy. After building the preliminary kriging response by using the initial sample points we may wish to enhance the model accuracy by applying a series of infill points. The success of constructed response using the infill points depends on the infill criteria. The infill points are typically chosen either in areas where the response is found to be inaccurate (exploration) or where the surrogate model suggests that the optimal design may be found (exploitation). By exploring the design space, the response surface can be modified to predict the complex behavior of the true function, and by exploiting the surrogate model the attractive areas of objective space can be improved. We know that to exploit the surrogate before the design space has been explored sufficiently may result in the wrong global optimum, while over exploration is a waste of resources. Therefore providing a useful way to achieve the balance between exploration and exploitation is required.

As mentioned before, one of the kriging model's features, which makes it a popular surrogate model, is its statistical interpretation. This interpretation not only allows us to predict the function, but also allows us to find the possible error in the predictor. The availability of predicted function and estimated error in kriging can help us in achieving a balance between exploration and exploitation. One way of balancing exploitation of the predicted function $\hat{y}(x)$ and exploration using Mean Square Error (MSE) is to minimize a statistical lower bound [75]

$$\begin{aligned} LB(x) &= \hat{y}(x) - As(x) \\ s(x) &= \sqrt{MSE(\hat{y}(x))} \end{aligned} \tag{7-5}$$

where A is a constant that controls the exploitation and exploration balance. From the literature review [75], $A=5$ may be a proper choice.

In the statistical lower bound approach, the additional points are chosen where the minimums of statistical lower bound occur. In order to test this approach, a simply-supported rectangular plate is chosen. The baseline panel configuration, loading, and material properties, provided by Lockheed Martin Aeronautics Company (Lockheed Martin), are shown in Fig. 7-3 and the material properties used for analysis of this panel are given in Table 7-2. The kriging response for buckling parameter versus starting point of curvilinearly stiffener is shown in Fig. 7-4. As can be seen in Fig. 7-4, in addition to the kriging predictor and FEM response, the estimated error is also presented. The estimated error is zero at the sampled points, indicating that the predicted function and FEM analysis match. As we go further from the sampled point, the more uncertain the predicted function is, and the higher is the estimated error.

In Fig. 7-5, this approach is evaluated and as can be seen the quality of objective function is improved at the end of each iteration.

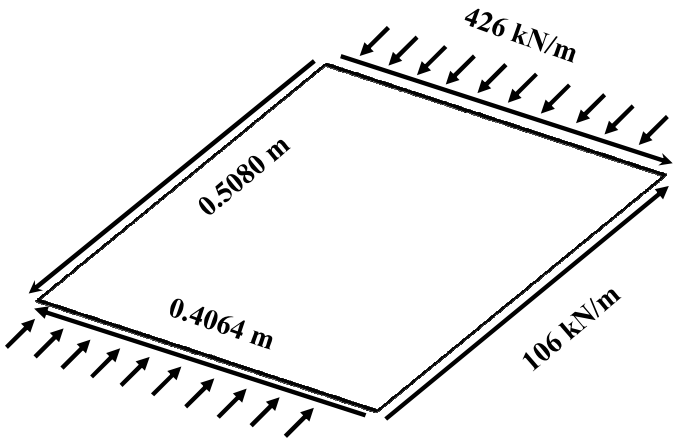

Fig. 7-3 Panel dimensions and loading conditions

Table 7-2 Material properties of curvilinearly stiffened plate

Modulus of Elasticity	73×10^9 *Pa*
Density	2795 kg/m^3
Poisson's Ratio	0.33

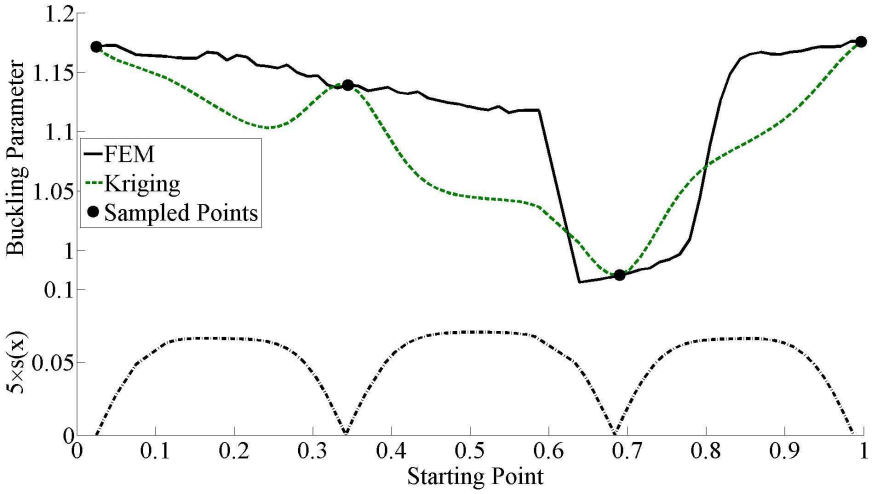

Fig. 7-4 The kriging predictor and estimated error

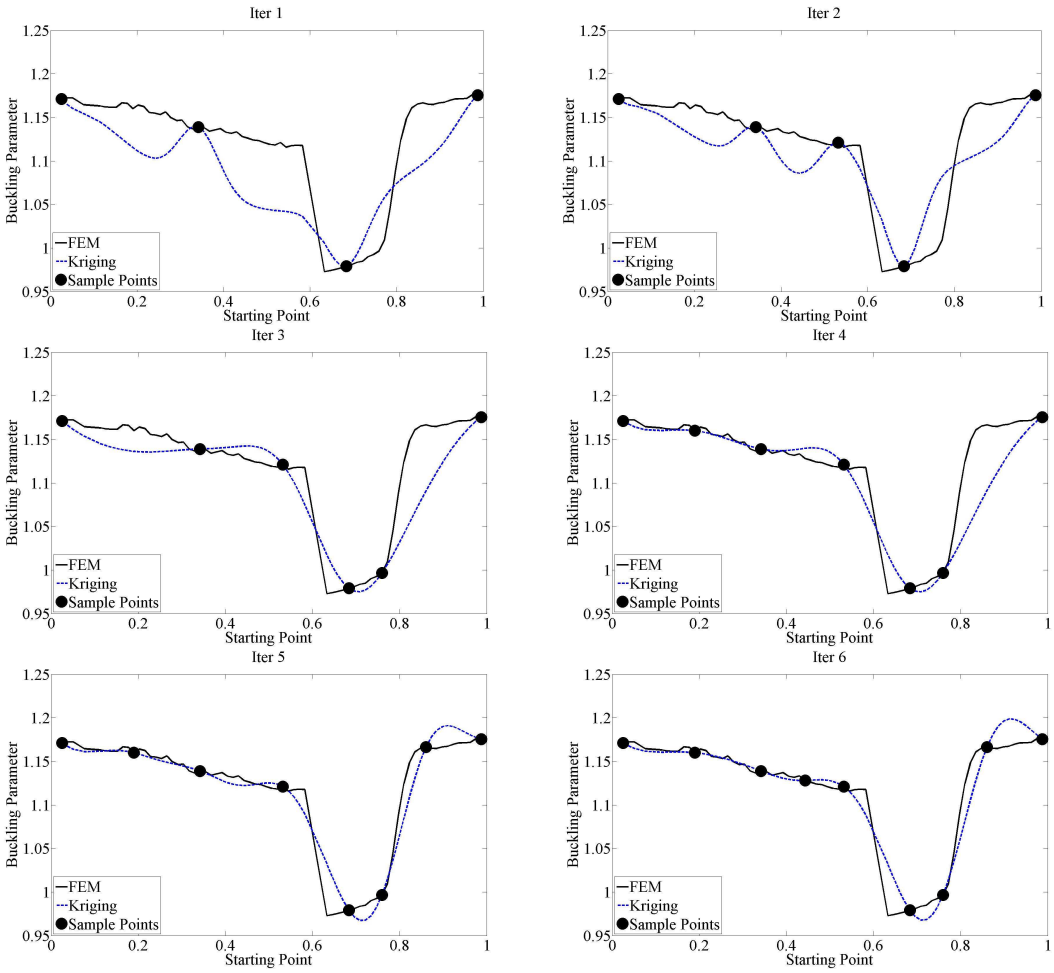

Fig. 7-5 Iterations of enhanced kriging model

- ***Reciprocal Variable***

As mentioned in introduction, Schmit and Farshi [69] looked at various approximation concepts to improve the efficiency of structural optimization. One of those concepts was reciprocal variables and it was shown that it can improve the quality of the displacement and stress response. By looking through the buckling equations for curvilinearly stiffened plate, it can be seen that the buckling eigenvalue is proportional to the square of thickness of plate (h_p), so the buckling parameter (1/buckling eigenvalue) is inversely proportional to the square of thickness of plate. Let the square of thickness of plate be defined as a design variable. By using the fact that for linearly buckling problem, the buckling parameter is inversely proportional to h_p, the reciprocal design variable can be defined as:

$$\beta = 1/h_p^2 \tag{7-6}$$

The kriging response for buckling parameter versus thickness of plate is shown in Fig. 7-6 for two choices of design variables. As can be seen in this figure, the kriging prediction with reciprocal design variable is closer to the FEM results. In the current research the quality of kriging approximation is enhanced by using the reciprocal design variable.

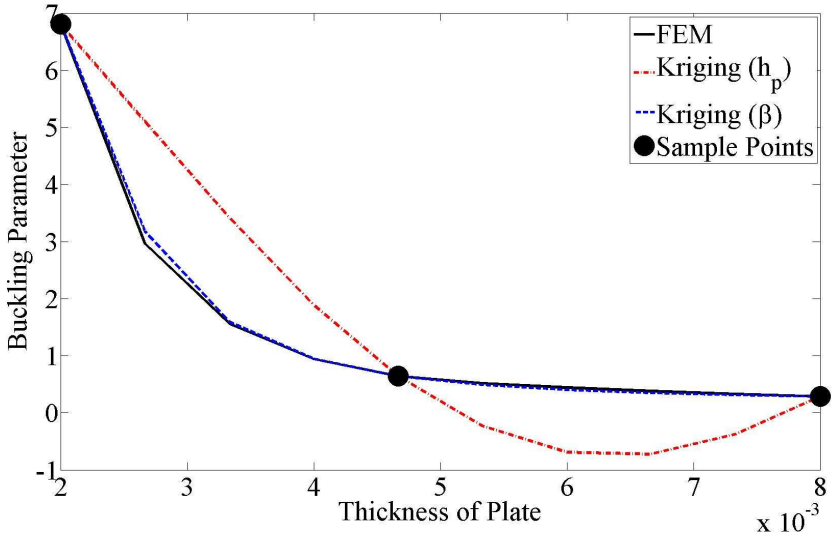

Fig. 7-6 The kriging predictor using reciprocal variable

7.4 Results

Numerical results have been obtained for optimization of plate with curvilinear stiffeners. The presented results compare minimum mass designs from three different optimization approaches. The performance and optimal results obtained using MD.PATRAN®, MD.NASTRAN®, and VisualDOC®, MD.PATRAN®, MD.NASTRAN®, kriging and GA, and meshfree, kriging and GA are compared. All optimizations for mass minimization have constraints on buckling eigenvalue. All FEM analyses are performed with NASTRAN using CTRIA3 shell finite element. The curvilinearly stiffened plate geometry and mesh are regenerated for each design point analysis during optimization. The details of this approach can be found in the paper by Gurav and Kapania [77]. The meshfree analyses are performed using the code developed by author.

A simply supported rectangular plate of size 0.4064 × 0.5080 m, as is shown in Fig. 7-3, and material properties listed in Table 7-2 is studied under combined shear and compression with dominant compression, Ny=2009.7kN/m and Nxy=462 kN/m. The optimum masses for each approach are listed in Table 7-3, and the stiffener configurations from each approach are shown in Fig. 7-7. Comparing the

performance of each method show that the meshfree, kriging and GA is able to almost obtain the same configuration and optimal mass in far less CPU time. By using the meshfree method we could improve the CPU time of each analysis and by using the surrogate model we could reduce the number of iterations.

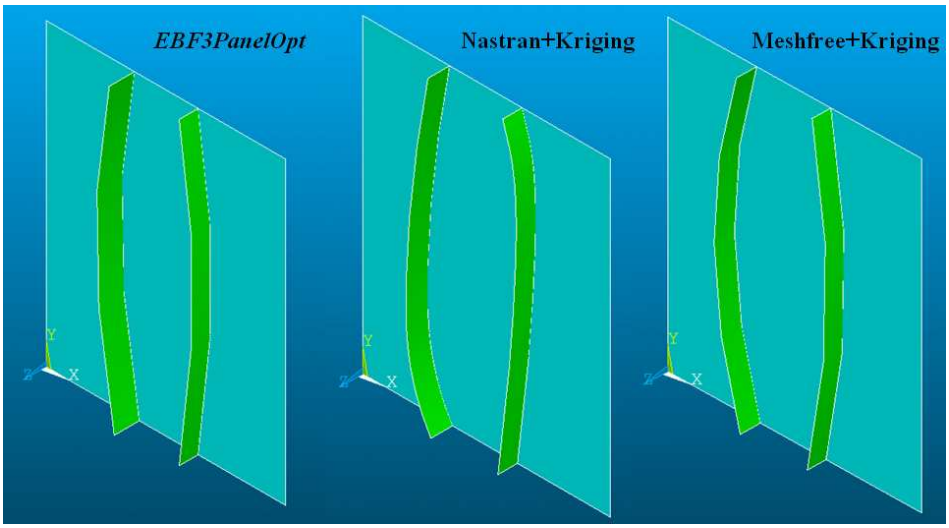

Fig. 7-7 Comparison of optimum stiffener configurations obtained using three approaches

Table 7-3 Optimum mass obtained using three approaches

EBF3PanelOpt		Nastran+Kriging		Meshfree+Kriging	
Mass (kg)	Buckling	Mass (kg)	Buckling	Mass (kg)	Buckling
2.02	1.00	2.08	1.02	2.09	1.01
10500 iterations (9hr)		3800 iterations (5hr)		3800 iterations (2hr)	

7.5 Conclusion

Since the FEM analysis of curvilinearly stiffened plate is quite expensive, the meshfree method is chosen as the analyzer to reduce the CPU time. However it will still require many simulations. Because of the number of simulations may be required in the solution of an engineering optimization problem, many researchers have tried to find approaches and techniques in optimization which can reduce the number of function evaluations. In these problems, surrogate models for analysis and optimization can be very efficient. The basic idea in surrogate model is to reduce the computational cost and giving a better understanding of the influence of the design variables on the different objectives and constrains. To use the advantage of both meshfree method and surrogate model in reducing CPU time, the meshfree method is used to generate the sample points and combination of Kriging (a surrogate model) and Genetic Algorithms is used for design of curvilinearly stiffened plate. The meshfree and kriging results and CPU time were compared with those obtained using *EBF3PanelOpt*.

8 Future Research

In the conducted research, the Element Free Galerkin (EFG) and Ritz methods were developed for vibration, random vibration, buckling and static analysis of plate with curvilinear stiffeners. The main advantage of meshfree formulations is that the stiffeners can be placed anywhere within the plate and they need not necessarily follow the nodal lines for the plate. This feature resulted in the placement and shape of a stiffener changing without re-meshing the entire domain, which can be very beneficial for performing optimization studies. To use the advantage of both meshfree method and surrogate model in reducing CPU time, the meshfree method was used to generate the sample points and combination of Kriging and Genetic Algorithms (GA), is used for design of curvilinearly stiffened plate.

As it was mentioned in the thesis, the stiffener cross section is assumed to be symmetric about the stiffener binormal axis and the stiffener is assumed to remain perpendicular to the plate during deformation. Developing the equations for the stiffener with unsymmetric cross section is necessary for analyzing “L” stiffener.

Also it is mentioned that in this research the linear buckling and static analysis of curvilinearly-stiffened plate are considered. In many engineering applications, the structure may experience the nonlinearity. Investigating nonlinearity in both the deformation and material is very important and can be the subject of future research.

The nonlinear random vibration of structures is one of the serious problems facing designers and engineers. Developing an Element Free Galerkin formulation using von Karman plate theory for the analysis of random response of curvilinearly stiffened plate could be an extension to the current research.

Changing the shape and size of curvilinear stiffeners can passively control natural frequencies, mode shapes, mechanical and thermal stresses and acoustic behavior of structure. In addition to the mentioned capability of curvilinear stiffeners, the potential efficiency gains of adaptive structures can be also used to control the behavior of unitized structure. Adaptive structures typically comprise unconventional materials (e.g., piezoelectrics, shape memory alloys or polymers, electroactive polymers) that respond to environmental and/or artificially imposed fields. In the proposed research, the placement of piezoelectric stiffener can be investigated using the meshfree method and discrete optimization formulation (e.g. Genetic Algorithm (GA)), to determine the location of piezoelectric sensor and actuator for damage detection in the structure.

References

[1] Renton, W. J., Olcott, D., Roeseler, W., Batzer, R., Baron, W., and Velicki, A., "Future of Flight Vehicle Structures (2000-2023)," Journal of Aircraft, Vol. 41, No.5, 2004, pp. 986-997.

[2] Kapania, R. K., Li, J. and Kapoor, H., "Optimal Design of Unitized Panels with Curvilinear Stiffeners," AIAA 5th ATIO and the AIAA 16th Lighter-than-Air Systems Technology Conference and Balloon Systems Conference, v 3, 2005, pp. 1708-1737.

[3] Matheron, G., "Principles of geostatistics". Economic Geology, Vol. 58, No. 8, 1963, pp.1246–1266.

[4] Cressie, N., "The origins of Kriging", Mathematical Geology, Vol. 22, No. 3, 1990, pp. 239–252.

[5] Kendrick, S., "The Analysis of a Flat Plated Grillage," European Shipbuilding, Vol. 27, 1956, pp. 923-935.

[6] Schade, H. A., "The Orthogonally Stiffened Plate under Uniform Lateral Load," Journal of Applied Mechanics, Vol. 7, 1940, pp. 143-146.

[7] Olson, M. D. and Hazell, C. R., "Vibration Studies of Some Integral Rib-Stiffened Plates," Journal of Sound and Vibration, Vol. 50, No. 1, 1977, pp. 43-61.

[8] Bhimaraddi, A., Carr, A. J. and Moss, M. J., "Finite Element Analysis of Laminated Shells of Revolution with Laminated Stiffeners," Computers and Structures, Vol. 33, No. 1, 1989, pp. 295-305.

[9] Holopainen, T. P., "Finite Element Free Vibration Analysis of Eccentrically Stiffened Plates," Computers and Structures, Vol. 56, No. 6, 1995, pp. 993-1007.

[10] Kumar, Y. V. S. and Mukhopadhyay, M., "A New Triangular Stiffened Plate Element for Laminate Analysis," Composites Science and Technology, Vol. 60, No. 6, 2000, pp. 935-943.

[11] Gangadhara Prusty, B. and Satsangi, S. K., "Analysis of Stiffened Shell for Ships and Ocean Structures by Finite Element Method," Ocean Engineering, Vol. 28, No. 6, 2001, pp. 621-638.

[12] Barik, M. and Mukhopadhyay, M., "A New Stiffened Plate Element for the Analysis of Arbitrary Plates," Thin-Walled Structures, Vol. 40, No. 7, 2002, pp. 625-639.

[13] Chen, C. J., Liu, W. and Chern, S. M., "Vibration Analysis of Stiffened Plate," Computers and Structures, Vol. 50, No. 4, 1994, pp. 471-480.

[14] Liew, K. M., Xiang, Y., Kitipornchai, S., Lim, M. K., "Vibration of Rectangular Mindlin Plates with Intermediate Stiffeners," Journal of Vibration and Acoustics, Vol. 116, No. 4, 1994, pp. 529-535.

[15] Liew, K. M., Xiang, Y., Kitipornchai, S., Meek, J. L., "Formulation of Mindlin-Engesser Model for Stiffened Plate Vibration," Computer Methods in Applied Mechanics and Engineering, Vol. 120, No. 3, 1995, pp. 339-353.

[16] Smith, S. T., Bradford, M. A. and Oehlers, D. J., "Numerical Convergence of Simple and Orthogonal Polynomials for the Unilateral Plate Buckling Problem Using the Rayleigh-Ritz Method," International Journal for Numerical Methods in Engineering, Vol. 44, 1999, pp. 1685-1707.

[17] Bellman, R., Kashef, B. G. and Casti, J., "Differential Quadrature: A Technique for The Rapid Solution of Nonlinear Partial Differential Equations," Journal of Computational Physics, Vol. 10, No. 1, 1972, pp.40-52.

[18] Zeng, A. and Bert, C. W., "A Differential Quadrature Analysis of Vibration for Rectangular Stiffened Plates," Journal of Sound and Vibration, Vol. 241, No. 2, 2001, pp. 247-252.

[19] Wei, G. W., Zhao, Y. B. and Xiang, Y., "Discrete Singular Convolution and Its Application to the Analysis of Plates with Internal Supports. Part 1: Theory and Algorithm," International Journal for Numerical Methods in Engineering, Vol. 55, 2002, pp. 913-946.

[20] Zhao, Y. B., Wei, G. W. and Xiang, Y., "Discrete Singular Convolution for the Prediction of High Frequency Vibration of Plates," International Journal of Solids and Structures, Vol. 39, No. 20, 2002, pp. 65-88.

[21] Belytschko, T., Lu, Y. Y., Gu, L., "Element-Free Galerkin Methods," International Journal for Numerical Methods in Engineering, Vol. 37, No. 2, 1994, pp. 229-256.

[22] Krysl, P. and Belytschko, T., "Analysis of Thin Shells by the Element Free Galerkin Method," International Journal of Solids and Structures, Vol. 33, No. 20, 1996, pp. 3057-3080.

[23] Belytschko, T., Krongauz, Y., Organ, D., Fleming, M., and Krysl, P., "Meshless Methods: An Overview and Recent Developments," Computer Methods in Applied Mechanics and Engineering, Vol. 139, 1996, pp. 3-47.

[24] Peng, L. X., Kitipornchai, S. and Liew, K. M., "Analysis of Rectangular Stiffened Plates under Uniform Lateral Load Based On FSDT and Element-Free Galerkin Method," International Journal of Mechanical Sciences, Vol. 47, No. 2, 2005, pp. 251-276.

[25] Peng, L. X., Liew K.M. and Kitipornchai, S., "Buckling and Free Vibration Analyses of Stiffened Plates Using the FSDT Meshfree Method," Journal of Sound and Vibration, Vol. 289, No. 3, 2006, pp. 421-449.

[26] Zhou, L. and Zheng, W.X., "Moving Least Square Ritz Method for Vibration Analysis of Plates," Journal of Sound and Vibration, Vol. 290, No. 3-5, 2006, pp. 968-990.

[27] Bobaru, F., and Mukherjee, S., "Shape Sensitivity Analysis and Shape Optimization in Planar Elasticity Using the Element-Free Galerkin Method," Computer Methods in Applied Mechanics and Engineering, Vol. 190, 2001, pp. 4319-4337.

[28] Olson, M. D. and Lindberg G. M., "Jet Noise Excitation of an Integrally Stiffened Panel," Journal of Aircraft, Vol. 8, No. 11, 1971, pp. 847-855.

[29] Dey, S. S., "Finite Element Method for Random Response of Structures Due to Stochastic Excitation," Computer Methods in Applied Mechanics and Engineering, Vol. 20, No. 2, 1979, pp. 173-194.

[30] Yang, T. Y. and Kapania, R. K., "Finite Element Random Response Analysis of Cooling Tower," Journal of Engineering Mechanics, Vol. 110, No. 4, 1984, pp. 589-609.

[31] Mukherjee, A. and Mukhopadhyay, M., "Response of Stiffened Plated Structures under Stochastic Excitation," Computer Methods in Applied Mechanics and Engineering, Vol. 71, No. 3, 1988, pp. 273-292.

[32] Lyrintzis, C. S. and Vaicaitis, R., "Random Response and Noise Transmission of Discretely Stiffened Composite Panels," Journal of Aircraft, Vol. 27, No. 2, 1990, pp. 176-184.

[33] Liu, Q., Orisamolu, I. R. and Chernuka, M. W., "Consistent Finite Element Discretization of Distributed Random," Journal of Aircraft, Vol. 51, No. 1, 1994, pp. 39-45.

[34] Dogan, V., "Vibration of Anti-Symmetric Angle-ply Composite Plates under Random Excitation," Aircraft Engineering and Aerospace Technology, Vol. 79, No. 5, 2007, pp. 475-484.

[35] Joshi, P., Mulani, S. B., Gurav, S. P. and Kapania, R. K., "Design Optimization for Minimum Sound Radiation from Point-Excited Curvilinearly Stiffened Panel," Journal of Aircraft, Vol. 47, No. 4, 2010, pp. 1100-1110.

[36] Praveen, G. N., and Reddy, J. N., “Nonlinear Transient Thermoelastic Analysis of Functionally Graded Ceramic-Metal Plates”, International Journal of Solids and Structures, Vol.35, 1998, pp. 4457-4476.

[37] Loy, C. T., Lam, K. Y., and Reddy, J. N., “Vibration of Functionally Graded Cylindrical Shells”, International Journal of Mechanical Sciences, Vol. 41, 1999, pp. 309-324.

[38] Yang, J., and Shen, H. S., “Dynamic Response of Initially Stressed Functionally Graded Rectangular Thin Plates”, Composite Structures, Vol. 54, 2001, pp. 497-508.

[39] Qian, L. F., Batra, R. C., and Chen, L. M., “Static and Dynamic Deformations of Thick Functionally Graded Elastic Plates by Using Higher-Order Shear and Normal Deformable Plate Theory and Meshless Local Petrov–Galerkin Method”, Composites: Part B, Vol. 35, 2004, pp. 685-697.

[40] Zhao, X., Lee, Y. Y., and Liew, K. M., “Free Vibration Analysis of Functionally Graded Plates Using the Element-Free kp-Ritz Method”, Journal of Sound and Vibration, Vol. 319, 2009, pp. 918-939.

[41] He, X. Q., Ng, T. Y., Sivashanker, S., and Liew, K. M., “Active control of FGM plates with integrated piezoelectric sensors and actuators”, International Journal of Solids and Structures, Vol. 38, pp. 1641-1655, 2001.

[42] Sheng, G. G., and Wang, X., “Effects of Thermal Loading on the Buckling and Vibration of Ring-Stiffened Functionally Graded Shell”, Journal of Thermal Stresses, Vol. 30, 2007, pp. 1249-1267.

[43] Birman, V., and Byrd, L. W., “Stability and Natural Frequencies of Functionally Graded Stringer-Reinforced Panels”, Composites: Part B, Vol. 39, 2008, pp. 816-825.

[44] Najafizadeh, M. M., Hasani, A., and Khazaeinejad, P., “Mechanical Stability of Functionally Graded Stiffened Cylindrical Shells”, Applied Mathematical Modeling, Vol. 33, 2009, pp. 1151-1157.

[45] Chen, C. S., Hsu, C. Y., and Tzou, G. J., “Vibration and Stability of Functionally Graded Plates Based on a Higher-order Deformation Theory”, Journal of Reinforced Plastics and Composites, Vol. 28, 2009, pp. 1215-1234.

[46] Malekzadeh, P., Shahpari, S. A., and Ziaee, H. R., “Three-dimensional Free Vibration of Thick Functionally Graded Annular Plates in Thermal Environment”, Journal of Sound and Vibration, Vol. 329, 2010, pp. 425-442.

[47] Malekzadeh, P., Three-dimensional Free Vibration Analysis of Thick Functionally Graded Plates on Elastic Foundations. Composite Structures, Vol. 89, 2009, pp. 367-373.

[48] Timoshenko, S. P. and Gere, J. M., "Theory of Elastic Stability," McGraw-Hill, New York, 1961.

[49] Seide, P., "The Effect of Longitudinal Stiffeners Located on One Side of A Plate on The Compressive Buckling Stress of the Plate Stiffener Combination," Report No. NASA TN 2873, 1953.

[50] Kolakowski, Z., "A Semi-Analytical Method for the Analysis of The Interactive Buckling of Thin-Walled Elastic Structures In The Second Order Approximation," International Journal of Solids and Structures, Vol. 33, No. 25, 1996, pp. 3779-3790.

[51] Byklum, E., Steen, E. and Amdahl, J., "A Semi-Analytical Model for Global Buckling and Postbuckling Analysis of Stiffened Panels," Thin-Walled Structures, Vol. 42, No. 5, 2004, pp. 701–717.

[52] Brubak, L., Hellesland, J. and Steen, E., "Semi-Analytical Buckling Strength Analysis of Plates with Arbitrary Stiffener Arrangements," Journal of Constructional Steel Research, Vol. 63, No. 4, 2007, pp. 532–543.

[53] Bedair, O., "Discussion on Semi-Analytical Buckling Strength Analysis of Plates with Arbitrary Stiffener Arrangements by Brubak, J. Hellesland and E. Steen," Journal of Constructional Steel Research, Vol. 63, No. 12, 2007, pp. 1616–1617.

[54] Shastry, B. P., Venkateswara Rao, G. and Reddy, M. N., "Stability of Stiffened Plates Using High Precision Finite Element," Nuclear Engineering and Design, Vol. 36, No. 1, 1976, pp. 91-95.

[55] Mukhopadhyay, M. and Mukherjee, A., "Finite Element Buckling Analysis of Stiffened Plates," Computers and Structures, Vol. 34, No. 6, 1990, pp.795-803.

[56] Biswal, K. C. and Ghosh, A. K., "Finite Element Analysis For Stiffened Laminated Plates Using Higher Order Shear Deformation Theory," Computers and Structures, Vol. 53, No. 1, 1994, pp. 161-171.

[57] Sadek, E. A. and Tawfik, S. A., "A Finite Element Model for the Analysis of Stiffened Laminated Plates," Computers and Structures, Vol. 75, No. 4, 2000, pp. 369-383.

[58] Guot, Yan-Lin and Lindner, J., "Analysis of Elastic-Plastic Interaction Buckling of Stiffened Panels by Spline Finite Strip Method," Computers and Structures, Vol. 46, No. 3, 1993, pp. 529-536.

[59] Kapania, R. K and Li, J., "On a Geometrically Exact Curved/Twisted Beam Theory under Rigid Cross-Section Assumption," Computational Mechanics, Vol. 30, No. 5-6, 2003, pp. 428-443.

[60] Kapania, R. K and Li, J., “A Formulation and Implementation of Geometrically Exact Curved Beam Elements Incorporating Finite Strains and Finite Rotations,” Computational Mechanics, Vol. 30, No. 5-6, 2003, pp. 444-459.

[61] Atluri, S. N. and Zhu, T. L., “A New Meshless Local Petrov–Galerkin (MLPG) Approach in Computational Mechanics,” Computational Mechanics, Vol. 22, No. 2, 1998, pp. 117-127.

[62] Batra, R. C. and Zhang, G. M., “SSPH Basis Functions for Meshless Methods, and Comparison of Solutions with Strong and Weak Formulations,” Computational Mechanics, Vol. 41, No. 4, 2008, pp. 527-545.

[63] Liew, K. M., Peng, L. X., and Kitipornchai, S., “Buckling of Folded Plate Structures Subjected to Partial In-plane Edge Loads by the FSDT Meshfree Galerkin Method,” International Journal for Numerical Methods in Engineering, Vol. 65, 2006, pp. 1495-1526.

[64] Smith, G. A., Laura, P. A., and Matis, M., “Experimental and analytical study of vibrating stiffened rectangular plates subjected to in-plane loading,” Journal of the Acoustical Society of America, Vol. 48, No. 3, 1970, pp. 707-713.

[65] Kielb, R. E. and Han, L. S., “Vibration and Buckling of Rectangular Plates Under In-Plane Hydrostatic Loading,” Journal of Sound and Vibration, Vol. 70, No. 4, 1980, pp. 543-55.

[66] Attaf, B. and Hollaway, L., “Vibrational Analyses of Stiffened and Unstiffened Composite Plates Subjected to In-plane Loads,” Composites, Vol. 21, No. 2, 1990, pp. 117-126.

[67] Srivastava, A. K. L., Datta, P. K. and Sheikh, A. H., “Buckling and Vibration of Stiffened Plates Subjected to Partial Edge Loading,” International Journal of Mechanical Sciences, Vol. 45, No. 1, 2003, pp. 73-93.

[68] Srivastava, A. K. L., Datta, P. K. and Sheikh, A. H., “Transverse Vibration of Stiffened Plates with Cutouts Subjected to In-Plane Uniform Edge Loading at the Plate Boundary,” Shock and Vibration, Vol. 11, No. 1, 2004, pp. 9-19.

[69] Schmit Jr, L. A., and Farshi, B., “Some Approximation Concepts for Structural Synthesis,” AIAA Journal, Vol. 12, No. 5, 1974, pp. 692-699.

[70] Jones, D. R., “A Taxonomy of Global Optimization Methods Based on Response Surface,” Journal of Global Optimization, Vol. 21, 2001, pp. 345-383.

[71] Simpson, T. W., Mauery, T. M., Korte, J. J., and Mistree, F., "Comparison of Response Surface and Kriging Models For Multidisciplinary Design Optimization," Technical Report, AIAA- 98-4755, 1998.

[72] Carpenter, W. C, and Barthelemy, J. F. M., "A Comparison of Polynomial Approximations and Artificial Neural Nets as Response Surfaces," Structural Optimization, Vol. 5, 1993, pp. 166-174.

[73] Sakata, S., Ashida, F., and Zako, M., "Structural Optimization Using Kriging Approximation," Computer Methods in Applied Mechanics and Engineering, Vol. 192, 2003, pp. 923-939.

[74] Queipo, N. V., Haftka, R. T., Shyy, W., Goel, T., Vaidyanathan R., and Tucker, K., "Surrogate-Based Analysis and Optimization," Progress in Aerospace Sciences, Vol. 41, 2005, pp. 1-28.

[75] Forrester, A. I. J., and Keane, A. J., "Recent Advances in Surrogate-based Optimization," Progress in Aerospace Sciences, Vol. 45, 2009, pp. 50-79.

[76] Sakata, S., Ashida, F., and Zako, M., "Eigenfrequency Optimization of Stiffened Plate Using Kriging Estimation," Computational Mechanics, Vol. 31, 2003, pp. 409-418.

[77] Gurav, S. P., and Kapania, R. K., "Development of a Framework for the Design Optimization of Unitized Structures," 50th AIAA/ASME/ASCE/AHS/ASC Structures, Structural Dynamics, and Materials Conference, 4-7 May 2009, Palm Springs,

[78] Dang, T. D., Kapania, R. K., and Gurav, S. P. "Optimization of Unitized Structures under Damage Tolerance Constraints," 50th AIAA/ASME/ASCE/AHS/ASC Structures, Structural Dynamics, and Materials Conference, 4-7 May 2009, Palm Springs,

[79] Reddy, J. N., "Mechanics of Laminated Composite Plates and Shells," CRC Press, Boca Raton, 2004.

[80] Martini, L. and Vitaliani, R., "On the Polynomial Convergent Formulation of a C_0 Isoparametric Skew Beam Element," Computers and Structures, Vol. 29, No. 3, 1988, pp. 437-449.

[81] Zhu, T. and Atluri, S. N., "On A Modified Collocation Method and a Penalty Formulation for Enforcing the Essential Boundary Conditions in the Element Free Galerkin Method," Computational Mechanics, Vol. 21, No. 3, 1998, pp. 211-222.

[82] Kapania R. K. and Singhvi, S., "Free vibration analyses of generally laminated tapered skew plates," Composites Engineering, Vol. 2, No. 3, pp. 197-212, 1992.

[83] Kapania R. K. and Lovejoy, A. E., “Free vibration of thick generally laminated cantilever quadrilateral plates,” AIAA Journal, Vol. 34, No. 7, pp. 1474-1486, 1996.

[84] Kapania R. K., Kim, Y, “Flexural-Torsional Coupled Vibration of Slewing Beams Using Various Types of Orthogonal Polynomials,” Journal of Mechanical Science and Technology, Vol. 20, No. 1, 2006, pp. 1790-1800.

[85] STAR Modal (Version 6.4.0.0) [Computer software]. 2730 Orchard Parkway, San Jose, CA 95134-2012: Spectral Dynamics, Inc. Available from http://www.spectraldynamics.com/

[86] Wessel, James K., Handbook of Advanced Materials: Enabling New Designs, Hoboken, NJ, WileyInterscience, 2004.

[87] Zienkiewicz, O. C., “The Finite Element Method,” McGraw-Hill, New York, 1977.

[88] Rossow, M. P., Ibrahimkhail, A. K., “Constraint Method Analysis of Stiffened Plates,” Computers and Structures, Vol. 8, No. 1, 1978, pp. 51–60.

[89] McBean, R. P., “Analysis of Stiffened Plates by the Finite Element Method,” Ph.D. thesis, Stanford University, Palo Alto, CA, 1968.

[90] Chang, S. P., “Analysis of Eccentrically Stiffened Plates,” Ph.D. thesis, University of Missouri, Columbia, MO, 1973.

[91] Lin, Y. K., “Probabilistic Theory of Structural Dynamics,” R. E. Krieger Pub. Co, Huntington, New York, 1976.

[92] Sacks, J., Welch , W. J., Mitchell, T. J., and Wynn, H. P., “Design for Computer Experiments,” Technometric, Vol. 31, No. 1, 1989, pp. 41-47.